Development of a Strategy for the Management and Control of Multiple Energy Sources within Series Hybrid Electric Vehicles

Theodorus Antonius Hendrik Kok

A doctoral report submitted in partial fulfilment of the requirements of the University of Sunderland for the degree of Doctor of Philosophy

August 2015

amap University of Sunderland
automotive & manufacturing advanced practice

Philippa - for unwavering dedicated support, I love you

Isla and Elwyn - for always smiling and making my days brighter

Acknowledgements

I want to thank my manager and Director of Studies Adrian Morris for the opportunity offered, now 6 years ago, and for the time and dedication he has given me to be able to complete this project. I also would like to thank Professor Alan Wheatley for supporting the opportunity and his time to this project.

The journey has been an interesting one and has taught me many things, but without the teachings, support and understanding from my parents I would have never made it this far. A big thanks to my Dad and his wife for all practical advice and my Mum and her husband for a listening ear and the time to relax. I would like to thank my sisters, my brothers and their families and my friends in the Netherlands, England and around the world. Without their support I would not have been able to complete this project. I say thank you for keeping me sane.

I would like to thank all the staff at AMAP for their support and contributions. A special thanks to Phil Johnson, for IT support in both hardware and software, Helen Scott for her assistance with statistics, Dr Michael Knowles for his overall knowledge on engineering subjects and Dr. Kevin Burn for his contributions on control techniques.

Lastly, I would like to thank the University of Sunderland as my employer and educational institution.

Abstract

The battery in an EV is designed according to a power to energy ratio and is a trade-off in the design of the pack. It also suffers from effects such as rate capacity effect, ripple effects and inefficiency under charging. These effects result in losses through which the capacity and life span of the batteries are compromised affecting range and drivability.

In this thesis a novel development path resulting in a novel Power and Energy Management Strategy (PEMS) is presented. The effects of (dis)charging a battery are researched and converted to an energy optimisation formula and result in reduced power demand for the converter which reduces weight. The resulting Power Management Strategy (PMS) aims to recover energy more efficiently into UC while responding fast to a change in demand.

The effects of converters on the battery current ripple are researched and discussed, resulting in an optimal topology layout, improved battery life and reduced losses. Through the use of Markov Chain analysis and a newly derived Bias function a predictive Energy Management Strategy (EMS) is developed which is practical to use in EVs.

This resulted in a PEMS which because of the fast PMS results in a fast response time. The use of Markov Chain results in predictive EMS and improves the efficiency of the energy sources and allows the design to be reduced in size.

Through the design methodology used the parallel topology (the battery converter parallel to the UC Module) was rated preferred choice over battery only and battery with UC Module. The rating was based on capacity, ripple control, weight, 10 year cost, potential for motor controller efficiency improvement, range and efficiency.

The combination of method and PEMS resulted in an improved life expectancy of the pack to over 10 year (up from 7) while increasing range and without sacrificing drivability.

Nomenclature

Notation	Description	Unit	
SoC	State of Charge	-	[%]
Q	Capacity	Ampere-hours	[Ah]
I	current (DC)	Ampere	[A]
i	Current (AC)	Ampere	[A]
t	Time	Seconds	[S]
h	hourly time interval	hours	[h]
E	Energy	Joules	[J]
		Watt-Seconds	[Ws]
		Watt-hour	[Wh]
		kilo-Watt-hour	[kWh]
P	Power	Watt	W
		kilo-Watt	kW
C	Capacitance	Farad	[F]
U, V	Voltage	Volt	[V]
L	Inductance	Henry	[H]
D, d	Duty Cycle	-	-
T	Time period	Seconds	[S]
Δi	Current ripple	Ampere	[A]
f	Frequency	Hertz	[H]
Δv	voltage ripple	Voltage	[V]
R	Resistance	Ohm	[Ω]
X	Reactance	Ohm	[Ω]
η	Efficiency	-	[%]
M	Transition matrix of possibilities	-	-
p	probability	-	-
B	Bias vector	-	-
S	State of probability	-	-
F_{te}	Tractive Effort	Newton	[N]
F_{rr}	Force through rolling resistance	Newton	[N]
F_{ad}	Force through aero dynamic drag	Newton	[N]
F_{hc}	Force through incline / decline	Newton	[N]
F_{la}	Lateral acceleration force	Newton	[N]
1.05	inertia effort on lateral acceleration force	Newton	[N]
μ_{rr}	rolling resistance coefficient	-	-
m	mass of the vehicle	kilogram	[kg]

g	gravitation constant	metre per second squared	[m/s^2]
ρ	air density	kilogram per meter cubed	[kg/m^3]
A	Frontal surface area	metre squared	[m^2]
C_d	Drag Coefficient	-	-
v	Velocity	metre per second	[m/s]
α	Angle of the slope	degrees	[°]
a	Acceleration	metres per second squared	[m/s^2]
G	Gear ratio	-	-
r	Tyre radius	metre	[m]
T_m	Torque at the motor	Newton-metre	[Nm]
ω	Angular speed at the motor	radians per second	[rad/s]
v	Vehicle velocity	meters per second	[m/s]
Kp	proportional control variable	-	-
Ki	integral control variable	-	-
Ma	Compensation ramp variable	-	-
Ibat_max	Temporary limit to battery current	Ampere	[A]
Idem	Bus current demand	Ampere	[A]
Iuc	UC current	Ampere	[A]
Ibat	battery current	Ampere	[A]
Vuc_max	UC maximum voltage	Volt	[V]
Vuc_min	UC minimum voltage	Volt	[V]
Vuc_target / Vuc_nom	UC target voltage	Volt	[V]
Cycle Range	Driveable range on a full battery charge	kilometre / cycle	km / cycle
P_{ri}	Power lost in internal Resistance of the UC	Watt	[W]
P_{out}	Total UC power	Watt	[W]
$P_{dissConv}$	Converter power losses	Watt	[W]
P_{Conv}	Total Converter Power	Watt	[W]
η_{uc}	UC Efficiency	-	[%]
η_{conv}	Converter Efficiency	-	[%]
η_{total}	UC Module Efficiency	-	[%]

Abbreviations

EV	Electric Vehicle
BEV	Battery Electric Vehicle
HEV	Hybrid Electric Vehicle
ICE	Internal Combustion Engine
FC	Fuel Cell
DG	Diesel Generators
UC	Ultra Capacitor
SC	Super Capacitor
EDLC	Electrical Double Layer Capacitor
DC-DC Converter	Direct Current to Direct Current Converter
UC Module	Combination of UC and DC-DC Converter
PEMS	Power and Energy Management Strategy
PMS	Power Management Strategy
EMS	Energy Management Strategy
SPS	SimPowerSystems, toolbox within Simulink
SoC	State of Charge – present capacity of the battery
SoD	State of Discharge – measure of charge removed
DoD	Depth of Discharge
SoH	State of Health
BMS	Battery Management System
GhG	Greenhouse Gas
VC	Vector Control
FOC	Field Oriented Control
AEV	All Electric Vehicle
RLC	Resistor – Inductor – Capacitor network
RC	Resistor – Capacitor network
CCM	Continuous Conduction Mode
DCM	Discontinuous Conduction Mode
DG	Dynamic Programming
MPC	Model Predictive Control
RB	Rule Based
NN	Neural Networks
ECMS	Equivalent Consumption Minimisation Strategy

Contents

List of Tables

List of Figures

Introduction

1.1.Motivation

The Battery Electric Vehicle (BEV) is seen as an important component and a learning step to the introduction of Fuel Cell (FC) vehicles (Bitsche and Gutmann, 2004, NAIGT, 2009). The reason for using FC vehicles is the speed of fuelling which is similar to that of current Internal Combustion Engines (ICE). Battery fast charging times are around 20-30 minutes and will enable a range of 100 miles (compared to 300+ miles in 5 minutes for diesel ICE).

One reason for viewing the BEV as a stepping stone to FC vehicles is due to the current price of FC systems. These costs may be reduced by using a smaller FC system supplemented with a supportive or multiple supportive systems (battery and/or ultra capacitor combination). The management of these supportive systems and their interaction is the focus of this thesis.

The cost of the battery pack ($400-$600 /kWh (Schoenung, 2011)) means that BEVs are expensive. The cost of the battery pack is defined by the need for energy to ensure suitable range, the need for power to achieve required acceleration and the need for durability (Burke, 2002, Bradley and Frank, 2009). Any reduction to the size of the pack without sacrificing range and driveability would thus be an improvement. The aim for the electric vehicle system is to improve their performance: size, temperature and efficiency (ieee.tv, 2010). The benefits of optimisation include reduced discharge and charge losses over time with the age of the battery.

Crolla et al (2008) has identified 3 areas for additional research that are more specific to electric vehicles:

1. driveability – optimisation research is currently based around driving cycles, but it is widely acknowledged that people are not likely to drive exactly that way
2. braking behaviour – braking energy can be won back but these systems should not put the drivers lives on the line or affect driveability
3. practical design – research currently done leaves many implementation issues; the practical designs should not affect safety or driveability

The main criteria used when considering buying a vehicle appears to be price and performance (Lane and Potter, 2007). The CENEX - The Smart Move Case Studies report stated that Electric Vehicle (EV) utilisation was increased through opportunity charging (Carroll, 2011), the participants rated the performance of EVs over the ICE equivalent. An important factor of the research into optimisation of the EV drive train is to maintain driveability of the vehicle in such a way that people want to drive it. EVs do not have the range people have come to expect from their personal transport and this so called “range anxiety” remains a worry since people’s expectations are very rigid (Valentine-Urbschat and Bernhart, 2009).

A fuel cell system alone, while able to output high power, responds slowly to a change in power demand. FCs, unlike batteries, are not able to accept charge (from regenerative energy). To increase their efficiency it would be best to use a smaller stack and operate it at its most optimum point while storing any generated energy that is not directly used temporarily in batteries and use these batteries to cover the peak power events (Simoes et al., 2014). Batteries on their own lose additional potential capacity under high discharge currents

(Donghwa et al., 2011). Ultra Capacitors (UC) would be able to supplement peak power demand since their losses under high demands are significantly less but their low energy density limits the time they can supply their power, which means they add weight if the efficiency of their use is not high enough. The peak power smoothing achieved through the use of UCs can thus improve available battery capacity. However in a vehicle any additional weight leads to an increase in power demand to maintain the same drive characteristics. This additional required power would result in an increased level of current draw from the battery. It is therefore necessary to not just simply add the UC and converter to the vehicle but to free up an equal amount of weight (or more) for the system to be beneficial or to gain a sufficient increase in driving range to justify the added weight.

Unlike the voltage level of a battery, which is often considered to be constant, the voltage level of an UC changes faster with current drawn (because of the lower energy density) as does the voltage level of a FC systems under load (Larminie and Dicks, 2003). In order to work with these changing voltage levels, Direct Current to Direct Current (DC-DC) converters are introduced. These converters can step up (boost) or step down (buck) the changing input voltage level to a constant output level.

These combinations of a slow energy source and a faster power source will become common because of the potential for overall improved efficiency, system stability, reduced size and reduced component size, such as in the use of hydraulic systems (Bender et al., 2013), FC systems (Thounthong et al., 2009a) or electric generators (Di Napoli et al., 2002b). This combining of different energy and power sources will also be found in battery packs using

different technologies to support each other, for example, non-metal-air packs supporting metal-air technologies (Stewart et al., 2012b, Stewart et al., 2012a). This thesis focuses specifically on the BEV drive train with a supporting power source in the form of an UC with DC-DC converter. It analyses the weaknesses of the batteries and the supporting role of the UC. The trade off in battery pack design (energy versus power ratio) is the result of the high current demand the battery pack has to supply and the frequency at which this demand occurs (Donghwa et al., 2011). The additions of a supporting power source is not without challenges such as: the power source does not necessarily add the same energy to weight ratio as a battery (often less energy for more weight) which requires the added components to provide an energy saving through other means. This means that the additional components should be designed towards some optimised cost function in order to keep its weight low and its size small. The reason for this is that in automotive design, any additional weight directly results in loss of efficiency. As the mass of the vehicle increases acceleration, cruising and deceleration are directly affected because an increase in mass would require additional energy and power to maintain the proposed driveability.

1.2. Problem Scope

The scope of this project is to design and test a novel Power and Energy Management Strategy (PEMS) for use in BEVs. The aim is to reduce the overall size of the energy components of the drive train without sacrificing the range or driveability. The driveability is characterised by the power required and the range by the available energy. Reducing the size of the battery pack to free up space for a support mechanism to increase power would reduce the available energy. Reducing the power rating of the battery would allow for an increase in

available energy (but at lower peak power demand) affecting driveability. The combination of a battery pack with an UC module (UC with DC-DC Converter) potentially allows for the required power demand to retain driveability while at the same time reduce the power as seen by the battery resulting in an increase of available energy.

The new PEMS optimises the usage of power between the energy sources, while optimising energy efficiency resulting in increased driving range without increasing the overall weight of the sources. As a result the new PEMS also improves battery life expectancy without affecting driveability.

This research extends to the topology used for the drive train and has an additional aim in reducing the battery ripple effects which will result in improved battery life expectancy. The scope of the problem is multi faceted:

i. Reduce the size and weight of the battery pack without reducing range or affecting driveability

ii. Add specific components that allow the reduction in size of the battery pack.

   a. The added component weight should be equal or less than the combined weight of the removed cells.

   b. The added cost of the components should be equal or less than the cost saving as a result of the removed cells.

iii. Design of a PEMS to control the different sources (battery and UC module) such that the desired optimisations, discussed previously in this section, are achieved

This thesis will include a holistic approach which will include the individual components: Battery, UC, DC-DC Converters.

1.3.**Hypothesis**

An improvement in Power and Energy Management Control Strategy will result in the downsizing of drive train component for electric vehicles, without sacrificing driveability or range.

1.4.**Methodology**

The methodology employed starts with an extensive literature review detailing the strength and weakness of the individual drive train components and their individual models.

The rate capacity effect of batteries is investigated to acquire an efficiency formula for batteries. This is validated through the author's own research. Efficiency formulas will also be established for use with converters and UCs. This will enhance the simulations by being able to estimate overall efficiency of the drive train.

In this thesis the interaction of power and energy sources through different topologies and the behaviour of different popular topologies on battery current ripple will be investigated. Part of this problem definition is the need to establish the predicted power and energy requirements in a given drive cycle. This knowledge will enable the author to optimise the size of the battery pack and UC module. Drive cycles will be analysed for energy management optimisation through the use of Markov Chain analysis. The Markov Chain analysis is not computationally intensive and as such provides a practical method to design a Power and Energy Management Strategy (PEMS).

Based upon an extensive literature review and methodical research on battery rate capacity effect, topology battery current ripple analysis and drive cycle analysis a new PEMS is developed. The development process results in a new

set of design rules to optimise the UC Module and reduce weight, volume and cost.

Using the individual models found in the literature complete drive train models are created and simulated using the Matlab / Simulink software environment. A number of simulations will be carried out using Mathworks Simulation packages Matlab / Simulink and additional toolboxes. These toolboxes include: SimPowerSystems (SPS), Symbolic Math toolbox, Simulink Control Design, Simulink Design Optimisation.

Finally full drive train simulations will be presented simulating different topologies over different drive cycles. The results will be analysed for efficiency, weight, volume and cost. The results and outcomes will be discussed and validated against the hypothesis.

1.5. Key Contributions

The key contributions in this thesis are:

- ✓ Method to design an optimised power train with multiple sources while targeting driveability, which can be extended to online adjustment
- ✓ A novel Power Management Strategy (PMS) that includes the Operational Control
- ✓ The new PMS allows for continued driveability even when the UC module is depleted but rewards ECO driving behaviour by further increasing efficiency
- ✓ A novel Energy Management Strategy (EMS) to optimise the contribution of each energy source through the use of Markov Chain analysis
- ✓ Increased knowledge on the effect of topologies on battery current ripple

- ✓ Research and analysis showing the reasons for a preference for a parallel topology over a cascaded topology
- ✓ Research and analysis showing a preference for using converters in parallel configuration
- ✓ Research showing the effect of battery energy loss under constant load conditions resulting in a formula for battery efficiency based on C-rating
- ✓ Method to assess the efficiency of batteries under simulation.
- ✓ A feed forward control for bus monitoring has been designed which will keep the bus voltage at a constant level under regeneration and does not require a torque reference to function. This solution is ideal for simulation purposes.

1.6. Thesis Outline

Chapter two describes the literature review in which the different BEV drive train components are described. This includes, the battery, the UC and the DC-DC converter, their control and power and energy management strategies. It also describes the models necessary for simulation in Matlab / Simulink.

In chapter three the topology selection for use in simulation will be explained, the battery efficiency markers will be analysed to establish an efficiency formula related to battery C–rating to enhance simulation results. In this chapter the efficiency formulas for the UC module and converters in general will be explained. The chosen drive cycles will be explained as well as the final simulation setup.

Chapter four describes the development of the Power Management Strategy and the simulation setup. Chapter five shows the use of Markov Chain analysis and the development of a Bias variable which sets up the design of the Energy

Management Strategy as well as the parameters for the development of the drive train components (Battery, UC, Converters).

Chapter six will discuss the results of the simulation. In chapter seven the hypothesis will be verified and closing thoughts will be presented.

1.7. Publications

HU, Z., REN, Q., CROLLA, D. A., MORRIS, A., **KOK, D.** & HU, M. (**2010**) **'Design and Implementation of Power Management System for Fuel Cell and Battery Powered Buses'**, 25th World Electric Vehicle Symposium and Exposition (EVS25). Shenzhen, China, 5-9 November 2010, p. 5

Knowles, M., **Kok, D.,** Baglee, D., Morris, A. (**2012) Design and Development of a Electric Vehicle Drive Train Test Bed***, presented at the Condition Monitoring and Machine Failure Prevention Technology (BINDT),* London UK

KOK, D., KNOWLES, M. & MORRIS, A. (**2012**) **'Building a Driving Simulator as an Electric Vehicle Hardware Development Tool'**, *Driving Simulation Conference 2012.* Paris, 325-333

KOK, D., MORRIS, A. & KNOWLES, M. (**2013**) **Novel EV drive train topology - A review of the current topologies and proposal for a model for improved drivability**:*Power Electronics and Applications (EPE), 2013 15th European Conference* on. 2-6 Sept. 2013.

KOK, D., MORRIS, A., KNOWLES, M. & BAGLEE, D. (**2013**) **Converter simulation using SimPowerSystems: a comparison of drive cycles and control strategies**, *Renewable Energy Research and Applications (ICRERA), 2013 International Conference on*. 20-23 Oct. 2013.

Kok, D., Morris, A., Knowles, M. and Baglee, D. (**2015**) '**Battery ripple effects in cascaded and parallel connected converters**', *IET Power Electronics*, 8(5), pp. 841-849

1.8. Presentations

Baglee, D., **Kok, D.,** Morris, A., (**2014**) **Prototype Pre-Heat System for Electric Vehicles**, *Keynote presentation at the Next Generation Batteries 2014 conference*, April 29-30, San Diego, CA, USA

Literature Review

A Battery Electric Vehicle (BEV) drive train generally consists of an energy source, a motor controller and a motor (Chan, 2007, Høyer, 2008). Adding DC-DC Converters in combination with UCs are considered an option to improve the performance of the energy source for future EVs. This is achieved by allowing energy sources with different power response rates to work together through the use of such converters.

The management of different power and energy sources in BEV drive trains are an important feature for future vehicles; especially the management of energy to weight ratio and the way in which the available power is optimised to achieve maximum energy flow.

In this chapter the different components of the drive train are described and analysed. First the different energy sources will be discussed followed by the converter and then the motor and control after which different topologies are described. These topologies are combinations of energy sources and / or power sources and converters. Finally the control and management strategies are discussed.

2.1. Introduction

A common feature of different energy sources is that they each operate at highest efficiency within a specific operating range. Outside of this their performance is reduced for a variety of reasons, such as sensitivity to changes in demand (Battery, FC) or by having to function under low load (FC and ICE). In electrochemical devices, such as FCs (and to a lesser extent batteries but

still significant), the chemical process has inertia and as such does not respond immediately to changes in demand. This inertia can also be observed in Internal Combustion Engines (ICE) and Diesel Generators (DG). They are generally inefficient under varying and low loads (Bose et al., 1996). This inertia effect takes time to overcome. In a FC system it takes time for the chemical reaction to build up during which the voltage across the stack will drop under the applied demand (Larminie and Dicks, 2003). It takes time for the FC to increase the airflow and thus increase the current output, there is the potential that the bus voltage may drop below operating specification or even that the demand is so high that fuel starvation occurs. In order to overcome this delay a source that is capable of a faster response can be employed to assist during these moments of transition. It is expected that FC systems will operate in conjunction with batteries to provide responsive acceleration and reduce the size of the necessary FC stacks but batteries have their own limitations under high current demand (Bitsche and Gutmann, 2004). The UC has low energy density but does not suffer from the electrochemical effects that FCs and batteries have as so may prove an ideal supporting system for short period of high demands. In this chapter the limitations to the battery will be explained as well as the benefits of the ultra capacitor and DC-DC converters. The control strategies for different drive train topologies will also be discussed.

2.2. Battery

A battery is an electro-chemical device, in which chemical energy is converted into electricity. The energy the battery holds is given in Watt-hours (Wh) or kilo-Watt-hours (kWh) which is the capacity in Ampere-hour (Ah) of the battery times its average or nominal rated voltage. A measurement to indicate how much capacity is left in the battery is called the State of Charge (SoC) and is

measured on a range of 0% (empty) to 100% (full) and is calculated by the amount of current drawn over time; i.e. the capacity removed from the battery (Husain, 2003).

Another metric used in energy sources for comparison from one source to another are the specific energy (Watt-hour per kilogram) and specific power (Watt per kilogram). Figure 2.1 shows the difference for various technologies between specific energy and specific power.

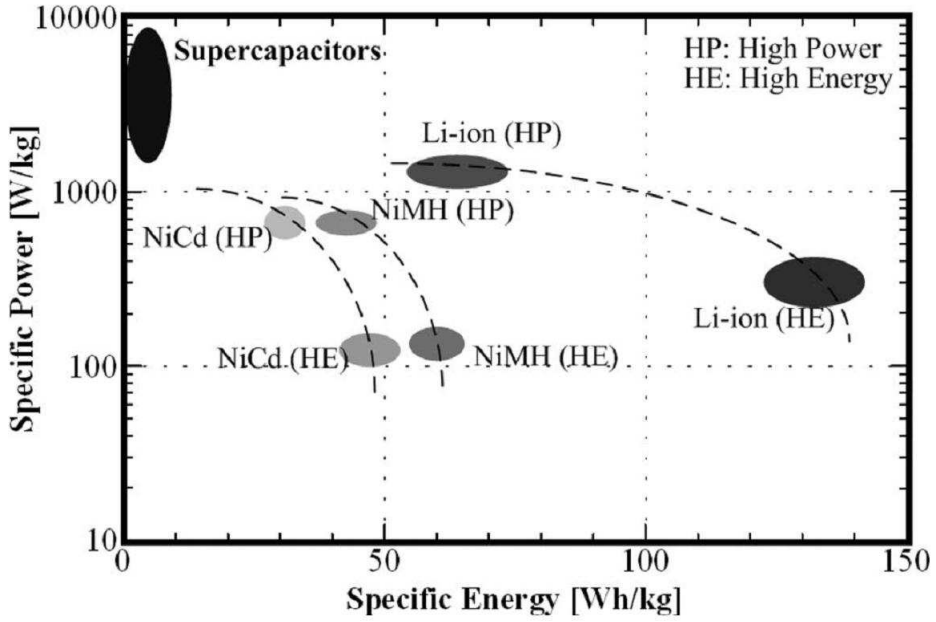

(Thounthong et al., 2009a) © 2009 IEEE

Figure 2.1: Specific power versus specific energy

There are various battery technologies which can be used in EV applications such as: Lead-Acid, Zebra, Nickel Metal Hydride, Lithium-Ion (Krutak et al., 2013). A discussion on the different technologies is outside the scope of this thesis. A good overview with detailed applications is given in (Divya and Østergaard, 2009). In this thesis the main battery technology discussed is the lithium-ion battery which is used in the Nissan LEAF among other vehicles.

In a standard BEV drive train (battery + motor controller + motor) the battery supplies power as the motor controller demands it. This includes sudden

acceleration and braking which present short term peak power demand as well as the low frequency components of the inverter. These peak power moments have the following effects on batteries:

- Rate Capacity effect, where the capacity is reduced at high discharge rate (Donghwa et al., 2011)
- Intercalation (the insertion of lithium ions in the anode), which at high currents is limited and increases the resistance at the anode and thus increases heat (Jongh and Notten, 2002)
- Plating effect (deposition of lithium on the anode of the battery). This reduces the reaction area at the anode and reduces the amount of available lithium ions. In worst case, this deposition can cause a short circuit in the battery which would result in complete battery failure (Jongh and Notten, 2002, Miller et al., 2009b)

Other issues that affect Battery State of Health (SoH) arise from the effects of current ripple as a consequence of switching frequencies, such as arises from the inverter:

- Low frequency ripple (<1kHz) results in greater ohmic resistance (Kowal et al., 2010), increases heat generation in the cells and can affect cell balancing systems (Divan, 1989, Bala et al., 2012)

Or from higher switching devices:

- High frequency ripple (> 1kHz) results in higher inductance (Kowal et al., 2010) and can potentially cause skin effects (unequal distribution of ac current within a conductor) and proximity effects (the current through one conductor affects the behaviour of another conductor) (Jin et al., 2010)

In the case of a lithium-ion battery pack, typically used in BEV applications, high current peaks increase ohmic losses which leads to increased temperature and

as a consequence reduced battery life (Harris et al., 2010, Di Napoli et al., 1999).

A ripple will be present in inductors and capacitors as a result of the switching nature of converters and inverters. A high frequency current ripple with a high level of energy can cause skin and proximity effects both of which increase resistance of the battery (Jin et al., 2010). An increase in resistance leads to an increase in heat generation which is a major factor in battery aging (Lacey et al., 2013, Wang et al., 2014). In fuel cells this ripple increases aging effects (Gerard et al., 2010) as well as losses and fuel waste (Ferrero et al., 2012).

Reducing the current input ripple of a converter, as seen by the FC, is an important field of research since the effect of double-layer capacitance defines the behaviour of the transfer of electrons and ions. The behaviour prevents (part) functioning of the FC as a result of current ripple (Bard and Faulkner, 2000, Ksiazek and Ordonez, 2014). Hence, not only is a small ripple desired but also the knowledge that, that ripple remains small. As a consequence it is recommend that battery current ripple should be kept to below 10% of rated current (Qing-Chang et al., 2012).

In Figure 2.2 two different discharge rates are shown for the same battery. A battery under discharge experiences different effects (polarisations) as marked on the graph. As can be seen the higher discharge current results in a steeper drop in the 3 identified regions as well as less available energy.

Temperature and discharge rates also affect the behaviour of this curve (Doerffel and Sharkh, 2006). As remarked by Onar and Khaligh (2008), cycling of batteries at high C ratings (quickly charging and discharging at high currents) causes additional friction in the battery which reduces capacity and increased heat generation.

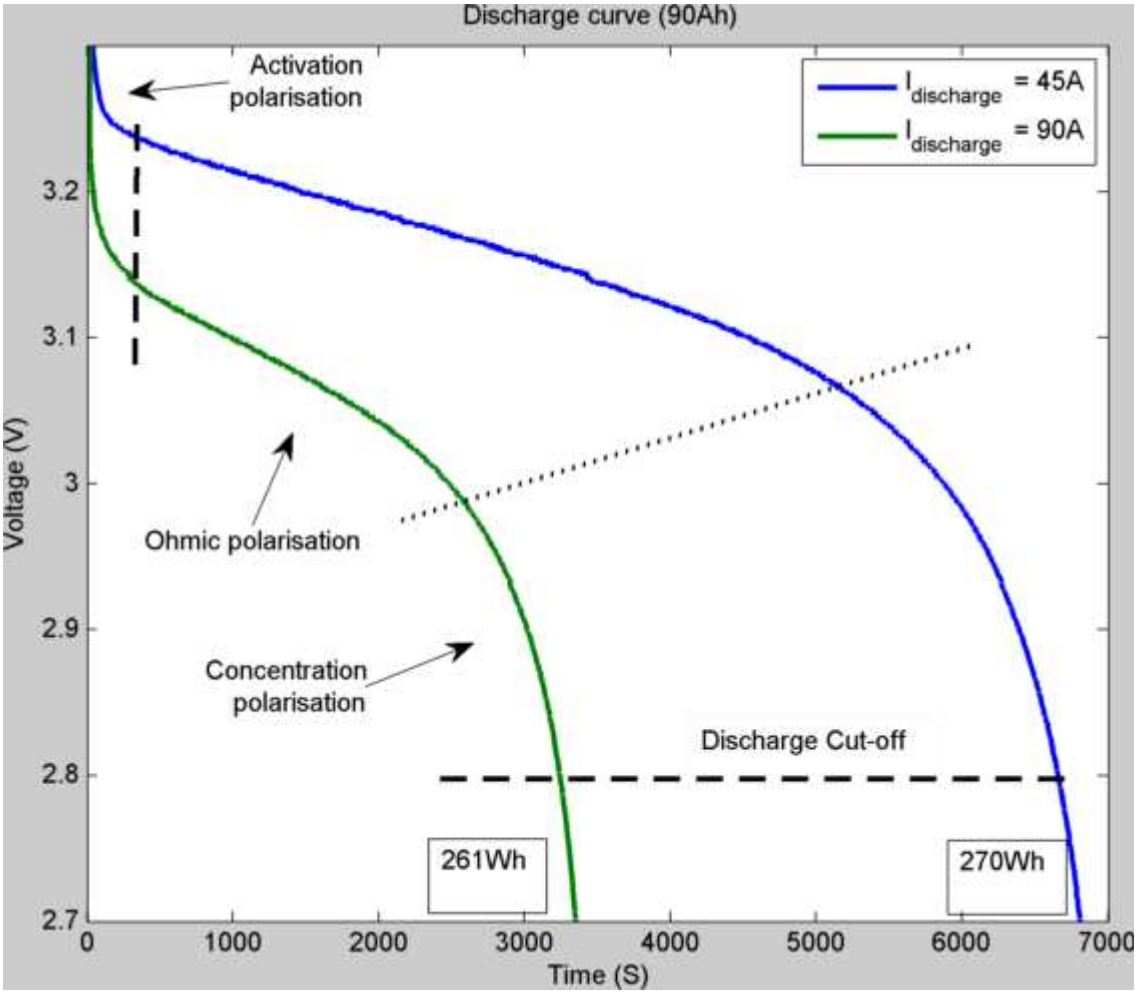

Figure 2.2: Discharge curve for different discharge rates

2.2.1. Temperature effects on batteries

The temperature affects battery performance in the following ways:

- ... Electrochemical system;
- Round trip efficiency;
- Charge acceptance;
- Power and energy capability;
- Reliability;
- Life and life cycle cost.

(Pesaran, 2002, p. 377)

It is reported that the optimum temperature range for lithium-ion phosphate batteries is between 25 and 40 degrees centigrade (Pesaran, 2002). At temperatures below 20 degrees a reduction in capacity can be observed (Baglee et al., 2014) while at temperatures above 40 degrees the rate of aging is increased (Niculuţă and Veje, 2012) As a result thermal energy management is very important to the life time and behaviour of the battery (Niculuţă and Veje, 2012). Thermal management employs the following techniques:

- Air / liquid cooling by providing a flow of air / liquid which transfers heat away from the battery packs, but not necessarily equally distributed (Ji et al., 2013)
- Phase Change Material (PCM), a material which changes its state under the influence of heat and as such removes heat away from the battery pack and is able to reinsert heat when the pack cools down and the state returns to its original (Al-Hallaj et al., 2005).

The latter technique is not common in that no reference of commercial use has been found but research is increasing since first being proposed in 2005 and is now focussing on how the material controls the temperature and which material performs best (Ling et al., 2014).

In cold climates it is actually necessary to warm the batteries to avoid increased losses as a result of reduced flow of the electrolyte (Miller et al., 2008) using techniques as heating elements or AC heating - a high frequency (10kHz) and high current (60A) is used to pre-heat the battery to operating temperature from -40℃ in 3 minutes (Pesaran et al., 2003).

Heat generation in a battery is higher during fast charge / discharge cycles compared to constant supply at a lower level. Reducing the peak power seen by the battery reduces the current and internal stresses on the battery which

reduces the temperature increase. By using an UC module it is possible to reduce the effects of peak power events due to fast demand changes. This represents two benefits an UC module can provide (Rao and Wang, 2011). As a result, reducing peak current demand will improve the batteries expected life span.

2.2.2. Regenerative effects on the battery

A battery can accept regenerative energy, much like it would accept charging energy but if the charging time is below 20 seconds the round trip efficiency of charge acceptance versus discharge is less than 60%. At around 30 seconds this round trip efficiency rises to around 92%. (Miller et al., 2009a). This energy is lost in the battery's greater ohmic resistance as a result of the low frequency ripple (Kowal et al., 2010). In other words, lithium-ion batteries do not recover energy efficiently if the regenerative period is short.

2.2.3. Life span

Battery life span is measured in either one of two methods: cycle life (cycles) or calendar life (years). The end is defined as 80% of initial full charge remaining and the target for manufacturers of battery packs is 80% capacity remaining after ten years (Makansi and Bergholtz, 2010).

The vehicle is expected to have a life span of fifteen years and 180 000 miles (290 000 km). The battery pack is designed to last the life time of the vehicle but some suggest a full replacement is necessary to maintain continued operating range (Aguirre et al., 2012). Leuenberger and Frischknecht (2010) anticipates that the battery pack will be changed at least once in 93 000 miles (150 000 km). Ortuzar (2005) estimates the life span of a Lithium-Ion battery in HEV at six years and the vehicle at twelve years. It seems reasonable to assume that

the battery lifespan has increased since 2005. Van den Bossche et al. (2006) choose a life span of 112 000 miles (180 000 km) which was a result of choosing 3 000 cycles at 80% DoD (at 60 km per discharge), which in turn at 12 000 miles (20 000 km) per year (*Average Annual Car Miles UK*, 2014) would result in a life span of around nine years. The value calculated based on the information provided by Van den Bossche et al. (2006) was felt to be optimistic because more recent work suggests a lower life span, for example, Gerssen-Gondelach and Faaij (2012) state that the lifetime of a battery pack is approximately seven years.

The life expectancy of a battery is subject to operating temperature and peak power demand over the life of the battery. The main contributors to battery life span degradation are: temperature, charge / discharge rate, average state of charge and change in SOC (i.e. depth of discharge) (Lacey et al., 2013). More aggressive driving results in higher peak demands, which in turn results in higher battery pack temperature, which results in faster aging of the pack. For analysis within this thesis the life span of the battery has been chosen as seven years mirroring Gerssen-Gondelach and Faaij and Leuenberger and Frischknecht.

2.2.4. Battery size

Another factor in the choice of battery is its amp-hour rating, which will increase in the future as can be seen from Figure 2.3. The Lithium-Sulphur batteries have shown good practical energy but at the time of writing are not fully in mass production (OXIS Energy, 2014). Other battery technologies suitable for BEV, such as Lithium zinc and Lithium air, are not expected to be available until 2020 at its earliest (Newton, 2012).

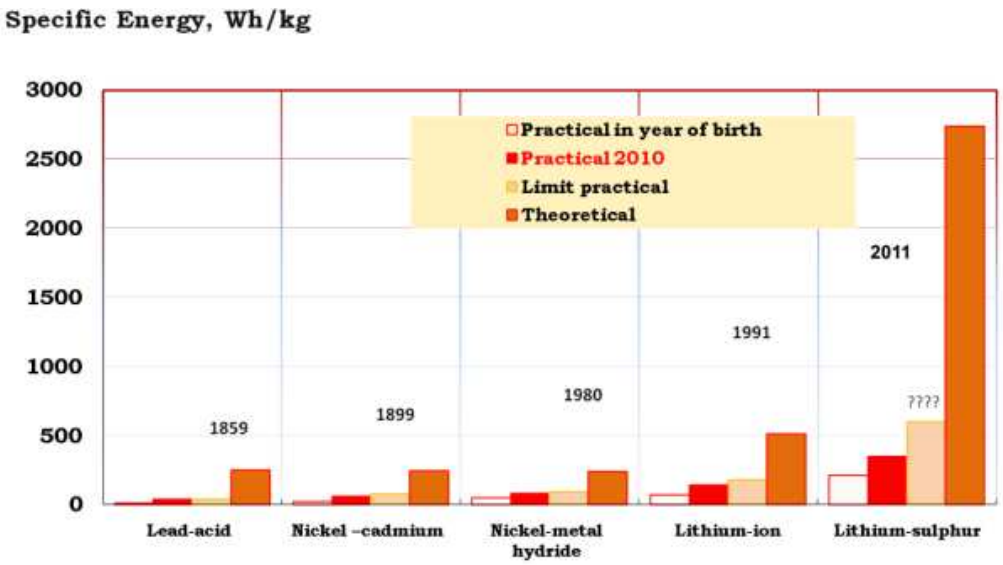

(Hampson-Jones, 2012) © 2012 IET

Figure 2.3: Future expectation of battery specific energy

2.2.5. Sizing the battery for EV

In 2004 the specification of a small electric vehicle could be described as: a driving range of around 60 miles (100 kilometre), 25-30kW peak power, pack weight of around 120kg and a pack voltage of around 300V (Bitsche and Gutmann, 2004).

In 2013 this has been adjusted to: 100 miles (about 160km) which requires energy storage of around 20 - 40kWh, peak power range of 50-100kW and a series voltage of 300 to 500 volt (Tie and Tan, 2013). One reason for this increase is due to increased battery capacity. As discussed earlier, the energy density of the battery has increased (more Wh per kilogram). This has resulted in an increase in energy storage while not increasing the weight of the pack.

The sizing of the pack is thus a trade-off between expected range and pack weight, which, in turn has a bearing on acceleration and driveability. The size of the pack is also a compromise in design between available energy and useable power, with batteries tailored for power demand and not necessary for available energy (Bradley and Frank, 2009). Hybridization of the battery pack would

potentially allow the battery to be designed for energy, increasing the available energy in the same volume and weight of a battery. The required power can be supplemented with a UC + converter setup (Miller et al., 2009a). One reason for the trade off between energy and power is that a vehicle requires a certain amount of power for acceleration, with faster acceleration requiring higher power. If a system can be designed that allows for appropriate acceleration with the peak demand deferred from the battery to an auxiliary supply, then batteries could be designed for a lower power to energy ratio, which increases battery energy content. The required power from the battery (the main source) under cruising conditions should be within the allowable range of the battery such that the additional weight of the UC module does not cause the power demand to increase above this set maximum.

There are continuous discussions on the expected range of a BEV. People have come to expect 300+ miles range from conventionally fuelled vehicles, which with technology of today using only battery is not possible (taking in account affordability and driveability). A large pack is heavy and will affect performance. Another issue BEV vehicles face is charging time: the larger the pack the longer the charging time. (Tie and Tan, 2013) provide a detailed description of current and proposed chargers for BEV, Figure 2.4:

Classification	**On-board method Residential/Level 1**				**Public/Level 2**	**Off-board method Fast or ultra-fast/Level 3** [82]
	Mode 1		**Mode 2**		**Mode 3**	**Mode 4**
Electrical characteristic	1-Phase 120/240 V_{ac} 16 A 3.3 kW	3-Phase 400 V_{ac} 16 A 10 kW	1-Phase 240 V_{ac} 32 A 7 kW	3-phase 400 V_{ac} 32 A 24 kW	3-Phase 400 V_{ac} 63 A 43 kW	Direct current 50–700 V_{dc}, 100–125 A, 50–300 kW
Charging period	6-8 h	2-3 hours	3-4 h	1-2 hours	20-30 min	< 20 min
Safety	Circuit breaker to protect against overload		Basic protection * with In-cable protection device		Basic protection* with control system	Basic protection with control system
Standard[83]	local NF-C-15100		IEC 61851-1 IEC 60309		IEC 61851-1	IEC 62196 IEC 61851-1
Socket	Household socket		Domestic socket		Dedicated circuit-socket	DC connection socket

* Such as earthling system, circuit breaker to protect against overload and an earth leakage protection.

(Tie and Tan, 2013) © 2013 Elsevier

Figure 2.4: Classification and technologies of available EV charging stations

In the UK, a 24kWh battery pack could be charged at home, over night, using a mode 1 charger since most houses would be able to accommodate this. This would result in 3.3 kWh charging for 6-8 hours for a full pack. Since 24 kWh can provide a range of around 100 miles a pack 3 times its size (assuming the weight remains the same) would give the coveted 300 miles. However, home charging would become top-up charging due to the time it would take to charge the batteries from a mode 1 charger. Fast chargers could be installed which would increase the demand from the grid which substations would not be able to support yet (and probably not for the foreseeable future) on a house by house installation.

Currently most installed fast chargers are level 2 (mode 3), allowing a 24kWh - 100 mile- pack to be charged in 20-30 minutes up to 80% SOC. In theory a 300 mile pack could fast charge in 1-1.5 hours up to 80% SOC. Ultra fast charging could reduce this time, but the high current this requires could increase battery aging rate as well as result in significant temperature increases at stand still, when air cooling might be used at pack level.

2.2.6. Battery Management System

The operating range of the battery pack depends on its single cell range and how many have been placed in series. However due to manufacturing tolerances the internal resistance differs a little from battery to battery. This difference in internal resistance means that each cell experiences different losses ($P_{loss} = I^2 \cdot R$). These losses are cell dependent and result in less charge stored when charging or more charge lost when discharging. This means that while at the beginning a string of cells might have been equally charged (showing equal voltage per cell) over time this is no longer the case potentially resulting in unsafe cell behaviour (under voltage or over voltage conditions).

These discrepancies, which are exacerbated through the aging process and temperature differences, while small, need to be compensated for. This can be done through the use of a Battery Management System (BMS). In basic principle, a BMS removes some of the excess charge from the cell with the highest voltage and either burns it or transfers it to a lower voltage cell. A reason to keep the length of strings short is to reduce the complexity of the BMS (Xing et al., 2011). In their comprehensive review of battery balancing systems Jian et al. (2008) show that most simple balancing systems only influence the cell directly adjacent to the unbalanced cell. More complex balancing systems use switching topologies to temporarily store energy in a capacitor or inductor and then switch between the highest and lowest cells. In these systems there is use of at least a single inductor but more often multiple transformers, and converters which inherently add to weight and complexity of the overall system. The benefit of the BMS is the equal cell voltage from one cell to the next; i.e. the whole string has a stable voltage which improves energy density and voltage stability. The latter allows for reducing of the number of cells per string which reduces weight, provided the BMS does not increase the weight more than the reduction as a result of the shorter string.

2.2.7. Modelling the battery

There are 3 basic ways of realising a battery model: electrochemical, mathematical (black box model) and electric circuit approximations (Tremblay et al., 2007). Of these three the best approach to calculate SoC is the electric circuit approximation since the other 2 methods are computationally intensive or require in depth information about the battery (Kroeze and Krein, 2008, Tremblay, 2009, Dong et al., 2011). Dong et al. (2011) concludes that impedance models (electric circuit models) are highly suited for BEV drive train

battery modelling because of the reasonable level of accuracy, their high dynamic range and scalability.

The electrical model sees the battery as a non ideal voltage source and can as such be represented as a voltage source with internal resistance (Floyd, 1997), see Figure 2.5. This model can be further expanded by including more components representing effects such as self-discharge and low frequency and high frequency impedance, such as shown by (Rosario, 2007, Kroeze and Krein, 2008, Jin et al., 2010). This electrical model also forms the basis for any thermal models and aging models (Kowal et al., 2010). Newer battery models include: capacity fading models as proposed by (Long and Bauer, 2013).

This thesis focuses on the optimisation of control and energy management and as such not on the internal workings of a battery. The author's interest in the accuracy of the model is the loading effect on the battery voltage since a higher load results in a larger voltage drop across the internal resistance and as such will influence the final current value; a voltage drop requires a rise in current to achieve the same power output. Modelling of a battery depends very much on the data available, the accuracy needed and the type of battery.

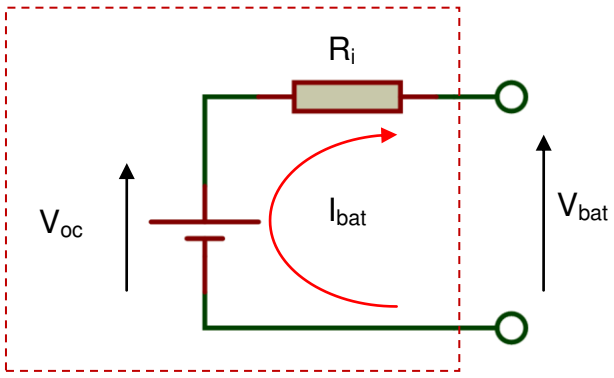

Figure 2.5: Battery as a non-ideal voltage source

Tremblay et al. (2007) presents a generic model for which parameters can be extracted from the manufacturers supplied power curve. This has the advantage

that the internals of the battery need not be known. The model estimates SoC as well as voltage and current. This model is readily available in Simulink as a battery component within the SPS toolbox and will be used during the simulations.

The model used is chosen to mimic the behaviour of a battery and not the aging process or heat factors. It is assumed that during drive cycle test that aging has little influence. The heat factor is assumed constant by keeping charge / discharge cycles well within operating conditions. Any benefits or downsides in terms of aging and heat factors to a battery pack are related to the occurrence of excessive peaks as opposed to a low constant current draw and affect the efficiency of the battery.

2.2.8. Summary

The price of the Lithium-ion battery is still very high in comparison with lead acid. The trade-off between energy density and power density as a design requirement directly affects the range.

There are two major causes that influence the battery lifetime and capacity:

- Peak current demand
- Ripple effects

Both can result in increased heat which is directly related to a reduced available battery capacity and reduced life span. By reducing the peak current demand and reducing current ripple battery life can be improved and efficiency increased which results in more available capacity, prolongs battery life span and increases range per cycle.

One way to reduce the current as seen by the battery pack is to increase the number of cells in series but this increases complexity of the BMS which also could increase weight of the overall pack.

A battery under regenerative conditions is not functioning effectively due to the short periods of recovery which is also found in high frequent pulse demand – for example – start stop driving. It would make sense to incorporate these as design features in a new PEMS.

2.3. Ultra Capacitor

The name Ultra Capacitor (UC) is a trade name, as is super capacitor and Electrochemical Double-Layer Capacitor (EDLC), the later referring to its construction and method of storing energy (Sharma and Bhatti, 2010). In this thesis the name Ultra Capacitor will be used. The name Ultra Capacitor (UC) will be used in this thesis for all such devices.

An UC stores energy in the form of static electricity on 2 opposing plates which are separated by an insulator (Ribeiro et al., 2001).

The energy a Maxwell UC can store is described in (2.1) where E is the energy stored, C is the capacity and V is the voltage potential.

$$E = \frac{1}{2} C V^2 \tag{2.1}$$

The Maxwell UC can access the full range from zero to operating voltage (2.5V). However, it is not realistic to operate the UC in voltage range of zero to maximum cell voltage because in a conversion the current increases inversely proportionally with a voltage decrease. If the voltage drops the current increases in order to maintain the power balance. Another reason is instability of the converter at low input voltages (Giaouris et al., 2009).

A minimum voltage is often set as the lower limit of operation to protect the system and to preserve efficiency of the system. While the internal resistance of a UC is generally low (in the region of milliohms) at high currents this will result in significant losses.

While the operating range of the Maxwell looks good it is actually a lot smaller because of system design limitations. These limitations result in an energy calculation as shown in (2.2), where V_{max} and V_{min} are the upper and lower system limits of the UC, respectively.

$$E = \frac{1}{2} C (V_{max} - V_{min})^2 \quad \textbf{(2.2)}$$

A Lithium-ion UC uses a different technology akin to Lithium-ion batteries. The lithiated electrode (negative) holds a fixed lower potential compared to the activated-carbon electrode (positive), which allows for a higher voltage and since the voltage is squared to achieve energy (2.1) results in a higher energy density. The lithiated electrode also provides a larger surface area for storage and thus a higher capacitance per unit weight allowing the Lithium-ion UC to be designed at a lower weight for an overall increase in energy density despite voltage operating range limitations. In addition this UC also has a lower self discharge rate (Smith et al., 2013). The voltage range limitation is a result of the lithiated electrode losing li-ions when operated below the set range (Sivakkumar and Pandolfo, 2012).

Example specifications of 2 different UC technologies are shown in Table 2.1. In this comparison conducted by (Lambert et al., 2010) the Lithium-ion capacitor shows an improvement of 2.7 times in weight and at a higher voltage an improved energy density compared to an off-the-shelf equivalent Maxwell PC2500 (Lambert et al., 2010).

Assuming the full voltage is available then the Li-Ion UC shows an improvement of 3.4 times energy density compared to the Maxwell (see Table 2.1. However, as reported it is not always practical to use the full voltage range.

The voltage level of an individual lithium-ion UC cell has a similar range as a lithium-ion battery but since the energy is stored as electricity there is no delay

in converting the energy to electricity as there is in a lithium-ion battery. However, as the electricity is stored as static charge on the available surface area inside the capacitor the amount is an order of magnitude smaller than the energy stored in a battery (Thounthong et al., 2009a).

Table 2.1: Ultra Capacitor technology comparison

	Maxwell PC2500	Lithium-Ion Capacitor
Nominal Capacitance	2700F	2200F
Usable Voltage Range[1]	0 – 2.5V	2.2 - 3.8V
Maximum Current	± 625A	± 250A
Cell Mass	711.8g	261.0g
Dimensions	61 x 61 x 158 mm	10 x 125 x 180 mm
Operating Temperature	-40°C to +70°C	-20°C to +70°C
Energy (full range)	2.34 Wh	2.93 Wh
Energy Density	3.29 Wh/kg	11.24 Wh/kg

Adapted from Lambert et al., (2010) © 2010 IET

This allows the UCs to have a high power rating, but at the expense of a low specific energy rating. Recall from Figure 2.1 the UC's specific energy (how much energy a source can hold in Wh/kg) is an order of magnitude smaller compared to Li-Ion batteries. The UC's specific power (how much power a unit can supply in W/kg) on the other hand is an order of magnitude larger in comparison with Li-Ion batteries.

The high specific power rating allows the UCs to support a slower acting energy source by providing peak power assistance (Uzunoglu and Alam, 2006, Thounthong et al., 2009a). The support reduces the stresses on the slower source by reducing peak current demand and thus reducing temperature increase and increases life expectancy without limiting acceleration

[1] This is not necessary a practical design voltage range.

performance of the electric vehicle, while potentially reducing the size of the overall energy pack (Takehara et al., 1996, Di Napoli et al., 1999, Jinrui et al., 2006a, Jinrui et al., 2006b, Rosario, 2007).

This supporting of battery packs or FC systems by peak current or power smoothing is generally accepted as a potential useful improvement to EVs and in particular support points 1 and 2 raised by Crolla et al. (2008).

2.3.1. Temperature effects on Ultra Capacitors

The working operating range of the UC is -45 ℃ to + 60 ℃ (Mallika and Saravana Kumar, 2011) which makes it a good supporting unit in cold climates or even cold days as a support for cold starting instead of burdening the lead-acid battery with the high power current draw and seriously reducing the life span of the battery (Miller and Sartorelli, 2010).

2.3.2. Charging the UC

The UC behaves very different under short charging periods as a result of the way it stores energy; there is no conversion necessary from one form of energy to another. As a result unlike the Li-ion battery the UC has very good storage behaviour for time periods under 20 seconds. The UC can return the energy it has stored as a result of –for example – a regenerative event with higher than 90% efficiency (Loukakou et al., 2010).

2.3.3. UC cell management

Much like the individual battery cells, the individual cells of an UC string suffer from manufacturing discrepancies and because of the much higher currents the lower internal resistance does not negate the challenge. A short string, as in the case with batteries, keeps the system simple and light.

2.3.4. UC model

As in the case of a battery model there are various approaches that can be used. Smith et al. (2002) shows the accuracy of a first order RLC model, where the inductor (L) adjusts for frequency influences on the UC. But with the magnitude of the model nearly linear at higher frequencies this model can be simplified by reducing it to its RC equivalent. The choice of model for simulation depends on the available model parameters. Its basic circuit equivalent model (RC model) is presented in Figure 2.6. More extensive models are provided by Grbovic et al. (2011) and Xu and Riley (2011) but the benefits of these models in simulation are depending on the type of research. The latter providing the background for the Matlab model that can be found in SPS.

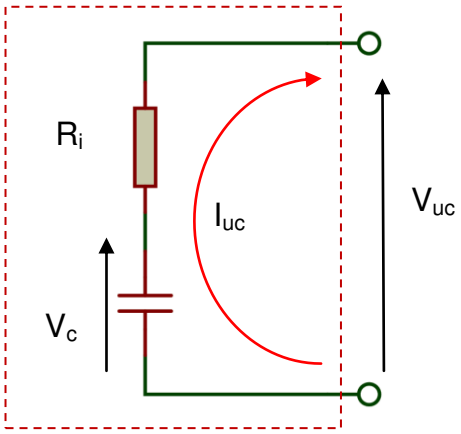

Figure 2.6: UC equivalent circuit model

In this thesis, a basic State of Charge (SOC) module (such as the Simulink model described earlier) is sufficient since the internal parameters of the UC are unknown to us. As in the battery model case, this UC model can be given the basic information (information that is available from data sheets) to get a accurate model of a super capacitor.

2.4. The UC module

In this thesis the combination of UC and DC-DC converter is referred to as a UC module. The addition of an UC module to the drive train should be measured on four points in order to prove a benefit to the system:

1) to improve vehicle acceleration;
2) to improve overall drive efficiency, thereby increasing the driving range;
3) to reduce life cycle cost by extending battery life;
4) to reduce capital cost by direct replacement of some batteries.

(Carter et al., 2012, p. 1526)

The author does not consider this list complete. Vehicle acceleration does not necessarily need improving since a vehicle such as the Nissan LEAF has acceptable acceleration. In the author's opinion it is more important that any improvement should not reduce the driveability of the vehicle while lessening the peak load demand on the battery. An additional point would be that the total weight of the solution should not be increased unless compensated by a gain in energy from the battery. UC modules can also be applied for use in ICE which result in different benefit aims (Lugert and Knorr, 2002).

2.4.1. Summary

The UC has the potential of delivering high power for short periods of time but its fast changing voltage level means it requires additional electronics to control and stabilise the voltage swing. Due to its low energy density, the energy to weight ratio is a lot less than a battery which implies that to be a good support

the benefits of the UC module has to outweigh the introduced weight and cost factors. There is likely an optimum solution between usability and weight.

2.5. DC-DC Converter

The basic functioning of the Direct Current to Direct Current (DC-DC) Converter is to convert an input voltage to a different level output voltage. This output can be lower, higher, both or negative depending on the circuit used. In this thesis, the Half H-Bridge converter will be used which is shown in Figure 2.7. DC-DC converters find a very wide area of implementation in today's society (Lung-Sheng and Tsorng-Juu, 2012). The circuit is well described in literature for example by (Caricchi et al., 1994, Rosario, 2007).

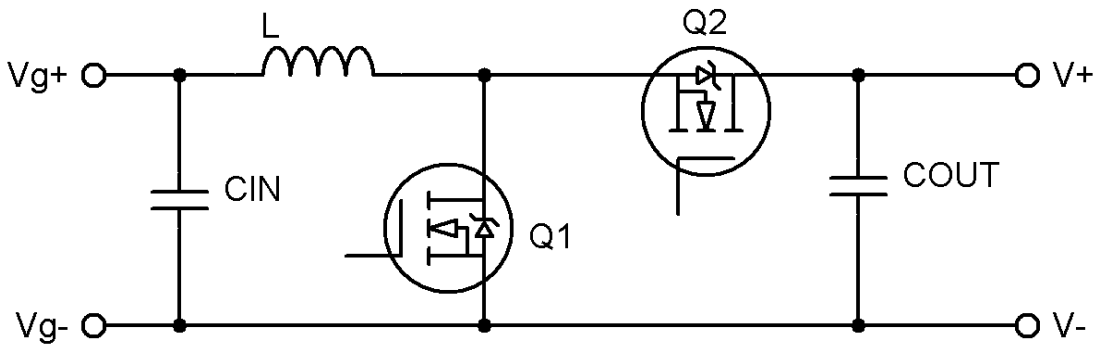

Figure 2.7: Half H-bridge converter

2.5.1. Introduction

The main reason for using UCs is their ability to instantaneously supply large amounts of power; this ability protects slower sources against peak power demands in a variety of applications. The UC voltage is dependent on the current drawn or returned and so may fluctuate widely. The main benefit of using an UC setup and a bi-directional DC-DC converter is the ability to manage the SoC of the UC (Jayawickrama and Rajakaruna, 2004). This can then be

used to supplement the power demand with UC power instead of drawing all power from the battery.

Introducing DC-DC converters into the drive train reduces low frequency ripple propagation - noise from the inverter - and improves recuperation of energy through multi-quadrant operation (Divan, 1989). The controllable bus voltage allows for control strategies to increase the efficiency of the controller and motor operation by keeping a high voltage at high motor speed when the back Electromagnetic Force is high and low voltage at low velocity (Estima and Marques Cardoso, 2012). As reported (2.2.2 Regenerative effects on the battery and 2.3.2 Charging the UC), both the battery and UC could facilitate recuperation of energy, which can be improved through converters but only UC has the efficiency to do this over short term periods (periods lasting less than 20 seconds).

A battery could also be fitted with a converter to achieve a higher voltage level but a battery pack has a more stable voltage level; it changes less quickly with charge removed compared to UC. The battery does have an operating range but the design of most inverters allows for a wide operating range. An example inverter such as the Curtis 1238-6501 AC Induction Motor Controller has a nominal input voltage range of 40-80 volt. If a single lithium cell has a nominal voltage of 3.2V, with max voltage of 4V and a minimum voltage of 2.5, one could string together 20 cells and be well within operating conditions at all times (64V nominal).

DC-DC converters would allow the designer to use fewer batteries in series while still achieving a set target voltage. This would achieve a more stable bus voltage as the voltage swing as seen by the motor controller would be reduced.

A strong argument against using converters in combination with batteries would be the potential rise of current as seen by the battery as a result of the power balance:

$$P_{out} = P_{in} \tag{2.3}$$

$$V_{out} * I_{out} = V_{in} * I_{in} \tag{2.4}$$

If the output voltage and current are fixed and the input voltage is lower than the output voltage then the input current will need to increase to maintain the power balance. At an input voltage of half the output voltage the input current is double the output current.

$$I_{in} = \frac{V_{out}}{V_{in}} * I_{out} = \frac{V_{out}}{\frac{1}{2}V_{out}} I_{out} = 2 * I_{out} \tag{2.5}$$

In real circuits this effect is even further increased because of component losses.

The reduction of the string length through the use of converters would result in a higher current as seen by the battery under cruising conditions. To counter this effect multiple strings and multiple converters would be necessary. Any negative effects are most noticeable under high way cruising conditions when the driving demand is constant and at a high level.

Multiple device converters including interleaved multiple device converters can help in reducing the size (but increasing the number) of the components. The reduction in component size combined with the doubling of frequency increases the efficiency by reducing the losses (Hegazy et al., 2012).

Using multiple converters has 2 key advantages:

- The weight of each inductor can be more than halved because the size of the inductor is in direct relation to the supported current and the surface area of the diameter of the wire,

- The output voltage ripple can be reduced (theoretically removed but this is not possible in practise) by creating interleaved converters (Giaouris et al., 2013).

Various studies (Ortuzar, 2005, Rosario, 2007, Miller and Sartorelli, 2010, Khaligh and Zhihao, 2010) have been conducted to investigate the effectiveness of the addition of UCs and converters to the electric drive train and their benefit to the weight ratio of the pack and the cost effectiveness of the solution. The effectiveness of the UC module and converter configuration is partly due to the effectiveness of the converter itself, which in well designed converters can reach up to 97% efficiency for a 50kW converter (Pickert et al., 2010).

DC-DC converters are non-linear switching systems and their behaviour is characterized by various modes of instability because of moments of switching. Within converter operation there are two main modes that define the moment of switching: Continuous Conduction Mode (CCM) and Discontinuous Conduction Mode (DCM). In DCM the voltage across the inductor during the switching period falls below the forwarding voltage of the opposing diode (the diode not paralleled to the switching MOSFET). Because the diode is no longer forward biased the current through the inductor falls to zero instead of the continuous ripple in CCM (Erickson and Maksimovic, 2001). In this thesis only CCM is used for modelling, while the simulation incorporates both as part of the setup chosen.

However in vehicles weight is a significant contribution to the overall efficiency of the tank-to-wheel energy conversion. Some weight factors are:

Cooling

Converters can be found in different sizes and topologies. According to Pickert et al. (2010) one third of a converter's weight is accounted for by a water cooled heat sink if used. Air cooled converters are possible but their power output is limited by the wire gauge used and the presence of an airflow.

Inductor

The inductor is the component which allows the step up or down of the voltage in a converter by temporarily storing energy. The size of the inductor is defined by the carrying current and the frequency used.

The latter is described in (2.6), with L = inductor (H), V_g = input voltage (V), D = duty cycle, T = interval period ($T = \frac{1}{f}$) f = frequency and Δi_L= allowed peak current ripple (Erickson and Maksimovic, 2001).

$$L = \frac{V_g}{2\Delta i_L} DT \tag{2.6}$$

The inductor calculation for a buck converter is given in (2.8) where V=output voltage (V).

$$L = \frac{(V_g - V)DT}{2\Delta i_L} \tag{2.7}$$

In high frequency switching power electronics there is the issue of switching spikes; voltage peaks that arise because there is parasitic inductance in the system. Part of this inductance in the system is defined as "*the inductance of the commutation loop*" (Caponet et al., 2000, p. 919) which include: the inductance from the bus bar, the capacitors, screw terminals and the switching module. The voltage drop across the inductor is described in (2.8) (Floyd, 1997).

$$V_{ind} = L\frac{di}{dt} \quad \textbf{(2.8)}$$

At a higher frequency the current rate of change increases. Enhanced by the added parasitic inductance this will result in a larger change in $\frac{di}{dt}$ and as such a higher voltage overshoot as well as higher losses due to switching (Giaouris et al., 2008). The effects of stray inductance become more apparent when the frequency is increased and an increase in power is demanded (Skibinski and Divan, 1993). A smaller current ripple will result in reduced voltage spikes as a result of parasitic inductance while reducing losses will improve efficiency and lead to the reducing the dimensions of converter components.

Bus Capacitors

The output capacitors in a converter setup are designed to smooth the output ripple. Switching converters have an inherent ripple as a result of their operation. The output capacitor provides a degree of smoothing. The equations are given in (2.9) and (2.10) (Erickson and Maksimovic, 2001). The equation for the boost converter is given by the (2.9) where V = output voltage (V), R is the load represented as a resistor (Ω), Δv = the desired voltage ripple.

$$C_{boost} = \frac{\Delta \mathrm{i}}{2\Delta \mathrm{v}} DT \quad \textbf{(2.9)}$$

Similarly, the equation for the buck converter is provided in (2.10).

$$C_{buck} = \frac{\Delta \mathrm{i} \cdot \mathrm{T}}{8\Delta \mathrm{v}} \quad \textbf{(2.10)}$$

The capacitor boost equation shows that the value for the bus capacitance depends on the load ripple (Δi) and the desired voltage ripple (Δv).

The bus capacitance is often designed larger than calculated to avoid instability at the bus (Jamshidpour et al., 2011). In the same paper a control adjustment is presented to reduce the bus capacitor size by factor 2. This point is made by

(Payman et al., 2011). Another solution to reduce the capacitor size is to use a UC + converter as an adaptive active capacitor converter solution as presented by (Zhang et al., 2013b).

2.5.2. The Converter model

There are various types of converters as described in (Williams, 2013), for the research in this thesis a Half H-Bridge converter layout is used, shown in Figure 2.7 (page 32), repeated in Figure 2.8 for convenience. This layout has been described as the best optimum for BEV (Schupbach and Balda, 2004, Amjadi and Williamson, 2010). In this thesis the converter is connected with a source lower in voltage than then the output voltage, which means the voltage is boosted from the source to the bus and bucked from the bus to the source. It is possible to implement the converter in reverse but this would require a larger string of cells to achieve voltage higher than bus voltage and as found by Miller and Sartorelli (2010) the power profile would be very similar and as a result the voltage level would define the current draw; a larger current for the boost option but as discussed the current draw is not an issue for the UC. The longer string – on the other hand - is considered a disadvantage due to issues with cell balancing, weight and cost, as mentioned in section 2.2.6 (Battery Management System).

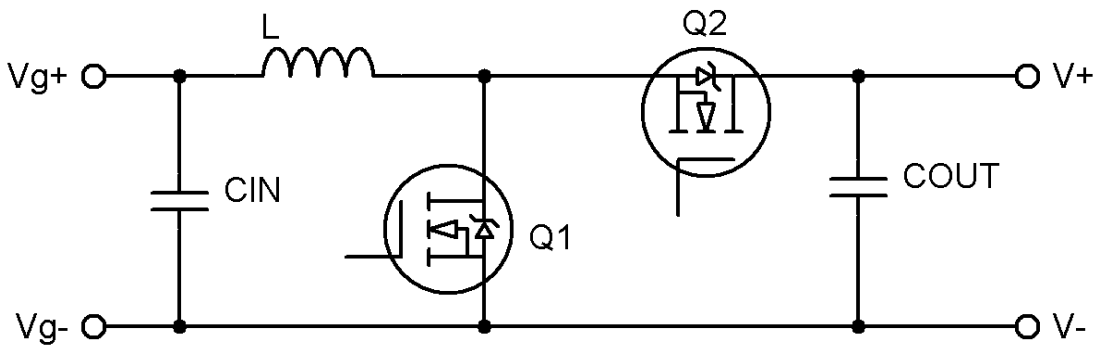

Figure 2.8: Half H-bridge buck boost converter

The component variables can be found from the equations shown in (2.6), (2.9) and (2.10). To establish the values for the Proportional Integral (PI) control loop a Simulink model is build based on the state space averaging method. The half H-Bridge converter can be approached as two individual converters: a boost converter as shown in Figure 2.9, where only switch S is toggled through a Pulse Width Modulated (PWM) signal or as a buck converter as shown in Figure 2.10. The basic buck converter circuit is shown as per convention. It should be noted that in the bi-directional setup the input of the buck converter is the output of the boost converter.

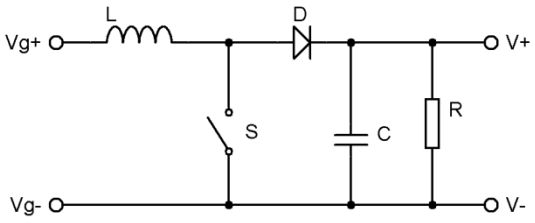

Figure 2.9: Basic boost converter

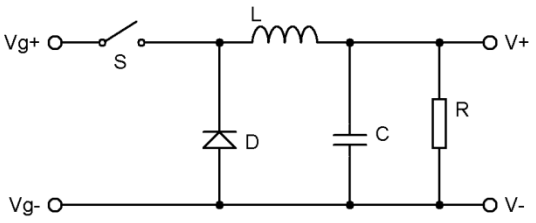

Figure 2.10: Basic buck converter

These ideal converters can be described using the state space equations, which are shown in Table 2.2 - 2.3.

Table 2.2: Ideal Boost Converter

S closed		S open	
$L\frac{di_L}{dt} = V_g$	(2.11)	$L\frac{di_L}{dt} = V_g - V$	(2.14)
$C\frac{dV}{dt} = -\frac{V}{R}$	(2.12)	$C\frac{dV}{dt} = i_L - \frac{V}{R}$	(2.15)
$i_g = i_L$	(2.13)	$i_g = i_L$	(2.16)

Table 2.3: Ideal Buck Converter

S closed		S open	
$L\frac{di_L}{dt} = V_g - V$	(2.17)	$L\frac{di_L}{dt} = V$	(2.20)
$C\frac{dV}{dt} = i_L - \frac{V}{R}$	(2.18)	$C\frac{dV}{dt} = i_L - \frac{V}{R}$	(2.21)
$i_g = i_L$	(2.19)	$i_g = 0$	(2.22)

2.5.3. Converter control

There are two main modes of converter control which are named after their way of operation: Current Mode Control (CMC) and Voltage Mode Control (VMC). VMC converters are controlled through a basic voltage loop, which reads the voltage level at the output and compares this to a reference voltage followed by PI controller which generates the Pulse Width Modulated (PWM) signal to toggle the appropriate switch. The disadvantage of this approach is the control is slow. A slow control results in a slow response to changes in the load, which requires a larger output capacitor to compensate. CMC is faster and as such has a better feedback loop response compared to VMC.

Boost converter topologies are often controlled using a current control strategy while a voltage loop is used in a slower control loop and is necessary if the load conditions are changing (Tse, 2004).

Two commonly used current control modes are peak current control and average current control (Giaouris et al., 2009). Dixon (1998) states that peak current control has various negative drawbacks such as poor noise immunity, slope compensation needed and peak-to-average current errors. Under average current control K_p can be proportional only or proportional-integral but

in both cases its output value needs to be limited to avoid period doubling as a result of border collisions which cause instability (Tonicello, 2002).

Giaouris et al. (2009) states that it is clear that average current control has other control and design issues of which setting the control parameters is the main one, which make it easier to implement peak current control. Peak current control has another big advantage and that is the speed of the control loop. The low frequency ripple propagation from an inverter drive can be reduced by using a fast current control loop when the DC-DC converter is designed separately from the inverter (Jih-Sheng, 2009).

As shown in Figure 2.8 (page 38) the actual converter can easily be modelled in the Matlab / Simulink toolbox SimPowerSystems and the control system can then be designed in Simulink itself.

2.5.4. Peak current control setup within Matlab / Simulink:

The inductor current is measured and compared to a reference value. The error signal is then sent to a RS flip-flop which has its Set input connected to a clock signal, see Figure 2.11. Table 2.4 shows the truth table of the SR flip flop. At the start of every period the flip-flop is set (Q = 1) and thus boost switch is on. The output remains high until a reset value is presented at the Reset input. This happens when the inductor current is equal or higher than the reference current.

Table 2.4: SR Flip-flop truth table

S	R	Qn	!Qn
0	0	Qn-1	!Qn-1
0	1	0	1
1	0	1	0
1	1	0	0

Converter and stability

The duty cycle of the PWM control signal is a direct relation to the input to output ratio of the half H-bridge converter. The duty cycle for the buck converter is given in (2.23) (Erickson and Maksimovic, 2001).

$$\frac{V_{out}}{V_{in}} = D \tag{2.23}$$

While the duty cycle for the boost converter is given in equation (2.24).

$$\frac{V_{out}}{V_{in}} = \frac{1}{1-D} \tag{2.24}$$

Peak current control looses stability at duty cycles over 0.5. This effect is countered by introducing a ramp with a slope equal and inversely proportional to the slope of the inductor current (Dixon, 1998, Erickson and Maksimovic, 2001). In this control setup a ramp compensation of 0.5 of the inductor ripple current was chosen as shown in (2.25) where m_L is the inductor current ramp is during the off-period of the switch; i.e. when the current through the inductor falls.

$$m_a = \frac{1}{2} m_L \tag{2.25}$$

O'Loughlin (2012) notes that before the start of a period a blanking interval is needed to avoid the duty cycle being able to be on for the whole period (D=100%). Under boost conditions the duty ratio v_{out}/v_{in} goes to infinity under ideal conditions and still is excessively large under non-ideal conditions causing instability. This blanking interval was implemented with the use of a second timer and logic shown in the highlighted area of Figure 2.11; the derivation of the Karnaugh map for the logic used can be found in Appendix 3.

This logic has two effects: a) it ensures that at the beginning of the period the flip-flop is always set (Q=1), while the last 10% of the period is always reset (Q=0).

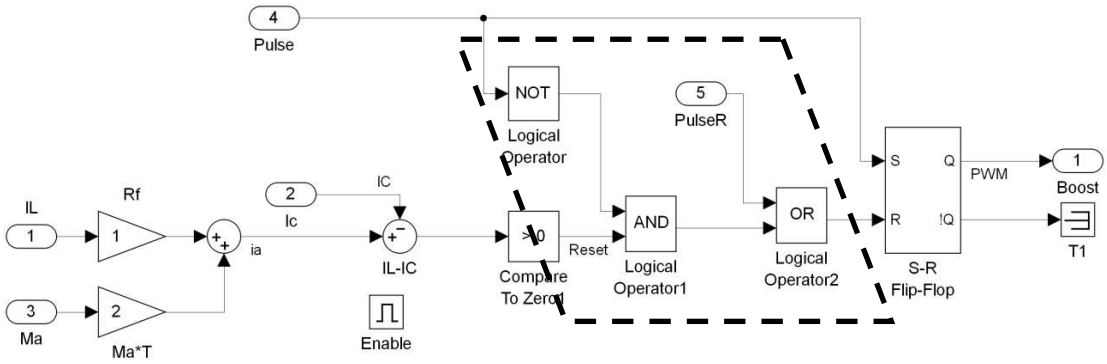

Figure 2.11: Peak Current Control Mode

Due to the internal resistance of both the battery and UC it is common to charge at low SoC with a constant current and switch to voltage control when the maximum charging voltage is reached and reduce the charging current to ensure no overcharging occurs which could damage the receiving source.

To simplify the control setup the following assumptions are made:

- The preferred method of converter control is through a peak current controller with an outer voltage control loop in order to maintain a stable bus voltage except when the bus voltage is defined by the battery.
- When the battery defines the bus voltage the assumption is made that no damage is sustained by the battery under charging moments.

To establish the controller parameters the transfer functions are required. These transfer functions are derived through state space modelling and fully described in Erickson and Maksimovic (2001).

The state space equations are then setup in Simulink as shown in Figure 2.12 (adapted from (Erickson and Maksimovic, 2001)) and then the control optimisation toolbox (Simulink) can be used to quickly derive the most optimum control settings. The optimisation toolbox requires the use of the transfer functions and cannot be directly applied to the implementation in Simulink / SPS

since the setup relies on switching which the optimisation protocol sees as either on or off for the duration of the optimisation strategy.

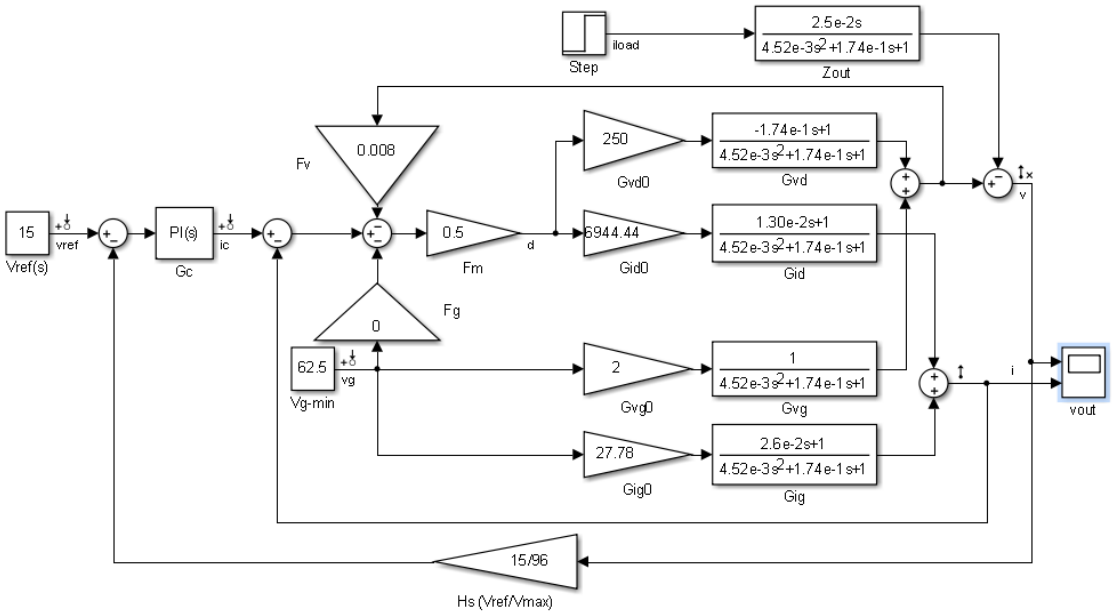

Figure 2.12: Averaged model in Simulink boost converter

The control loop under buck conditions is only a CMC loop to simplify the simulation. The reference current estimation is difficult under a changing bus demand or supply. Under buck conditions a torque reference is often used to calculate a power reference for energy recuperation (Dusmez and Khaligh, 2013). In the simulations the bus demand is represented by a Current Controlled Source (see chapter on motor and controller) which means that a torque reference is not available in the simulation setup used. A reference from the current supplied into or out off the bus does not work in the case of charging an UC because the switch disconnects the bus from the output. A current reference only validates against the reference current for part of the period. As compensation the current sensor was placed just after the inductor such that under buck conditions the output current would be measured and slightly smoothed as a result of the output capacitor (Lynch, 2003). If the reference current is derived from the current supplied to the bus then during the on period

the current through the inductor rises until the measured current is equal to the reference current then the switch is opened but there is still a capacity added to the bus equal to the reference current multiplied by the duration of the off period. This is illustrated Figure 2.13 (page 46), where V_{in} is the bus voltage, V_{bat} is the output voltage as seen by the buck converter and current is the inductor current. Increasing the reference current would result in a less steep slope at the bus (V_{in}) but it would always rise. Inversely, increasing the reference value above a certain point would deplete the input capacitor because during the on period of the switch more current would be removed than supplied during the whole switching period. This behaviour is recognised especially in renewable energy sources where the source supply is not constant and as such robustly designed input filters are necessary which incidentally adds cost weight and volume to the design (Williams, 2013).

In order to overcome this effect during our simulations the author assumed that the amount of power being recovered would not exceed the rated charge current of the battery or the UC. This is an appropriate assumption since the interest is in current ramp effects and (for the moment) not in the effects of emergency stop.

A feed forward loop was developed based on the converter input impedance, the aim of this loop is to measure the bus voltage and combined with the averaged input impedance a current reference was created. The bus voltage was monitored and the reference current adjusted to maintain a stable bus voltage and as such protect the bus against over/under voltage conditions. The assumption made here was that the battery or UC would be able to handle the current provided under regenerative conditions and that the regenerative current would not exceed the converter maximum. The result is shown in Figure

2.15. The outcome of the test simulation is shown in Figure 2.14. The derivation of the transfer function is explained in Appendix 4.

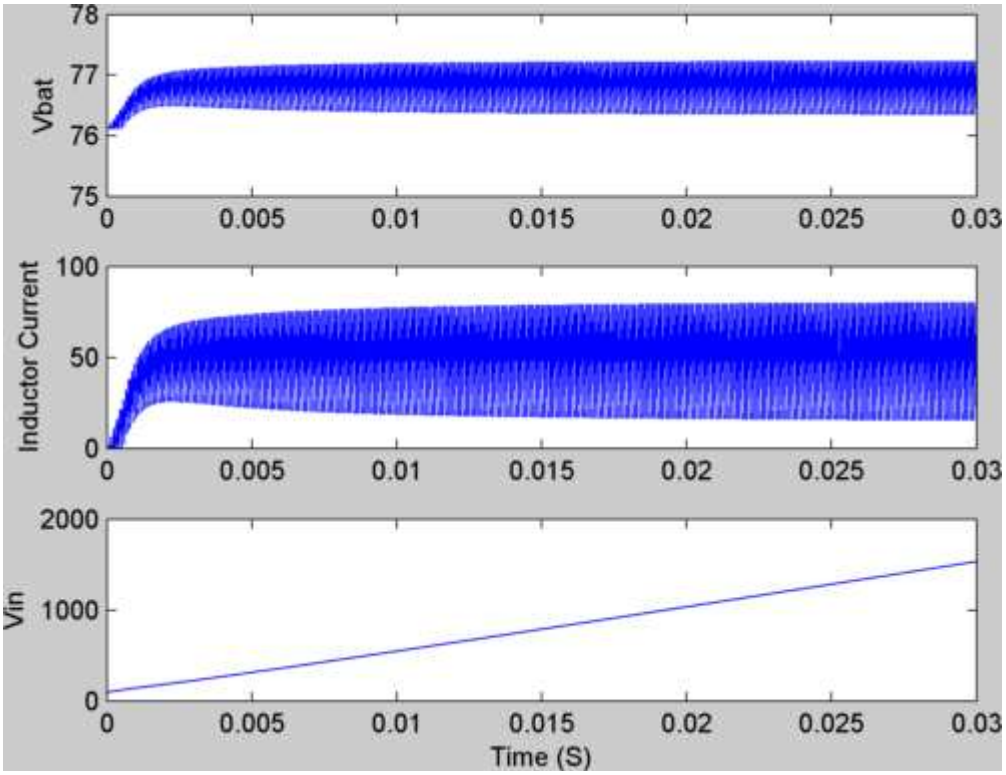

Figure 2.13: Simulation output fixed reference current

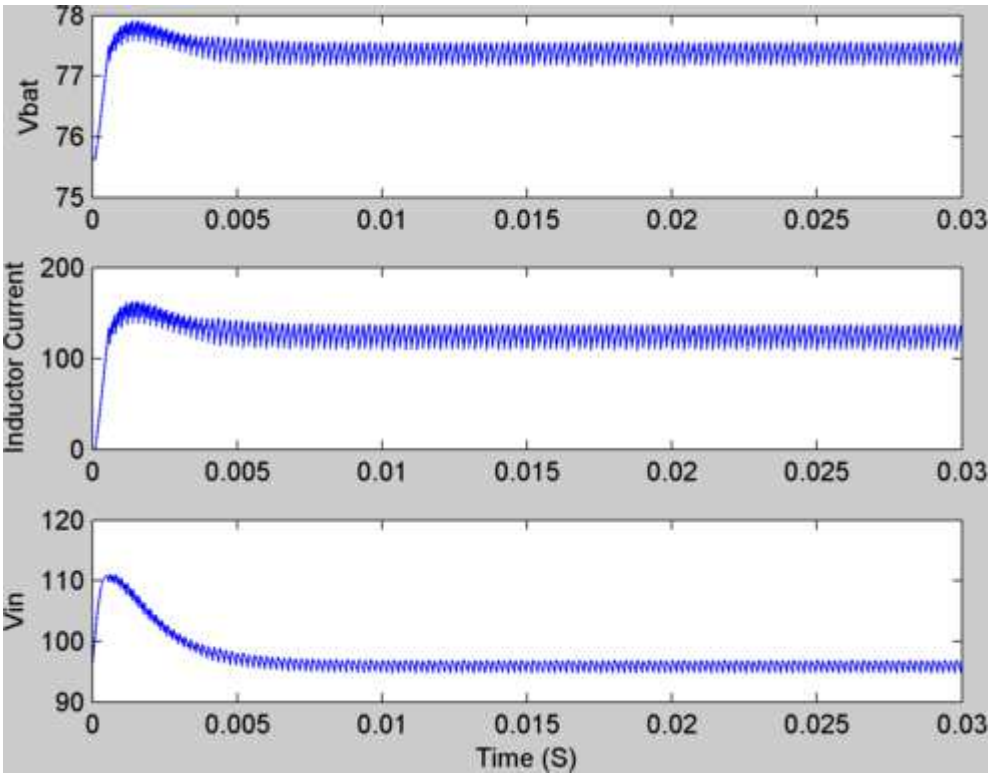

Figure 2.14: Simulation output controlled reference current

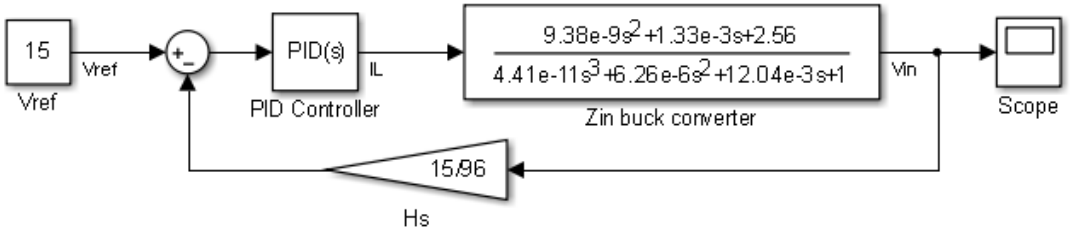

Figure 2.15: establishing control parameters for buck converter

2.5.5. Summary

The main benefits of using a converter are that the system is able to access all the available energy from the UC whilst controlling current and current ripple. In addition a more stable bus voltage may be achieved.

A disadvantage of using a converter with a battery is the increase in current demand as seen by the battery based on the power balance equation.

2.6. Establishing the size of the support module

The sizing of the UC module depends on 3 aspects that define the size, weight and cost: a) Peak power demand b) Useable energy and c) Converter ripple. In addition, adding the UC module should result in some kind of gain, for example: overall reduced weight, improved battery efficiency and thus improved driving range without affecting driveability, less batteries in a string and thus reduced overall cost or any combination of these features, otherwise the system is not viable. In other words, the addition is a trade-off between the UC module's size, weight and cost, and the gains it brings.

Peak power demand affects the size of the current carrying components of which the inductor forms a very large and heavy part. The peak demand also affects the size of the output capacitor, where a larger peak demand requires a larger capacitor to avoid under voltage (or over voltage) situations. The useable energy depends in part on the working range of the UC but also on the number

of UC strings in series and in parallel. If more energy is required the module will be heavier. The choice of PEMS influences the size of the UC module and as a consequence its weight (Mesbahi et al., 2014).

The converter ripple consists of two components; the inductor current ripple and the output voltage ripple. The size of the allowable inductor current ripple defines the value of the inductance and with a higher inductance more windings are needed which results in a heavier inductor. The wire diameter and thus its weight are dependent on the current carrying capacity; i.e. the maximum allowed current (Miller et al., 2008). The size of the allowable voltage ripple as seen by the output defines the output capacitance with a higher capacitance resulting in a smaller ripple.

For the current state of the art in converter design the following values can be used: 5 kW / kg (Miller, 2004) which is expected to rise to 14.1 kW / kg in 2020 (Rosario, 2007).

In FC systems the complementing energy source (which can be a battery or UC) is determined on the basis of current slope limitations (to avoid fuel starvation which can seriously damage the stack (Payman et al., 2011)). Hence, “Worst case scenarios from drive cycle determine size of the storage devices. - (Thounthong et al., 2009a, p. 250)”. The worst case scenario in this case is defined as the fastest allowable response from the system minus the fastest allowable response of the second source. This means that the supporting source needs to be able to complement 2 aspects: 1) being able to support the power requirements and 2) being able to support the energy requirements. As a reminder: The power requirements are dependent on the weight of the vehicle (and any associated friction and losses) and the manner in which it is being driven with a requirement for fast acceleration resulting in a higher peak

demand. The energy requirements are dependent on the amount of power the supplementing unit should provide and the duration this power is required for.

In case of an UC system designed for elevators the system should be designed to deal with the instantaneous required maximum power for the period of acceleration under maximum load as a priority. This leads directly to the energy requirements (Rufer and Barrade, 2002). Similarly, for ride through systems, which are systems to overcome brown-outs, small interruptions in the energy supply, the UC module would need to be sized for maximum power requirements after which the energy requirements are determined by the duration the system should sustain this power (Grbovic et al., 2011). The next limitation could be either space or cost. A brown-out is typically a small interruption in the supply which lasts from milliseconds to several seconds. For larger interruptions batteries or even FCs might be more appropriate; although FCs suffer from a start up delay, which require an UC module to support (Maxwell Technologies Inc., 2007).

UC Systems used as primary power sources require very different considerations. An UC system used as a mobile quick charge receiver, for instance, where the charge provided at one station allows a tram to reach the next station where it is charged again. Here the energy requirements define the size of the module while the charging power (P_{ch}) is limited by the charging time (t_{ch}) allowed (Rufer et al., 2003) and not by the drive cycle since the power under discharge (P_{dis}) would be spread out over a period of driving (t_{dis}) while the charging period is a lot shorter and thus the power demand is higher to achieve the same energy.

$$P_{ch} * t_{ch} = P_{dis} * t_{dis} \quad \textbf{(2.26)}$$

A FC has a slow response to changes in load demand and can be damaged if demand is higher than capability of supply, which provides a time segment during which a supporting system or systems should be able to supply; this approach can be seen as bus regulation while the FC system gets up to speed (Thounthong et al., 2009b) and as such prevent rapid changes in demand as seen by the FC (Thounthong et al., 2006). This relation is shown in equation (2.4); with the split in time is indicated for the different power durations.

$$P_{bus} = P_{uc}(t < t_{uc}) + P_{bat}(t_{uc} > t < t_{fc}) + P_{fc}(t > t_{fc}) \quad \textbf{(2.27)}$$

In applications where an ICE is involved the sizing of the UC is suggested to encompass peak shaving and the estimation of the peak power is defined as the: “maximum power demand for system under the target drive cycle, (Yu et al., 2012, p. 1645)”

This means that if a different drive cycle is chosen the power expenditure could be overrated or underrated. It assumes that that power from the individual sources is available at all times; an UC might not be fully charged, which would imply that the remaining power comes from the battery.

In electric vehicle systems a major objective is to satisfy regenerative and acceleration specifications (Di Napoli et al., 2002b),

> An Ultra Capacitor tank must supply all the power required in excess of the batteries rated power, if its state of charge is greater than a specified minimum - (Di Napoli et al., 1999, p. 2)

In this definition the changing voltage levels of the UC are taken in account as part of the power requirements. The remainder of the quote can be summarised as:

$$P_{req} = P_{bat-rated} + P_{uc}\,, with\, V_{uc} > V_{uc-min} \quad \textbf{(2.28)}$$

With $P_{req}$the required power, $P_{bat-rated}$= rated battery power, P_{uc}= power from the UC. The UC module should be able to supply this power as long as the UC voltage (V_{uc}) is larger than a set minimum (V_{uc-min}) at the moment of the initial demand. The inclusion of the minimum statement is to protect the system since at lower SoC the battery's voltage level is lower and thus the current is higher. If the demanded power doesn't change the current needs to increase when the voltage drops.

In order to protect the battery from high frequency drive patterns the current demand can be split into a high and low frequency parts (through the use of filters) with the UC module responding to the high frequency demand and the battery supporting the low frequency. Defining the size of the UC module can be done through empirical simulation tests (Blanes et al., 2013, Etxeberria et al., 2012). The aim is to smooth battery peak demand while maintaining UC voltage between set minimum and maximum, see also (Rosario, 2007, Grbovic et al., 2011). The use of filters generally includes introducing a delay in the system, which should be avoided if possible or negated by introducing that delay to the battery converter as well, which introduces delays in the system and a large drop in voltage at the bus which potentially causes instability. A popular design approach to sizing the UC pack is to look at the maximum acceleration time and required power in a drive cycle and then reverse engineer a pack size from this (Thounthong et al., 2009a). However, the maximum acceleration is variable from drive cycle to drive cycle and as such leads to over dimensioning of the UC pack to compensate for all eventualities.

Ideally, an UC module should be designed to cover all the peak power above a certain mean value but there is no fixed mean value for a vehicle since every

vehicle is different and for every trip the driving conditions will be different. Then there is the different driving behaviour of people.

Ortuzar (2005) proposed a strategy to add the energy needed for a 30 meter hill climb to the energy needed to accelerate to top speed from zero. This requires the converter to be designed for peak power up, over and above the battery power rating to be safe. Similar to the power demand increase when the acceleration is increased, an increase in gradient increases the power demanded. The problem with choosing a fixed value for a hill climb is the variability in hills. What happens if the hill climb is longer? Should the potential battery power be limited through a current restrained strategy? Limiting the battery power to a level below the power available when support is active reduces driveability.

Another approach is for the UC module only to support the battery when rated peak power is exceeded (Jinrui et al., 2006a, Sadoun et al., 2012), which leads to not being able to follow certain power profiles when the UC is depleted. Their argument is that limiting the battery current prevents the loss of capacity but it will also affect driving behaviour and potentially the safety of the driver which does not support points 1.1 and 1.2 raised by Crolla et al. (2008).

2.6.1. UC Module efficiency

The UC module adds weight and complexity to the drive train and compared to their battery counterparts are still very expensive for little energy. Under cruising conditions in battery powered electric vehicles an UC module is a weight that needs to be carried around, which in vehicles increases losses.

The UC module should also be designed for highest overall efficiency with the efficiency defined by losses in the UC and losses in the converter. The UC module should not function below 90% efficiency (Miller and Sartorelli, 2010,

Miller, 2007a). The current at which this limitation occurs can be calculated through the combination of UC efficiency:

$$\eta_{uc} = \frac{1}{1 + \frac{P_{ri}}{P_{out}}} \tag{2.29}$$

Together with the efficiency of the power electronics:

$$\eta_{conv} = \frac{1}{1 + \frac{d \cdot P_{dissConv}}{P_{conv}}} \tag{2.30}$$

For a final efficiency of:

$$\eta_{total} = \eta_{uc} * \eta_{conv} \tag{2.31}$$

A Matlab program was written, see Appendix 1, - the UC cell used for this example is the Lithium-Ion capacitor cell - the output which is shown in Figure 2.16 is based on a UC open circuit voltage of 3.6 and an internal resistance of 1.4mΩ (Miller, 2007a, Miller and Everett, 2004).

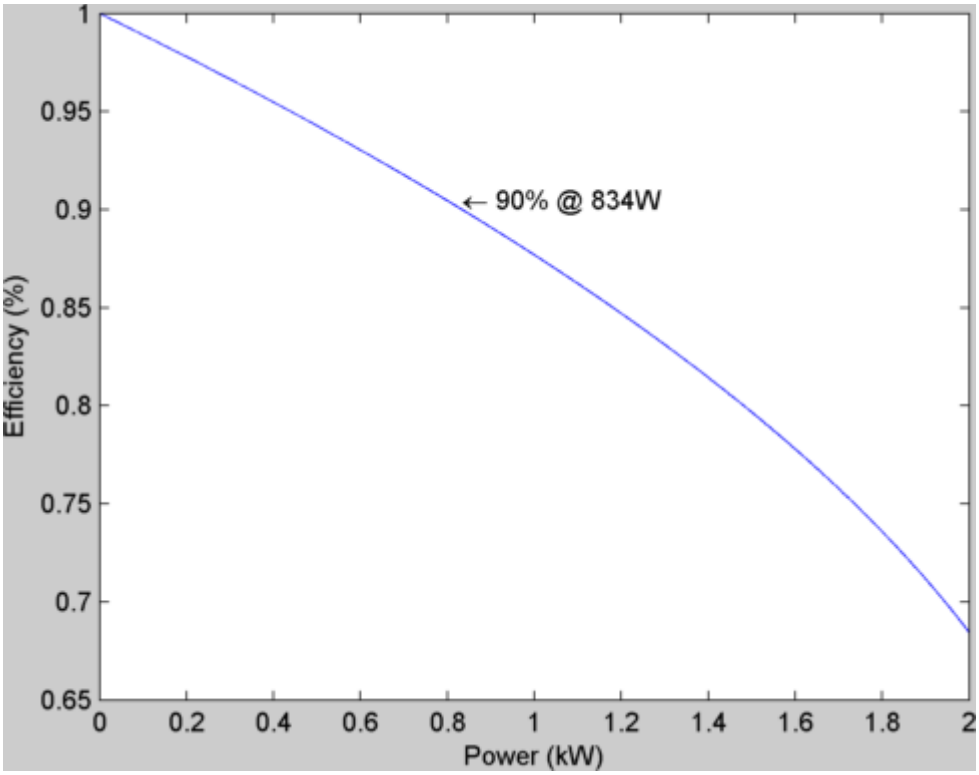

Figure 2.16: UC Cell Power versus Efficiency graph

The marker shows an UC operating point of 90% efficiency. In order to keep the efficiency above 90% the current from the UC should be limited to $\frac{834}{3.6} = 232A$ per cell.

The efficiency of the converter is depended on the switching duty cycle. The calculation of efficiency can be a complex calculation (Hegazy et al., 2012), but are often simplified to the following individual equations (for both boost and buck converter) (Miller and Sartorelli, 2010):

$$P_{Losses} = P_{inductor} + P_{switch} \cdot d + P_{diode} \cdot (1 - d) \quad \textbf{(2.32)}$$

A Matlab program is provided in Appendix 2 and a sample plot is shown in Figure 2.17.

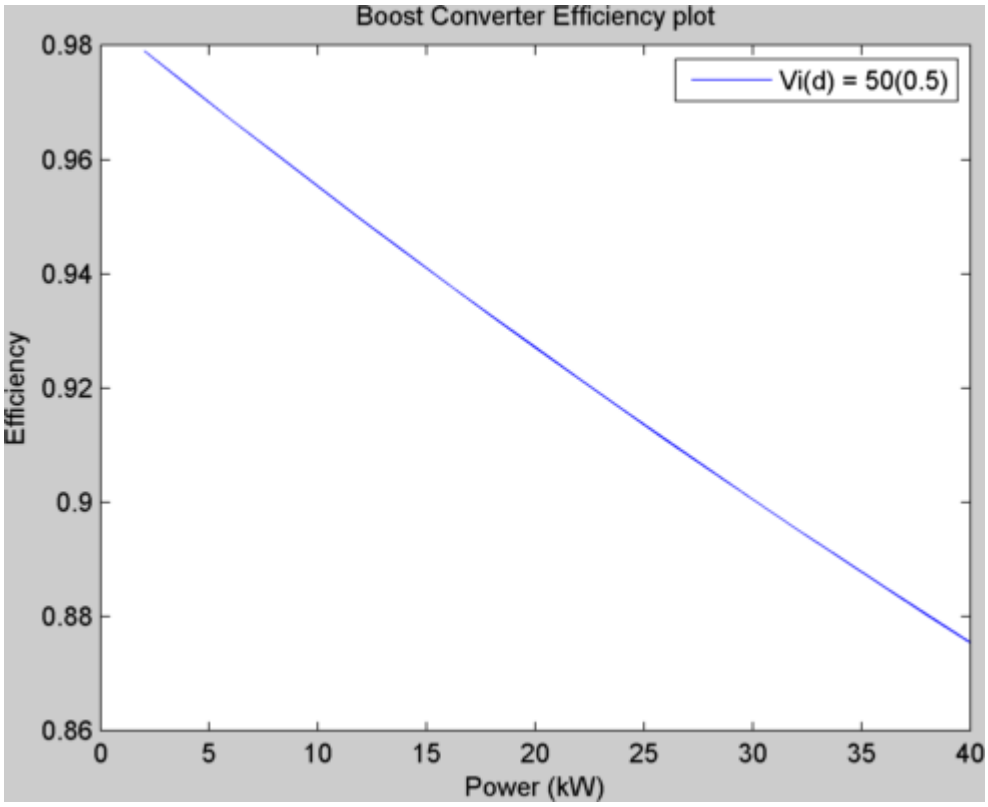

Figure 2.17: Boost Converter Efficiency plot

2.6.2. Driveability

Eco Driving is where the driving behaviour is modified through training to improve fuel economy and tail pipe emissions by “applying a smooth and progressive driving style” (Scott et al., 2012).

Eco-driving features actions such as:

- Moderately accelerating
- Anticipation of traffic flow and signals
- Not exceeding the speed limits
- Regular maintenance

It is recognised that eco-driving – if followed by the masses – will positively contribute to the reduction of Greenhouse Gasses as well as providing a safer driving environment and reduced cost for the individual driver (Barkenbus, 2010). The specific style of driving would be of particular interest to batteries since it will smooth part of the acceleration.

The way in which a vehicle is driven is also dependent on the age of the driver and is related to the drivers experience and cognitive ability (Knowles et al., 2012b).

A key aspect of vehicle behaviour is driveability, which is defined as:

> ...the difference between the vehicle response to the driver request and that expected from the driver - (Eller et al., 2010, p. 2251)

The definition of drivability is understood to be the response of a vehicle based on acceleration, braking and general driving behaviour (Crolla et al., 2008).

2.6.3. Summary

In (Kok et al., 2013b) the authors highlighted the affects of smoothing the battery current under complete drive cycle conditions by using an UC with converter module. They also highlighted the relation between drive cycle and the use of the UC pack: under cruising conditions the UC module is hardly used since there are no changes to the speed and thus the UC module is effectively dead weight and could result in a loss in driving range. As such it would make sense to design the module to be as small as possible and use the battery's energy and power to complement the UC module.

The UC module should thus be designed to achieve the following:

- Protect the battery from high frequency peak power demand changes
- Support the battery under acceleration and deceleration as long as this happens above a certain frequency
- Reduce the bus capacitance without sacrificing stability

This would result in an UC module design, which

- has the shortest set of UC in series (simplicity in BMS but lower voltage),
- has the least strings in parallel (but sufficient capacity),
- optimised power demand,
- with the lowest efficiency losses; because no large current draw would be required even at low SOC as such all components (including the bus capacitor),
- can be designed for minimum size and weight, smallest footprint under cruising conditions,
- does not sacrifice driveability.

2.7. Inverter and Induction motor

Induction motors are well described in literature (Krause and Thomas, 1965, Shi et al., 1999, Husain, 2003, Ehsani et al., 2004) as are inverters (Trzynadlowski, 2001, Synthesis Partners LLC, 2011). The purpose of this chapter is to provide an overview but since these items are not used in this thesis they are only included for completeness and to explain the model chosen. The main advantage of the induction motor over a permanent magnet motor is that an induction motor requires no rare earth metals to make, because the magnetic field is induced through current flow, however it has control problems at low speed due to the resistance of the inductors.

2.7.1. Induction motor

The popularity of the induction motor has been rising over the last couple of years with low maintenance being a major feature compared to –for example- commutation motors (Finch and Giaouris, 2008).

In principle the induction motor consists of two Y-connected or Delta-connected circuits a stator and a rotor. The stator layout is such that 3 coils are connected in a Y-formation and each branch is provided with 1 phase of an AC voltage source with the phases supplied at a phase shift of 120 degrees.

The principle of operation is based on mutual induction; when there is a current through the stator a magnetic field will be induced through the air gap into the rotor which results in an induced current on the rotor side which creates a magnetic field which in turn aims to align with the field generated in the stator, which results in the rotor turning. The rotor will rotate along with the frequency of the supplied electrical signal adjusted by the number of pole pairs.

The synchronous frequency is the frequency at which magnetomotive force rotates through the airgap. As a result of this force there the rotor is pulled along

and starts rotating with its rotor frequency which is very close to the speed at the air gap but with a slight delay (slip).

2.7.2. Induction motor as a Generator

An induction motor works by exciting the inductors in the stator which create a magnetic field which is the start of current induction and as such the creation of force. But the rotor is effectively a ladder with rods that does not have any excitation in them on their own. Turning the rotor without any other form of excitation does not generate current in the stator (because of a lack of magnetic field). If we would want to use the motor as a generator we are missing an essential component.

The stator contains a little flux from it being magnetised (as an effect of it constantly magnetized as part of its operations. This residual magnetism and resulting flux does react to the rotation of the rotor and applying some capacitors in a line to line configuration allows the build up of a voltage as a consequence of this reaction. With the voltage established on the stator a current will flow in the rotor and thus a force will be generated.

2.7.3. Induction Motor Control

Vector Control (VC) is also known as Field Oriented Control (FOC) is the control technique of choice for asynchronous induction motors because of the possibility to access parameters such as rotor currents by deductions of the vector control principles which allows for control techniques that do not require sensors (i.e. sensorless control methods), which inherently reduce maintenance and cost (Finch and Giaouris, 2008). These control techniques offer a very fast response to a change at the input which makes them ideal for electric vehicles.

The basic aim of VC is to imitate the rotating commutator of brushed motors as if the system is a DC motor and as such we can keep the magnetic field constant and perpendicular so the torque can be maintained at maximum level (Husain, 2003, Ehsani et al., 2004). The other aim of VC is the independent control of the current and field flux for speed control (Trzynadlowski, 2001).

2.7.4. The motor and Controller model

A bus connection feeding a motor controller with induction motor can be seen as a black box, where the current is either demanded (accelerating / cruising) or provided (braking / regenerative). As long as the bus voltage remains within operating parameters from a Current Controlled Source (CCS) can be a good stand in for the complex setup that is the motor and controller since they do not play a part – in terms of their control – in the development of the power and energy management strategy. The basic model is shown in Figure 2.18.

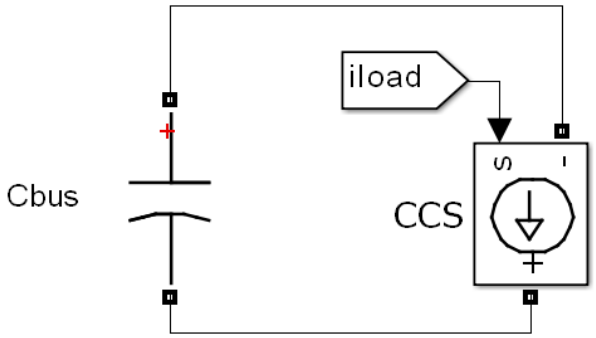

Figure 2.18: CCS model

The choice for this model was based on the number of switching components. If the choice was made to simulate the inverter and motor controller including the switching components the simulation time would increase significantly. Increasing the number of converters from one to two would increase the simulation time from an average of 2 hours to an average of 6 hours for the

NEDC. In addition, it was felt to be not necessary as they can be adequately approximated by a current controlled source.

2.7.5. Summary

The motor and controller described here are used as basic reference material to determine the bus voltage, operating voltage range and current limitation. While this thesis focuses on the optimisation in power and energy management and control of the battery with UC combination, the effects this control can have on the bus connected peripherals can be substantial. In Synthesis Partners LLC (2011) a list of identified features has been produced which shown expected cost drivers according to inverter manufacturers. This list includes: capacitors and thermal management, which both are a result of wide operating range and ripple effects. In the same document some manufacturers stated their belief that today's version of inverters are over-designed because of the unknown usage in operating range; i.e. more knowledge or tighter bus control would allow for a reduction in inverter cost and weight. The efficiency would also increase (Siang Fui and Chee Wei, 2012).

2.8. Topology Comparison

Having established that combining batteries with UC and or converters can bring significant benefits, in this chapter some different topologies and their benefits and deficits will be examined.

The different available energy and power sources available allow for different layout combinations of these component groups. The addition of converters allows for an even larger combination of these topologies and they are extensively studied and have their individual advantages and disadvantages. An extensive overview is shown in (Kok et al., 2013a).

This chapter provides an overview of the specific qualities that have been identified and which are specifically relevant in vehicles to improve driveability and user confidence.

In a basic BEV drive train, the string is a reference to the number of cells in series used for a particular setup. The string length for all electric vehicles is defined by the desired nominal operation voltage and the type of cell used. For example, the battery pack in the Nissan leaf consists of a total of 48 modules divided over two strings. Each string consists of 24 modules and each module consists of 4 cells, which means that each string consists of 96 cells. This provides a bus voltage of around 365V (U.S. Department of Energy, 2012, Blanco, 2010). Tesla Motors use a different setup due to the use of a different battery design. They use a 16 modules in series with each module contains 6 cells in series and 74 in parallel which means a total of 96 cells in series for a bus voltage of around 345V (Anderman, 2014). A discussion of all different possible configurations is outside the scope of this thesis.

In the conducted review this was seen as a long string and a disadvantage of this length was the need for cell balancing, which means that the total pack size would be heavy and the balancing process complex. A benefit of this setup, using two strings, is a partial smoothing effect compared to a single string; each string only carries half the demanded current.

Adding a string of UC directly in parallel to the basic drive train setup of batteries provides some smoothing but also requires a long set of UC cells as well as significant balancing at each cell (Miller, 2004). The benefits of this direct parallel topology is a proven reduction in transients during steps changes and runtime extension of the batteries (Smith et al., 2002, Uzunoglu and Alam, 2006). A disadvantage of this direct parallel setup is that not all of the potential

energy of the UC is available because the UC functions as a filter capacitor and smoothes only the ripple effects; i.e. the UC is recharged by the battery once the battery has overcome its inertia.

Figure 2.19 shows a popular topology; the so-called: cascaded topology (Mestre and Astier, 1997, Di Napoli et al., 1999, Di Napoli et al., 2001, Onar and Khaligh, 2008, Jian and Emadi, 2009). The first source can consist of a very short string with the second source a longer string (provided there are equal voltage levels per cell) while still shorter than the potential string length when directly connected to the bus. It is reported that if the first source is a battery and the second a UC then the UC can provide current smoothing for the battery and the battery does not see the any power demand under acceleration while under deceleration any recovery can be directed to the UC.

Kok et al. (2013b) shows that a limited amount of smoothing is possible but over long periods of acceleration and cruising condition, the UC will not be able to supply the necessary energy and as such the current demand as seen by the battery can rise and because of the two converters the current will rise inversely to the voltage, which results in increased losses and may damage the battery. This topology would not be suitable for BEV where limiting current draw is a necessity to achieve maximum energy draw from the battery pack. Cell balancing over a long string of cells makes monitoring and management potentially expensive and complex. A similar conclusion was reached by (Miller and Sartorelli, 2010), where a cascaded setup with a battery as lowest point was seen as not the most beneficial.

When the first source is an UC and the second source a battery (Figure 2.20) then the load current can be split between the battery and UC. The battery in this case can be protected from peak by the UC. Figure 2.20 is also referred to

as parallel since the battery is parallel to the UC module but the inverter here can also be preceded / replaced by a DC-DC converter as is shown here.

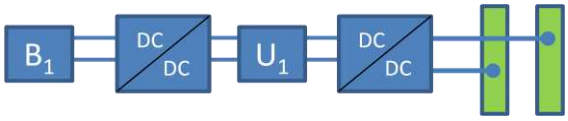

Figure 2.19: Cascaded Connection

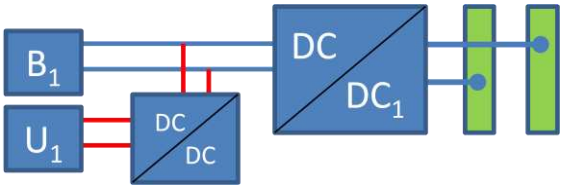

Figure 2.20: Battery + UC module Cascaded

Hence in this thesis this topology and others that use this approach are referred to as cascaded topologies. The described advantages are: bi-directionality, a constant voltage at the inverter and control over the state of charge of the capacitor (Mestre and Astier, 1997). This circuit overcomes the problem of the capacitor voltage needing to be as high as the battery voltage because of the DC-DC converter and at peak times the UC module can support the battery.

The voltage at the inverter is dependent upon the battery voltage (Di Napoli et al., 1999) if no converter is placed between battery and bus. An expansion is to insert a DC-DC converter before the inverter (Jang et al., 2012, Di Napoli et al., 2001). This has the benefit that the voltage can be boosted further before the inverter is reached and it provides smoothing against inverter ripple. The response from a DC-DC converter is fast enough to respond to changes from the inverter. This would increase the current draw as seen at the input of the converter but the peak current can still be supplied by the capacitor converter setup. Under cruising conditions this support will fade when the UC module is being depleted.

An expansion on the cascaded topology can be achieved by using a battery with converter to act as support for a FC system (Jang et al., 2012, Payman et al., 2011). This topology and its control system reduce stresses in the FC because peak demand is reduced and increase the lifespan by maintaining the

FC at a fixed output voltage. Current is supplied from the battery when a change in current demand occurs. Allowing the FC to run longer when the current demand falls will charge the battery and extend the time period the FC can run at high efficiency. If an acceleration moment follows shortly after braking the FC is already providing its available power. The battery also recoups energy under regenerative braking.

Figure 2.21 shows a parallel converter topology. The advantage of parallel connected power legs is the cumulative current at the same voltage to increase the total available power (Di Napoli et al., 2002a). It is possible to independently control the current demand from various sources. The response from a FC to changes on the bus is generally slow whereas the response from battery or UC is much faster. Using this topology the faster sources can support the slower sources while being independently controlled.

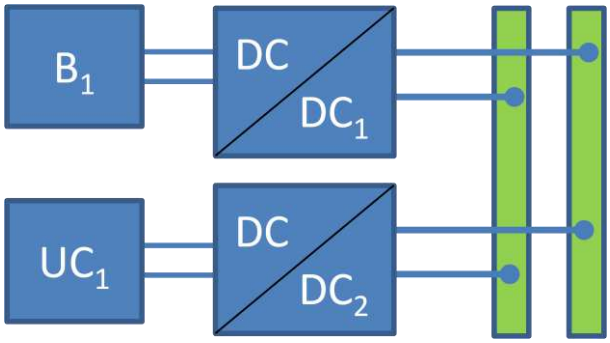

Figure 2.21: Bi-directional Converter topology

This design features various advantages over previously mentioned topologies (Rosario, 2007):

- Relatively low voltage needed from the energy sources compared to direct bus connection
- Modularity - The modular approach of the converter allows for standardised components which can be mass produced to improve

economies of scale offering cheaper components for use in these converters

- Full control over SoC of both the battery and capacitor

Some of the disadvantages reported:

- A relatively large series setup of capacitors needed compared to cascaded connection
- A higher current demand at the battery side as consequence of the reduced voltage
- UC capacity to be defined for a wide variety of peak power profiles

This parallel topology offers an advantage to FC systems because of the reduced ripple effects and peak power smoothing option (Jian and Emadi, 2009, Wuhua et al., 2010).

Another feature that parallel topologies provide and that can be beneficial for the driver experience in BEV is redundancy (Camara et al., 2008). The reasoning here is that paralleling sources and paralleling converters reduce the risk of unbalancing the sources and provides redundancy on string level and converter level. Here redundancy takes precedence over number of components.

Using switches at cell level Taesic et al. (2012) created a very flexible and redundant topology. Using the switches any desired topology can be created and if there is a unit failure this can be bypassed. This flexibility is a great advantage especially as it allows for redundancy but the number of components needed and their power rating makes this an expensive and potentially heavy solution

Another approach is too aim for reduced losses at the expense of redundancy by providing peak power smoothing and reducing the number of components.

The argument being that efficiency is of vital importance because fewer losses mean more power from a third source (Marchesoni and Vacca, 2007).

Multiple inputs can be connected to a single output through a traditional buck-boost converter a so called: single inductor multiple input converter. This topology allows for reduction in parts. The control scheme allows smoothing of the current by allowing duty cycles (to open the switches) to overlap from different sources (Dobbs and Chapman, 2003, Ahmadi et al., 2013). Further improvements using four quadrant converters allows for recuperation of energy within the same topology instead of needing a separate converter (Khaligh, 2008, Zhihao et al., 2009, Khaligh et al., 2009). The use of a single inductor compared to a multi-leg setup helps to reduce component cost and weight (Khaligh, 2008).

These single inductor circuits have the disadvantage that there is no redundancy after inductor or converter failure. The use of a single inductor for all currents requires the inductor to be rated for peak load demand. The inductor is only optimised for peak demand from the load and not peak ability from its individual source.

Song and Wang (2013) concludes that making a setup fault tolerant will increase the complexity and component count which can also impair the efficiency of the system. Therefore, if designing a fault tolerant system high efficiency at each stage is a necessity.

A common feature of all topologies using DC-DC converters is the reduction of low frequency ripple propagation although this is replaced by higher frequency ripple from the converter. This higher frequency mainly causes generation of heat since its effect is inductive and not resistive but this generation of heat is relatively small in comparison with the heat generated by the DC current draw.

The measurement of component reduction is difficult since it always needs to be compared against a specific topology. The measure of component reduction is better measured with the aim of overall cost reduction. It should be noted that costs may be reduced by using more cheaper/smaller components rather than a single component which is specifically designed and as a result more expensive. This improvement often requires additional control hardware and creates additional manufacturing costs associated with controlling, handling and building these extra components into systems. It should be noted that higher manufacturing volumes may reduce costs through orders of magnitude offsetting some of these cost increases (Kok et al., 2013a). Component reduction is seen as desirable however reducing components could result in reduced flexibility and redundancy, both of which are also desirable design features.

2.8.1. Summary

Adding converters to energy sources reduces the length of the string which has benefits in BMS complexity but increased the current draw. The control of the peak current demand from sources sensitive to this becomes important. The modular setup allows for increased redundancy. The use of converters in combination with UCs is highly recommended due to the increased voltage range which leads to an increase in available energy.

In Kok et al. (2013a), a novel approach to the topology setup was proposed based on the following design features:

- Cascaded topology
- Short UC string
- Redundancy
- Modularity

The design is shown in Figure 2.22. The author concludes that a parallel topology with multiple legs will reduce the current at each step. Support from the UC module reduces the current demand under acceleration conditions and cascading them limits the length of the strings. Under cruising conditions a reduced number of converters is active (i.e. only as many needed to achieve the desired demand) thus optimising efficiency by operating the converters at their most optimum point, while through the diodes the sources work together to reduce the current draw per source thus allowing the batteries to operate at low current demand reducing rate capacity effect and increasing range. The diodes also work together to balance the UCs and provide a parallel operation in case acceleration occurs which does not require maximum power but maximum energy.

In a comparison between battery drive train without converter and a battery drive train with converter, the current draw from the battery as a result of the converter use is higher as a result of the power balance equation (see equation (2.3) page 34), which is why the multiple legs are required.

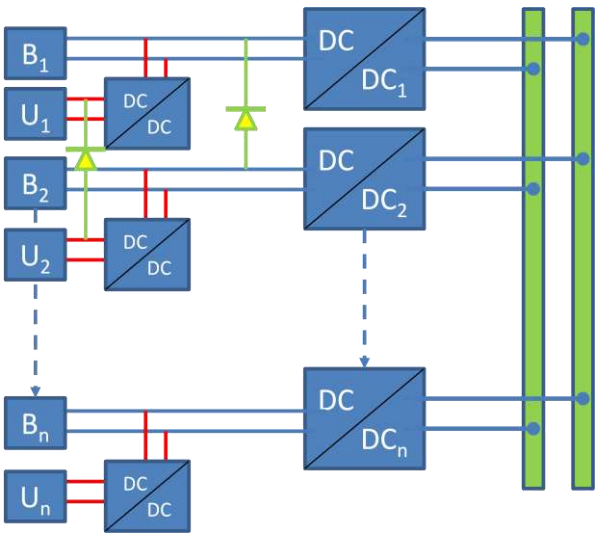

Figure 2.22: Novel Topology

The use of the cascaded structure would result in a ripple as seen by the battery which would be a function of the UC contribution, which will be explained in section 3.2.3 (page 84). This topology is not investigated further in this thesis because the ripple experienced by the battery – especially the high frequency component - would result in direct effect of battery aging. This would result in direct capacity loss and thus be a direct contradiction to the goal that is to be achieved; improvement of efficiency. The addition of the diodes will result in random current injections which add to the ripple problem.

2.9. Effectiveness of hybridization

The addition of a UC module should provide a benefit in some form to the vehicle such as –for example - overall reduced weight, improved driving range or reduced overall cost. Several case studies and research studies discuss and find whether there is a benefit that is worth for deployment in future vehicles ((Di Napoli et al., 2001, Ortuzar, 2005, Miller, 2008, Bo et al., 2009, Sadoun et al., 2012). Some findings are discussed here. For example, a 45kW converter design described in Ortuzar (2005) has a reported 22kg inductor and a water cooling system. In the same paper the UC pack of 20.45F has a weight of 95 kg adding to this the converter components for a total combined weight of 135 kg as reported in Dixon and Ortuzar (2002). This means the actual converter weight is 40 kg resulting in 1.125 kW / kg. This figure does not agree with the estimated 5 kW / kg (Rosario, 2007). The combined vehicle weight is reported to be 2 000 kg (Ortuzar, 2005). This equates to 6.75% of total vehicle weight. This increases the power demand under acceleration and will affect peak power demand from the battery.

The research concluded that if the life expectancy of the lead-acid batteries would be increased as result of the module addition to 50% it would make

financial sense over the life span of the vehicle, but it was recognised by the author that 50% would not be realistic.

Yet, using batteries in plug-in hybrid electric vehicles (PHEV) can reduce fuel consumption by up to 70% and with a marginal increased cost to the overall vehicle ($3500) the reduction in fuel cost - $8.33 / 100 miles for a conventional vehicles versus $2.26 / 100 miles for a full electric vehicle[2]. A breakeven point in terms of cost would be achieved after approximately 57 000 miles, which means hybridization has merit (IEEE Board of Directors, 2007) but at an average annual mileage in the UK of around 12 000 miles per year (*Average Annual Car Miles UK*, 2014), the payback would be just under 5 years (just over 4 if an annual mileage of 15 000 miles is assumed).

Under cycling condition using a constant current and a constant time period J.R. Miller (2007) showed that UCs have a higher round trip efficiency during regenerative period of under 10 seconds (>90%), while lithium-ion batteries only achieve this efficiency at around 30 seconds. The round trip efficiency of lithium-ion batteries at 10 seconds is close to 50%. In (Mallika and Saravana Kumar, 2011) this effect was mentioned as having a breakeven point of 10 seconds but the graph they used to arrive at their conclusion was taken from Miller (2007a) who used that particular graph as “illustrative only”.

Baisden and Emadi (2004) proved through simulation a 70% reduction in lead-acid battery pack size when using ultra capacitors in a HEV for a 2.41% improvement in MPG but at the expense of a heavier system which affects grade ability and top speed.

Burnett and Borle (2005) prove in their paper the possibility of optimising a FC system using solar, Li-ion battery and UC. They show a cost and weight

[2] Electric vehicle figures based on a Tesla 2007. The value derived for a Nissan Leaf will arguably look better since it has a smaller battery pack, smaller motor and overall less weight, which means the electric efficiency (kWh/mi) will be better and thus higher savings.

improvement by reducing the size of the FC to be able to supply cruising speed on its own, while power is supplemented from the battery and UC. Through the use of the UC the battery pack size is kept small by reducing initial peaks.

2.9.1. Summary

The use of converters does add to the effect of increased losses, but overall battery and ultra or super capacitor combinations have been proven to reduce the battery pack size while increasing the efficiency (more miles while using a smaller battery pack) but not reducing the overall weight volume, cost of the combined drive train (Miller et al., 2008).

Ortuzar (2005) states that no improvement in range was found and stipulated a theoretical improvement of 50% in battery life span was needed (lead-acid) but the UC module used was of significant weight (about 200 kg on a 2000kg vehicle).

Lithium-ion batteries generally have a much higher power rating, but their price is much higher which could make for a good cost argument. Their power rating is higher as well.

While it seems certainly true that the peak power can be supplemented by using an UC module the benefits are not always an optimum solution. Most often the weight of the added systems seems to increase despite the reduction in the number battery cells. The crux of the problem is the need for batteries under cruising conditions where the low energy UC module is just added weight.

2.10. Power and Energy Management

The aim of Power and Energy Management (PEM) control policies is to increase energy efficiency and lifespan of the energy sources and is considered to be of extreme importance for the acceptance of EV (Steinmauer and del Re,

2001, Rosario and Luk, 2006, Jinrui et al., 2006a). In addition to the technical and practical reasons there are economical advantages to optimising the drive train such as reducing the energy components and cost reduction of the total drive train (Di Napoli et al., 2001).

For hybrid electric vehicles there are 3 levels of control required (Rosario and Luk, 2007, Trovão et al., 2013).

I. Operational (Power electronics – microseconds)
II. Tactical (Power Management – Milliseconds)
III. Strategic (Energy management - Seconds)

Where operational is the switching control of the converter. This occurs at a set switching frequency which can be faster than microsecond intervals. Tactical is the power split between different sources, it defines which source supplies how much power at any given time and sets limits to how much power can be supplied by each source. Strategic is the overall management strategy to ensure that the limitations of each source are not violated. This level of control monitors the available energy in the different sources over time and decides on the best available strategy for the distribution of this energy. It informs the tactical management level on available power split options.

2.10.1. Operational

The operation of a converter is already discussed in an earlier chapter. In addition, within the control strategy for individual converters some accepted controls for Pulse Width Modulate (PWM) converters are current mode control (peak, averaged, charged) all three schemes can be supplemented with a voltage control loop (Cho et al., 2009) and voltage mode control. The main choice for a scheme is speed and stability under changing loads. A faster

controlled converter can control the output voltage better which results in smaller bus capacitance and it allows for better protection of slower sources.

2.10.2. Tactical

The power management strategy often boils down to the following equation:

$$P_t = P_1 + P_2 + P_3 + \cdots + P_n \quad \textbf{(2.33)}$$

Where n is the number of available sources and P is the power contribution of each individual source, which results in the total requested power (P_t).

In HEV the power split is often designed to maintain a certain range of SoC of the battery with the ICE running in an optimised zone only; i.e. outside this zone the ICE will be switched off or other changes are made to bring the ICE back in optimum operation zone. The UC will support the battery at moments of peak demand, this often results in different modes of operation with each mode having a different set of operating parameters (Stienecker et al., 2005).

The mode of operation is often used to identify a basic approach to the way in which the total power should be distributed, for example in a hybrid DC, source control is based around a rectifier and UC module to maintain a stable bus voltage but care must be taken to avoid chatter when switching between modes (Ayad et al., 2007). These are phenomena that occur when switching from mode to mode and happen when the control point occurs in border situations such as switching from acceleration to regenerative. These can be avoided using hysteresis or continuous and differentiable functions.

Another reason for this approach is the realisation that when the UC module has been discharged it requires charging again, which can be done either through regenerative braking or from the battery. Regenerative braking has not got the potential to charge the UC back to full because of losses in the system. With these limitations it is generally agreed that around 30-50% of available

kinetic energy can be recovered. The battery will have to provide the missing charge. Charging an UC requires time and can be optimised if the required acceleration is known in advance (Trovao et al., 2010). Since most driving patterns are to a certain extend unique (either because of route, traffic or other factors), the UC module needs to be ready to be able to supply a certain value at any given time with the probability that at lower speeds an acceleration event is more likely than a regenerative event while at higher speeds it is more likely for a regenerative event to occur. Similarly, it is also not likely that an acceleration event always constitutes from 0-70MPH.

The conclusion is that the converter does not need to be designed to supply up to maximum acceleration, while the UC does not need to be designed to have the energy to cover a full acceleration profile. While, this data looks good in test and a person might want this opportunity in case he/she needs to accelerate out of a situation the probability of any occurrences of these events is low.

In Payman et al. (2011) the suggested control strategy directly incorporated the energy management strategy with the FC being able to supply all the power but under changing conditions the FC is supported by a UC module which only controls the current slope of the FC. The FC is allowed to rise as quickly as it can while anything faster the UC module supports. The flatness based control used allows for a certain minimisation of the bus capacitance because the flatness based technique allows for the definition of the combined reaction speed of the different sources.

The inclusion of the energy management strategy directly in the control strategy has a disadvantage in that the FC output is directly related to changes at the output, which apart from the fast changes that are filtered by the UC module, still shows a changing load, while a FC prefers a more stable condition and has

an optimum working range. The approach does allow for the removal of operating modes and thus avoid chatter phenomena.

2.10.3. Strategic

A major problem in optimisation strategies is the difficulty in implementing the optimum energy strategy. The optimisation strategy involves the optimisation of a cost function such as optimised fuel consumption, reduced peak demands, reducing weight without sacrificing other features such as driveability (acceleration and deceleration response) and safety. The number of variables can be large which increases complexity of the equations. The best optimisation strategies can only be calculated offline and often rely on a-priory knowledge of the proposed drive aspects and require large databases of look up tables which requires seconds or even minutes to look through (stochastic optimal control, dynamic programming (DP)) (Hofman et al., 2007, Malikopoulos, 2014).

Model Predictive Control (MPC) aims to overcome the problems of DP by tuning the system offline and applying it online (Hredzak et al., 2014). The tuning requires a lot of in depth knowledge and does not allow for easy adjustments.

Predictive control as demonstrated by (Bender et al., 2013) show that while the possibility for optimisation is significant it requires a lot of storage space and computational energy and a baseline strategy is still needed in case a route has not been driven before.

Drive Cycle prediction based on past events while seemingly very suitable for recurring routes, fails to deal with traffic effects and weather influences (Bender et al., 2013).

Energy management strategies based on predictive control are potentially complicated to understand and modify and often slow due to number of

computations that are needed (Byeon et al., 2013). It is therefore important that energy management strategies also focus on the sub-optimal strategies.

Equivalent Consumption Minimisation Strategy (ECMS) which aims to simplify the control problem by applying optimal combination of variables and is rated in optimisation capability close to MPC (Malikopoulos, 2014). However, it does not look at driving behaviour or tries to predict influences from outside (Borhan et al., 2012)

Heuristic control strategies – Rule Based (RB) strategies. The strategy does not actively search for the most optimised solution but assumes a solution based on the limitations set (Pisu and Rizzoni, 2007). The limitations are fixed points in the operation which results in susceptibility to noise. The addition of fuzzy logic allows for smoother transitions between operation points which improves continuity and robustness but at the expense of increase computation requirements and data storage (Gurkaynak et al., 2009). Rule-based Control, such as Solid State Machines and fuzzy logic controllers have the advantage of being able to function in real-time and are robust but are not as rigorous in optimisation as for example a DP or MPC strategy (Simoes et al., 2014).

Learning strategies such as Neural Networks (NN) promise good optimisation but are dependent on available training data (Moreno et al., 2006, Gurkaynak et al., 2009). According to Gurkaynak et al. (2009) NN are better than RB strategies and can be further improved through fuzzy logic. A NN is not considered as good as a MPC (Hredzak et al., 2014).

Energy Management in vehicles can also be done through flexible electric load demand (Kessels et al., 2005, Masjosthusmann et al., 2012) where the converter to charge the auxiliary battery is switched on and off as part of the load control. The auxiliary battery can sustain the load (from auxiliary

equipment, such as radio, heaters, window wipers, light, electric windows etc) on its own for a limited amount of time.

In his thesis Rosario (2007) describes a power energy management setup which approaches the setup as a management of resources, where the three levels are associated with a 3 tier management system (top, middle ,low); i.e. a top down approach see also (Rosario and Luk, 2007). The management strategy is encapsulated in a fuzzy logic set, which assumes three variables: fast, medium, slow. This three level rule based decision framework is enhanced upon by Trovão et al. (2013), who further map out the limitation of the battery and UC module, making the decision a further fine tuned system by applying simulated annealing algorithm to their rule based maps.

The fuzzy rules were based on the assumption that at lower speeds the likely hood of an acceleration event occurring was high thus the UC SoC should be high while at high speed the likely hood of accelerations was low, but the likely hood of deceleration was high thus the UC SoC required to be low in readiness for an influx of energy from regenerative braking. This allows for the reduction of the energy needs of the UC module and thus a lighter setup, but the definition is vague, since there is no definite certainty that at 60 km/h the probability of an acceleration event is higher or lower than a regenerative event and the duration and power requirements are not known either.

The distribution of timing is an important factor in the application of this management strategy as described by (Rosario, 2007) the tactical power management implementation can be a source of delays for which one needs to compensate with a larger bus capacitance to prevent instability. The reason for this is the time restriction implemented in the tactical level of the system. The power electronics can function at switching frequency which is in micro seconds

intervals. The tactical or power management level feeds these signals on a millisecond bases. Estimation on the necessary bus capacitance is calculated based on the switching frequency (micro seconds), but the introduction of the millisecond power level means that the bus capacitance is calculated based on this frequency. Thus the bus capacitor needs to be able to filter for a time length up to a 1000 times longer (depending on the switching frequency), which requires a much larger capacitor.

2.10.4. Summary

The three levels of control provide a good break down of the problems encountered designing a Power and Energy Management (PEM) strategy but provide their own issues such as the possible introduction of chatter and the increased size of bus capacitance. In the power strategy it will be important to swiftly provide a reference value to the power electronics to be able to keep the bus capacitance small.

The research in this chapter focuses on the smoothing of peak power with a certain (unwritten rule) that the battery power never exceeds a certain threshold for a longer period of time for example during NEDC driving cycle where the total cruising time at high velocity (100km/h or more) is only 40 seconds which is only a fraction (3.2%) of the total 1220 seconds of the drive cycle. Luk and Rosario (2005) state that the load requirements for electric vehicles are constantly varying and thus very user specific.

Influences such as road gradient, weather, tire degradation, etc, all contribute to the load profile (Souffran et al., 2012). Test routes used in research are often limited in driving under cruising conditions. The reason for mentioning this is that a short period of high speed is treated as a short term peak demand as if part of start stop driving and this can be compensated through the use of UC

module and sizing. Sizing the UC for a cruising condition or long term acceleration (hill climb) will deplete the UC and drop the demand back on the battery, which means that either you continue limiting the current from the pack or allow it to rise; in the former situation drivability is limited (imagine going into limp mode during a drive up hill) and in the later drivability is maintained at the expense of temporary loading the battery at a higher current.

2.11. Literature Review Conclusions

In Mesbahi et al. (2014, p. 5) 4 different power control strategies are classified:

- Battery power limitation with UC recharge during stop phase
- Battery power limitation with UC SoC management
- Dynamic battery power limitation according to UC SoC
- Dynamic battery power limitation according to UC SoC with limits based on UC SoC

The PEM system introduced in this paper will have dynamic battery power limitation based on power demand and adjustable SoC level management, with the aim to keep the current demand from the battery as low as possible and approaching average over a period of time. The adjustable UC SoC level allows accepting all regenerative energy and is high enough to provide acceleration up to a probable velocity. The target is to not change mode from a battery perspective since this will result in very short charge / discharge cycles that are highly inefficient.

The energy stage will focus on setting limits for the battery and SoC target for the UC with the aim to keep the UC module as small as possible while providing optimum support for the battery. The battery power will not be limited because this would limit driveability. A set of recorded drive cycles will be analysed and probable events will be derived through Markov Chain analysis. This will help in

defining the size of the UC module, the time period it needs to cover, the delay that can be applied before introducing the battery and the amount of power required to top-up the UC in case the UC SoC drops too low.

Maximising the life span of the battery pack is seen as an important area of research which requires tools to test (Knowles et al., 2012a). A hardware dynamometer tool was developed for this purpose as described in the same paper. This was later further developed for direct connection to a simulator (Kok et al., 2012), to create a Human-in-the-Loop setup.

In the next chapter the rate capacity effect of batteries and battery ripple effect will be investigated further. Both have a direct connection to life span of batteries. The research will focus on the development of a method to assess battery life span through efficiency improvement and as such provide a computer approach to life span assessment.

The research presented will also focus on the ripple effect as seen by the battery and which topology is best for the introduction of UC in the drive train, the development of a control strategy to manage the power split between the energy sources and the development of the energy management control strategy. This will then lead to the design a control system which has an integrated tactical and power stage which will allow the decrease in size of the bus capacitor and assist in chatter avoidance.

Predictive control through Markov Chain analysis will be investigated for the development of an improved Energy Management Strategy.

Simulation and Analysis Requirements

3.1.Introduction

In the previous chapter the following has been identified as a necessity to an optimum power and energy management system:

- Smooth peak battery current; keeping the battery current as low as possible
- Fast power control
- Optimised power management strategy
- Optimised Energy management strategy

It is not clear what the effects of different topologies are on battery current ripple and if this would influence the choice of topology. A method of assessing the effect of the optimisation in simulation is required. In the next chapters the PMS will be designed followed by the energy management strategy. The complete PMS strategy will then be tested through simulation. This chapter will focus on developing an approach to assess how the proposed PEMS will improve the efficiency of the system.

3.2.Topology Selection

3.2.1. Topology selection based on Battery current ripple

It is reported that a major drawback for boost conditions of the half bridge converter is the discontinuous output current (Siang Fui and Chee Wei, 2012). Similarly, under buck conditions this discontinuous current can be found at the input. In this section the effect of phenomenon will be further discussed, more

specifically what the effects are on combining switching converters. The basic premise of operation of a switching converter is the on-off behaviour of a switch which results in a temporary storage of energy in a storage medium (inductor or capacitor) before the temporarily stored energy is transferred to the output. The transferred energy results in an output ripple normally smoothed by the output capacitor but when the output capacitor has a fixed voltage because it is connected to a battery then another phenomenon is observed which will be discussed here.

In Payman et al. (2011) the following graph (see Figure 3.1) was shown which depicts a FC configuration with UC module; the UC module is switching in (mark point A) and out (marked point B). The combined setup is directly connected to the bus. It was noticed that the presented FC current showed a ripple doubling from 2 $A_{peak\text{-}peak}$ to around 4 $A_{peak\text{-}peak}$, which seemed a very large increment on a total of 16A load current demand (25% ripple).

The aim of the research presented here is to investigate the effect different topologies have on the battery ripple and the way in which this affects the life of the battery. In this chapter, simulations done in Matlab / Simulink with the use of the SPS toolbox will be used.

Note: The ripple effect at the bus is also observed by Miller and Sartorelli (2010) who showed in their research that a battery supplied by a UC module has more ripple than an UC supplied by a battery with converter. They concluded that the Energy Management System (EMS) was the cause for this, but the author will demonstrate that this ripple effect is a result of the topology configuration.

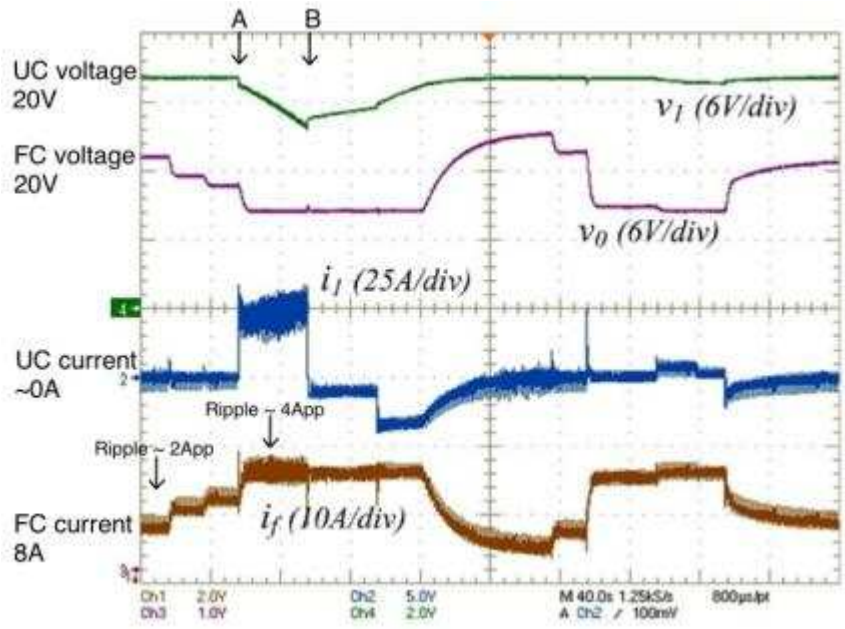

annotated from (Payman et al., 2011) © 2011 IEEE

Figure 3.1: Cascaded converter ripple effect

3.2.2. Topology: Battery with UC Module

Battery + UC Module - Boost Mode

Here the battery is directly connected to the bus – i.e. using no converters (keeping the strings long) - and a UC with converter is added. The circuit is shown in Figure 3.2. This results in a ripple effect as a consequence of the addition. The reason for this ripple is the switching effect of the converter.

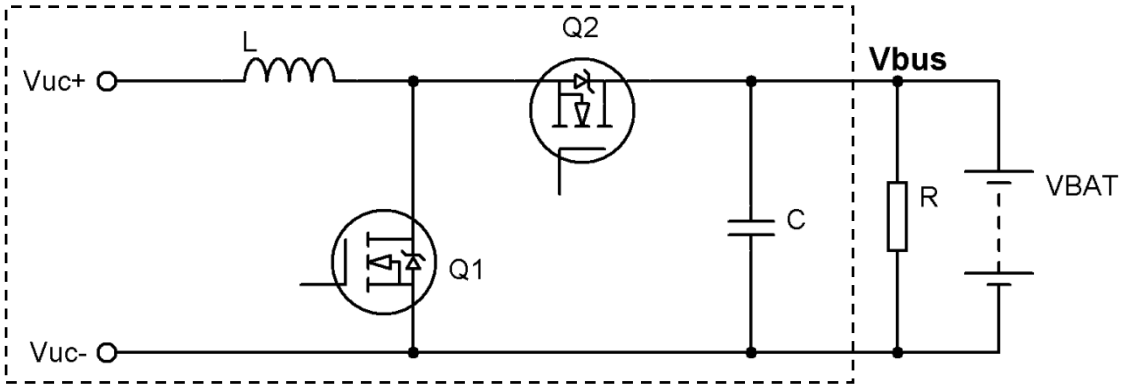

Figure 3.2: Battery + UC Module

In this case the bus is connected to a battery and the bus voltage can be considered constant. The resistor represents the load.

3.2.3. Simulation setup Battery + UC Module

The bus voltage for this simulation and in this thesis is chosen to be 96 V with its maximum being 125V and a minimum of 72V. The choice for this bus voltage came about as a result of calculation for a conversion project. The SPS battery model was set to Lithium-ion battery and the nominal voltage to 96 V (30 cells in series with a nominal voltage of 3.2V). The model's capacity was set to 50Ah (which is an arbitrary chosen capacity since capacity is not of relevance in this research because the simulation time is short) and the SoC at 75%. The SoC charge was chosen such that the battery would have room to receive some charge if so required. The battery is directly connected to the bus which is represented by a Current Controlled Source (CCS). The UC was modelled as a basic capacitor with internal resistance and based on the Lithium-Ion capacitor discussed in section 2.3 Ultra Capacitor (p26). The internal resistance of an individual cell is 1.4mΩ (Lambert et al., 2010). The operating voltage of the complete string was chosen as a value below the battery minimum. This was chosen to avoid diode forward bias which can occur when the UC voltage becomes higher than the converter output voltage and results in loss of control. The UC simulation parameters are given in Table 3.1. The UC voltage at start is set to 60V.

Table 3.1: UC parameters (18 cells)

Capacity	122.22	F
Voltage range	39.60 – 68.40	V
Internal resistance	25.2	mΩ

The converter topology used for the UC module is a Half H-bridge converter. It should be noted that the author is aware that interleaved converters would normally be used because of the large currents involved to reduce the size and weight of the inductor components and increase efficiency but interleaved converters increase the number of switching components and as such would increase simulation time.

The converter parameters for the UC module converter are given in Table 3.2. The parameters were calculated based on a peak current ripple of 2% of a maximum 300 A continuous, while the output voltage ripple was set at 5% bus voltage. The duty cycle was calculated based on the maximum ratio which would be the minimum input of 39.6V (2.2V*18 Cells) and the maximum bus voltage of 125V. When the converter is operating under buck conditions the output ripple (at the side of the UC) is set to 5%. This is included for completeness but it is recognised that that capacitor will have little effect compared to the large capacitance of the UC. The duty cycle under buck conditions was calculated using the largest ratio of input and output, which is the nominal bus voltage of 96V and the 66.6V, which is the maximum voltage of the UC (3.7V*18 Cells).

Table 3.2: Battery + UC module Converter Parameters

Inductor	225	µH
Cout	3.71	mF
Cin	21.7	µF
Switching frequency	10	kHz
Stability variable (m_a)	20	-

The simulation was setup such that a single reference current (I_{Ref}) or load current demand (I_{Load}) could be set. During the tests only one variable was

altered while the other was kept static. The simulation would run using peak current control as shown in Figure 2.11 (p43). The simulation would be run for 0.5 of a second which is to allow the simulation to stabilise. The simulation layout as used in Simulink SPS is shown in Appendix 7.

3.2.4. Simulation result Battery + UC Module

A battery is directly connected to a bus with an UC module in support with a fixed reference current ($I_{Ref} = 50A$). The load demand (I_{Load}) is varied (20A – 100A). The battery current ripple effects as observed by the battery can be seen in Figure 3.3. As can be seen the battery current ripple does not change with a changing load and fixed UC module supply (fixed reference current).

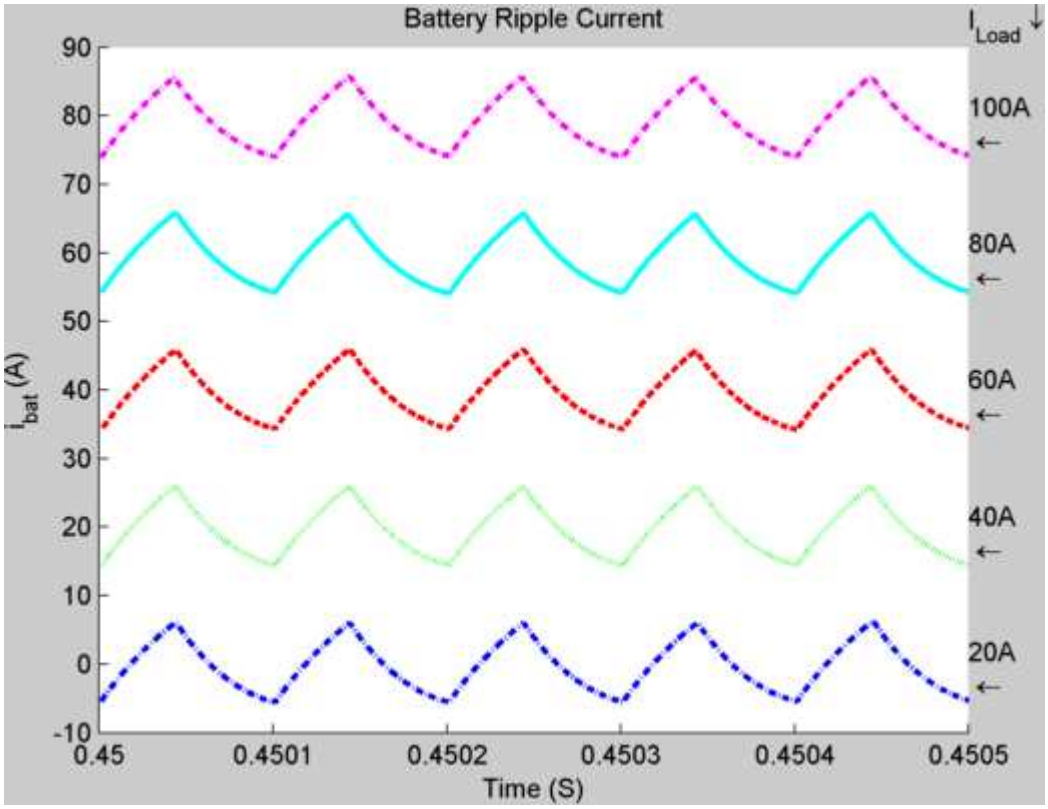

Figure 3.3: Battery ripple current for varying Load - Boost Mode

The situation was then changed and the load ($I_{Load} = 100A$) was kept constant and the reference current (I_{Ref}) varied from 20-100A. The ripple increases in direct relation to the level of current supplied from the UC Module (Figure 3.4).

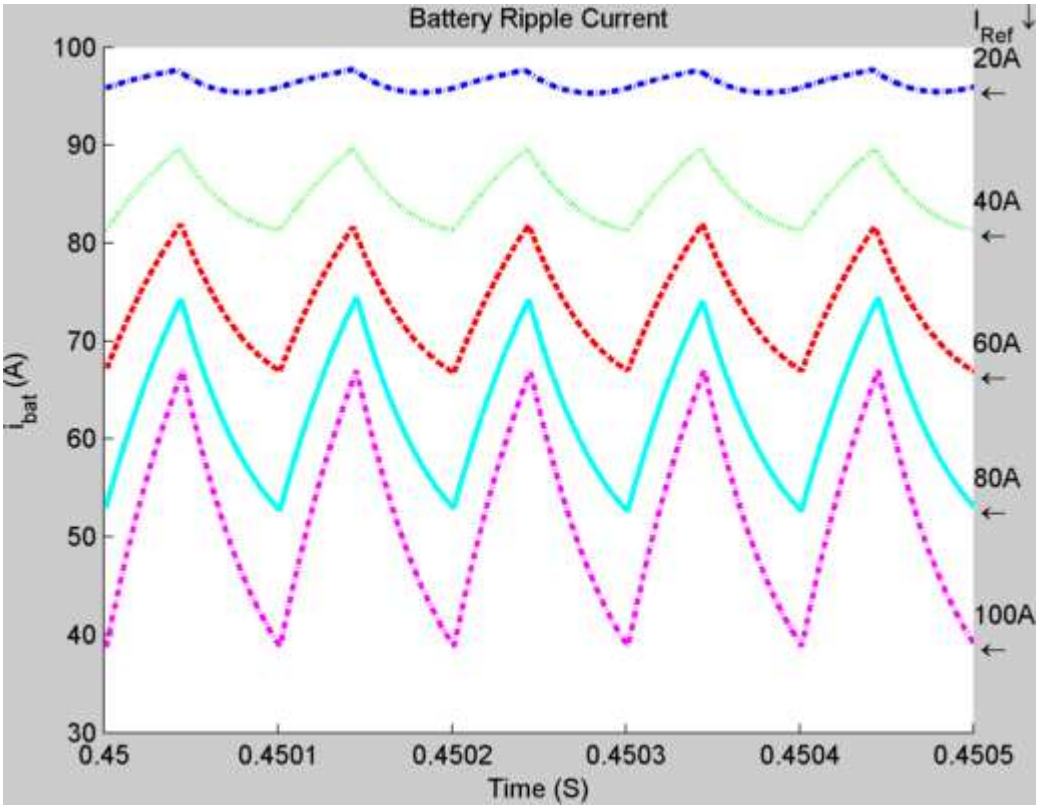

Figure 3.4: Battery ripple current with varying Reference - Boost Mode

The two individual states the converter can assume are shown in Figure 3.5 and 3.6. From these figures it is clear that when switch Q1 of the UC module is in the “on” position the battery is providing all demanded load (Figure 3.5), while when “off” (Figure 3.6) the UC module supplies the reference value reducing the battery current by that amount until a new period starts and switch Q1 is closed again.

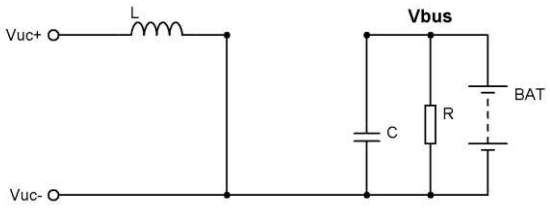

Figure 3.5: Battery + UC Module – Boost On

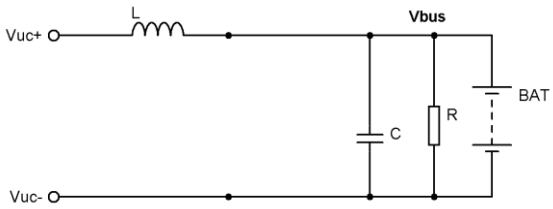

Figure 3.6: Battery + UC Module – Boost Off

In Table 3.3 the state space equations are given that describe the different states the converter topology can be in. The assumption made here is that

because of the battery the bus capacitor remains constant. It will provide some smoothing but for principle of operation it can be considered constant.

Table 3.3: Topology equations – Boost conditions

Q1 closed		Q1 open	
$L\frac{di_L}{dt} = V_{uc}$	(3.1)	$L\frac{di_L}{dt} = V_{uc} - V_{bus}$	(3.4)
$C\frac{dV}{dt} = 0, \quad \frac{V_{bus}}{R} = i_{bat}$	(3.2)	$C\frac{dV}{dt} = 0, \frac{V_{bus}}{R} = i_L + i_{bat}$	(3.5)
$i_{uc} = i_L$	(3.3)	$i_{uc} = i_L$	(3.6)

The difference between these equations and the equations of an ideal boost converter are that the output voltage ripple as seen by the battery is zero (3.2) and (3.5) and the load during the on period is supplied from the battery which will aim to supply all of the demand current while during the off period the converter supplies the requested reference current thus reducing the required contribution from the battery, which results in the ripple effect.

Battery + UC module - Buck Mode

In Figure 3.7 and 3.8 the circuit options for the converter under buck conditions are given. The bus current is represented by a current source. The capacitor is considered to have a much lower in value than the UC and thus not included in calculations. The resistance has been included to simulate the load as seen under buck conditions. The simulation was run with the same settings as previous except that the load demand is now negative as is the UC module current reference. Figure 3.9 shows the simulation result with a constant reference ($I_{Ref} = -50A$) current for the UC module and variable load current

(I_{Load}) ranging from -20A to -100A. Figure 3.10 shows the results of the simulation with a constant load demand ($I_{Load} = -100A$) and variable UC module reference (I_{Ref}) ranging from -20 to -100A.

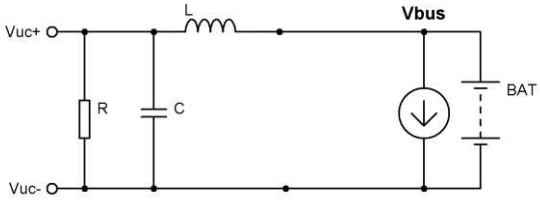

Figure 3.7: Battery + UC Module – Buck On

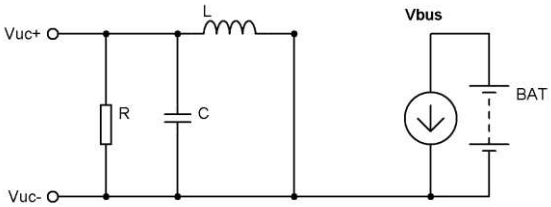

Figure 3.8: Battery + UC Module – Buck Off

Both figures are opposite to the graphs reported in Figure 3.3 and Figure 3.4. The equations are provided in Table 3.4 which show the similarity for the battery current equations: (3.2) = (3.12) and (3.5) = (3.9).

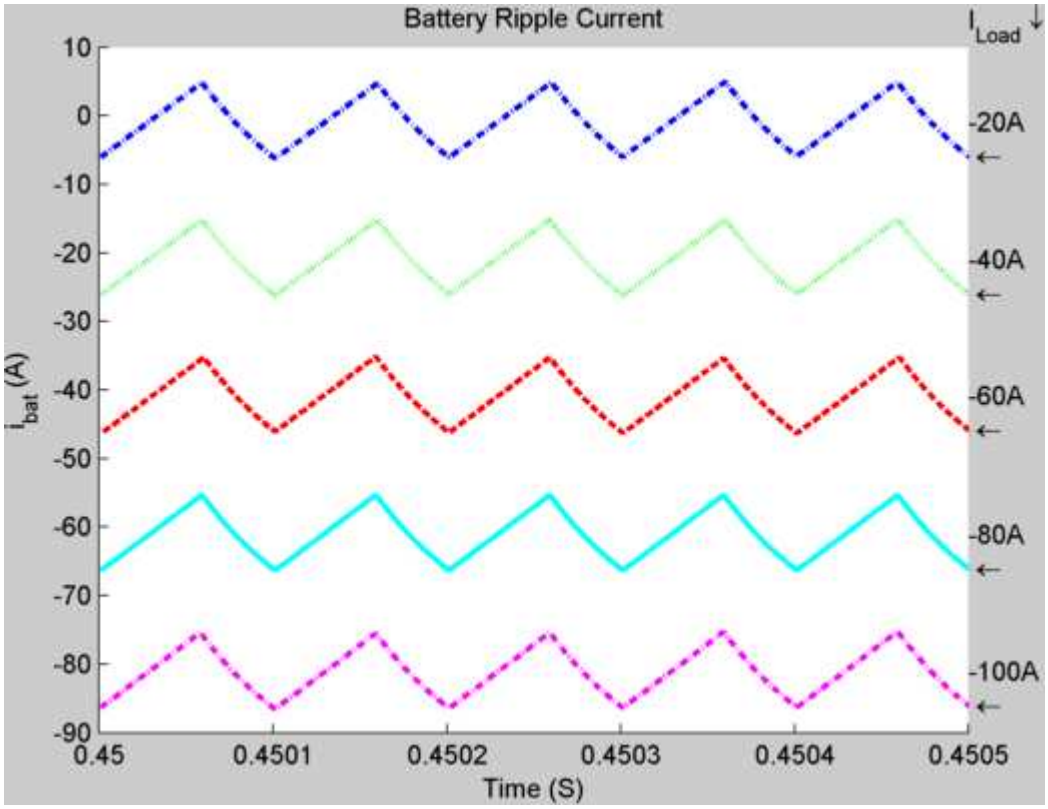

Figure 3.9: Battery ripple current for varying Load– Buck Mode

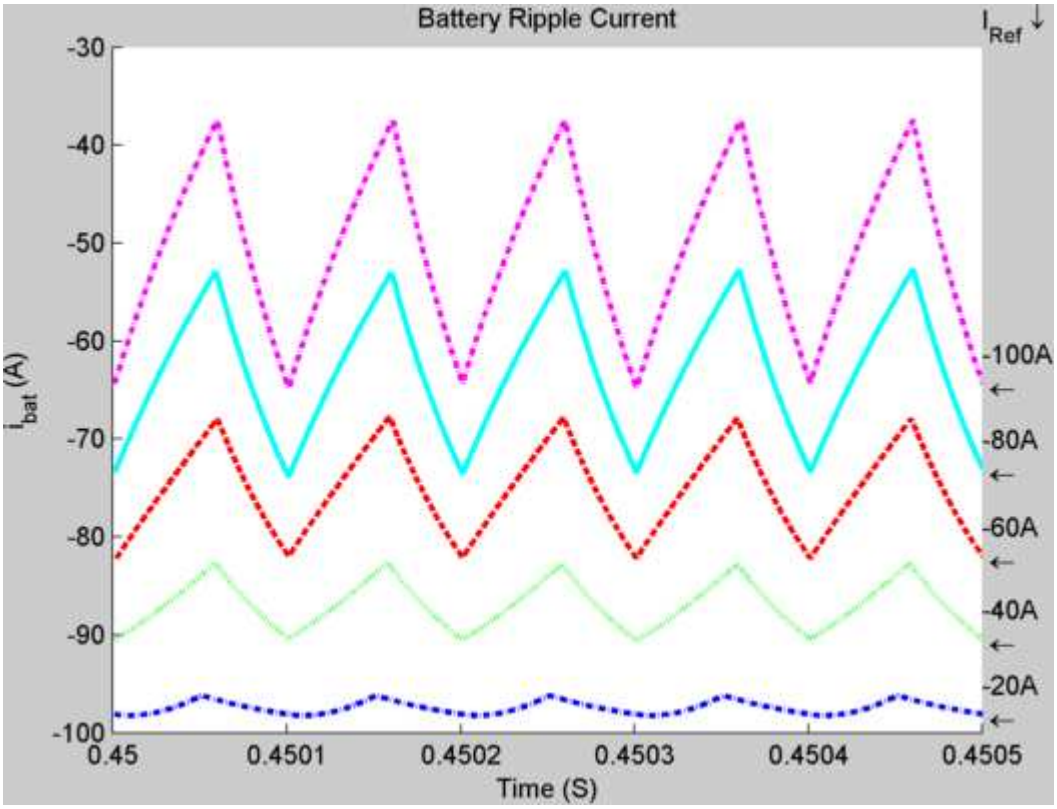

Figure 3.10: Battery ripple current for varying Reference – Buck Mode

Table 3.4: Topology equations – Buck conditions

Q2 closed		Q2 open	
$L\frac{di_L}{dt} = V_{bus} - V_{uc}$	(3.7)	$L\frac{di_L}{dt} = V_{bus}$	(3.10)
$C_{uc}\frac{dV_{uc}}{dt} = i_L - \frac{V_{uc}}{R}$	(3.8)	$C_{uc}\frac{dV_{uc}}{dt} = i_L - \frac{V_{uc}}{R}$	(3.11)
$i_g = i_L, i_{load} = i_L + i_{bat}$	(3.9)	$i_g = 0, i_{load} = i_{bat}$	(3.12)

3.2.5. Topology: Cascaded

Cascaded Converter – Bus Converter Boost Mode

In Figure 3.11 the layout of a cascaded topology is shown. It can be recognised that the left hand side of this circuit (to the left of the Battery) is the circuit discussed previously. The right hand side is the converter providing the bus with the demanded current.

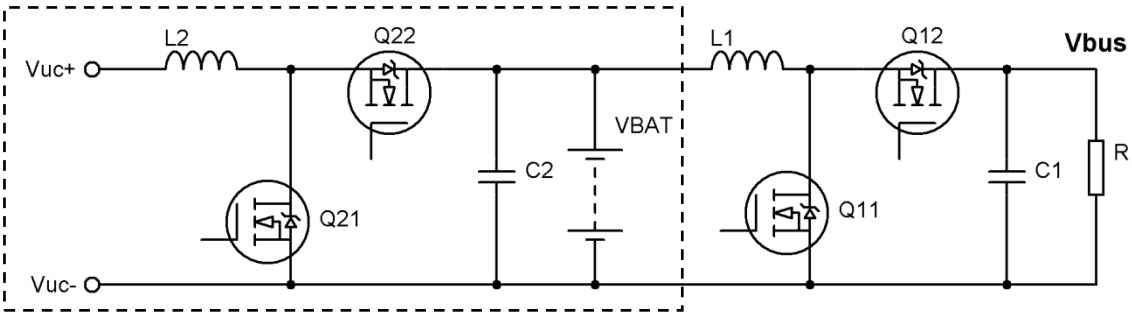

Figure 3.11: Cascaded Topology

The input current for a basic boost converter in both on and off conditions is given in Table 2.2 (page 39) and repeated in (3.13), with i_g renamed to i_{bat}. From the previous topology it is known that the battery current can be described by the inductor current from the UC module and the load demand current. This means that when the bus converter is functioning under boost conditions the ripple effects the battery experiences are the same as reported earlier.

$$i_{bat} = i_{L1} \tag{3.13}$$

Setting $i_{L1} = \frac{V}{R}$ then the battery current ripple in cascaded topology, with both converters under boost conditions, is described by equations (3.2) and (3.5) for the different states.

If only the bus converter is in boost mode (UC module in buck mode) then the relevant equations are given by (3.9) and (3.12). This would mean that any simulation results show a degree of similarity.

3.2.6. Simulation setup - Cascaded Converters

The bus voltage is again fixed at 96V which means that to avoid diode bias the battery voltage is lowered to 76.8 V (this would equate to 24 cells in series of 3.2 V nominal voltage – the battery minimum and maximum voltages are 60V and 87V respectively) to ensure this is avoided. Because of the lower battery voltage the UC Module converter requires different parameters to deal with the different input (39.6V) – output (87V) ratio while ensuring the same peak current ripple through the inductor. The inductor ripple current was set to 2% of 500A continuous which would be a 10A peak-peak ripple, while the output ripple was established at 5% of the bus voltage. The parameters for the bus converter and the new parameters for the UC Module converter are shown in Table 3.5. The parameters for buck converter operation of the UC module are now define through the battery nominal voltage and the maximum UC capacitor voltage. The output capacitor under buck conditions is 5% of the output maximum voltage.

The converter control is again peak current control only, while the bus converter has a voltage controller setting the reference current. The values for the PI controller are: P = 2, and I = 1000. The simulation layout as used in Simulink SPS is shown in Appendix 7.

Table 3.5: Cascaded topology - Converter Parameters

Bus Converter			UC Module Converter		
Inductor	156	µH	**Inductor**	180	µH
Cout	4.70	mF	**Cout**	3.09	mF
Cin	23.5	µF	**Cin**	22.5	µF

3.2.7. Simulation results – Cascaded Converters

The first simulation is run with I_{Ref} = 50A while I_{Load} is varied from 20 – 100A in 5 steps. This simulation is shown in Figure 3.12 and shows a good similarity with Figure 3.3. It should also be noted that the ripple design was set at $10A_{pp}$ and the ripple has doubled as a result of the converter-converter interaction.

Figure 3.13 shows a similarity to Figure 3.4 but the effect of the inductor current from the bus converter can clearly be seen. Despite this, the ripple still increases with the contribution provided.

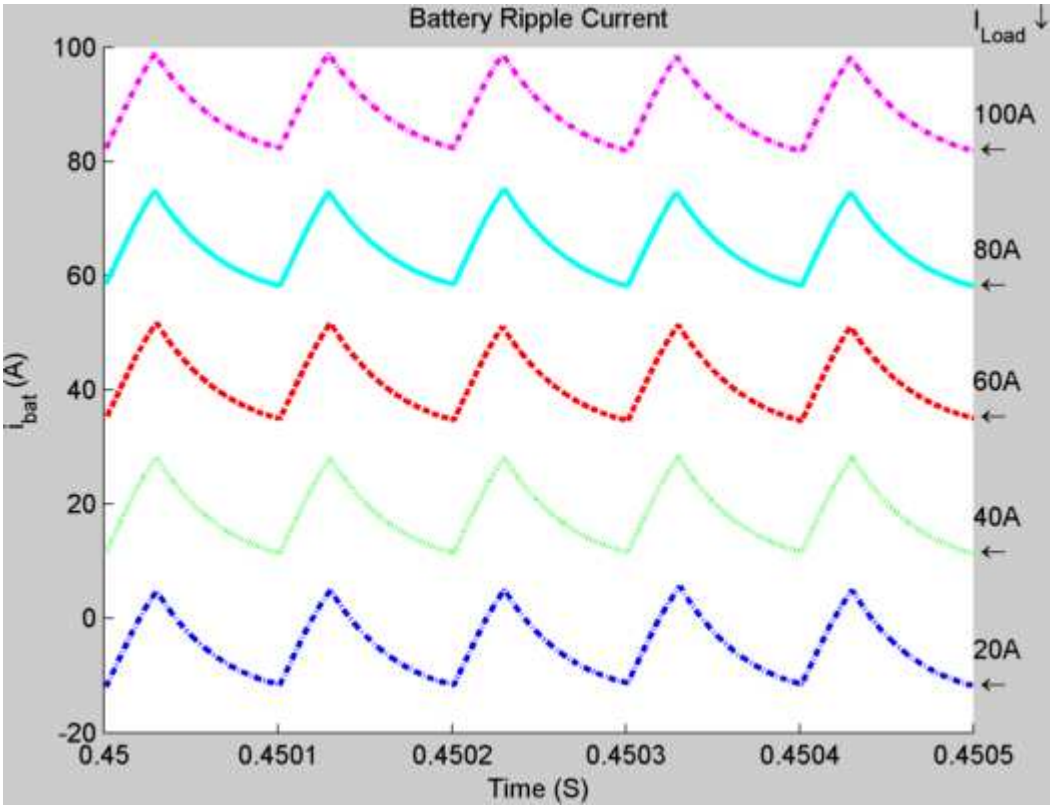

Figure 3.12: Cascaded Converters - Battery ripple current for varying Load– Boost Mode

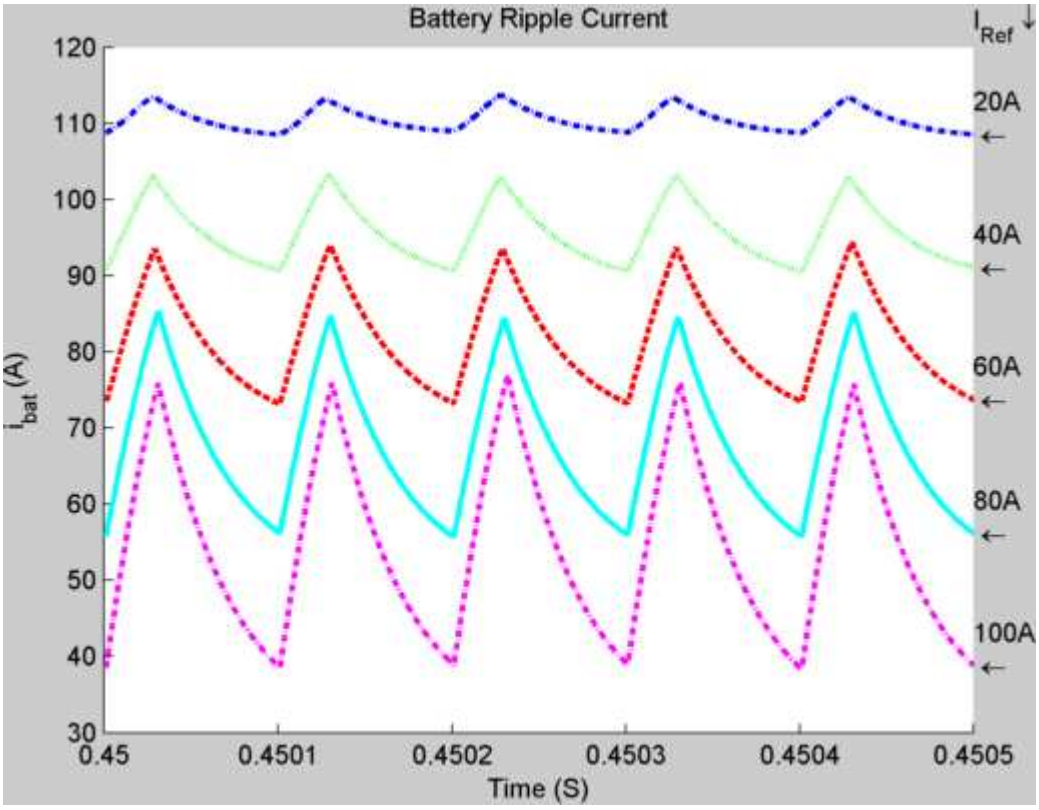

Figure 3.13: Cascaded Converters - Battery ripple current for varying Reference – Boost Mode

The next simulation shows the UC Module converter operating in buck mode and the bus converter in boost mode. Figure 3.14 shows the simulation with varying I_{Load} (20-100A) and constant I_{Ref}= -50A. The difference here is that the ripple remains constant but shifted upwards as a result of the load through the converter. Figure 3.15 shows the simulation with constant I_{Load} = 100A and varying I_{Ref} (-20 to -100A) and this shows the same shift effect.

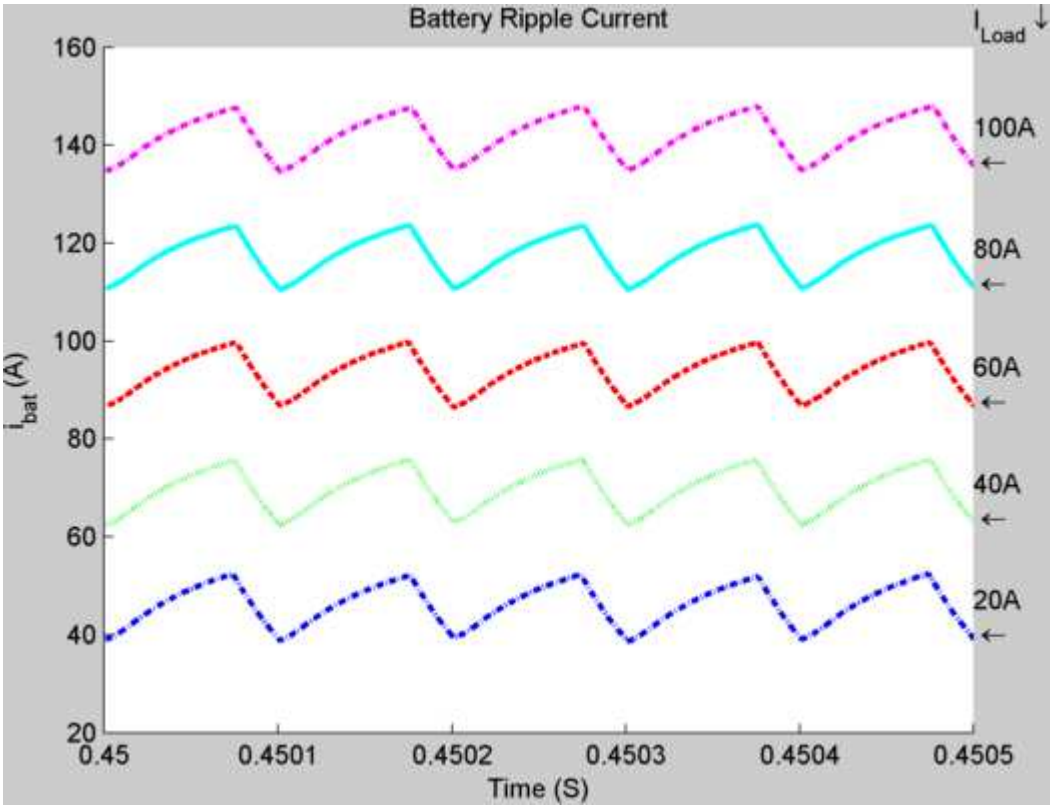

Figure 3.14: Cascaded converters - Battery ripple current for varying Load – Buck Mode

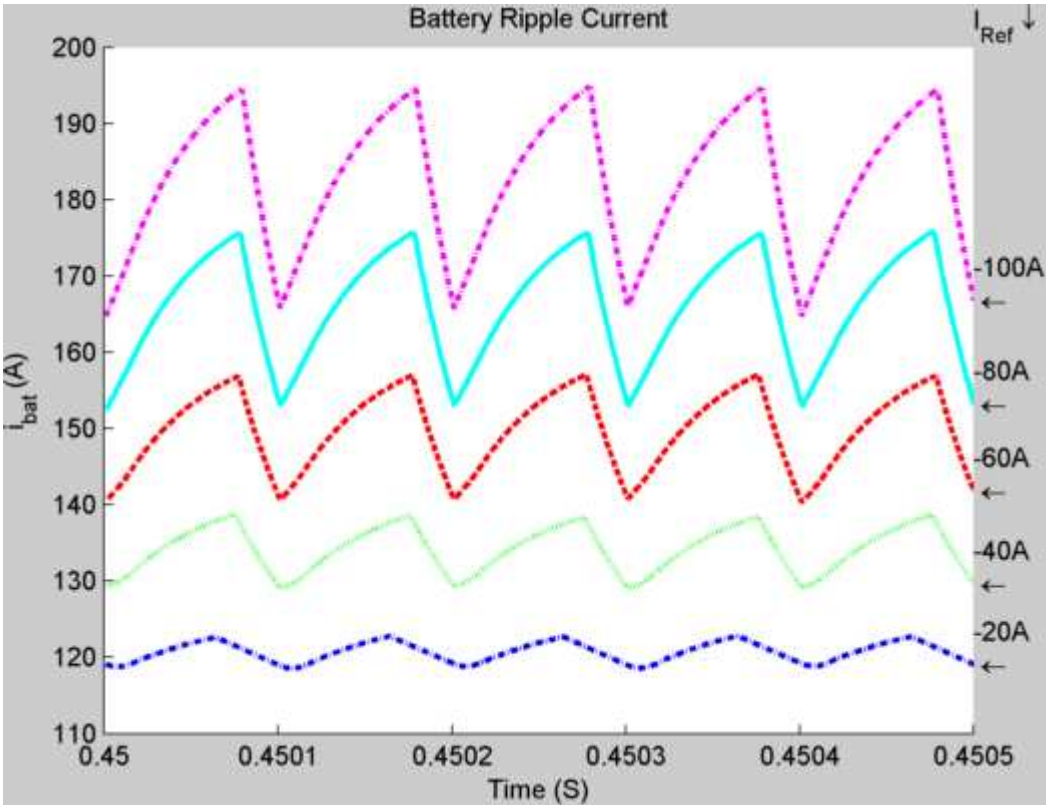

Figure 3.15: Cascaded converters - Battery ripple current for varying Reference – Buck Mode

Cascaded Converter – Bus Converter Buck Mode

When the bus converter operates under buck conditions the output current (i_{L1}) is given for both the on and off condition in an ideal converter (Table 2.3, repeated here (3.14)).

$$C\frac{dV}{dt} = i_{L1} - \frac{V}{R} \tag{3.14}$$

The battery replaces the capacitor but the output current is depending on switch Q22 (3.15).

Q22 is on	Q22 is off	
$i_{bat} = i_{L1} - i_{L2}$	$i_{bat} = i_{L1}$	**(3.15)**

These equations that define the battery ripple are the same as found in (3.9) and (3.12), which would indicate that the ripple effects are similar as well.

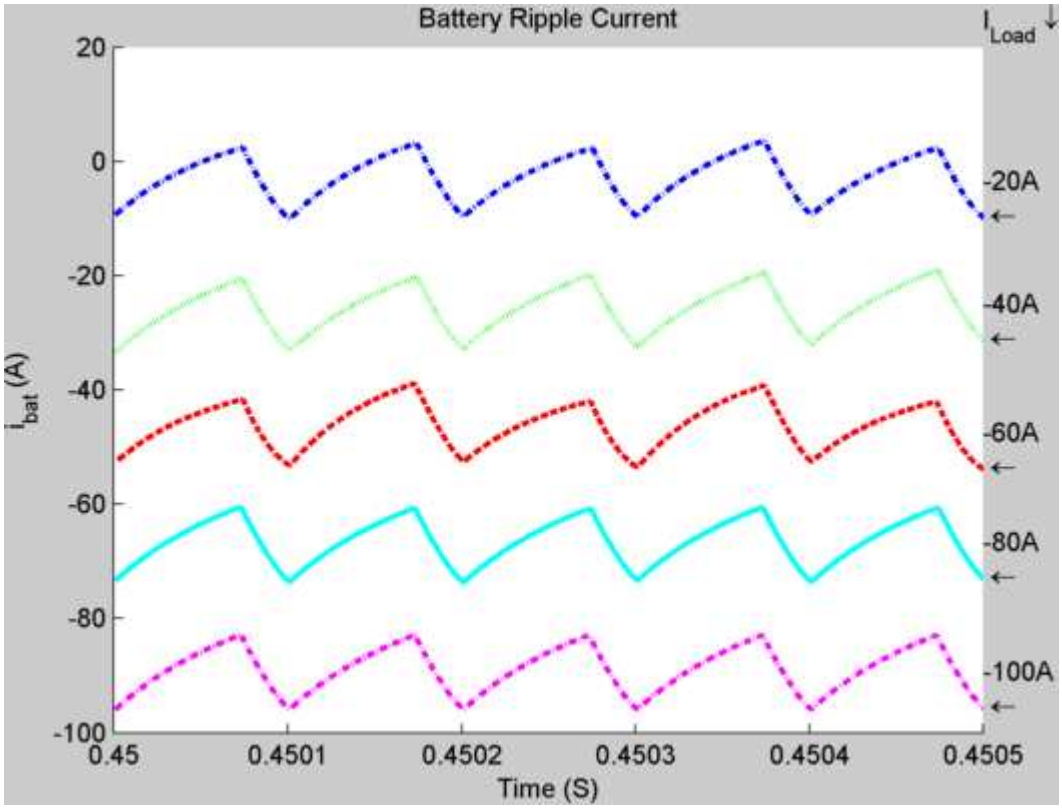

Figure 3.16: Battery ripple (buck-buck) – constant UC module support

For simulation the bus demand was in a range of -20 to -100A, while the UC module recovery was set to 50A. The results are shown in Figure 3.16. The

combination of inductors before and after the battery combined with the filter capacitors provide a degree of smoothing which brings the ripple down compared to Figure 3.9.

For the variable UC module reference simulation the reference was set in the range of -20 to -100A while the bus demand was kept constant at -100A.The results are shown in Figure 3.17. The figure is much like Figure 3.10 showing an increase in ripple when the UC module increases the amount it recovers.

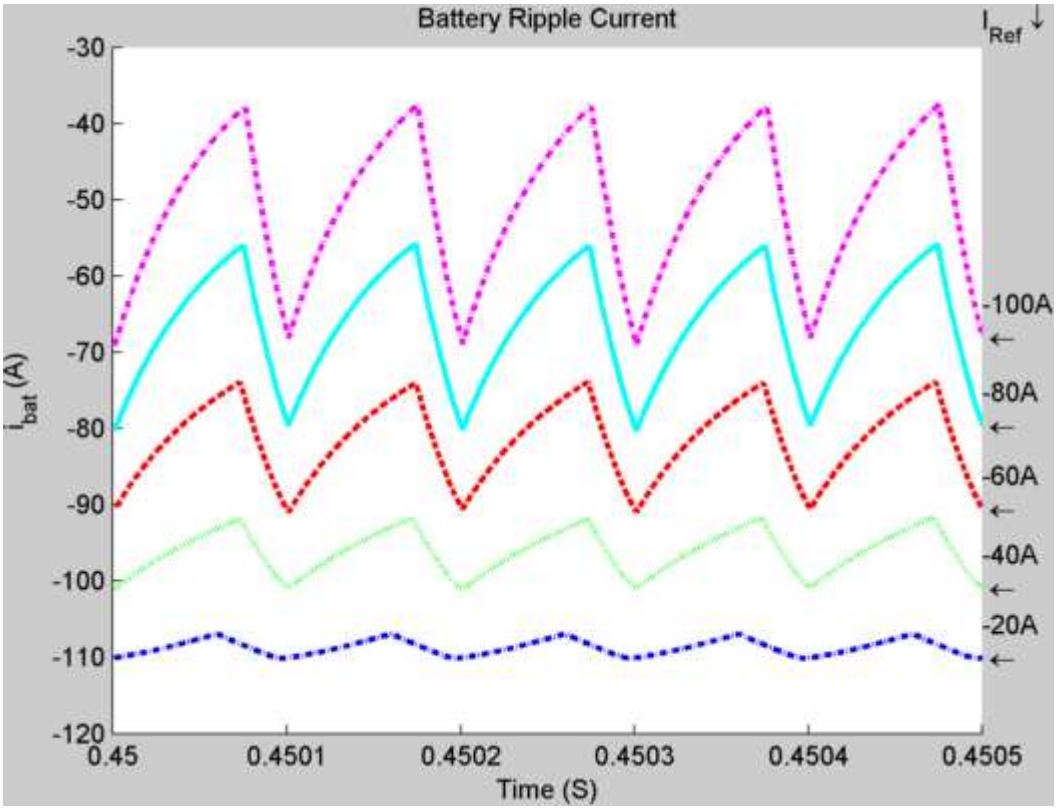

Figure 3.17: Battery ripple (buck-buck) – constant load demand

In the operation of a BEV with UC module the control strategy is often to a) support under acceleration (Figure 3.10) or b) maintain a certain target SoC by charging the UC with or without battery support - in preparation for another acceleration event (Figure 3.17). Under both conditions the battery ripple is a direct relation to the amount of support from the UC module.

3.2.8. Topology: Parallel

In the parallel topology (Figure 3.18) the sources are separated from one another and as a result the battery ripple current is the same as the inductor current of the ideal converter – buck and boost - as shown in Table 2.2 and Table 2.3.

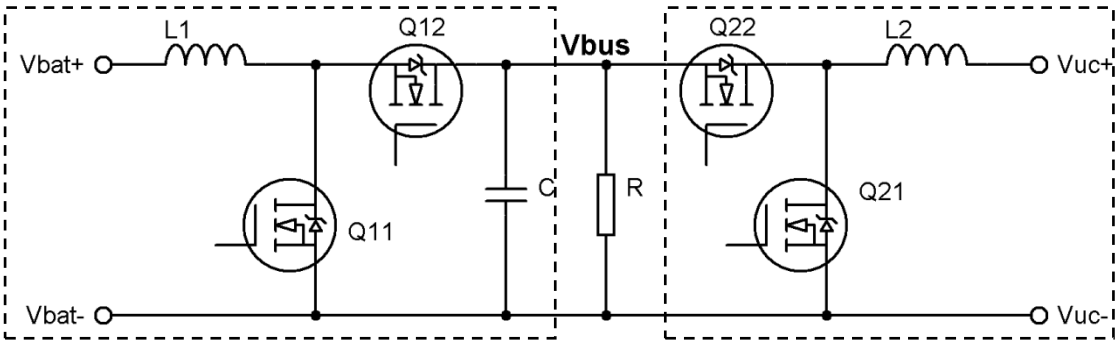

Figure 3.18: Parallel Topology

Simulation Setup – Parallel converters

The bus voltage is again set at 96V. The battery and converter setup and control are the same as in the Cascaded Topology (section 3.2.6) while the UC Module setup is the same as in section 3.2.3 (Battery + UC Module). The simulation layout as used in Simulink SPS is shown in Appendix 7.

Parallel converter – boost condition

The simulation results of both converters operating under boost conditions are shown in Figure 3.19 and 3.20. The results showing a fixed ripple under the different operating conditions and the size of the ripple is as specified in the design specifications. Here it can be seen that the effect of the switching has no effect on the inductor current ripple. The reason is that the diodes block any return current provided the bus voltage is well controlled and does not fall below the voltage level of any of the sources. In Figure 3.19 at 20A load demand the

battery converter is operating under buck conditions since the UC module supply is more than demanded.

Operating the battery converter in boost mode and the UC Module converter in buck mode does not change the battery ripple current since the battery current is not affected by any other influences as shown in the previous topologies.

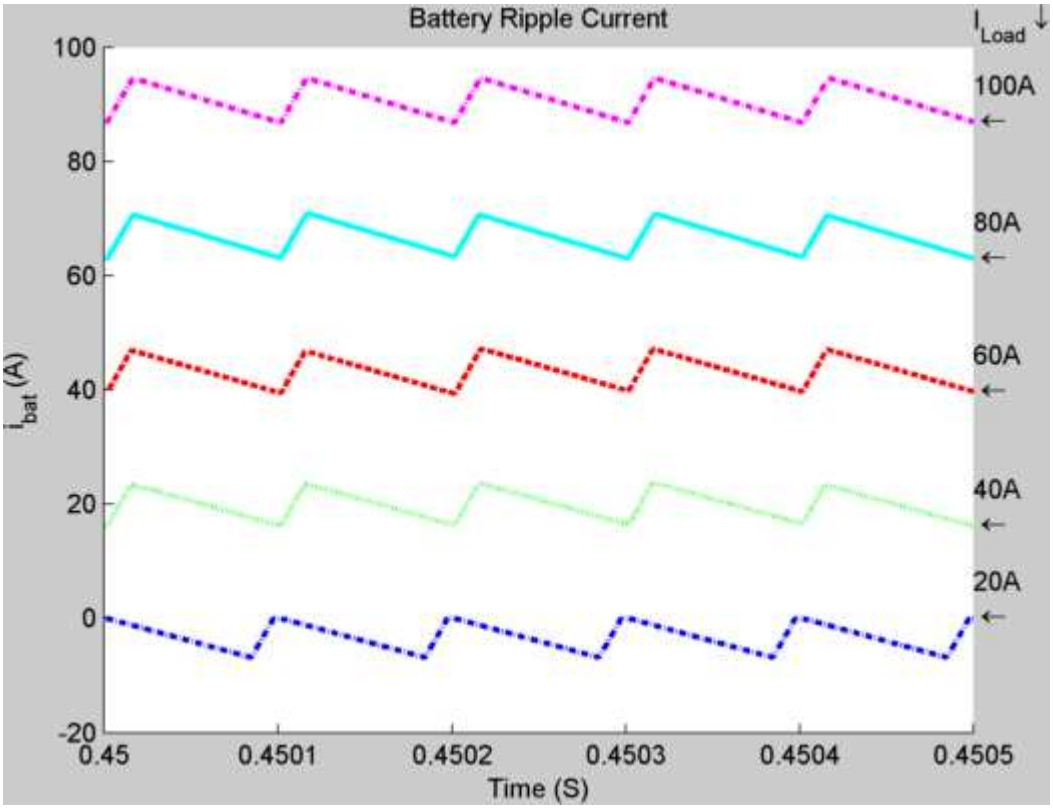

Figure 3.19: Parallel converters - Battery ripple current for varying Load

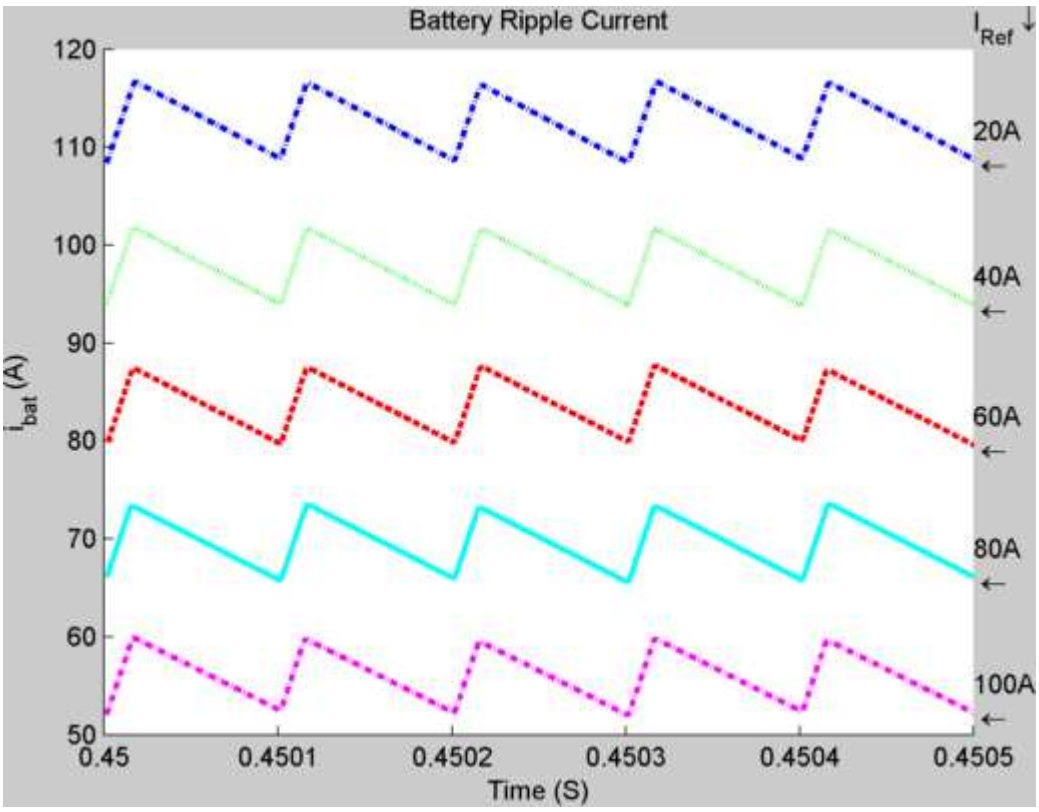

Figure 3.20: Parallel converters - Battery ripple current for varying Reference

Parallel converter – buck condition

The ripple effect is the same for the parallel converters with both converters operating under buck conditions (Figure 3.21 and 3.22) except that when both converters operate under buck conditions the control is sensitive to instability, which is a result of the bus being disconnected from both sources at sometime during the period. But since energy recovery in the battery is less efficient this is a situation that should be avoided.

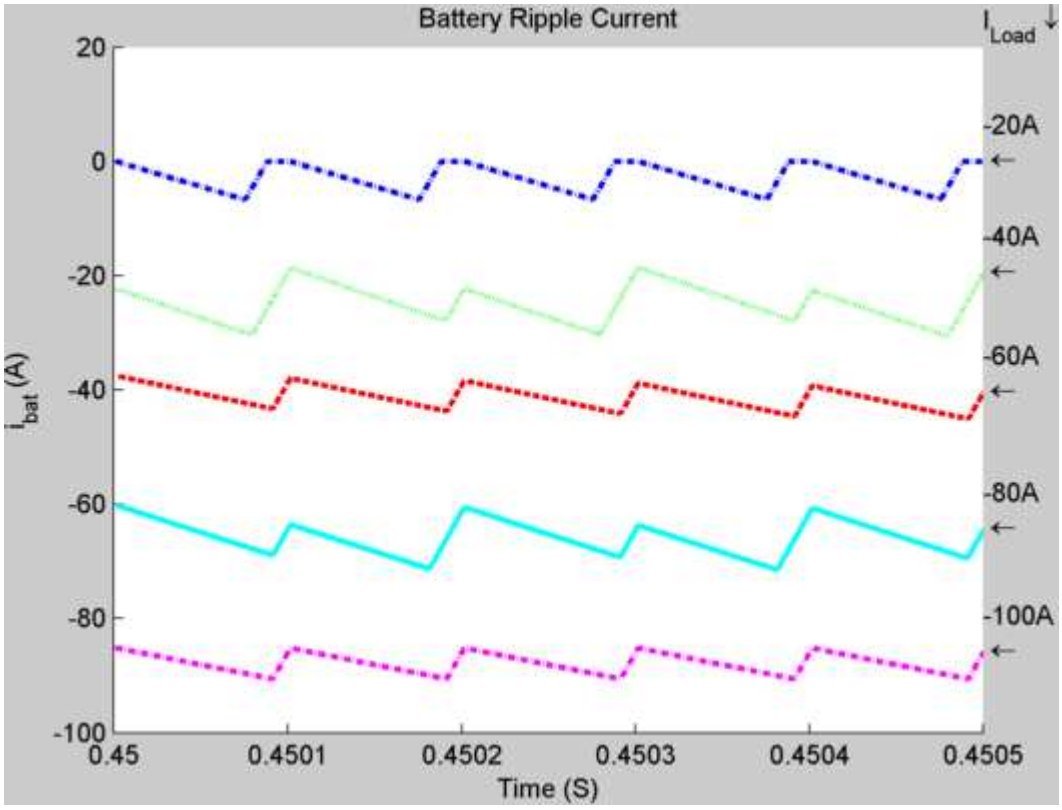

Figure 3.21: Parallel converters - Battery ripple current for varying Load

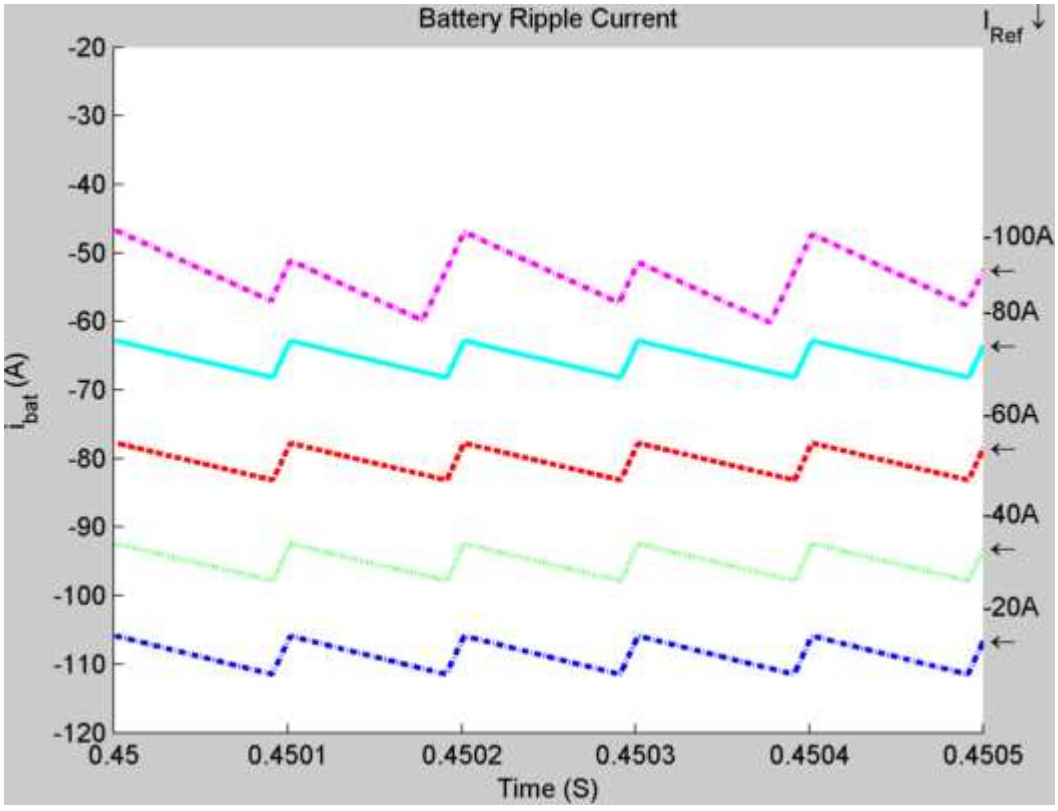

Figure 3.22: Parallel converters - Battery ripple current for varying

Parallel converter – bus capacitor

In Figure 3.23 the currents through the bus capacitor are shown (simulation data same as in Figure 3.20: i.e. a constant load with a varying value for the reference current of the UC Module converter). As can be seen the capacitor receives and supplies (smoothes) the current from the two converters providing a smooth bus voltage. Figure 3.24 shows a 50% timing offset to the converter of the UC module. Effectively 2 parallel converters (albeit with different sources) can be interleaved by offsetting one of the PWM signals as is done in interleaved converters.

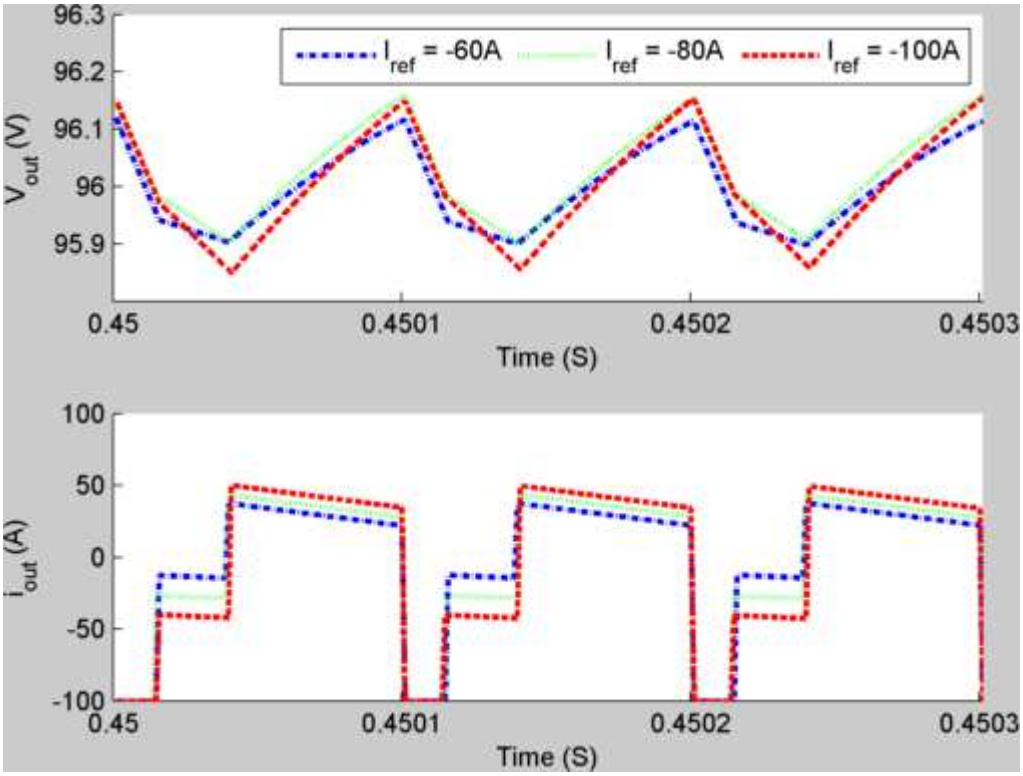

Figure 3.23: Parallel Topology - Bus Capacitor

Providing a timing offset to the operation of the two converters provides the same figure for the individual currents but an interesting effect occurs at the output as shown in Figure 3.24. The timing offset applied is 50% of the period which reduces the current ripple as seen by the bus capacitor. This will not necessarily allow for the capacitor size to be reduced but it will reduce the

stresses as experienced by the bus capacitor. From Figure 3.24 it can be seen that the current swing as experienced by the capacitor ranges from -50 to + 50A while the current swing without timing offset (Figure 3.23) ranges from -100 to + 50A.

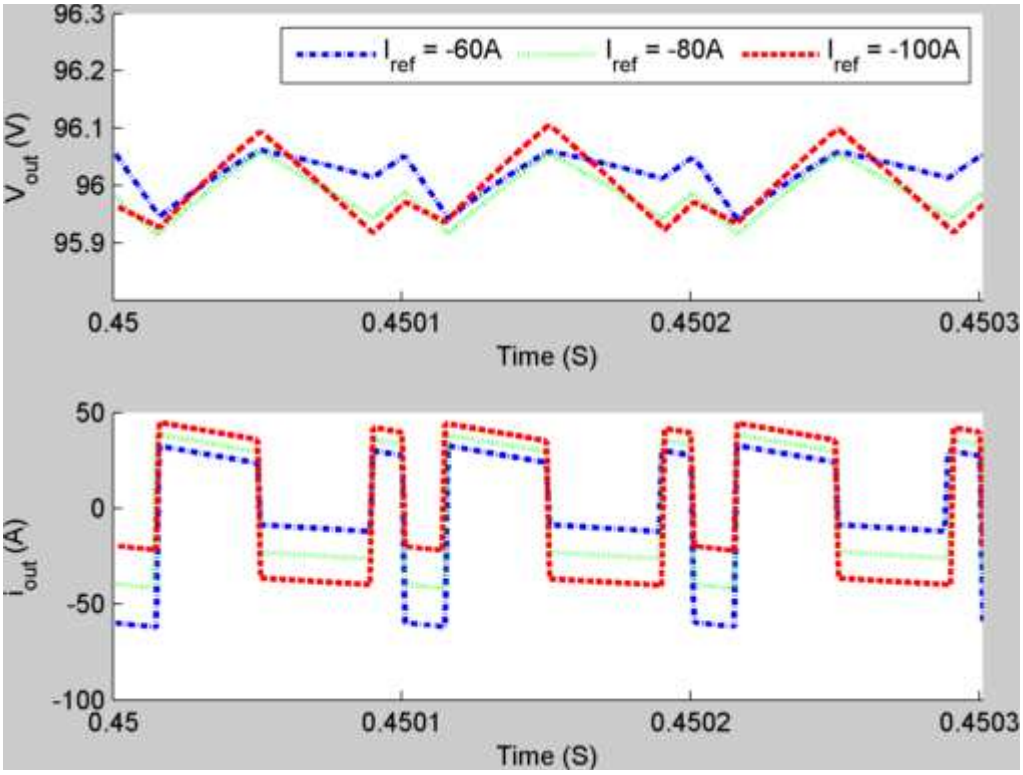

Figure 3.24: Parallel Topology - Bus Capacitor (with timing offset)

The duty cycle of each converter is defined by the ratio of output voltage over input voltage (Erickson and Maksimovic, 2001), which for the boost converter is defined as:

$$D = 1 - \frac{V_i}{V_o} \tag{3.16}$$

From equation (3.16) it will be clear that as V_i approaches V_o the duty cycle approaches 0. And vice versa, the duty cycle will approach 1 when V_i falls to a very low value. This means that the width of each pulse even when the converters are supplying the same current is different. Also, the amount of current each converter is contributing is not necessarily the same which means that at low battery current and high current from the UC the bus capacitor

responds differently to this then when reversed. The most optimum value for the delay is not just 50% (as in 2 interleaved converters from the same source) but it is a function of the ratio of input to output voltages and current contributions.

3.2.9. Summary

If the choice is made to use an UC module to supplement the power demand then the most optimum topology is the parallel topology based on the research presented here of which the advantages include:

- Individual source ripple control
- full control of the current ripple on each source independent of each other
- potential to reduce stresses for the bus capacitor under acceleration conditions

To counter the increased ripple effect in cascaded and single converters additional filtering is required, which in turn results in added weight, which is a function of the current it is required to support (Erickson and Maksimovic, 2001) (see also the Inductor on page 36). In addition, this setup sacrifices control from the batteries perspective because the battery ripple will now be a result from the total amount of power required during part of the period and the level of power contributed from the UC module during the other part. A converter would return control to the battery and allow a maximum battery current ripple to be set whereas a filter would just reduce the ripple but provide a simpler implementation. It is interesting to note that the inductor ripple current is not related to the ripple as experienced by the battery. The battery ripple is directly related to the amount the UC module is expected to support, which thus affects the size of the required filter: i.e. if the support required from the UC module is high the filter required needs to be able to filter these higher value peaks.

Another drawback found in the cascaded topology is that the bus converter has to be designed for peak current under all conditions (see equation (3.17)) compared to the parallel converter where each individual converter can be designed for a combined peak current, this is shown in equation (3.18).

$$I_{dem} = I_{L1max} \tag{3.17}$$

$$I_{dem} = I_{L1max} + I_{L2max} \tag{3.18}$$

The battery converter could be designed for cruising power, which would still be less than maximum allowed peak power while the UC can then be designed to supply the remaining power demand. This would keep the converter design smaller and lighter. This is further described in Kok et al. (2014). The results shown here also show that the novel design shown in chapter 2.8 Topology Comparison is likely not the best candidate due to ripple effects seen by the battery. This topology is not further investigated in this thesis because the ripple experienced by the battery would result in direct effect of battery aging, which would result in direct capacity loss and thus be a direct contradiction to the goal that is to be achieved; improvement of efficiency. The use of the cascaded structure would result in a ripple as seen by the battery which would be a function of the UC contribution, as explained in 3.2.1 Topology selection based on Battery current ripple (page 81). The effects of free flowing currents through the diodes would contribute to any ripple effect.

3.3. Chosen Topologies

The topologies chosen for simulation are shown in Figure 3.25 of which Topology 1 will serve as the baseline reference; Topology 2 is a reference for effects of current increase as seen by the battery as a result of using a converter; Topology 3 and 4 are chosen based on the research which suggests

these are the most likely candidates for future use in BEVs. The difference in efficiency will be a factor in deciding which topology is considered best.

Each topology will be simulated over four drive cycles in order to compare the performance of both the topologies and the PEM strategy. The performance improvement indicators will be: efficiency, weight, volume, cost and life span of the battery pack.

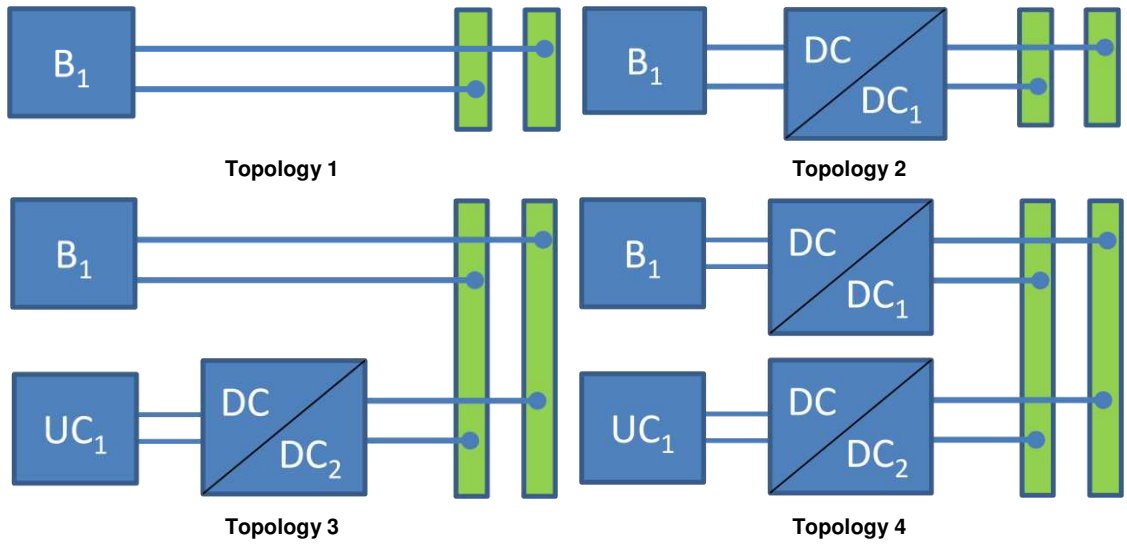

Figure 3.25: Topologies in Simulation

Topology 1: Battery only

Topology 2: Battery with Converter

Topology 3: Battery with UC Module

Topology 4: Battery with Converter and UC module (parallel)

3.4. Battery Efficiency - Rate capacity effect

3.4.1. Rate Capacity effect – constant current discharge

The rate capacity effect is visible in both lead acid and lithium-ion batteries (Doerffel and Sharkh, 2006). This makes the choice of allowed current demand a feature for trade-off in battery pack design. The rate capacity effect of high pulsed currents demand affects batteries more than equivalent constant current discharge (Donghwa et al., 2011) and the effects seem to be non linear, which

means that at lower levels and reduced pulses the available energy remains at highest level. For use in simulations it would be useful to know how the rate capacity effect changes under different current demands and whether this can be transferred across different batteries.

In order to gain a better understanding of the benefits of peak power reduction various constant current discharge tests were undertaken at the University of Sunderland. Two different batteries were repeatedly charged to full and then discharged using different currents. Two types of battery (90Ah and 130Ah) are used and are further described in Appendix 5.

Equipment

The equipment is supplied by MDL technologies (www.mdltechnologies.co.uk) and is comprised of:

- Chroma Programmable DC Electronic Load (63205)
- Chroma Programmable DC Power Supply (62100H-30)
- Chroma Battery Charge / Discharging software
- Datum XL100 Data logger for temperatures

The results of the different tests are shown in the figures below. The maximum discharge current possible was 180A. The tests were repeated with different batteries; with each test consisting of 22.5, 45, 90, 135, and 180A discharge rate. The results were averaged and plotted (Figure 3.26 - 3.27).

The standard deviations of all tests (Appendix 11) were found to lie within a 95% confidence interval from the mean value and it was concluded that the mean provides an adequate representative of the sample.

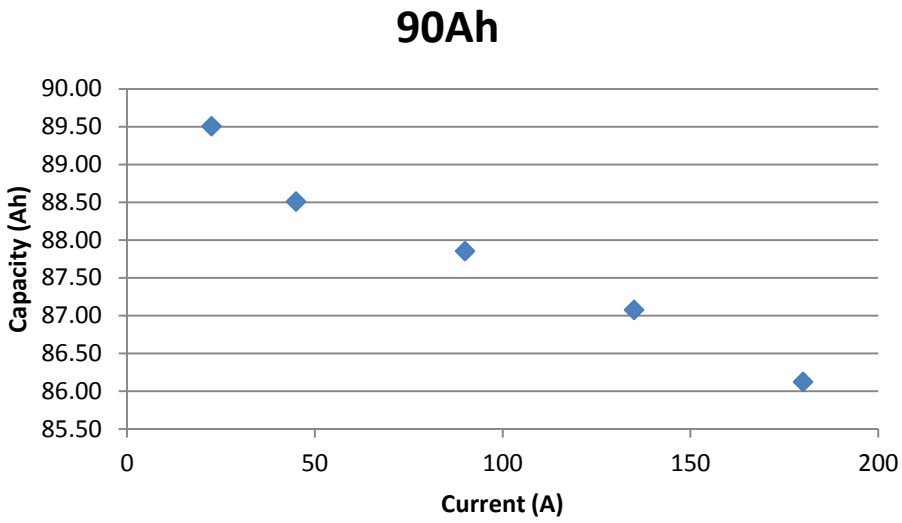

Figure 3.26: 90Ah Capacity Test

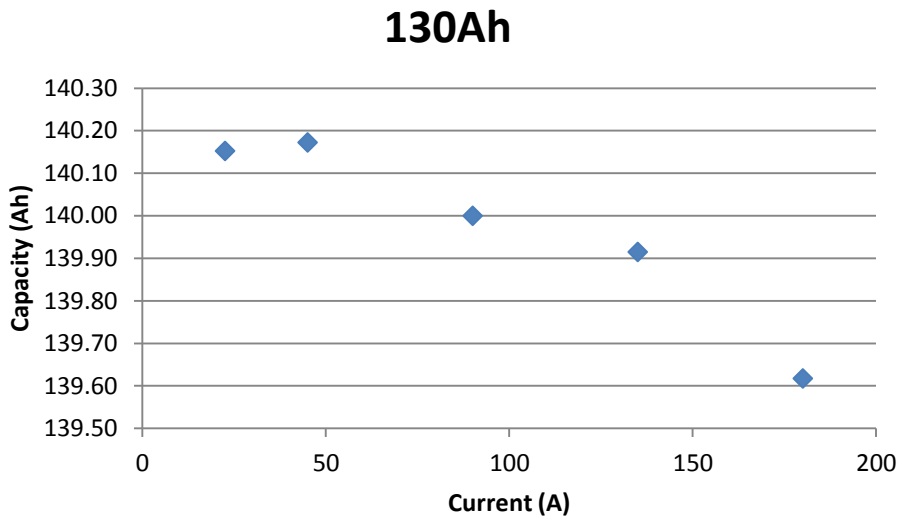

Figure 3.27: 130Ah Capacity Test

These results indicate that the savings in terms of capacity are not really impressive. Overall there is some improvement at lower currents but the difference between 180A and 25A discharge rate at 90Ah is only 3.37%. While for the 130Ah battery this is even less and is in the region of 0.5%.

The current discharge values were then multiplied with their accompanying voltage level and normalised on an hourly rate. The results are shown in Figure 3.28 and 3.29 .

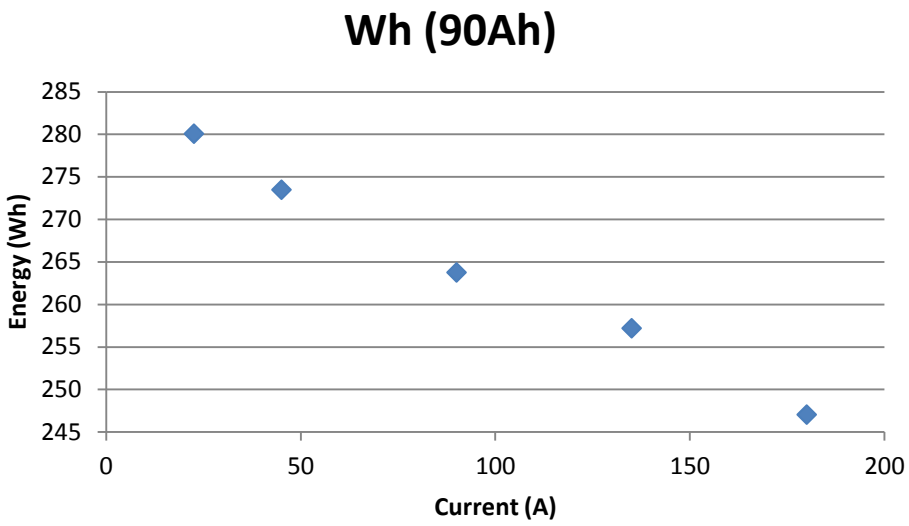

Figure 3.28: 90Ah Energy rating

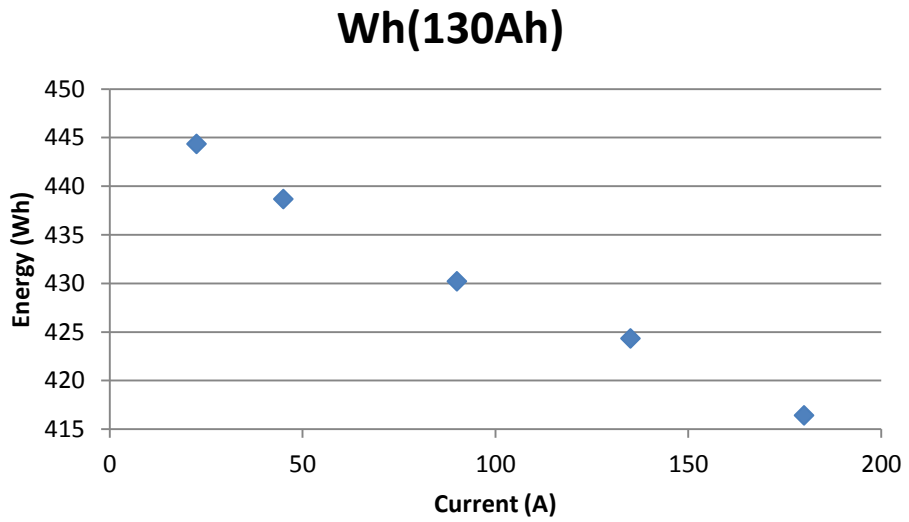

Figure 3.29: 130Ah Energy rating

At a lower discharge current the battery voltage remains higher which results in a high energy output. The data was then plotted on a C-rating scale and normalised, which then allows comparison between different batteries Figure 3.30. From (Donghwa et al., 2011) a data set for a 350mAh battery was retrieved. The data was presented in a C rating of 1 up to 6. For each battery a third order polynomial was derived based on the C-rating – Energy plot and then the polynomials were normalised and plotted on a range of 0 to 2C which

is shown below. Despite coming from different batteries (different C-ratings) with each having different nominal voltages, the 3 data sets show a very close approximation to each other. The polynomial is provided in (3.19).

$$y = -3.39e^{-3}x^3 + 17.34e^{-3}x^2 - 90.53e^{-3}x + 1 \quad \textbf{(3.19)}$$

Where y is the normalised energy output and x is the input in C-rating. The normalised energy output multiplied by 100% gives the percentage of energy available from the battery.

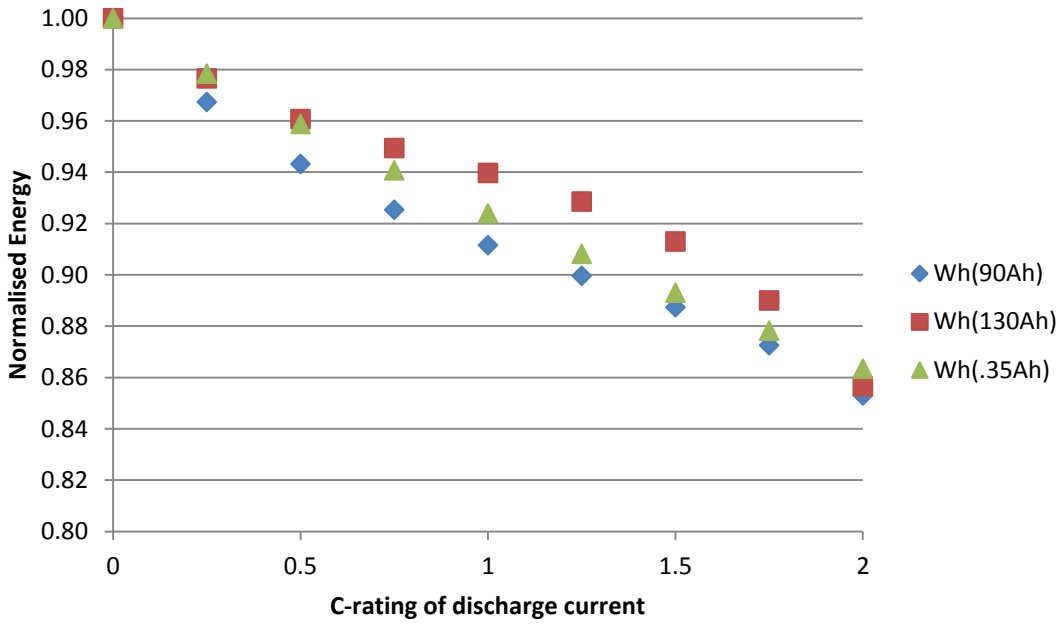

Figure 3.30: Battery test data normalised to C-rating

Since the polynomial function derived from the Donghwa et al. (2011) data is more accurate for higher ranges and the lower ranges show a good fit with the higher energy batteries this equation has been used to calculate a percentage improvement depending on discharge current. This is shown in Table 3.6. In this table each row shows the C-rating and how much energy can be retrieved (in percentage) from a battery. In the last two columns is shown how this C-rating then equates to a battery current based on the battery's Ah rating. The C-

rating is the input to equation (3.19), while the output times 100% is the percentage rating. Figure 3.31 shows the graph of the efficiency polynomial.

Table 3.6: Efficiency based on equivalent current

		Equivalent Current	
C rating	**Wh(%)**	**90Ah**	**130Ah**
0	100.00%	0	0
0.25	97.84%	22.5	32.5
0.5	95.88%	45	65
0.75	94.07%	67.5	97.5
1	92.40%	90	130
1.25	90.82%	112.5	162.5
1.5	89.31%	135	195
1.75	87.83%	157.5	227.5
2	86.35%	180	260
2.25	84.84%	202.5	292.5
2.5	83.27%	225	325
2.75	81.60%	247.5	357.5
3	79.81%	270	390
3.25	77.86%	292.5	422.5
3.5	75.72%	315	455
3.75	73.36%	337.5	487.5
4	70.75%	360	520

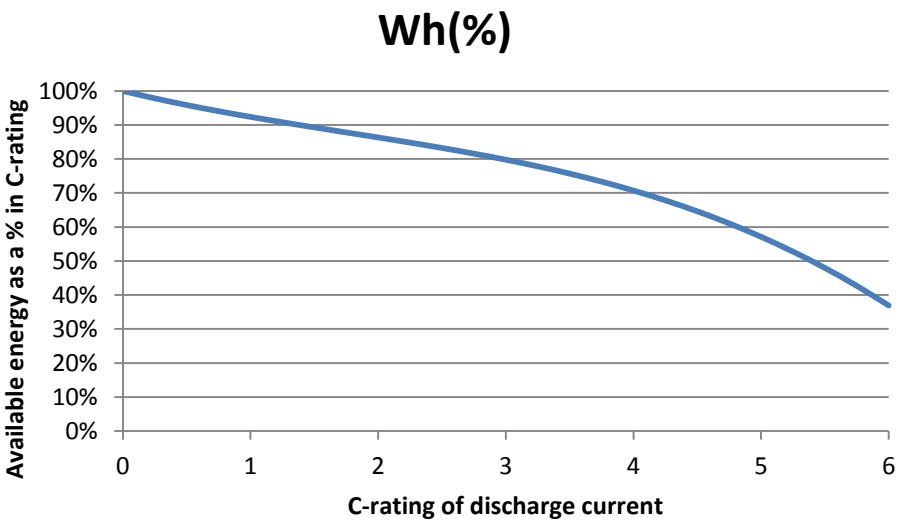

Figure 3.31: Battery Energy efficiency based on C-rating

Miller et al. (2009a) states that batteries prefer a C rating discharge of 2C or less; above this value there is increased temperature development. The difference between a 2C and a 0.25C discharge for any battery – according to the equation (3.19) is: 11.49%.

During operating conditions the current should be kept as low as possible since this provides the highest voltage level of the battery and thus the most energy from the battery. The reduced current results in reduced heat development which results in lower rate of temperature increase which allows for improved control to avoid overheating of the battery pack which is a main cause of aging and thus this would improve the live span of the battery (Lacey et al., 2013, Wang et al., 2014). Under cruising conditions the battery current should not exceed its 2C rating.

3.4.2. Rate capacity effects – pulsed discharge < 1C

It often seemed that the UC module was designed and controlled to supply the whole peak current from standstill as well as being the first to respond. To test the effect of current slopes on the capacity of batteries the following tests were conducted on a 90Ah battery, see Figure 3.32-3.34:

- Test 1 - Period of 20 second with a 50% duty cycle, peak current at 80A, no slope limitation
- Test 2 - Period of 10 seconds with a 50% duty cycle, and current slope limitation of 80A/s
- Test 3 - Period of 2 seconds with a 50% duty cycle and current slope limitation of 80A/s
- Control - Constant current discharge of 40A

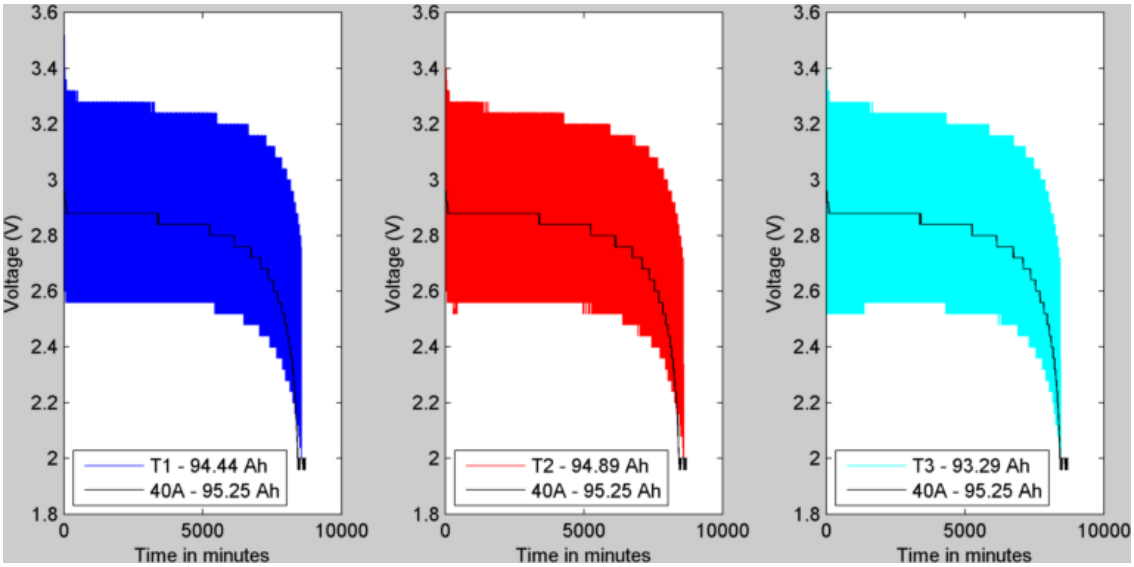

Figure 3.32: Different pulse test and the resulting capacity

Equipment

The test setup of for battery current slope testing is shown in Figure 3.33. The setup is comprised of a LD300 DC load, A DPO2014 Tektronix oscilloscope and a computer to store the recorded data. The interface for recording data is National Instruments' SignalExpress Software.

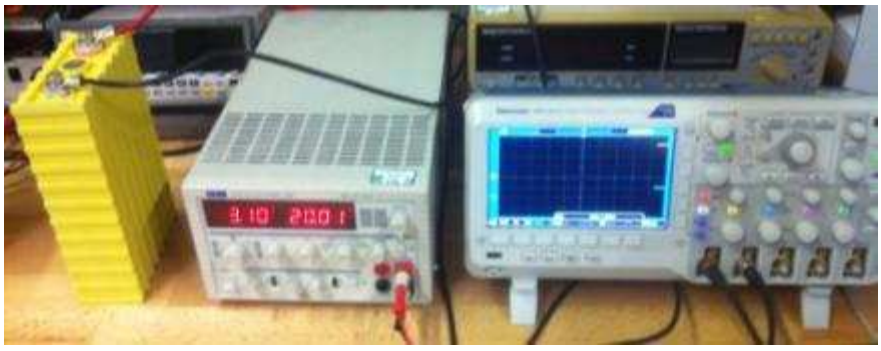

Figure 3.33: Battery test setup

Two types of battery (90Ah and 130Ah) have been tested; their respective full specifications are reported in Appendix 5.

3.4.3. Results

At 80A pulsed discharged (40A average) no significant results were found, which leads to the conclusion that while at high pulsed currents the battery suffers from rate capacity effect (Donghwa et al., 2011) this is not the case at below 1C pulsed discharge. In this test 80A pulsed with 50% duty cycle compared to 40A constant current discharge.

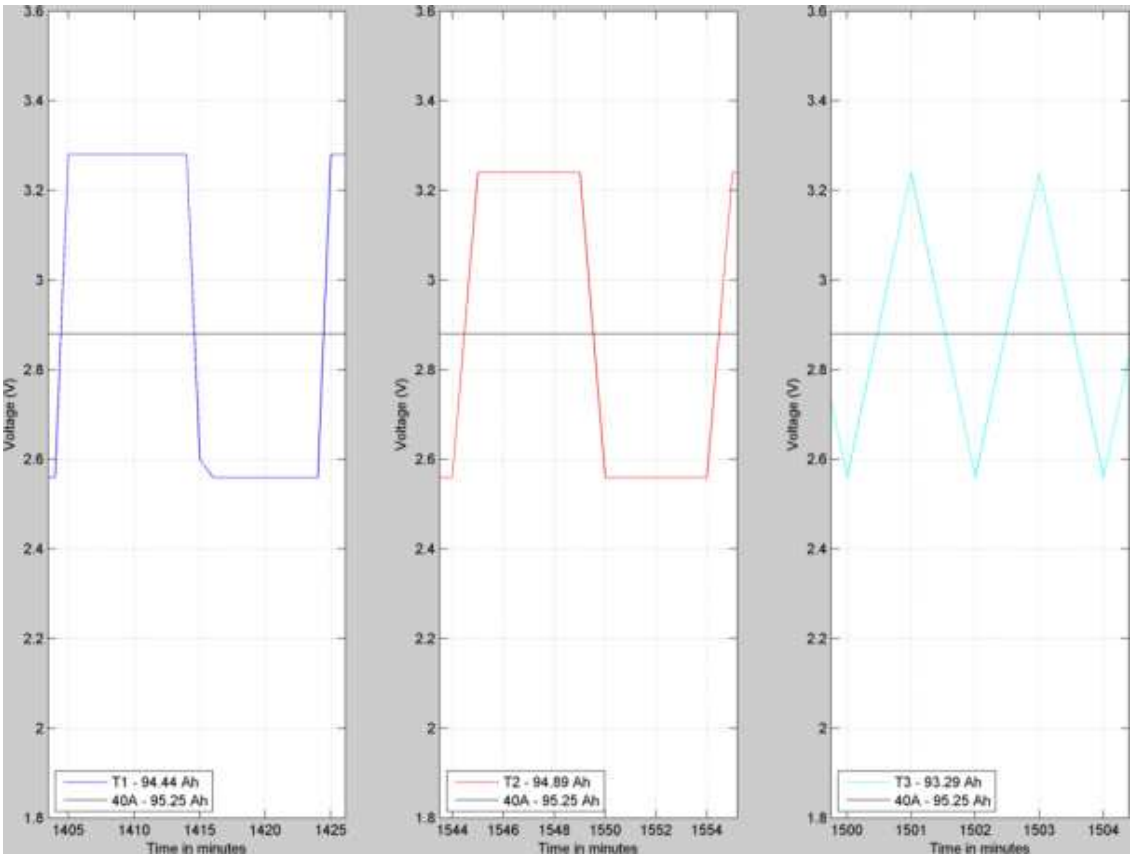

Figure 3.34: Pulsed zoom plot

This means that a battery could be the first to supply the current as long as the duration of the demand is longer than 2 seconds and the demanded current does not exceed half the battery's rated capacity. This also means that a battery and UC module could start at the same time to allow for combined peak power, which allows for the UC module converter to be designed to a lower power rating. The duration plays an important role here in that a shorter pulsed discharge could have an effect, but this can be filtered out with the use of the

UC module. For example: if the demanded current is pulsed, high and less than 2 seconds then the control should let the UC module supply the demand. The battery can then recharge the UC after the event at a) a lower averaged current and b) without ripple. This would extend the working time of the battery while the UC module reduced the peak demand. The effect where pulsed discharge and constant current are no longer similar could potentially be seen at higher currents but at the time the equipment did not allow us to investigate this.

3.4.4. Summary

Any pulsed demand current below 1C does not result in a significant difference towards the rate capacity effect, which combined with the results earlier allows for the battery to provide initial current provided this is limited (but still as low as possible) and the duration longer than 2 seconds.

The reasoning here is that immediately after an acceleration event the battery would need to supply current to the UC. The UC needs to be set at a predefined SoC in anticipation of another acceleration event. Combining the power supplied from both sources allows for a reduction in UC converter power and because of the direct support from the battery a potential reduction in size for the UC since its focus is on power supplement more than energy supplement. The proposed formula is for a period of constant discharge and is a good indicator of how efficient a battery will be for different currents on periods longer than 2 seconds.

3.5. Battery Efficiency – Under Regeneration

In Table 3.7 the differences between different drive cycles from the point of view of regeneration are shown. These drive cycles are described in full in section 3.8.2 (page 121). As can be seen from the table the total number of

regeneration events is equal across three of the drive cycles and low on the NEDC which can be expected because of the urban drive included. According to (Miller et al., 2009a) energy recovery for a battery during a regeneration event of less than 10 seconds is less than 60% effective, up to 20 seconds energy recovery will only reach up to 70% effectiveness, with energy recovered over a period longer than 20 seconds reaching around 90% round trip efficiency.

The data in Table 3.7 shows that over a whole drive cycle there are limited regeneration moments that last long enough (>20 seconds) to achieve 90% efficiency, most moments of regeneration are very short and below 10 seconds. For the two eco-drive cycles the energy recovered was calculated (not round trip but what the sensors reported was returned to the battery) and the values for ECOn and ECOp were 1111 kWs and 1100 kWs, respectively. This is a small difference and seems to suggest (the sample size is only two people) that the gain in energy between the two driving styles is largely due to the acceleration and vehicle speed; i.e. the most important aspect of the driving style is the current leaving the battery. While the amount of regeneration supports longer driving by recuperation of energy per person the difference is marginal. More in depth study is required in this area since it is not the focus of this thesis. The data suggest that the most number of regeneration events last less than 20 seconds and account for most of the regenerative energy available for recovery. As the average duration of all combined regeneration events is less than 10 seconds, the efficiency factor for regenerative energy will be set to 60% for analysis purposes.

The energy the battery stores (E_{stored}) is calculated based on how much energy is supplied ($-E_{bus}$) and the inefficiencies of the storage process and the

converters. If the energy is stored in the battery than the equation is provided in (3.20):

$$E_{stored} = -E_{bus} \cdot \eta_{batt} \cdot \eta_{conv} \quad \textbf{(3.20)}$$

Where η_{batt} the battery efficiency under charging is conditions less than 10 seconds (60%) and η_{conv} is the battery converter efficiency (95%) if applicable.

Table 3.7: Moments of Regeneration

	NEDC		NYCC		ECOn		ECOp	
		kWs		kWs		kWs		kWs
Moments of regeneration	18		41		41		41	
Total regeneration (time in s)	178	433	151	224	281	1111	294	1100
Duration of Drive Cycle (s)	1220		599		894		954	
Percentage time regen (%)	14.59		25.21		31.43		30.82	
Regen moments T >= 20 (s)	1	178	0	0	2	148	2	171
Regen moments T >= 10 < 20 (s)	8	146	2	26	7	452	11	589
Regen moments T < 10 (s)	9	109	39	198	32	511	28	339
average time (s)	9.89		3.68		6.85		7.17	

3.6. UC Module and Converter Efficiency

Next the efficiency of the UC module needs to be established as well as operating limitations.

Assuming the UC starts each drive cycle empty and requires charging from the start the UC module has 2 operating modes - the assumption is that the energy content of a charged UC pack does not contribute significantly to the driving range which in the proposed design the total energy of the UC pack would be around 1% of a 24 kWh pack:

- Recovery from regenerative conditions
- Charging from battery (top up)

During conditions where the UC is recovering energy from the bus, the current travels from the bus through the converter to the UC and afterwards back out from the UC through the converter results in equation (3.21). This equation describes a value for round trip efficiency: energy received * energy supplied

$$\eta_{mod} = \eta_{uc-in} \cdot \eta_{uc-out} \cdot \eta_{conv}^2 \quad \textbf{(3.21)}$$

The following assumption is made, because converters have reported efficiencies between 98% and 92%, an average of 95% has been chosen for simulation purposes (Miller et al., 2007, Ibanez et al., 2012).

The UC efficiency is split between recuperation / charge (η_{uc-in}) and discharge (η_{uc-out}). The discharge efficiency has been calculated to be 92% @ 62.5 V for 394A. A current of this magnitude would exceed the rated current of the capacitor. At lower 59.8V and 161A the efficiency is 95%. This means three strings of UCs are needed to achieve efficiency at the higher current. The calculated efficiency is in line with Fuyuan et al. (2010) who also show the UC regeneration / charge efficiency has the same efficiency level. Thus the efficiency calculation can be simplified to:

$$\eta_{mod} = \eta_{uc}^2 \cdot \eta_{conv}^2 \quad \textbf{(3.22)}$$

In the proposed setup the voltage is allowed to fall further but this should only happen (and at the maximum allowed current) in very rare occasions and with limited duration. The calculated value for UC Module round trip efficiency, the efficiency is: $0.95^2 * 0.92^2 = 0.76$ which is higher than the efficiency as seen by the battery at rates less than both 10 and 20 seconds. Thus it makes sense to design the system such that no energy will be recovered in to the battery if it can be avoided. In the simulations the UC will have its internal resistance modelled as part of the simulation but the efficiency is not included in the models.

It is suggested that an UC with converter should maintain an efficiency of greater than 92% (Miller, 2007b). This means a charge – discharge (round trip) efficiency of 84.6%. At high currents and low voltage this has already been proven to be difficult. This provides another reason to keep the UC voltage high: at low UC voltage the current needs to be higher from the battery to prepare the UC for another acceleration event compounding the inefficiencies of the system. Being able to delay the moment that the battery current reaches its maximum is thus also a desired feature in the energy management system.

The converter efficiency under previously calculated lowest UC efficiency should thus be 96.8%. Obviously the round trip efficiency will be impacted by the actual current drawn or supplied: at high currents the efficiency of the converter is lower as well. The converter efficiency for analysis will be set to an average of 95%.

3.7. Efficiency Analysis

From an efficiency perspective the bus will be used as reference. Since the simulations have been completed all the recorded variables should result in a stable bus voltage and equilibrium in current in and out.

The energy seen at the bus from the battery is calculated through:

$$E = \sum (P(i) + P(i) \cdot (1 - \eta_{bat} \cdot \eta_{conv})) \quad \textbf{(3.23)}$$

Where E is the energy used by the bus, $P(i)$ is the power as seen by the battery at 1 second interval (drive cycle interval), η_{bat} is the efficiency function which outputs the efficiency based on the current drawn and η_{conv} is the battery converter efficiency value if applicable. The converter efficiency is one if no converter is present.

The battery discharge efficiency has been included in this equation because it will provide an improvement with the proposed Power and Energy Management strategy. This improvement is expected to be offset against the introduction of the converter in line with the battery. Since the battery benefits from not having to supply peak demand the assertion is that the overall efficiency is higher: this provides an efficiency improvement from the battery perspective resulting in more energy where a non optimised system would have less energy. This does not include any energy recovered under regenerative braking. The energy recovered under braking will be set at 60% as discussed earlier.

From a similar perspective the energy supplied to and retrieved from the UC is calculated in round trip efficiency:

$$E_{uc} = \sum (P_{uc}(i) * \eta_{mod}), \qquad I_{uc} < 0 \tag{3.24}$$

Where $P_{uc}(i)$ is the power recovered from the bus in to the UC at 1 second intervals.

In order to test the hypothesis that an optimised power and energy management strategy can result in drive train downsizing a test metric has been developed that states that the total efficiency as seen by the bus is equal or higher than the efficiency as seen by the baseline measurement. In other words, the introduction of converters and UCs should improve the overall efficiency; resulting in current drawn from the battery at higher efficiency through the use of the UC module.

3.8. Simulation setup

3.8.1. Introduction

For the final simulation it was chosen to use a technique called forward inverse dynamic (Froberg and Nielsen, 2008). A drive cycle is used to create a power

profile which is then supplied as an input to a Simulink model. In the Simulink model the power demand is divided by the bus voltage to provide the current reference for the Current Controlled Source which is used to represent the bus demand. In this way the focus of the simulation is on the energy and power sources and the combining power electronics. The disadvantage of this approach is that any demand exceeding a designed maximum still need to be matched to avoid the bus to collapse. In converter / inverter design a limit would often be included in the maximum allowed power. In our simulations the assumption is made that the converter can handle any demand as seen by the bus. While this may not be entirely accurate it is in line with the design philosophy that the drive ability should not be compromised. This chapter explains the setup in detail of this simulation setup.

3.8.2. Drive Cycles used in Simulation

The different topologies will each be simulated over four different drive cycles, shown in Figure 3.35 - 3.38. The first two drive cycles represent urban and city driving respectively.

- New European Drive Cycle (NEDC)
- New York City Cycle (NYCC)

The NEDC is a drive cycle consists of 3 different accelerations. This is repeated 4 times after which a longer period of acceleration to higher velocities is done. The cycle represents urban and extra urban driving. Its maximum velocity is 120 km/h and it is the longest of the chosen drive cycles at 1220 seconds.

The NYCC represents city driving. It is characterised by a variety of sharp acceleration and deceleration moment. The achieved top speed is 50km/h and with 599 seconds it is the shortest drive cycle.

The third and fourth chosen cycles are real life recordings of two participants from a different study. The data from this study by Knowles et al. (2012b) was analysed for the best and worst lap in terms of total energy use, duration and acceleration and deceleration.

- Standard Lap non eco (ECOn)
- Standard Lap eco (ECOp)

The standard lap was 11.5km long. The main details are provided in Table 3.8.

Table 3.8: Standard Lap data summary

Driver	Energy (kWs)	duration (sec)	Max $\frac{m}{s^2}$	min $\frac{m}{s^2}$
ECOn	6535.38	863	2.24	-3.58
ECOp	4553.45	923	1.79	-2.24

The speed profile and calculated power profiles are shown in Figure 3.35 - 3.38. Interestingly despite the same distance the difference in energy between ECOn (6535 kWs) and ECOp (4553 kWs) is 1982 kWs which means the ECOn driver required 30% more energy.

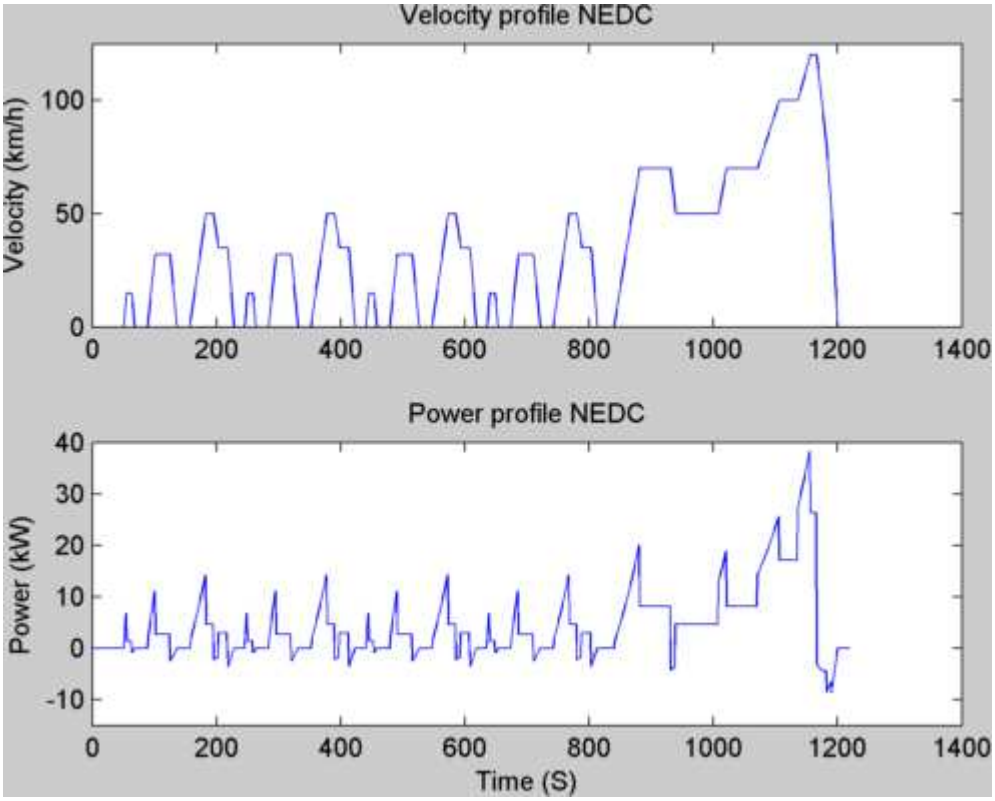

Figure 3.35: NEDC: New European Drive Cycle

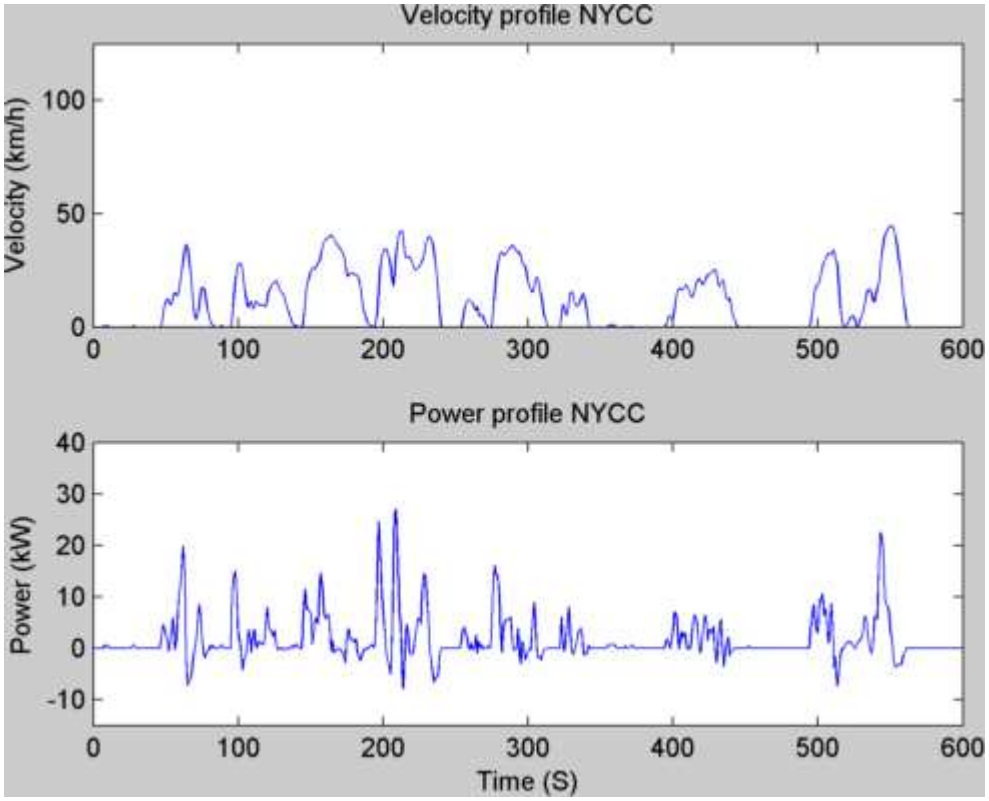

Figure 3.36: NYCC: New York City Cycle

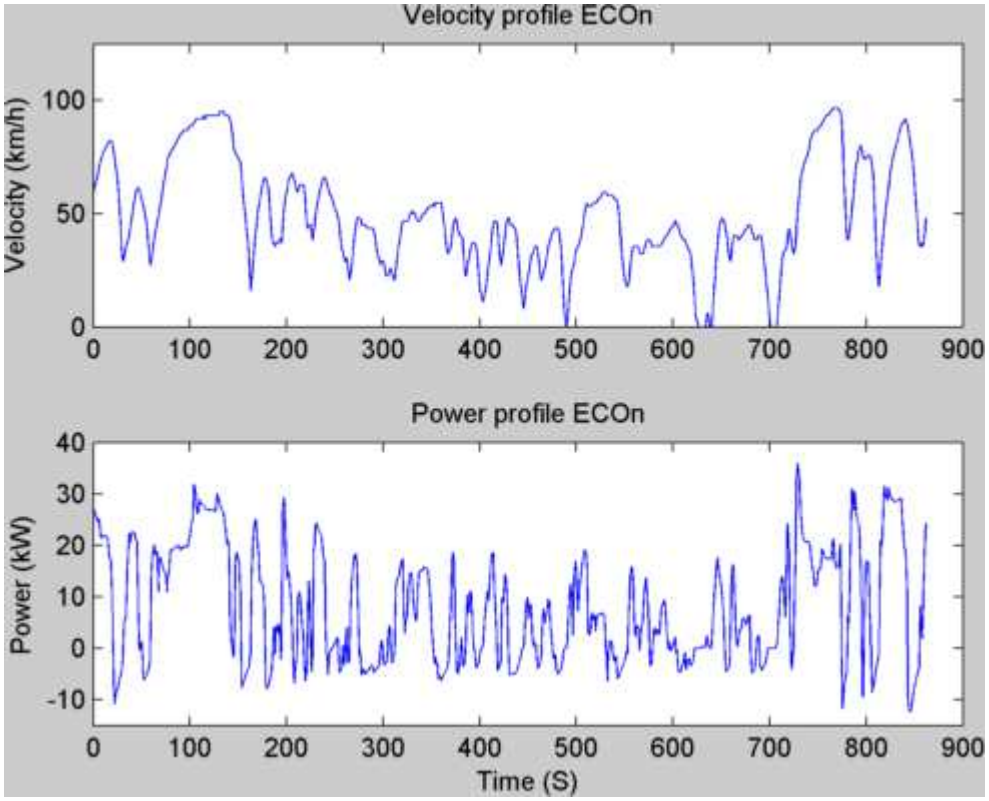

Figure 3.37: ECOn: ECO negative drive cycle

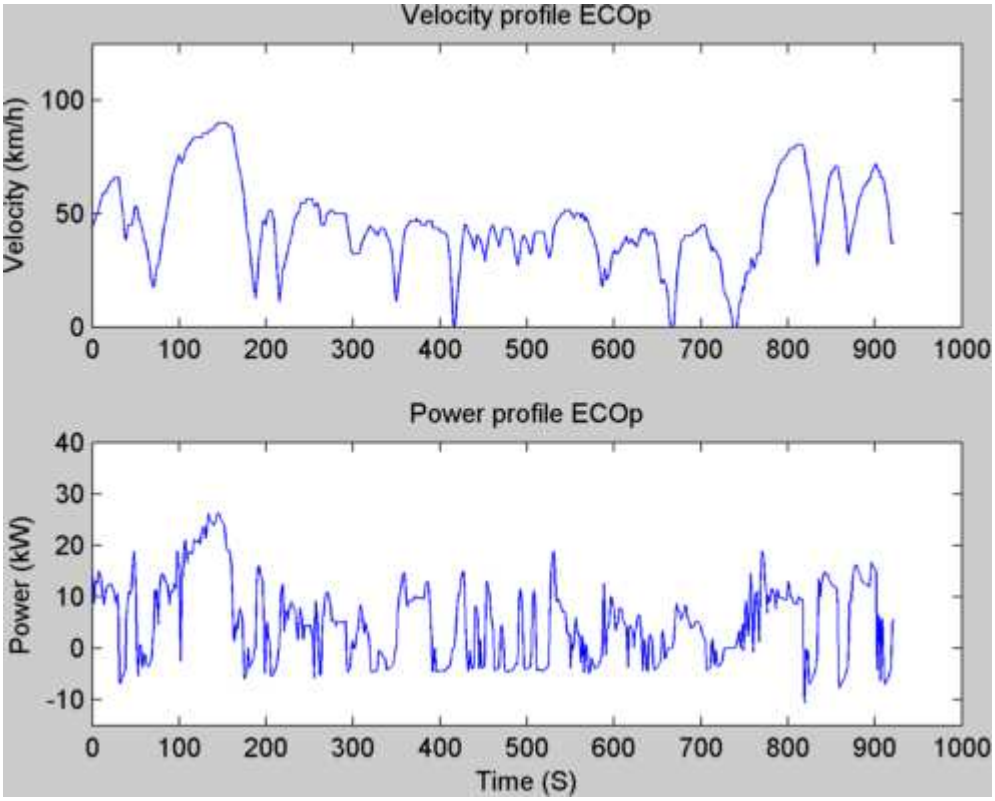

Figure 3.38: ECOp: ECO positive drive cycle

3.8.3. Vehicle

The forces working on a vehicle are well described by - for example Larminie and Lowry (2003) - and the basic equations are give here:

The necessary propulsion force (or tractive effort) is calculated through the following equation:

$$F_{\mathrm{te}} = F_{rr} + F_{\mathrm{ad}} + F_{\mathrm{hc}} + F_{\mathrm{la}} \cdot 1.05 \quad \textbf{(3.25)}$$

Where the individual elements of the equation are given below:

$$F_{rr} = \mu_{rr} \cdot m \cdot g \quad \textbf{(3.26)}$$

F_{rr} represents the force through rolling resistance and its components are : the rolling resistance coefficient (μ_{rr}), the mass of the vehicle (m) and g, the gravitational constant. The aero dynamic drag is defined as:

$$F_{ad} = \frac{1}{2} \cdot \rho \cdot A \cdot C_d \cdot v^2 \quad \textbf{(3.27)}$$

Where ρ is the air density, A is the frontal surface area of the vehicle, C_d is the drag coefficient and v is the velocity of the vehicle in m/s.

The third element is the hill climbing force, which is given by:

$$F_{hc} = m \cdot g \cdot \sin(\alpha) \quad \textbf{(3.28)}$$

In which α is the angle of the slope in degrees.

The final force acting on the vehicle is the lateral acceleration:

$$F_{la} = m \cdot a \cdot 1.05 \quad \textbf{(3.29)}$$

Where a is the acceleration of the vehicle in m/s^2. And the value of 1.05 represents the inertia effort based on a percentage of the lateral acceleration (F_{la}) instead of calculating the rotational acceleration from the motor.

Tractive effort can be defined by the force delivered from the motor, through the gears. This is dependent on the gear ration (G), tire radius (r), an efficiency factor (η) and the torque at the motor (T_m):

$$F_{te} = \frac{G}{r} \times \eta \times T_m \tag{3.30}$$

Motor velocity is defined by:

$$\omega = G \times \frac{v}{r} \tag{3.31}$$

The power at the wheels (P_w) is related by the power balance equations to the power supplied by the motor (P_m) and the power supplied by the bus (P_b). In the following equations these relations are shown and efficiencies (gear system - η_g and motor and motor controller efficiency - η_m) in the transfer of the power are included.

$$\begin{aligned} P_w &= \eta_g \cdot P_m \\ P_w &= F_{te} v \\ P_m &= T_m \omega \end{aligned} \tag{3.32}$$

Power at the bus and the power at the motor are related according to the following equations:

$$\begin{aligned} P_m &= \eta_m \cdot P_b \\ P_b &= V \cdot I \end{aligned} \tag{3.33}$$

The calculations are based on a previous project where a Nissan Micra was converted to run electric. For the current simulations the battery weight plus the laden weight is set to 1200kg. The auxiliary power drain was ignored since this can be seen as a constant small drain and would not significantly affect the traction pack in terms of losses. Kessels et al. (2005) report on 2 values for

average auxiliary load demand: 250W and 500W. In context this would mean an auxiliary power drain of 500W / 96V ≈ 5A on the traction pack.

The equations (3.25)-(3.33) were used in a Matlab program to calculate a power profile from a given drive cycle as shown in Appendix 8. This information was then loaded in the workspace for use by the Simulink model.

3.8.4. Basic Simulation Layout

Figure 3.39 shows a basic simulation layout of a battery and converter setup. The bus voltage was set at 96 volt (30 cells). The number of batteries cells in a string when connected to a converter was set to 25, which results in a nominal voltage of 80V. The battery model parameters were based on TS-LFP90AHA battery (see Appendix 5) and established according to Tremblay (2009). In Appendix 9 are provided the different setup variables for the two battery strings used. The UC specifications are given in section 5.4.2 UC Module (p155). The minimum and maximum bus voltages settings are set at 72 – 125V.

The “simin” block reads in data from the workspace in the form of the power profile for a particular drive cycle. A Matlab program was written that called the Simulink model while preparing the time the model should run for and the drive cycle power profile it should use. The Matlab program can be found in Appendix 10.

3.8.5. DC-DC converter

The simulation setup of the converter in SPS is shown in Figure 3.40. The method of operation, the converter control strategy setup as well as the tuning of the control variables are described in section 2.5) DC-DC Converter.

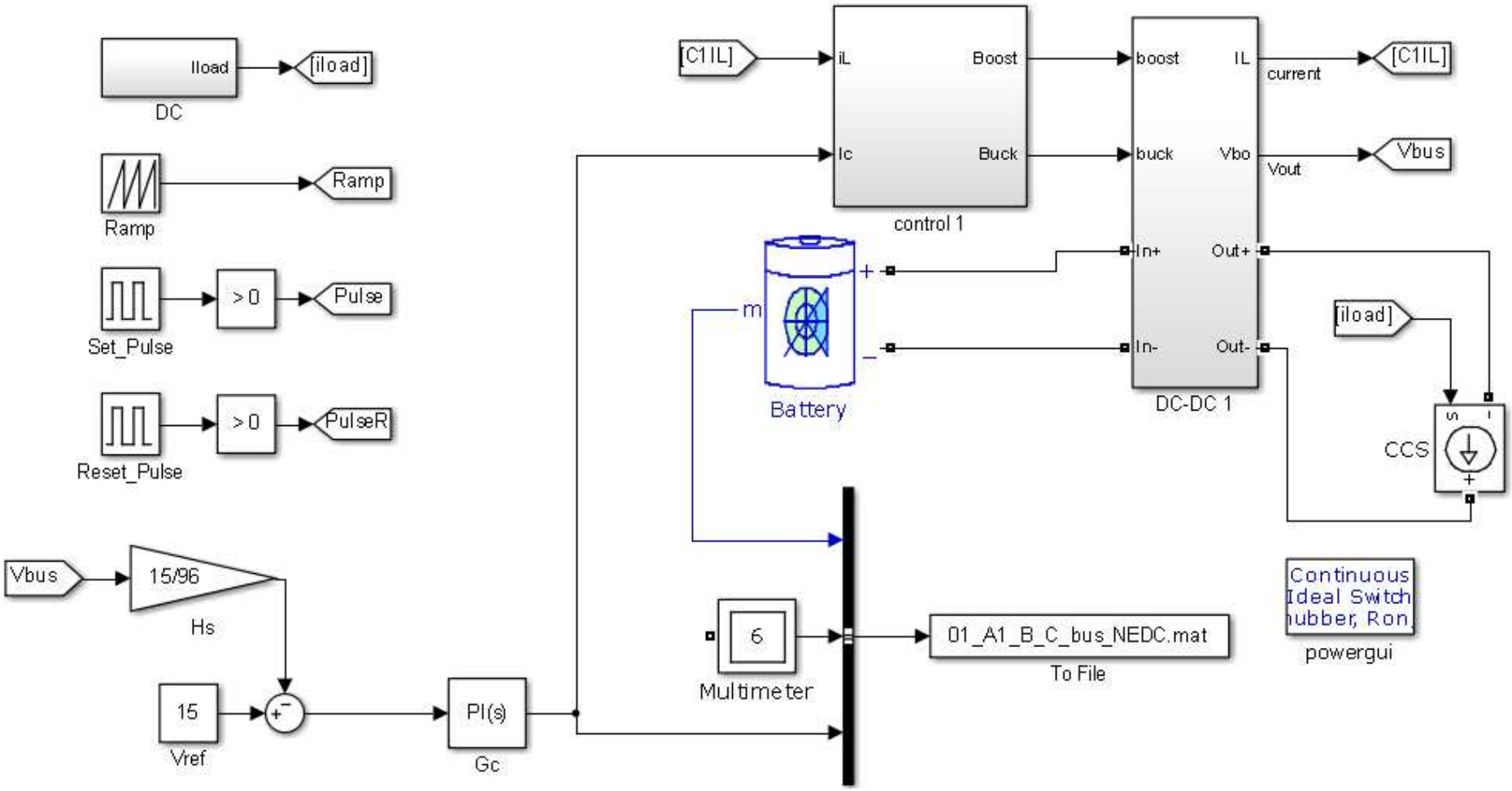

Figure 3.39: Topology 2 - Basic Simulation Layout

The switching from boost to buck state when required is achieved through the use of enabled subsystems around the different control layouts as is shown in Figure 3.41. The choice for buck or boost mode is defined by comparing the control signal from the PI controller to zero and when lower the buck mode is enabled, while when the result is higher the boost mode is enabled. The only exception is in the parallel topology for the battery control, since here the buck mode is only activated when the UC is full. Inside each subsystem the enabled port and “outport” need to reset when enabling and disabling respectively.

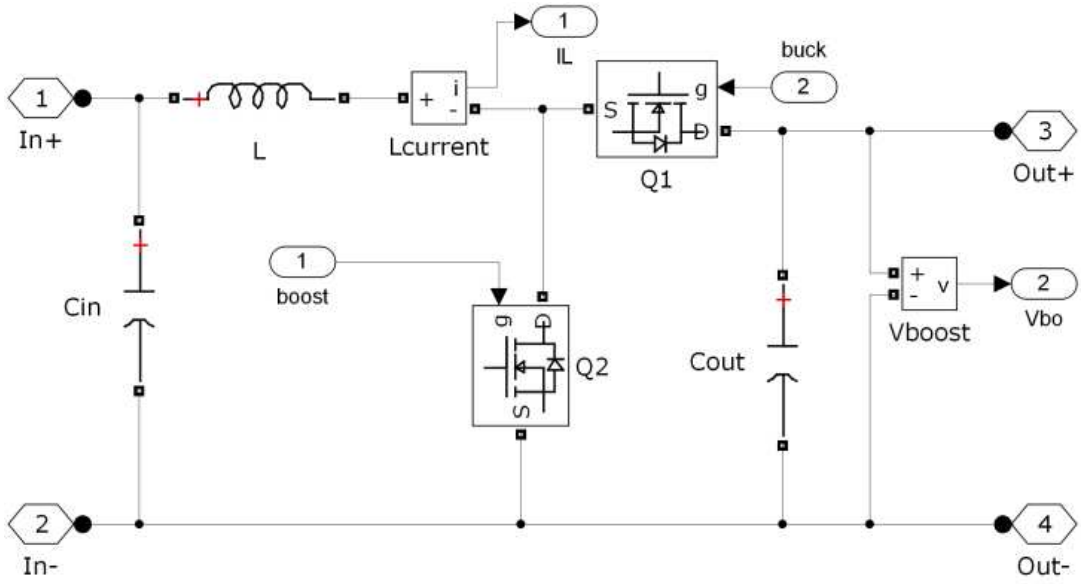

Figure 3.40: Bi-directional DC-DC Converter as modelled in SPS

3.8.6. Converter Parameters

Table 3.9 shows the parameters for the simulation of the 4 topologies identified in Figure 3.25. The parameters are established according to the formula’s provide for the inductor value for boost converter equation (2.6) which is based on the largest ratio of V_{out}/V_{in} and the allowed ripple (1A). The value for the output capacitor under boost conditions – equation (2.9) – also requires the value for bus voltage ripple, which is set at 0.48V. The input capacitor can be calculated by using equation (2.7) to calculate the resulting inductor ripple current under buck conditions using the nominal bus voltage (96V) and the

lowest output voltage (62.5V for the battery string and 50.6V for the UC string) to calculated the duty cycle. The allowed voltage ripple is set to 5% of the output voltage (the output voltage under buck mode is the input voltage for boost mode). For the converter supporting the UC a value for input capacitor was calculated based on a 5V allowed ripple. This capacitor has no influence compared to the much larger UC capacitor. The values for Ma were calculated according to equation (2.25).

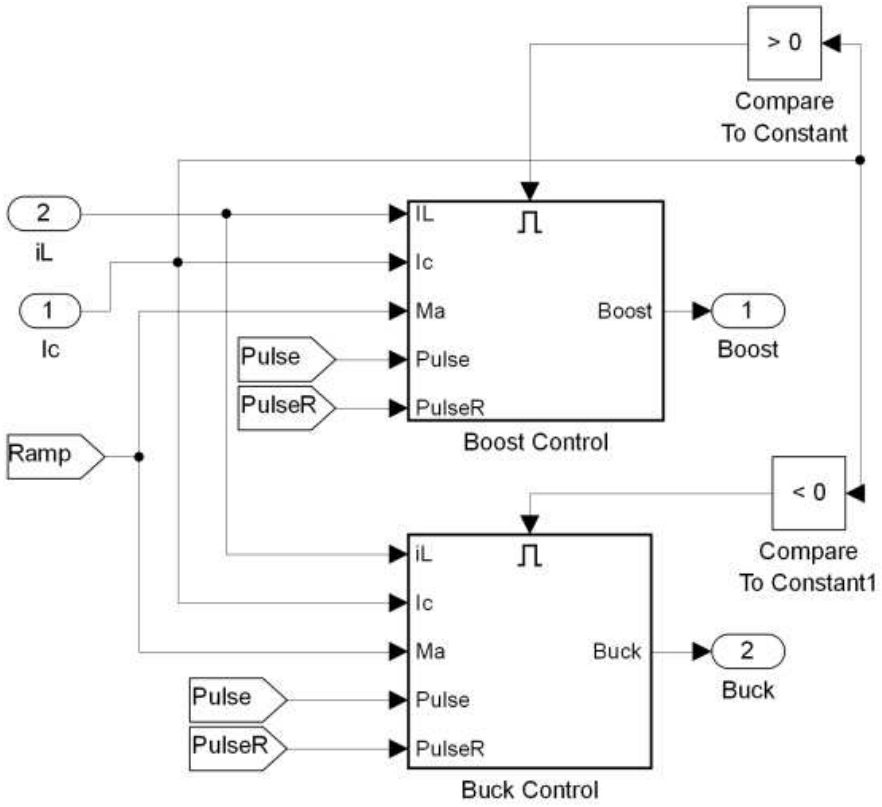

Figure 3.41: Buck - Boost selection

The converter parameters for the battery converter in Topology 4 are the same as in Topology 2 and the UC module parameters from topology 4 are the same as in Topology 3. Topology 3 does not have a voltage control loop since the battery voltage is the bus voltage. In the same table also the control variables (proportional and integral) are given as well as the stability variables. The values for the PI controller are established according to the method described in section 2.5.4 (page 41) and a stable solution was sought between the boost and

buck modes. Although converters can operate at much higher frequencies a lower frequency of operation was chosen to facilitate a fast simulation time.

Table 3.9: Simulation parameters

	Battery converter	UC Module Converter
Inductor	6.25 mH	6.02 mH
Cin	8.72 uF	7.95 uF
Cout	181 mF	172 mF
Kp	6	6
Ki	300	300
Frequency	2500 Hz	2500 Hz
Ma (boost / buck)	2 / 2	2.47 / 1.68

3.8.7. Data out

The requested output data is gathered either directly as a Simulink signal into the “Bus Creator” block or through the use of the multimeter which requires this measurement option to be activated in the converter components and CCS.

The “To-File” block gathers the data from the “Bus Creator” and outputs it as a Matlab Array file. The frequency used in the simulation can be fairly high and as a result the simulation step can be very small, which would result in a very large data file when simulating drive cycles. To this end, the “Sample Time” setting in the block is set to record at 0.1 second interval for drive cycle simulations. The reason for this is that the simulation seems to perform better. It can be set to smaller steps for testing step changes and stability issues but then simulation time needs to be limited to restrict the size of the data log.

Power Management Strategy Development

4.1. Introduction

From the literature it is clear that the addition of the converter for the battery and the UC module add a certain amount of weight without saving enough energy from the battery to justify this. Several reasons have been shown:

- Over dimensioning of the UC to capture all eventualities of acceleration
- Over dimensioning of the UC converter to achieve maximum acceleration without battery support

This resulted in the driveability being compromised because of increased weight or battery limitations. The proposed control strategy aims to reduce the size of the battery stack and size of the UC module while allowing for driveability and increasing efficiency.

In Figure 4.2 a power flow of the functional operation of the control strategy is shown. The aim of the control strategy at this point is to supplement the power demand as seen by the bus without exceeding an arbitrary value for a maximum battery current. The figure is divided in zones which explain the control principles.

4.2. Control Strategy Principles

Zone 1 - The battery is allowed a baseline maximum value at the start, since (as shown in the research) this does not affect its capacity or effect. The value for I_{bat_max} will be a controlled variable by the EMS and most likely start at zero value.

Zone 2 & 7 - Above this baseline the UC module will supplement the demanded power.

Zone 3 - Under cruising conditions the battery will continue to stay at its maximum value until the UC voltage has reached its target value then the battery current will drop to match the demanded value. As long as the target value of the UC SoC has not been achieved the battery will keep supplying its maximum value even if the demanded current has fallen to zero.

Zone 4 - Upon a regenerative event the regenerative energy is first collected by the UC module. If the UC SoC target has been reached then the battery will not supply any more current

Zone 5 - When the UC SoC has reached its maximum the battery will accept any remaining charge

Zone 6 - If the UC SoC is above its target value and an acceleration event is occurring then the UC will first supply the demanded value until target SoC is reached after which the battery is allowed to supply up to its maximum value.

The resulting control strategy is shown in Figure 4.1 for the parallel converter topology. The difference with the cascaded topology is that the cascaded topology adds the signals on electrical connection level and not in reference as in the parallel topology. The cascaded topology will not have the subtraction of the current signal from the battery reference. The functioning of this control strategy is further explained in (Kok et al., 2013b).

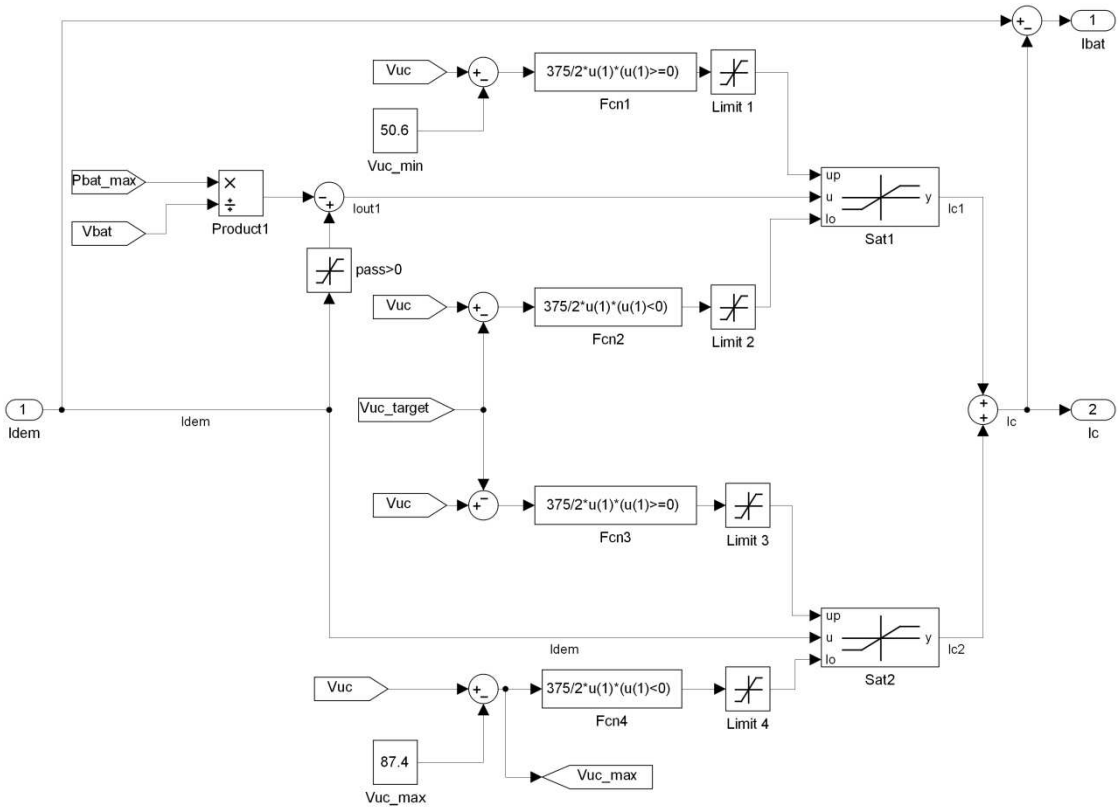

Figure 4.1: Control Strategy

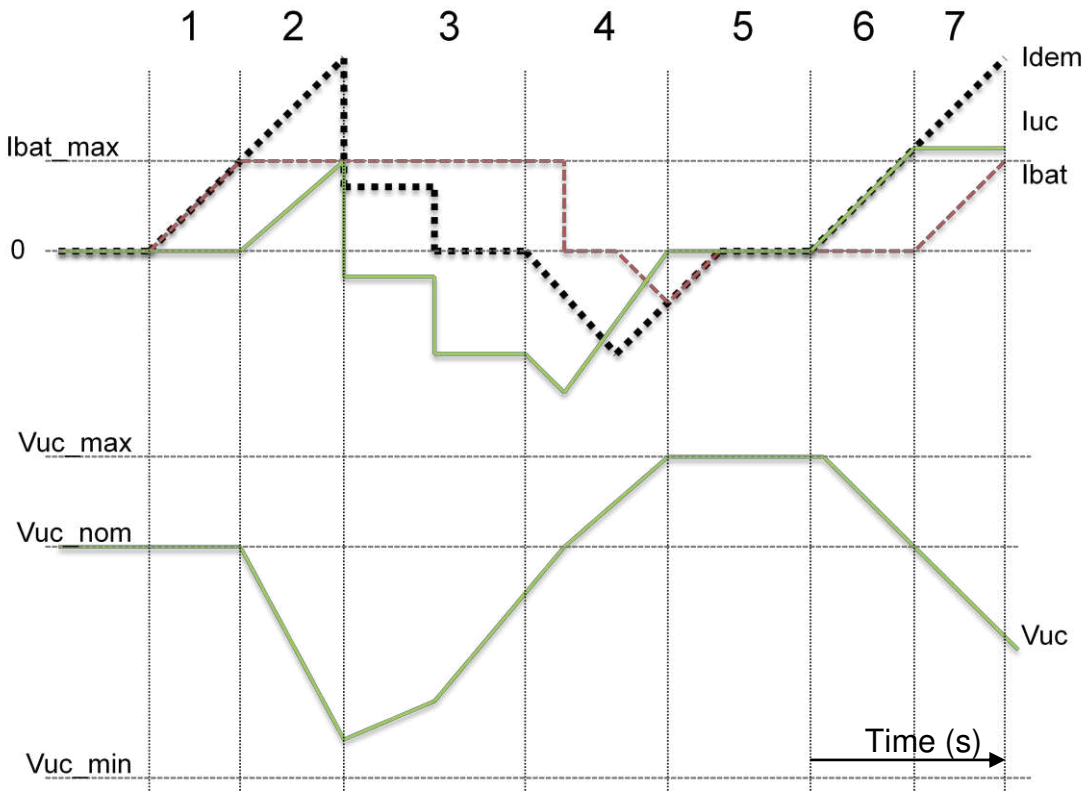

Figure 4.2: Control power flow

4.3.Control strategy

The main features of this control strategy are:

- The power split is defined as a reference value sent to the battery converter and not at the point of current combining such as in battery with UC module or the cascaded topology; this ensures the ripple of each source is individually controlled
- The power split decision is made fast and as such allows for a smaller bus capacitance by effectively combining the operational and tactical levels of control into one.
- The power split is dependent upon the amount of power available from the UC module
- If power is not available from the UC module the battery can still supply the demanded power even if the demanded power exceeds the set maximum. This allows for driveability but the occurrence of this event should be limited since it negatively affects the battery life time.

The control strategy is not intended to meet all eventualities but on prolonging the batteries' life without sacrificing driveability, while not increasing the weight of the total drive train. For example, continuous acceleration up to 120 km/h can be achieved but the final part of the acceleration will not be supported by the UC module instead the battery will take over since the UC module will not have the energy. The reason for this choice is that the battery should be able to support driveability of the vehicle.

4.4.Control limits

The amount of support the UC Module is providing is set by function (Fcn) blocks and limited by saturation (Sat) blocks as shown in Figure 4.1 (page 134) and explained here.

- Fcn1 controls the upper bound of Sat1 and is only closed when the UC is depleted. This function block controls the limit of the allowed current during acceleration events when $I_{dem} > I_{bat}$
- Fcn2 controls the lower bound of Sat1 and is dependent upon the value of the target level SoC of the UC. This function block controls the level of UC recharge during cruising conditions. If $I_{bat\_max} > I_{dem}$ and $V_{uc} < V_{uc\_target}$ then the difference between I_{bat_max} and I_{dem} is used to recharge the UC up to V_{uc_target}. If $V_{uc} > V_{uc\_target}$ then the function output is 0. The function value is set to limit the battery current. The control strategy allows the battery to keep supplying current even though a regeneration event is taking place. Combined with Fcn4 these two values work together to charge the UC to target voltage.
- Fcn3 controls the upper limit of Sat2 and operates opposite to Fcn2 in that when $V_{uc} > V_{uc\_target}$ the output is the value in the function and otherwise the value is zero. This function block is active when the UC is above its target value and thus will support the battery even if the $I_{dem} < I_{bat\_max}$. This is useful to ensure that the UC is brought to a level where any (at that moment) excess UC SoC is used first.
- Fnc4 control the lower bounds of the second saturation block (Sat2). The sum of V_{uc} - V_{ucmax} is almost always negative and thus allows for regeneration of energy into the UC until the UC is full ($I_{dem} < 0$). At this

moment the battery needs to accept the remaining regeneration energy. The “Goto block” sends a signal to the buck converter of the battery (if present) to make this happen.

The saturation blocks are controlled by the output of function blocks. The combination of function blocks and limit blocks is to limit jitter effects. Initially the difference between V_{uc} and V_{uc_target} was measured and based on this difference the lower limit of the “Sat1” block was set. But at high currents when the limit is set to zero as a result of the difference between the two values going to zero. The voltage of the UC is given according to equation (4.1). When the current is removed the value of V_{uc} will drop immediately because the internal resistance term is zero with the result that the voltage measured (V_{uc}) would drop below the target voltage (V_{uc_target}) and the limit would allow charging with high current again. To avoid this possibility a slope was introduced in the system. Now, when the difference between measured and target approaches zero the current is gradually reduced, thus eliminating jitter effects.

$$V_{uc} = \frac{1}{C}\int i_L dt + i_L \cdot R_i \tag{4.1}$$

The inclusion of the “Saturation” block (Pass>0) is to avoid the following situation:

$$\begin{aligned} -I_{bat\_max} - I_{dem} &= i_{c1} \\ -I_{dem} &= i_{c2} \\ i_c &= i_{c1} + i_{c2} \end{aligned} \tag{4.2}$$

As can be seen, in this situation a negative I_{dem} would appear twice at the exit and increase the current from the battery. The block is set to block negative signals.

The upper and lower limits are set by limiting the current as feature of protecting the electronics. Otherwise because of the power balance the current could potentially increase to unacceptable high levels.

The limits are defined by the final design for the converter in kW and the lowest operating voltage where this maximum power occurs.

$$\frac{P_{max}}{V_{op}} = I_{lim} \tag{4.3}$$

V_{op} is the voltage level at which the maximum power (P_{max}) of the converter is required. The point where this maximum power value is required is limited by the total power needed. The current limit (I_{lim}) is also subject to the efficiency of the UC operation as explained in chapter 2.

As established earlier, the maximum power of the converter has been established at 30kW which at a voltage of 23 x 3.6 = 82.8V means a current draw of 362A and higher if the voltage drops any further. Thus, under maximum power the efficiency of the system is not high enough to warrant its use or the system should have a SoC that is near the maximum voltage, which leaves little room for energy recovery.

From this it is clear that combining UC strings in parallel is necessary not only to achieve the desired energy available but also for the efficiency of the UC operation because the internal resistance of the paralleled UC strings is (assumed the internal resistances of each string are the same):

$$R_t = \frac{R_i}{n} \tag{4.4}$$

With R_t the total resistance, R_i is the individual resistance per string and n is the number of strings. The alternative is to increase the voltage level which reduces the current, but this would increase the number of cells in series and thus complicate the cell management system.

4.5.Simulation

During simulation tests of the control strategy with Topology 3 it was found that the difference between the battery reference target current and the battery current was significant. The battery current was higher than its target. This would result in the system reporting a lower efficiency than might be possible.

The reason for the difference lies in the power balance equation: with the load current as the base reference to determine the contribution of the UC module the step down in voltage of the UC is not taken in account.

The solution to this problem is to rework the PMS to use a power reference: the input is replaced with the bus power demand, the limits are set to 30kW and the power reference out is converted to a current reference by dividing with the appropriate source voltage. This solution is specific to Topology 3. Topology 4 will be simulated with the current reference because both sources are connected and controlled using a Proportional Integral (PI) loop; any mismatch in control is automatically corrected. Also, the more variable bus voltage (the bus capacitor is very small) compared to the stable battery voltage in Topology 3 result in instabilities in control since any change at the bus is transferred to the control signal

4.6.Summary

In this chapter a control strategy has been developed that ensures that each energy source is used in an appropriate manner at the correct time in order to ensure driveability, battery life and maintaining the size and weight of the energy sources within reasonable boundaries set by: I_{bat_max} and V_{uc_target}. The actual values for these parameters will be determined by the Energy Management Strategy.

Energy Management Strategy Development

5.1.Introduction

Since the power management strategy is designed to decide the power split based on two variables - the maximum battery current (I_{bat_max}) and the target Soc of the UC (V_{uc_target}) – the energy management strategy needs to set the values for these limits. The maximum battery current limit defines how much support is requested from the UC module. The UC SoC target defines how much energy can be recovered from that point and if the target is achieved how much acceleration the module can support.

The aim of the energy management strategy is to maintain a dynamic UC SoC and a dynamic current limit to smooth the battery dynamics and achieve optimum support from the UC module.

5.2.Drive Cycles

Drive cycles are lists of data points, often in 1 second intervals, representing a velocity value in time and are used to compare efficiency of PEMS in simulation and in the real world. They are useful to compare the efficiencies of different power and energy management strategies (Souffran et al., 2012).

5.3.Markov Chain Analysis

Knowles et al. (2012b) conducted a driveability study for which data was collected from a Mitsubishi iMiev electric vehicle, which was driven along a standardised route, see Figure 5.1 (the height of the polygon fence represents the speed of the vehicle during that time segment (1 second interval)).

The data from this study was analysed by the author and a Markov Chain transition matrix was developed. Markov's Chain's main property is that its next state only depends on the current state and not on its past.

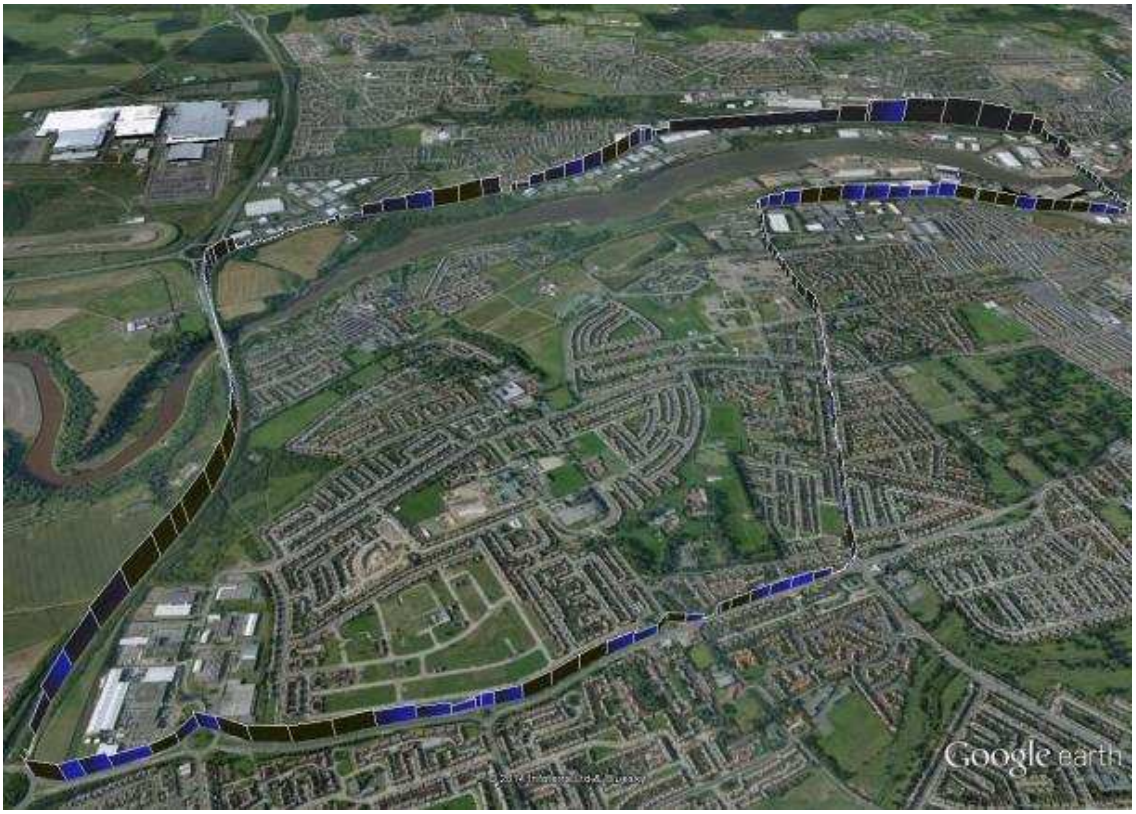

Figure 5.1: Standardised Drive Cycle Route

The recorded speed in kilometres per hour (km/h) of the 11 participants was recorded on a second by second basis. For analysis purposes the speed of each individual was rounded to the nearest 5 km/h interval. This data was read into Matlab for analysis. The Matlab program examined each column of data (each column represents the velocity of a participant during the test) and read the next velocity found from start to finish and mark every next velocity in a transition matrix to create a Markov Chain, where the rows represent the current state (current velocity) and the columns show the transition probability to achieve the next state; this is illustrated in equation (5.1).

If M is the transition matrix of possibilities then each value of the matrix is the probability (p) on achieving the next state (j) from the current state (i) (Souffran et al., 2012)

$$M = [p_{ij}]_{(i,j=1,\dots,n)} \tag{5.1}$$

Where:

$$p_{ij} = P[S(t+1) = Sj | S(t) = S_i] \tag{5.2}$$

In figures this looks like this, where the current and next state are given in km/h.

		Next State (Speed in km/h)				
		0	5	10	...	125
Current State (Speed in km/h)	0	i_1j_1	i_1j_2	i_1j_3	...	i_1j_{26}
	5	i_2J_1	i_2j_2	i_2j_3		
	10	i_3j_1	i_3j_2	i_3j_3		
	⋮	⋮			⋱	
	125	$i_{26}j_1$				$i_{26}j_{26}$

Probability (P_{ij}) **(5.3)**

Figure 5.2 shows two plots which show the relation between current state and next state with the colour map representing the value of the location at p_{ij}. In the figures the probability of transition from – current state - 125 km/h to – next state- 120 km/h equals 1 and there is no transition from 125 km/h to 125 km/h, which is caused by the small sample size and the limited top speed of the vehicle. There only was 1 person who achieved 125 km/h and that velocity was not sustained for longer than 5 seconds.

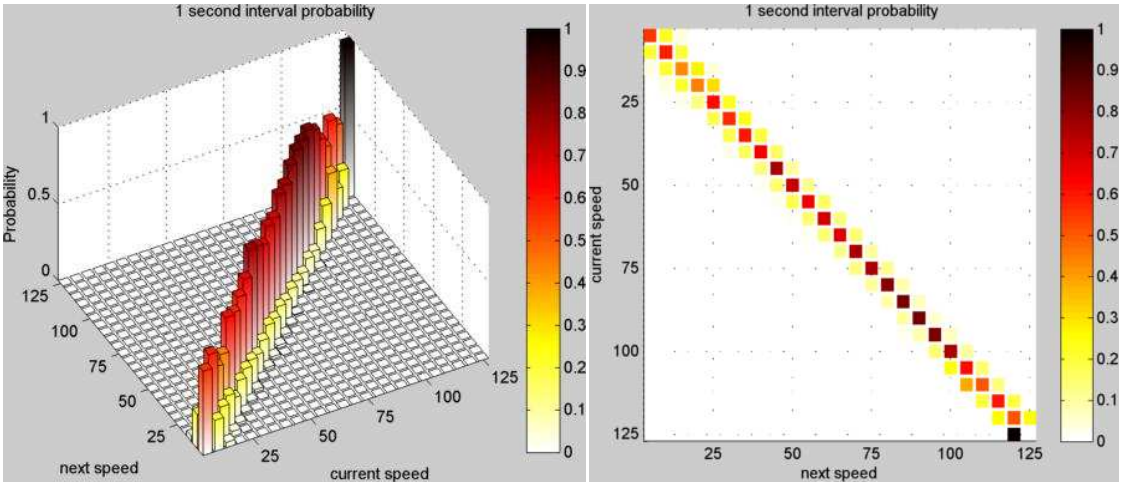

Figure 5.2: Transition Matrix plot

a - bar view

b - top view

Through the use of the transition matrix the probabilities were calculated at 5 second intervals as shown in Figure 5.3 where a sample collection is shown.

It can be seen that over time there is a development of maximum value lines appearing through the matrix, which indicates that starting –for example- at anywhere between 25 and 60 km/h the next velocity will be approximately 45 km/h. This trend is already visible at 20 seconds.

From this can be concluded that from an initial velocity the vehicle is likely to end up at a different target velocity after a certain amount of time. This information will allow us to slowly increase the battery supply over the set period of time while the peak demand is dealt with by the UC modules.

As mentioned in the literature, it is required that the SoC of the UC module is controlled in preparation of another acceleration or deceleration event. This SoC control on one hand happens through regenerative events and on the other hand by increasing the battery power demand, but this needs to be limited because any higher power demand than required for cruising conditions looses the battery pack valuable energy.

While it is clear from Figure 5.3 that the highest probability results in a target speed value the probability of achieving that value is dropping fairly quickly – from 50% at 5 seconds to 25% at 20 seconds which means that at 20 seconds there a 75% chance that this value is not achieved. The effect is of this remaining percentage results in a bias towards either a probability of velocity reduction or acceleration. Any current state resulting in a lower next state is indicative of a braking probability while when the next state is higher this is indicative of an acceleration probability.

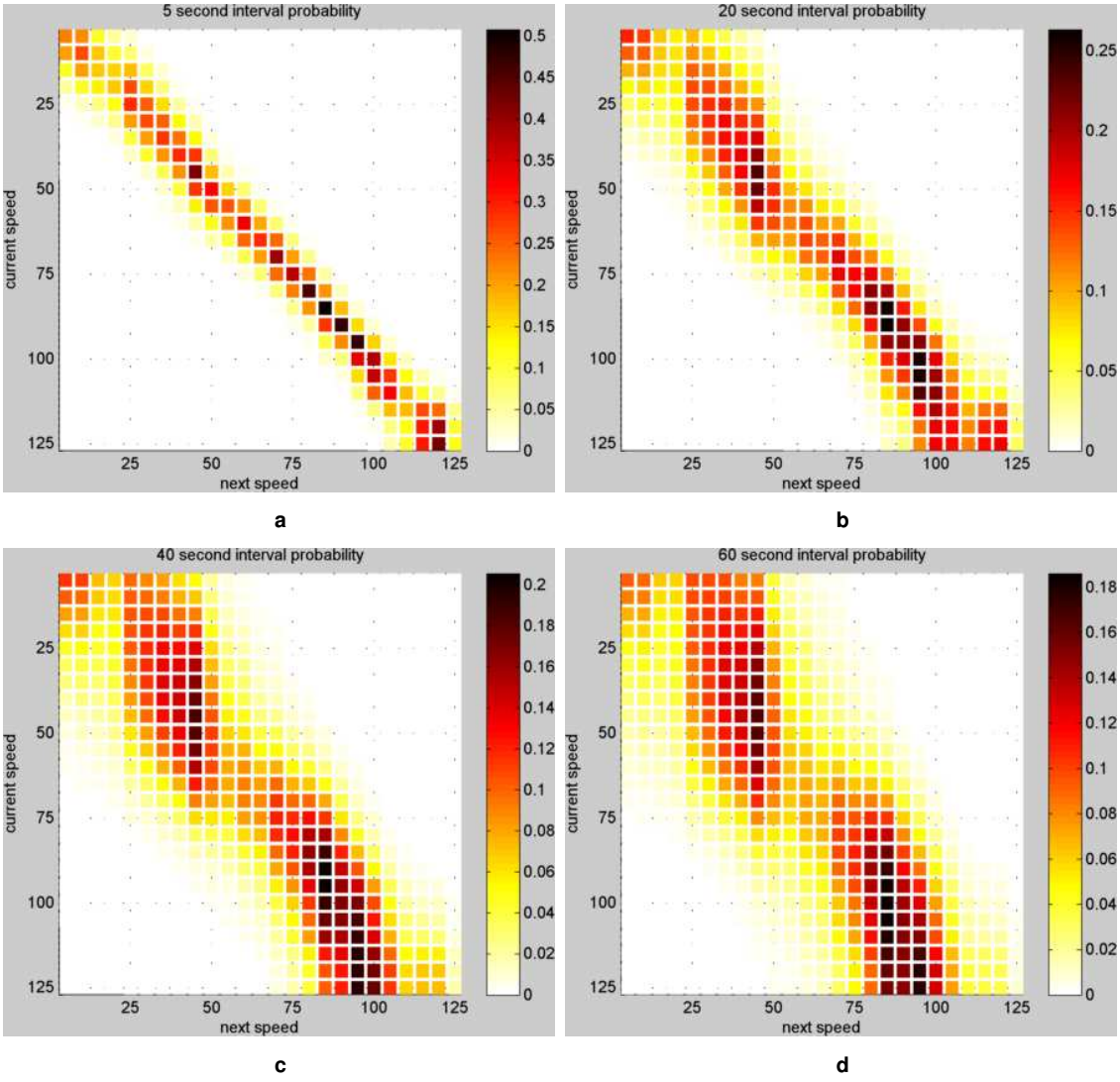

Figure 5.3: Probability matrices at different intervals

a - Probability after 5 seconds

b - Probability after 20 seconds

c - Probability after 40 seconds

d - Probability after 60 seconds

In Figure 5.4 graphs are drawn at similar intervals as in Figure 5.3 showing the maximum probability and the result of the following Bias equation (5.4). x is the interval period in seconds and M the original derived Markov chain matrix. B is a vector indicating if the long tail before and after the maximum (highest probable next state) is biased towards deceleration or acceleration (positive values for B_{ij} equal acceleration, negative values for B_{ij} equal deceleration). This is calculated by taking the sum of all the probability values after the location of the maximum value and subtracting this from the sum of all probability values before the location of the maximum value.

Within each row the location of the cell with the highest probability value is established. Its location is recorded. b is a vector containing integers representing the locations of the highest values on each row (the locations with the highest probability for the next velocity) and z equals the maximum value for j, then:

$$B = \begin{bmatrix} \sum_{j=b_1+1}^{z} p_{1j} - \sum_{j=1}^{b_1-1} p_{1j} \\ \sum_{j=b_2+1}^{z} p_{2j} - \sum_{j=1}^{b_2-1} p_{2j} \\ \vdots \\ \sum_{j=b_i+1}^{z} p_{ij} - \sum_{j=1}^{b_i-1} p_{ij} \end{bmatrix} \quad \textbf{(5.4)}$$

Where $[p_{ij}] = M^{(x)}$

The probability cannot exceed one, which means that each row should combine to a total probability of one. This is expressed in equation (5.5).

$$\begin{bmatrix} \sum_{j=b_1+1}^{z} p_{1j} + \sum_{j=1}^{b_1-1} p_{1j} + p_{1b_1} \\ \sum_{j=b_2+1}^{z} p_{2j} + \sum_{j=1}^{b_2-1} p_{2j} + p_{2b_2} \\ \vdots \\ \sum_{j=b_i+1}^{z} p_{ij} + \sum_{j=1}^{b_i-1} p_{ij} + p_{ib_i} \end{bmatrix} = \begin{bmatrix} 1 \\ 1 \\ \vdots \\ 1 \end{bmatrix} \quad \textbf{(5.5)}$$

B is the Bias vector of the probability matrix at x seconds; it is a measurement of difference. The Bias vector indicates whether the remainder of probabilities is biased toward braking or towards acceleration. The probability of the Bias is shown in Figure 5.4 (Bias towards braking is negative and towards acceleration is positive) together with the maximum probability and its next state velocity target. If the current state is 40 km/h then the next state after 20 seconds (5d) is most likely to be 45 km/h with the probability Bias towards deceleration. Even though, the highest probability is showing acceleration is expected there is a large Bias towards deceleration.

Similarly, if the current state indicates 60 km/h then the highest probability for the next state indicates a reduction in velocity to 45 km/h (5d), but the Bias now is towards acceleration. Through the progression of time intervals (5a-d) it is clear that different zones can be identified after 20 seconds:

- < 20 km/h
    - Here an acceleration event is most probable with the final point of acceleration being 50 km/h[3]. Basically, as long as the velocity remains under 20 km/h only the UC module should be active with

[3] While the graph shows 45 km/h it is assumed that 50km/h is the real target and that the 5km/h reduction is the result of rounding off data.

the battery only supporting when the SoC of the UC drops below a set point[4].

- 20 – 50 km/h
    - The Bias is towards deceleration, which allows the battery‘s supplied power to rise over the interval period while the UC module provides the peaks; at the end of the 20 second period the battery should be supplying the full demand with the UC at its next target SoC.
- 50 – 70 km/h
    - The Bias is towards acceleration, but the highest single probable outcome is a lower velocity, which indicates that if the battery power supply is set to this max value the system is prepared for the future since it has the possibility to charge the UC if so required while it can supply the battery current on its own. This could mean the battery current will be higher than demanded in order to charge the UC but will smooth a potential acceleration peak if it occurs.
- 70 – 90 km/h
    - The Bias probability is half of the maximum next state probability indicating that the moment 90 km/h is reached it is very likely that the next state will be at a lower value, again allowing the UC to refill the energy lost during this period of acceleration to achieve 90 km/h.

[4] Since the period of stopping is not quantified in terms of time any time spend at zero velocity skews the probabilities at low speed.

- 90 – 100 km/h
    - The likely event to occur upon arriving at the higher velocities is a regenerative event this is clear from the next state values which are lower than the initial values. Again, the UC should be readied to support acceleration to the next zone, but the need to recharge is not as high as at lower velocities.
- 100 – 110 km/h
    - It seems suggested here that the Bias is towards acceleration, but this is likely due to the limited events within each drive cycle and the limited number of drive cycles. In fact it is likely, that this zone is skewed by the effect of the single (probability 100%) of one person achieving a velocity greater than 110 km/h.
- > 110 km/h
    - The original recorded data only shows 1 person achieving a velocity above 110 km/h and only for 10 seconds which is likely the reason why the Bias is largely towards acceleration. This point is enhanced when the time interval is extended to 40 and 60 seconds as shown in Figure 5.5 from which it will be clear that the effect of the single high point in the Markov Chain disappears rapidly.

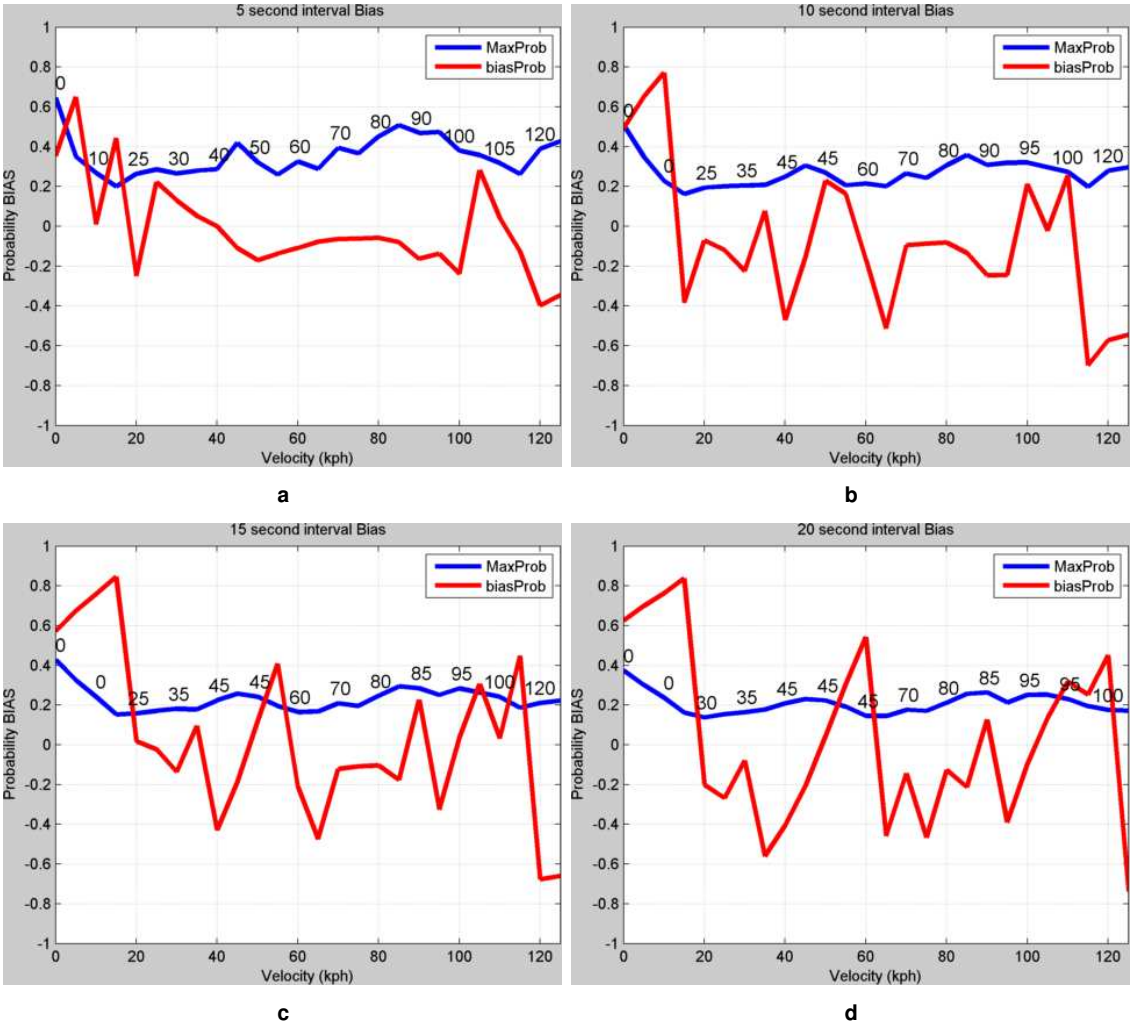

Figure 5.4: Bias and Maximum probability at different intervals

a - Probability after 5 seconds

b - Probability after 10 seconds

c - Probability after 15 seconds

d - Probability after 20 seconds

Also, in the iMiev the power from the battery is limited to 49 kW and a 130 km/h speed limit. The highest recorded value of power at the moment the peak velocity was achieved by this person is shown in Figure 5.6. From this figure it will be clear the battery current was limited as a form of protection. The power limiting is marked with a circle. The part of the road where this occurs is on a downward slope hence it was possible to continue acceleration despite the power being limited.

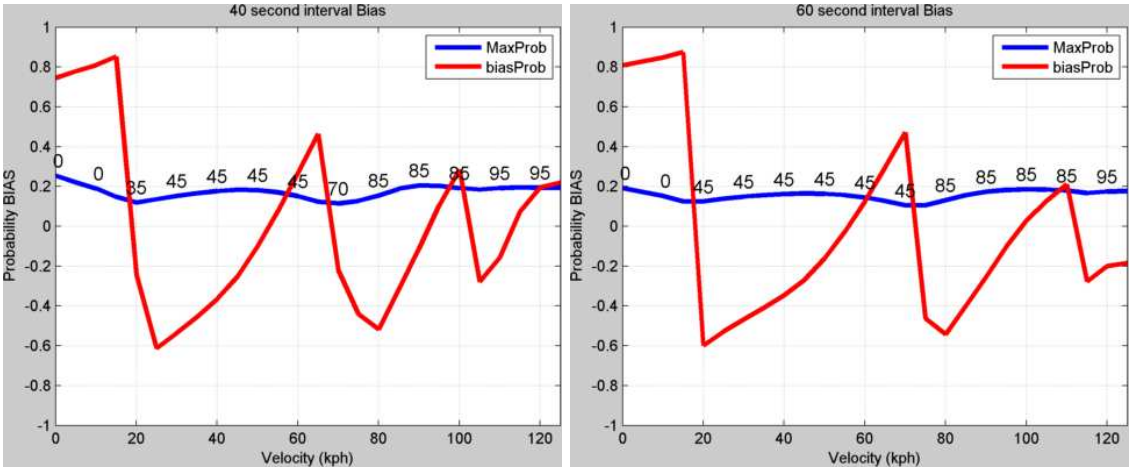

a b

Figure 5.5: Bias and Maximum probability

a - Probability after 40 seconds

b - Probability after 60 seconds

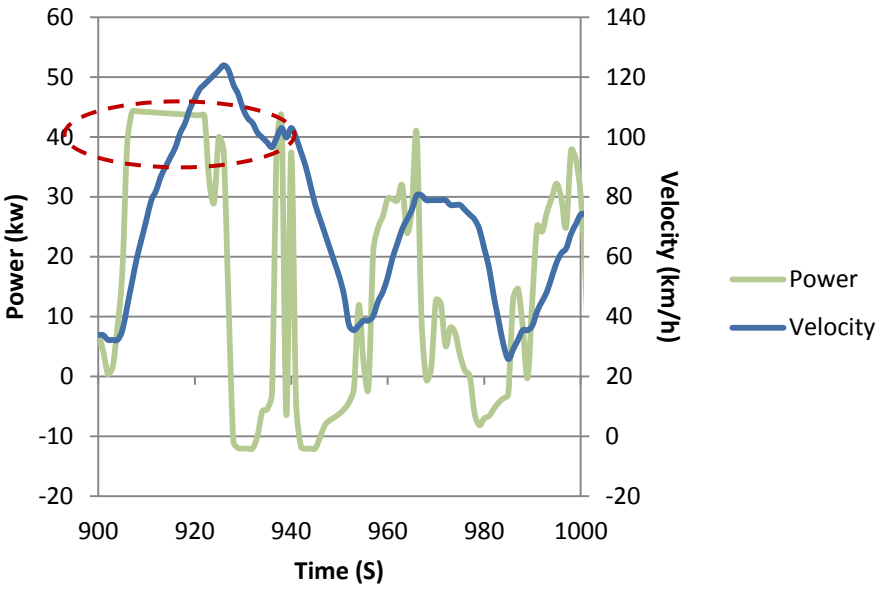

Figure 5.6: Drive Cycle snap shot

5.3.1. Discussion

The power demand as seen by the bus is variable and depends on mass of the vehicle, which is variable with the load and number of people as well as with the angle of the road surface (incline / decline) and other factors such as weather conditions and road surface. The final power demand of a vehicle at a fixed cruising velocity is difficult to predict. In the proposed energy management

strategy this limitation will be partially filtered as a result of the time interval choice. For example, suppose a vehicle is driving 50km/h and hits an incline the driver is likely to try and maintain that velocity but the power demand will rise requiring an acceleration to achieve this demand with the battery reaching the new target power at the end of the new time interval.

The speed at which the maximum value lines occur are dependent on factors such as speed restrictions and the duration that speed is maintained at each stretch of road driven during the test. The difference in position of the maximum value lines depends on the speed restriction over the different road stretches over the whole drive cycle. If there would be a change in speed restriction from 50km/h to 100km/h then these would likely become two maximum value lines as would the speed restrictions at other segments of the route.

A change from 50km/h (13.89 m/s) to 100 km/h (27.78 m/s) might happen at one stretch during the route but would register – depending on acceleration – as an increase for different time epochs. In establishing the matrix each speed is measured every 5 seconds and there will be more than 1 epoch needed to cover this increase at an average 2.68 m/s^2 (maximum acceleration in NYCC). This acceleration would show up (if it occurred regularly) as a Bias in reaching a particular speed over a particular period of time.

The bias effects caused as a result of the specifics of the route are not considered to be an issue for the validation of this approach. It is expected that – because the method is not computationally intensive – the algorithm would update the matrix all the time and adapt if a change in regular route occurs.

This algorithm is not expected to be fully optimised for every possible route but optimises regularly taken routes. The overall effect is shown later in this thesis when the final energy management strategy based on this standardised route is

applied to the unrelated NEDC and NYCC drive cycles and shown to provide a good efficiency optimisation.

5.3.2. Conclusion

Using Markov Chain analysis to analyse drive cycles is done for specific vehicles and specific routes (Souffran et al., 2012). Here it is shown that the Bias in the probability results is providing information on where braking and acceleration events are to be expected. This information will be used to design the energy management strategy.

In summary:

- the battery current limit should be set to the final power demand of the identified zones depending on the current state based on the chosen time interval
    - If the first velocity is assumed zero and the time interval chosen is 20 seconds then the final velocity (and the accompanying power) will be set at zero, while when the vehicle has accelerated to 20 km/h then the battery will be given 20 seconds to rise to the power requirements for 30 km/h.
- The UC module should be sized such that it can support the power demand during this time of transition.
- The target state of charge should reflect the energy remaining in the UC which allows acceleration up to the next zone, leaving enough room for recovery of all the energy in anticipation of a regenerative event
- While the control strategy is designed to be able to allow regenerative energy to be accepted by the battery the transition from supplying to accepting would constitute a ripple and as such is best avoided.

5.4. Implementation of the Energy Management Strategy

5.4.1. The battery maximum current

In Table 5.1, zone power values based on small vehicle (1200 kg) are given. These values have been calculated based on the velocities identified in the drive cycle chapter.

The zones are (illustrated in Figure 5.7 - 5.8) overlaid on the New European Drive Cycle (NEDC) and the New York City Cycle (NYCC). From these power values the maximum current can be established by dividing the power limit with the battery voltage.

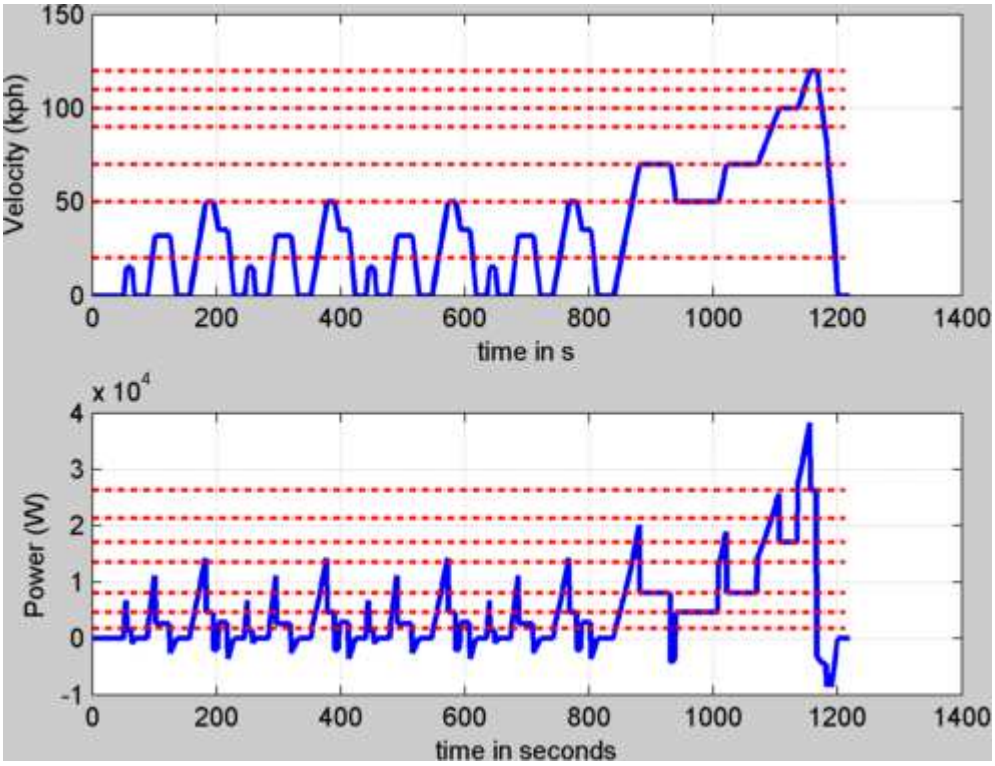

Figure 5.7: Zone overlay - NEDC

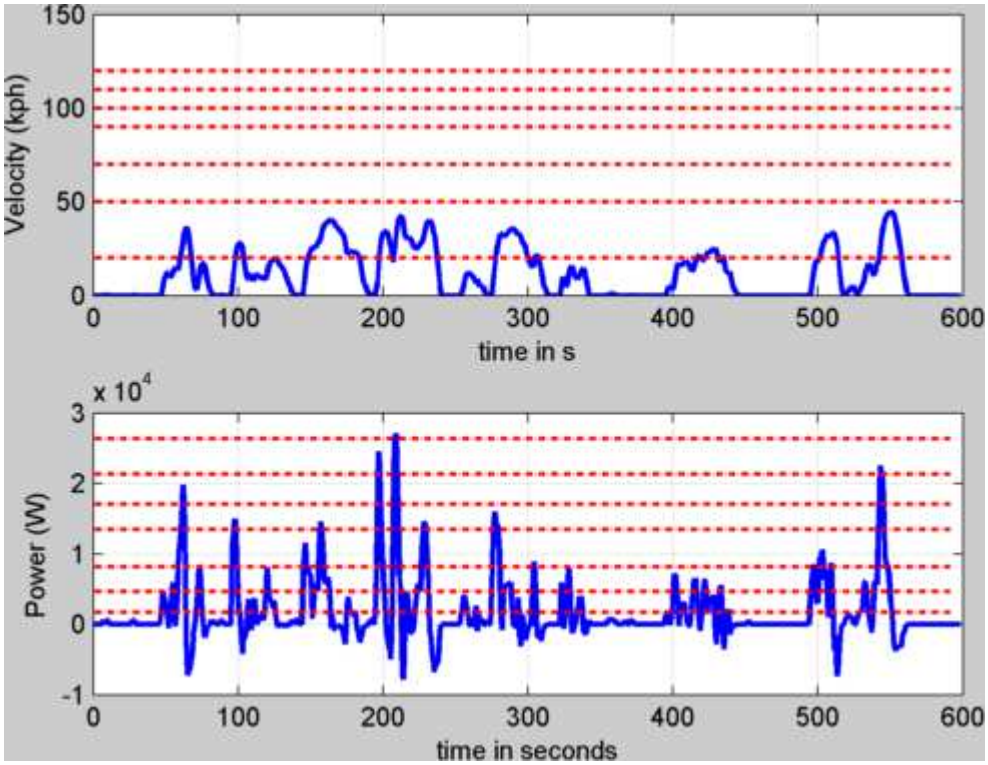

Figure 5.8: Zone overlay - NYCC

Table 5.1: Zone Power Values

Velocity (km/h)	20	50	70	90	100	110	120
Power at the Bus (W) @ 0% incline	1 744	4 617	8 108	13 492	17 064	21 313	26 309

The 20 second time interval was chosen based on the behaviour of the Bias curve which had stabilised after this time period (no major changes). It was also felt that a longer period would be unrealistic for the UC Module to support. Based on the chosen (20 second) interval a filter is designed to simulate the slow rise and to serve as a reference for a second by second update of the battery power limit.

A second order Butterworth low-pass filter is chosen of which the generic form is given in equation (5.6). The Butterworth filter was chosen because of its flat response up to the cut-off frequency.

$$Y(s) = \frac{\omega^2}{s^2 + 2 \cdot \beta \cdot \omega + \omega^2} \quad \textbf{(5.6)}$$

Where ω is the cut-off frequency in radians per second and β is the damping's factor. The damping factor is set to 1 which results in a critically damped response thus providing a flat response.

The timing interval is 20 seconds but this is only one quarter of the total frequency. The total period for purpose of use to calculate ω is therefore T = 80 seconds.

$$\omega = 2\pi f = \frac{2\pi}{T} \quad \textbf{(5.7)}$$

5.4.2. UC Module

For the module to be specified the following needs to be established:

- Maximum power for the converter
- Energy requirements of the UC

From Figure 5.8b it can be seen that the highest acceleration peak of the two drive cycles are located at around the 200 second mark, where the maximum power demand is around 26 kW, with the acceleration starting at zero velocity and without taking any potential battery contribution in account.

Using Simulink a simulation can be run using power profiles of drive cycles as input to the filter. The difference between the power profile and the filter output is the power demand the UC module should deal with. The results of these simulations are shown in Figure 5.9 - 5.12 from which it is clear that the expected maximum power is around ±30kW. An interesting effect the pictures are showing is that the ECO positive driver has lower power demand and seems to indicate an average almost equally distributed on each side of the zero marker, which means that this person would, based on his driving style, allow optimum use of peak power shaving technology and as a result the

battery would really benefit from the eco driving approach in combination with the UC module and PEM strategy.

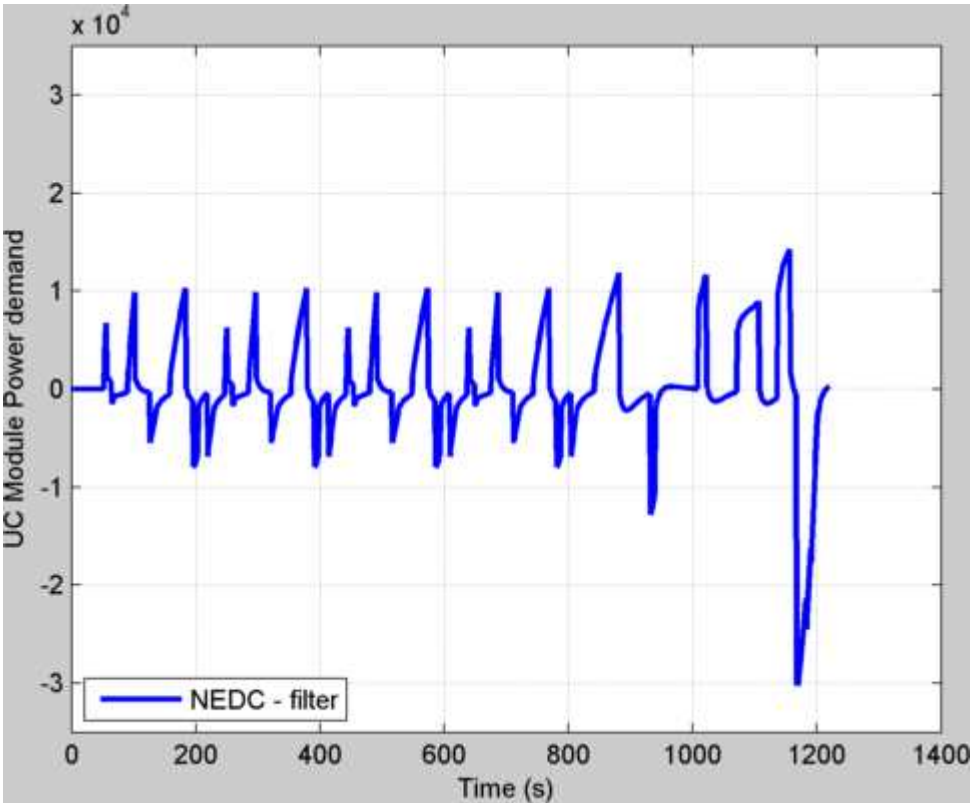

Figure 5.9: Expected UC Module power demand - NEDC

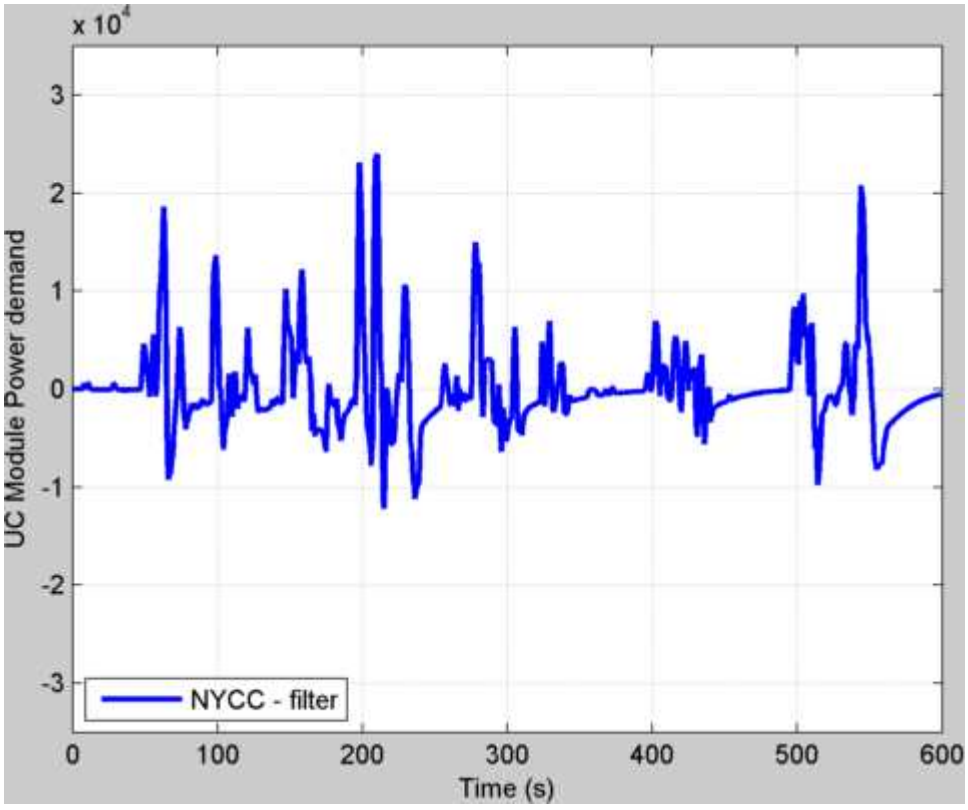

Figure 5.10: Expected UC Module power demand - NYCC

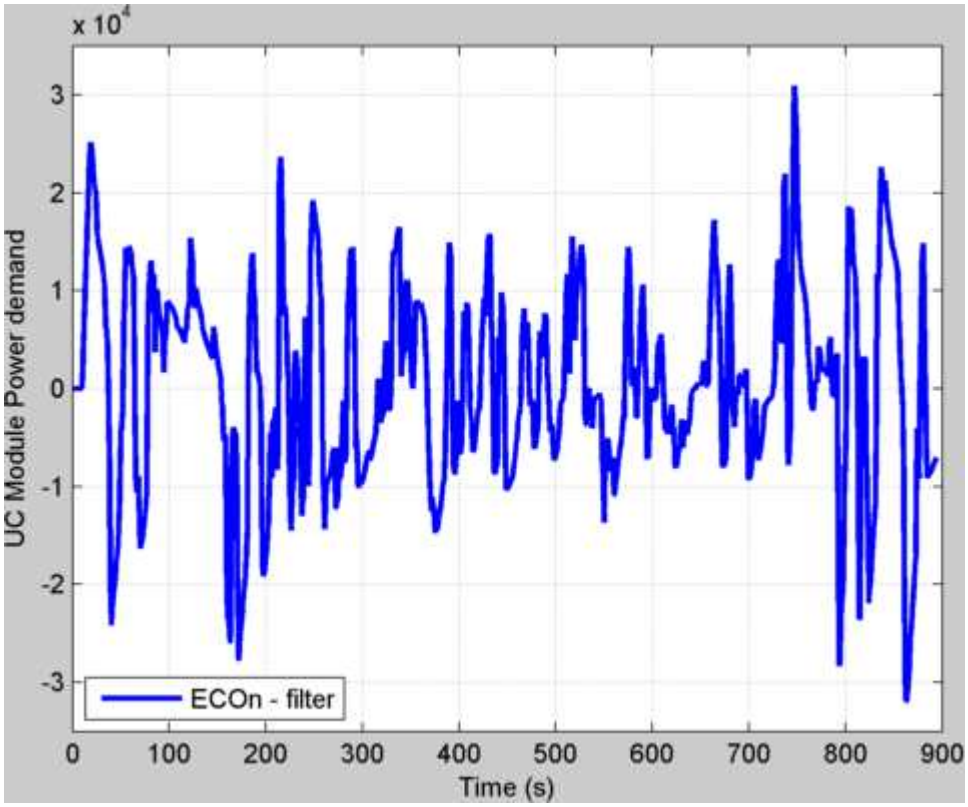

Figure 5.11: Expected UC Module power demand - ECOn

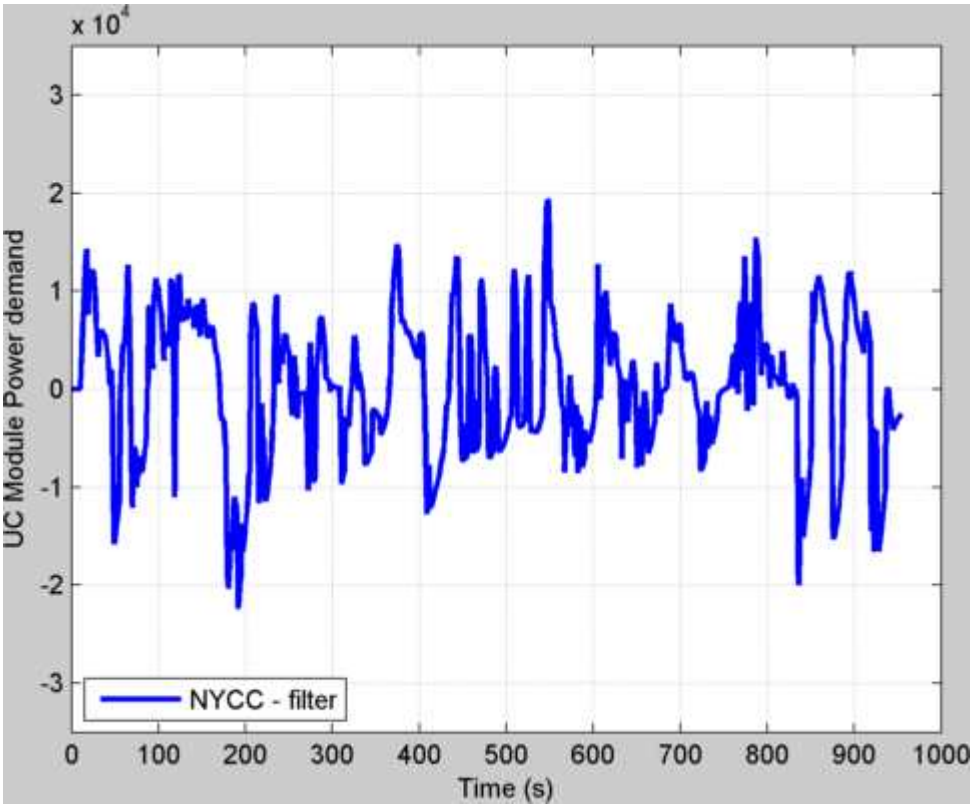

Figure 5.12: Expected UC Module power demand - ECOp

The energy requirement is dictated in two parts: a) the maximum power peak and b) the duration of the peak power demand. The chosen time interval is 20 seconds which results in an energy rating of 167 Wh (600 kWs).

The UC type chosen is the lithium-ion capacitor presented in (Lambert et al., 2010) of which a summary is presented in Table 2.1 in chapter 2.3. Based on an operating voltage of 50.60 V and 87.40 V (23 cells in series) with a capacity of 95.65 F per string (67.47Wh) and an internal resistance of 32.2mΩ. The required capacity would need 2.5 strings; which means 3 strings for a total usable energy of: 202 Wh at a capacity of 286.95 Farad and an internal resistance of 10.73mΩ.

The weight cost of this module would be

$$M = \frac{P_{converter}}{\rho_{converter}} + M_{cell} * Cell_{series} * String_{Parallel} \quad \textbf{(5.8)}$$

Where $P_{converter}$ is the maximum power of the converter and $\rho_{converter}$ is the power density of 5kg/kW. The UC cell used weighs 0.26kg and there are 23 in series per string and 3 strings are required. A packaging factor can be added if so required.

5.4.3. The UC target SoC

The energy recovery ratios range from 30% (Miller, 2004) to 87% (Gao et al., 1999) via (Carter et al., 2012). According to Zhang et al. (2013a) regenerative energy can constitute up to 60% of the overall consumed energy but only in start-stop driving cycles. Regenerative braking is also limited by the addition of friction brakes and legislation which requires the Anti-lock Braking System (ABS) to be in control of the braking torque (Oleksowicz et al., 2013).

According to Tie and Tan (2013) the energy recovery rate is limited to 50% because of losses in the system; this value has been used to set the UC target SoC.

For each zone the maximum value of recoverable energy has been calculated based on its kinetic energy value as per equation (5.9)

$$E_{rec} = \frac{1}{2} M v^2 * 0.5 \quad \textbf{(5.9)}$$

Where E_{rec}= the recoverable energy, M = mass of the vehicle and v is the vehicle velocity in meters per second (m/s). The extra factor of 0.5 is the 50% recovery rate.

The resulting energy levels are given in Table 5.2 with the mass of the vehicle set to 1200 kg.

Using the values from Table 5.2 and the equation to calculate UC energy as provided in equation (2.2) the corresponding voltage level can be calculated, see final column Table 5.2.

Table 5.2: Energy at different velocities

km/h	E available (kJ)	E recoverable (kJ)	Vuc Target (V)
0.00	0.00	0.00	87.40
20.00	18.52	9.26	87.03
50.00	115.74	57.87	85.06
70.00	226.85	113.43	82.75
90.00	375.00	187.50	79.57
100.00	462.96	231.48	77.62
110.00	560.19	280.09	75.41
120.00	666.67	333.33	72.91

5.4.4. Summary

Table 5.3 shows an overview of the target values. The targets for the UC SoC are based on the value of filtered power demand which sets the battery maximum power. These values will be updated every second. The control for this system in Simulink is shown in Figure 5.13. The “Management Timing Interval” block outputs a pulse every second from which the derivative is taken and only the positive ramp is passed on to the “enabled subsystem”. In this way, at the start of every full second the “Enabled Subsystem” is updated. This last block contains a “Matlab Function” block which is programmed with a rule based strategy to assign the right values. The code can be found in Appendix 6. This code also includes a line that avoids the maximum battery power becoming negative since this is controlled by the power management level if it is required that the battery accepts regenerative energy.

Table 5.3: Control Variables overview

km/h	Battery Power Limit (W)	Vuc Target
0.00	0	87.40
20.00	1744	87.03
50.00	4617	85.06
70.00	8108	82.75
90.00	13492	79.57
100.00	17064	77.62
110.00	21313	75.41
120.00	26309	72.91

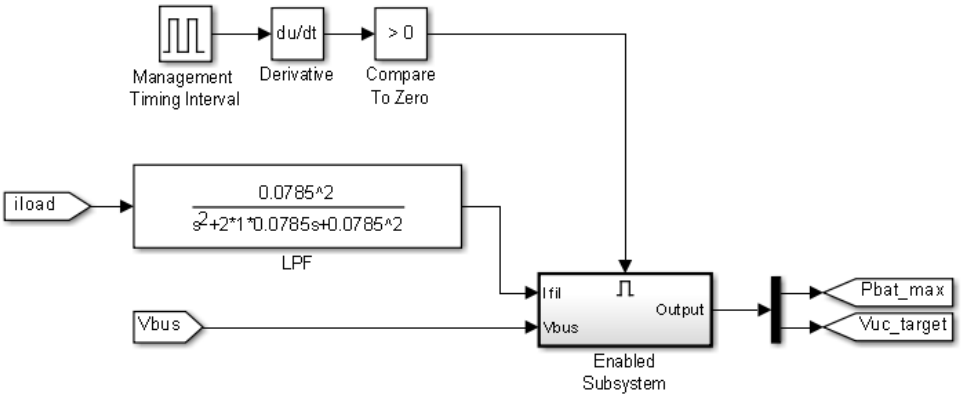

Figure 5.13: Energy Management Simulink Implementation

Simulation Results

6.1.Introduction

In previous chapters the current literature has been discussed and the different aspects for a PEMS have been analysed, which include: choice of topology, level of support required from the UC module and the efficiency of the whole power and energy elements of the drive train. A new PMS has been developed. Through the use of Markov Chain analysis power limits have been established as well as a time interval for a filter function culminating in a new PEMS.

In this chapter the results of different simulations will be discussed. There are 4 different topologies which are simulated using 4 different drive cycles. The results are then processed in a Matlab program for the effects of battery, converter and UC efficiency based on the efficiency algorithms established in chapter three.

6.2.Simulation Results

6.2.1. Topology 1

Figure 6.1 - 6.4 show the baseline simulations of each drive cycle for this topology. These graphs will function as a baseline measurement for the other topologies. The battery voltage and current are the bus voltage and current in this topology.

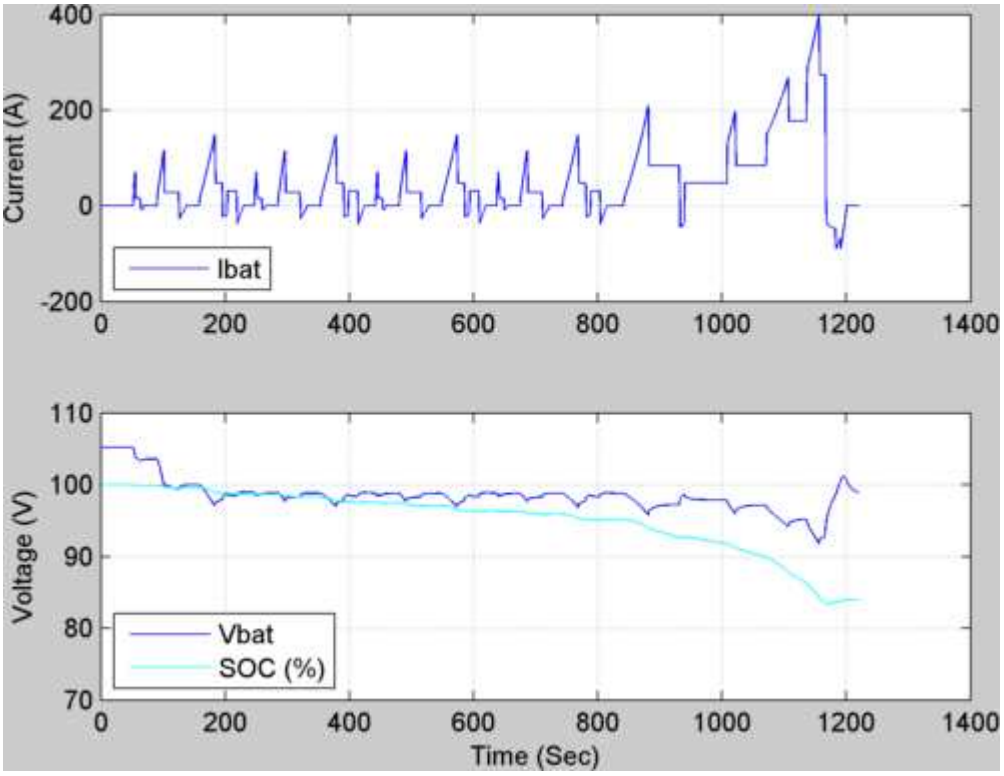

Figure 6.1: Topology 1 Simulation - Baseline NEDC

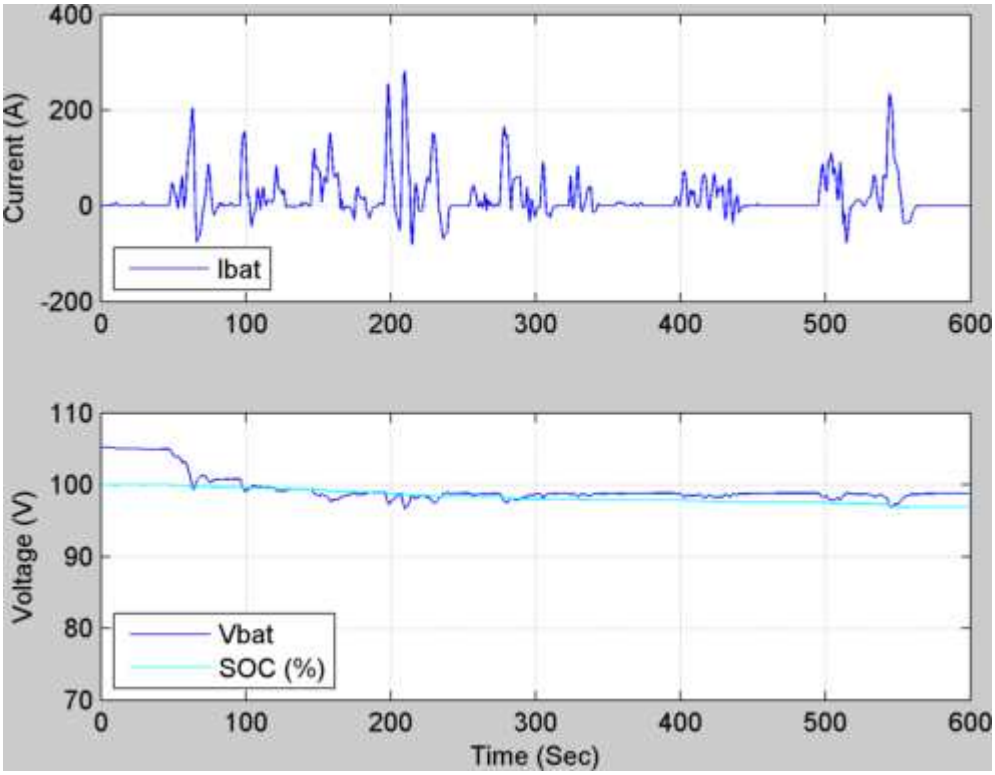

Figure 6.2: Topology 1 Simulation - Baseline NYCC

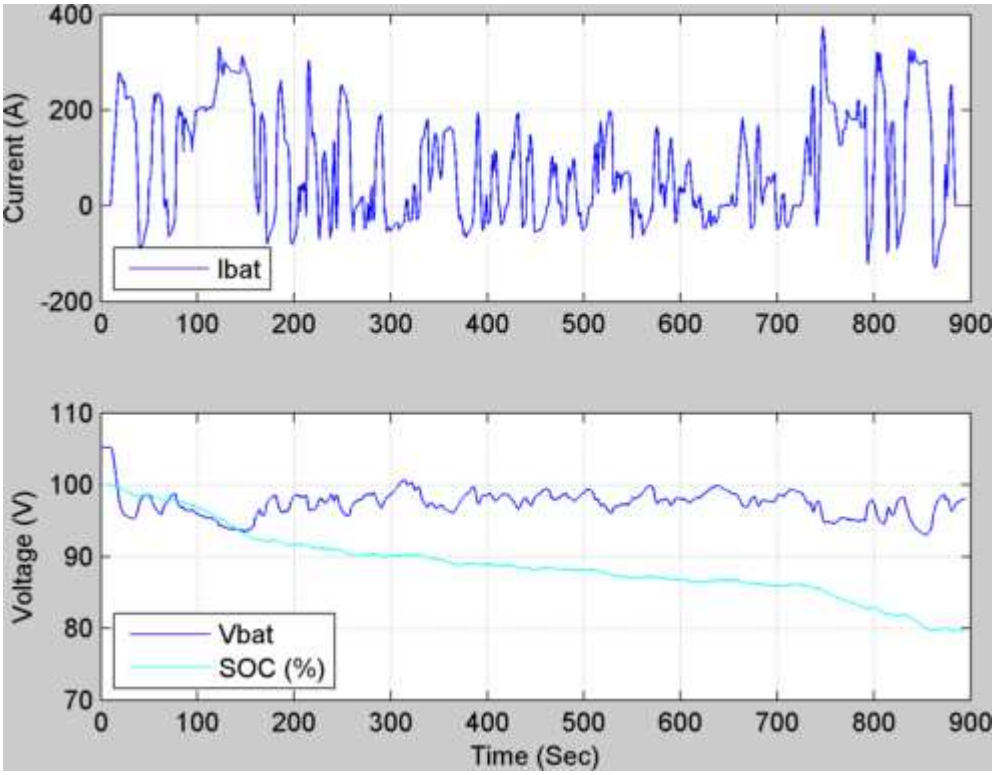

Figure 6.3: Topology 1 Simulation - Baseline ECOn

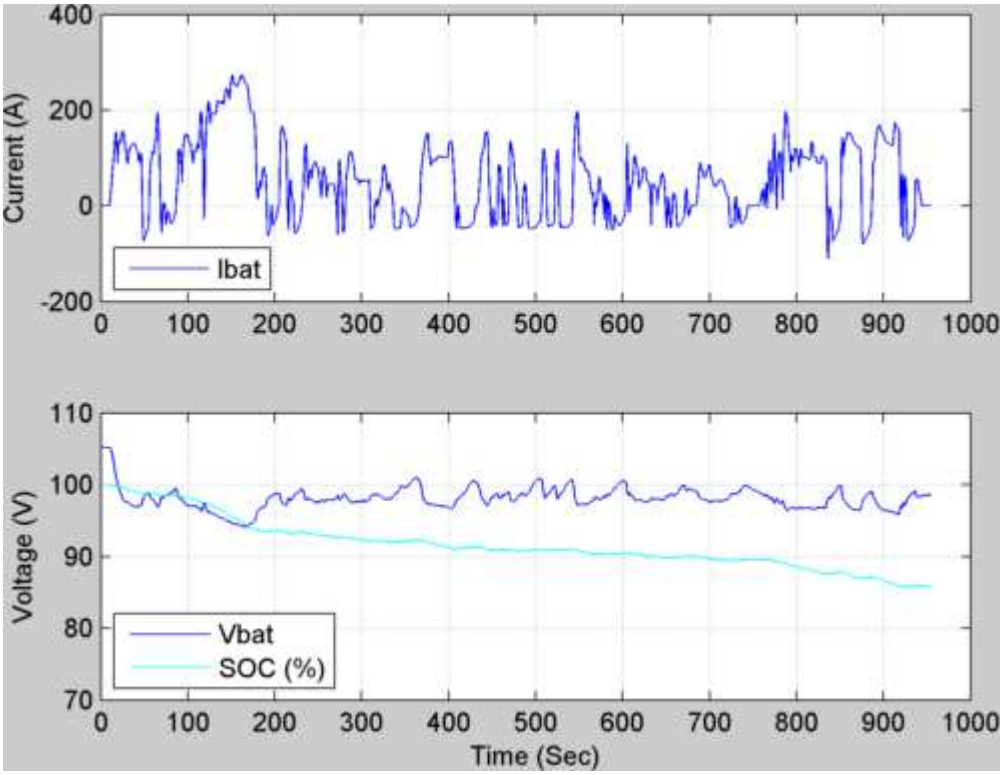

Figure 6.4: Topology 1 Simulation - Baseline ECOp

6.2.2. Topology 2

The effect of the converter is clearly visible in this topology as a result of the increased current demand from the battery, which directly results in a reduced battery SoC at the end of the drive cycle (shown in Figure 6.5 - 6.8).

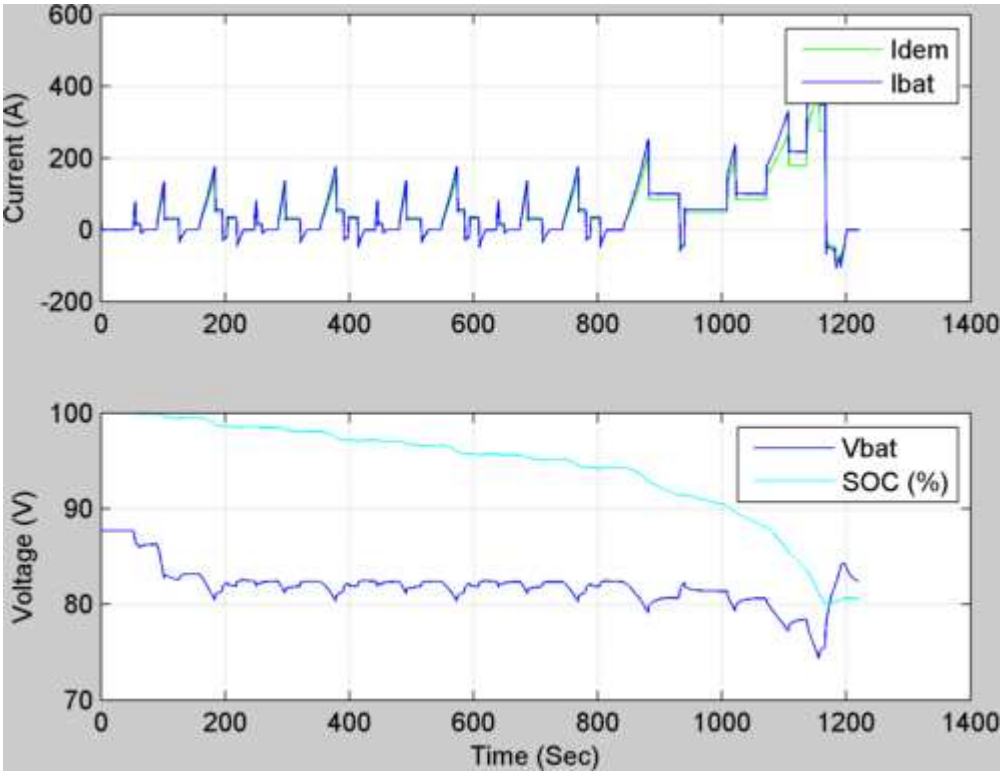

Figure 6.5: Topology 2 Simulation - NEDC

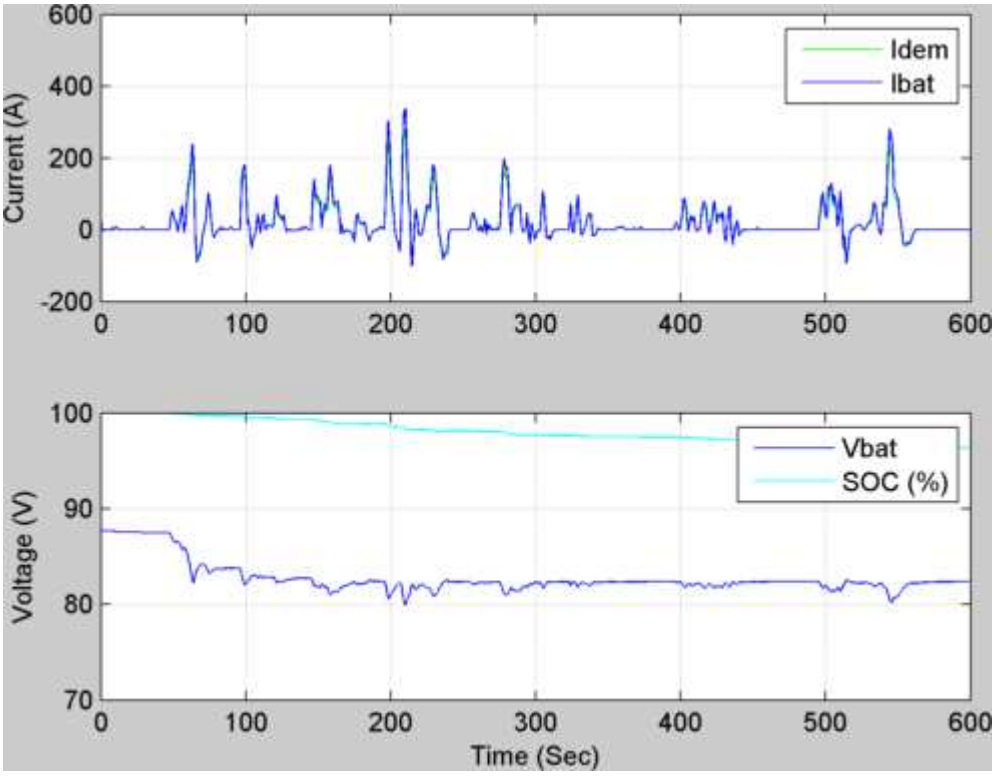

Figure 6.6: Topology 2 Simulation - NYCC

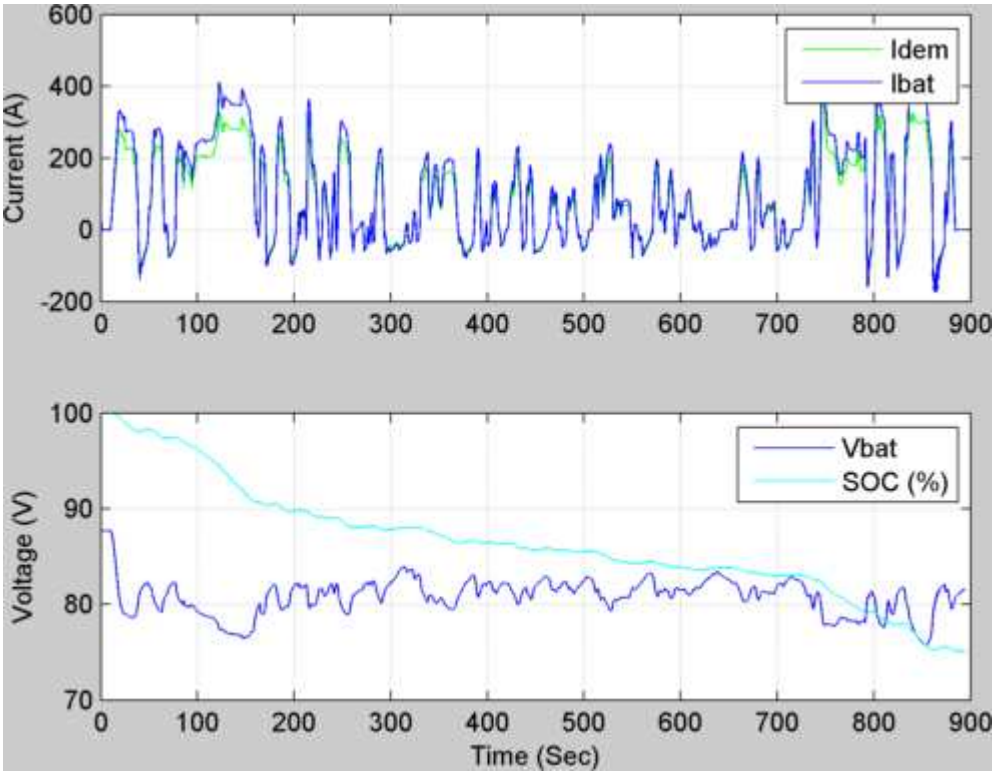

Figure 6.7: Topology 2 Simulation - ECOn

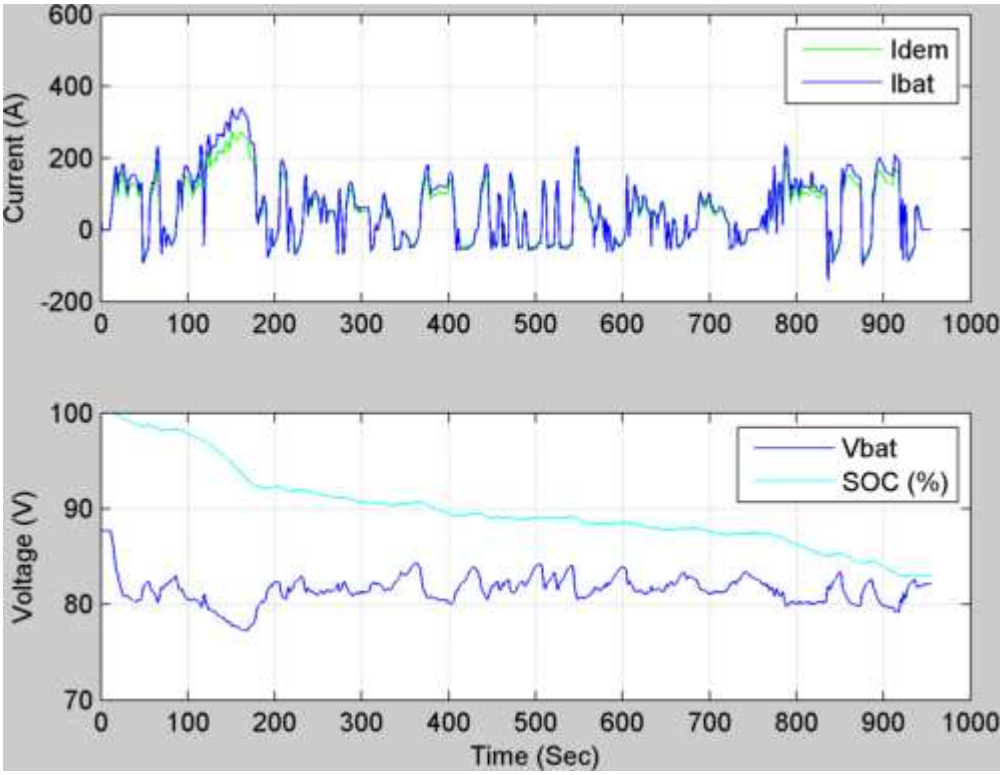

Figure 6.8: Topology 2 Simulation - ECOp

6.2.3. Topology 3

The effects on the UC can clearly be seen in the battery current behaviour, which is smoother, see Figure 6.9 - 6.12. The SoC is almost similar to Topology 1. The battery current shows some spikes at the moment of acceleration, these are the direct result of the topology: the battery is directly connected to the bus and as such will respond first to any change in demand. The control strategy is affected by the battery's direct connection to the bus. On transitions from acceleration / cruising to regeneration, initially the battery will see a falling demand and will follow this trend because it is directly connected to the bus.

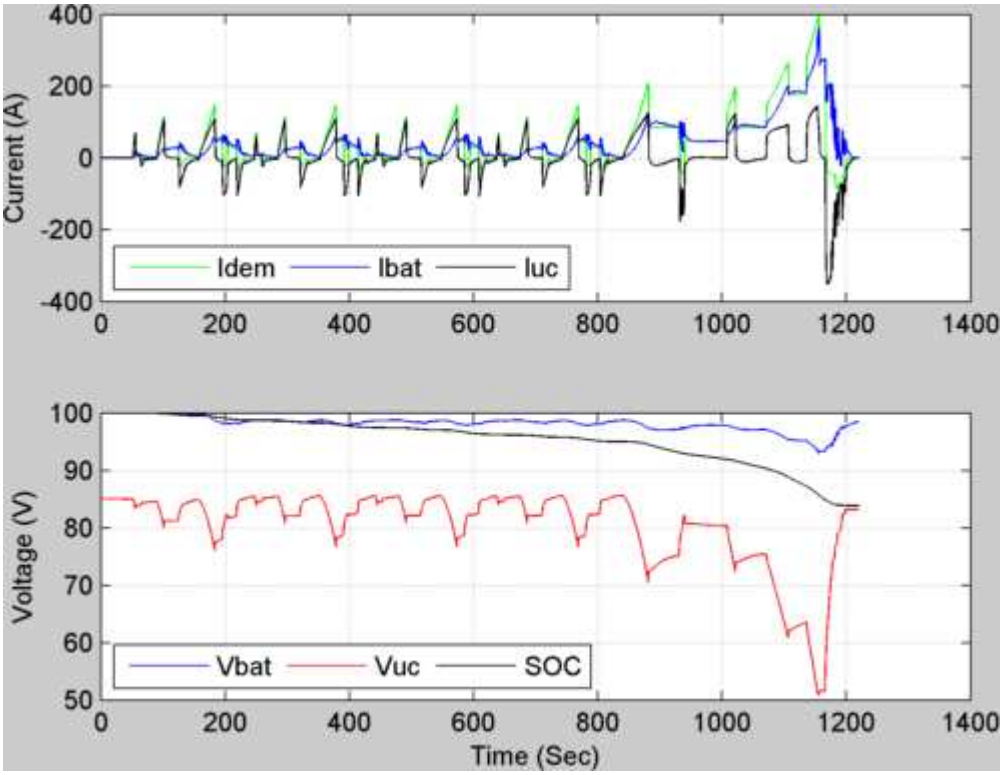

Figure 6.9: Topology 3 Simulation - NEDC

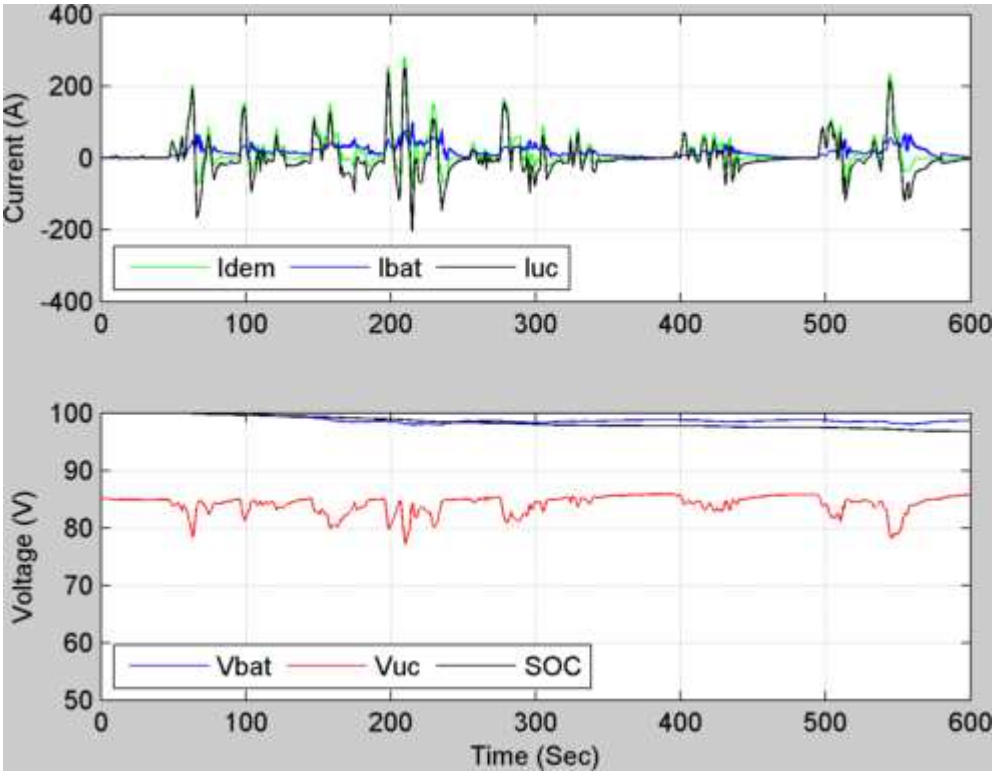

Figure 6.10: Topology 3 Simulation - NYCC

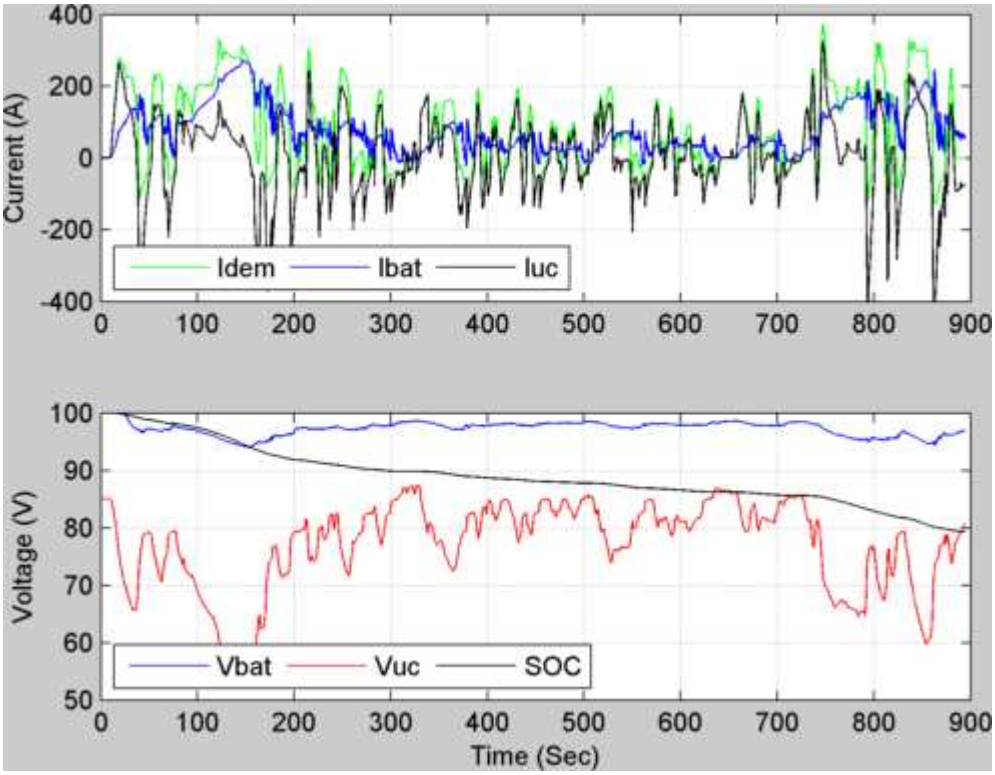

Figure 6.11: Topology 3 Simulation - ECOn

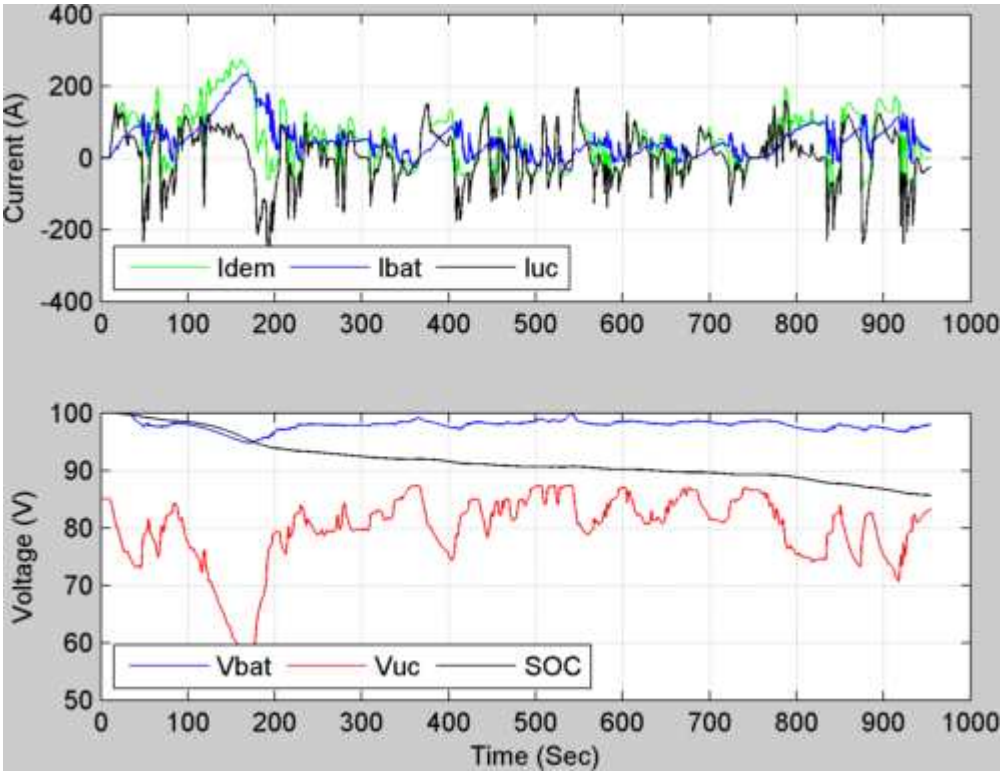

Figure 6.12: Topology 3 Simulation – ECOp

However, the requirement is to maintain a level that allows the UC to be charged to target voltage, but since the motor controller is functioning under regenerative conditions – recharging the bus capacitor – the battery will not respond. Only when the demand indicates regeneration can the control strategy start to demand the battery to assist in charging the UC; this is visible by the little dips at the moment the demand is negative.

6.2.4. Topology 4

The results in Figure 6.13 - 6.16 shows that the final acceleration of the NEDC relies less on direct battery supply. The sharp peak at the end of the NEDC is a result of the UC being depleted and the reported limited option for current limitation in the simulation: this would be where a limitation might be placed on battery current but because of the simulation approach taken this is not possible.

The ECOp driver provides better recovery of energy as a result of his (or her) driving style. The ECOn driver would potentially benefit from the UC module the most since the variance shown in the V_{uc} SoC is greatest, but also has likely the highest losses with high current demand at UC SoC below 62.5 V.

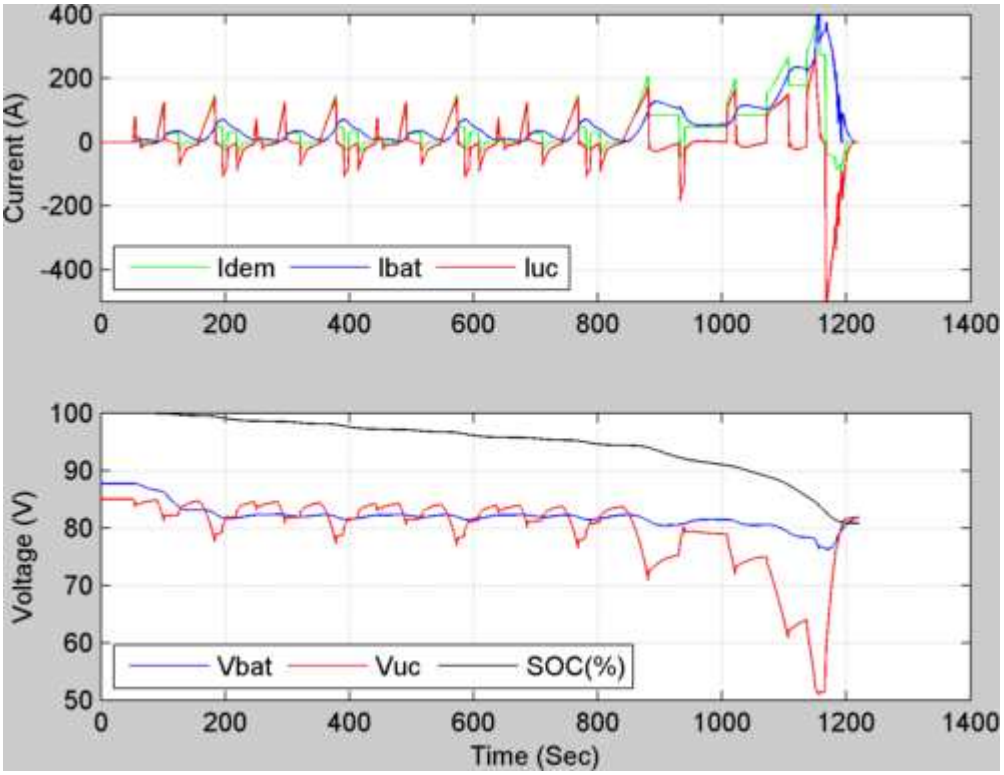

Figure 6.13: Topology 4 Simulation - NEDC

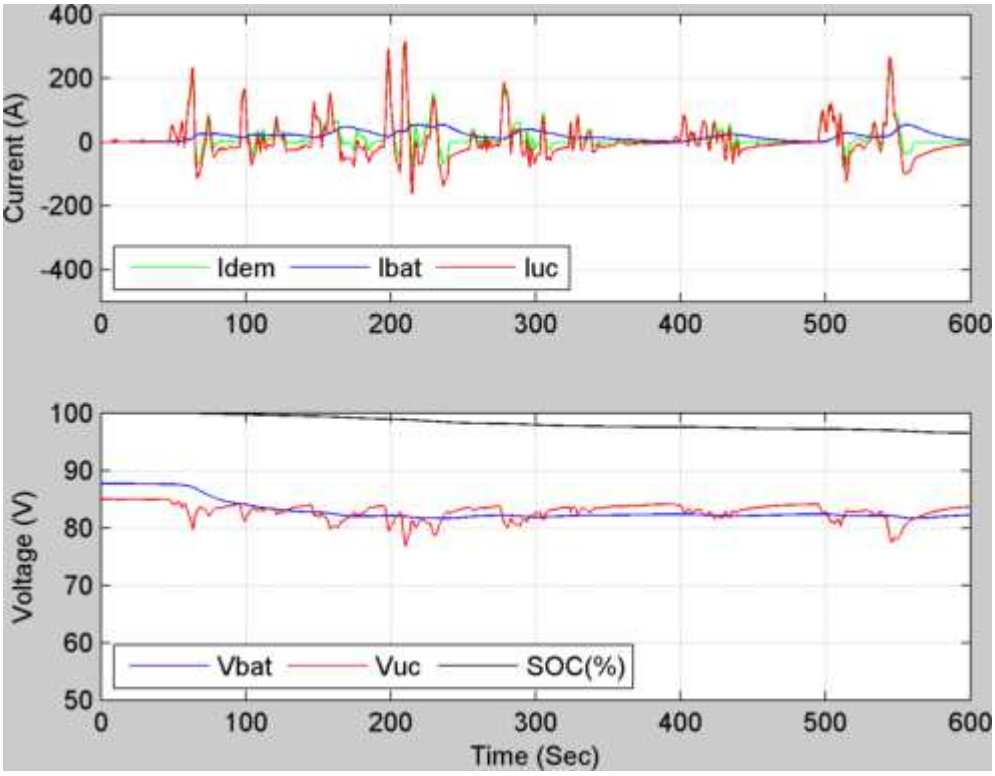

Figure 6.14: Topology 4 Simulation - NYCC

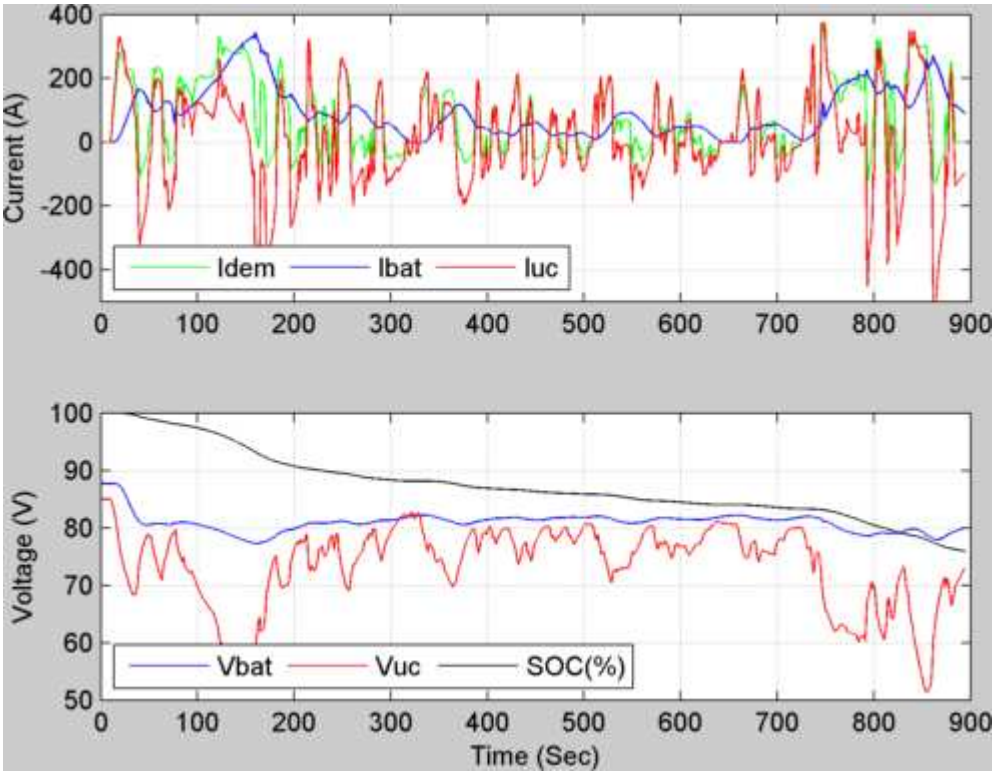

Figure 6.15: Topology 4 Simulation - ECOn

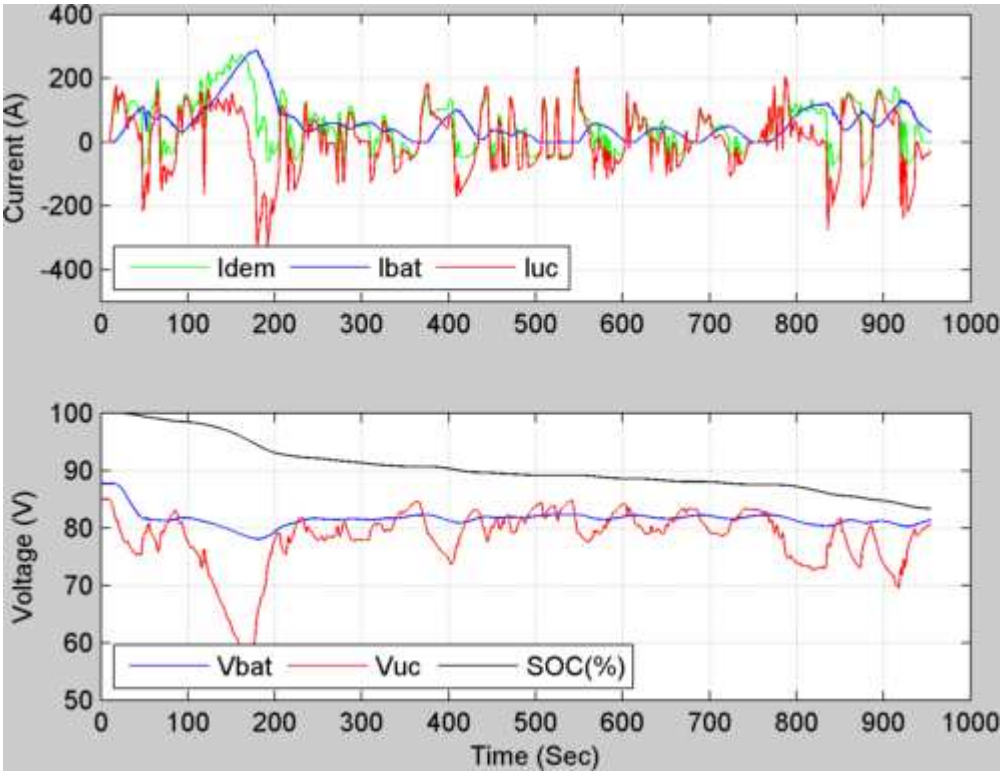

Figure 6.16: Topology 4 Simulation – ECOp

6.3. Discussion of the results

As reported in chapter 3 the efficiencies based on current demand will be calculated and then the effective energy used based on these efficiencies will be shown.

Figure 6.17 - 6.20 show the battery efficiency values based on the simulated battery current draws. In all situations Topology 2 has the worst efficiency as expected. The effect of converter addition (reducing the battery string length) is an increase in current and thus a loss of efficiency in current draw from the battery (higher current is less efficient) and the loss through converter efficiency. The losses as a result of the converter inefficiencies would realistically result in an increased current from a battery perspective. It has been assumed in these simulations that the effect of the converter inefficiencies on

the battery current increase can be neglected compared to the current increase as a result of the power balance.

The next least efficient topology is Topology 1, followed by Topology 4 then Topology 3. Interesting to note is that the ECOp driver also clearly shows a higher efficiency over all compared to the ECOn driver.

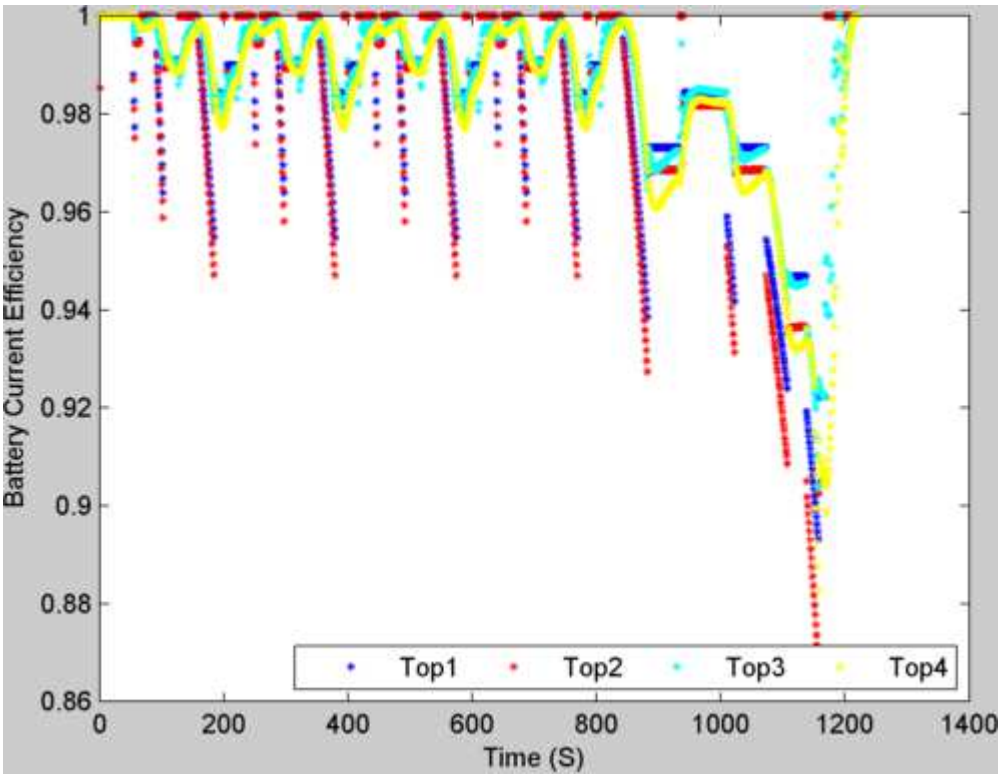

Figure 6.17: Battery Efficiency - NEDC

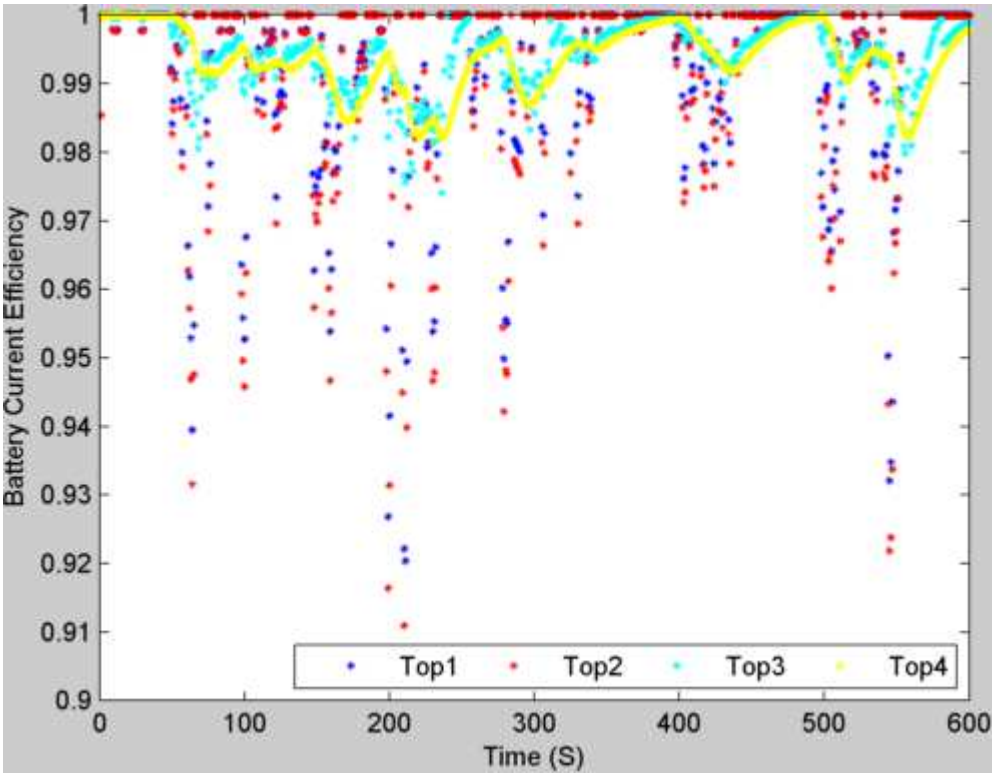

Figure 6.18: Battery Efficiency - NYCC

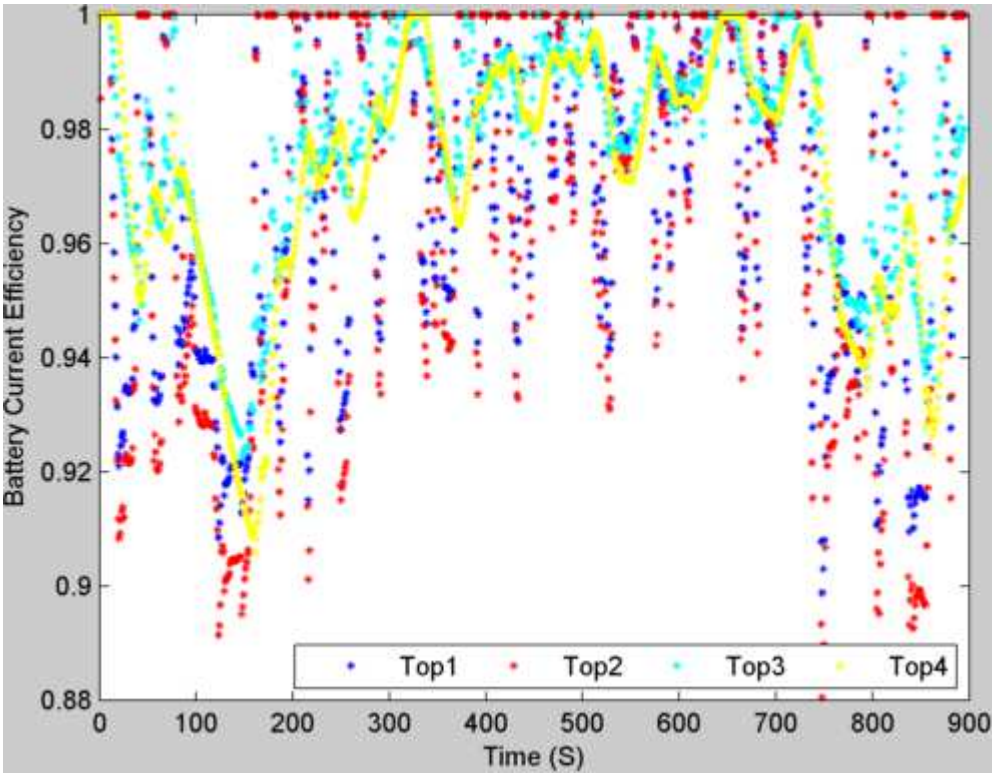

Figure 6.19: Battery Efficiency - ECOn

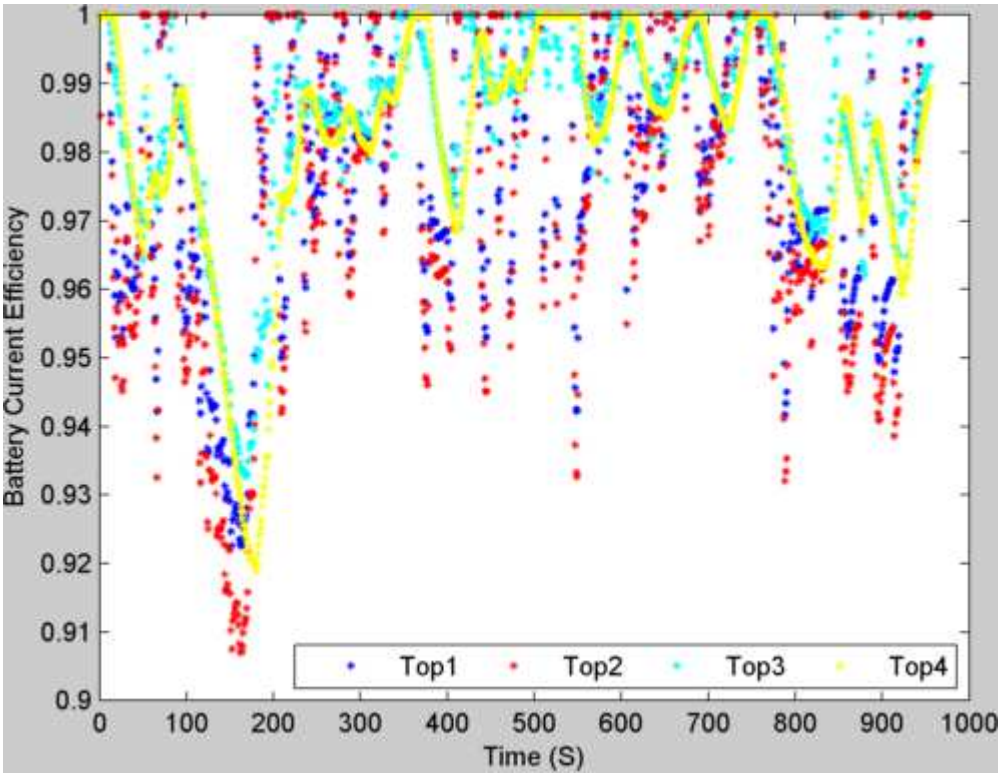

Figure 6.20: Battery Efficiency - ECOp

Shown in Table 6.1 are the calculated energies removed from the battery corrected for the inefficiencies based on the current demand. The value presented here represents how much energy is used in the different topologies with an overall efficiency assumed of 95% for the battery converter.

Based on these efficiencies Topology 3 is the most efficient (3 out of 4 topologies) and as a result has used the least amount of energy in each of the situations. The results also show that Topology 4 is more efficient than Topology 1. The most notable pattern is the direct relation between energy used under peak demand and the effect it has on the battery efficiency. The table shows all the energy registered from the battery to the bus including energy that then continued to be used to charge the UC. Already it can be seen that an improvement in overall efficiency is gained despite providing energy to the bus as well as charging the UC.

Table 6.1: Energy delivered from the battery to the bus (kWh)

	Topology 1	Topology 2	%	Topology 3	%	Topology 4	%
NEDC	1.762	1.871	6.19%	1.573	-10.73%	1.667	-5.39%
NYCC	0.374	0.383	2.41%	0.293	-21.66%	0.286	-23.53%
ECOn	2.484	2.651	6.72%	2.000	-19.48%	2.107	-15.18%
ECOp	1.762	1.841	4.48%	1.384	-21.45%	1.434	-18.62%

Table 6.2 shows the energy recovered from the bus into the battery. This table is showing a control issue within Topology 3. While the control is limited to maintaining a positive battery current a small amount of energy is still recovered into the battery as a result of the ripple effects described in chapter 3.2. While this energy does register here as data it probably would not register in the real world at all since the ripple duration is much lower than the 2 second duration required for our efficiency algorithm and in terms of efficiency it would probably not even get close to 60%. The improved control is clearly visible in Topology 4, where no current is recovered into the battery indicating no ripple issues.

Table 6.2: Energy recovered into the battery (Wh)

	Topology 1	Topology 2	Topology 3	Topology 4
NEDC	-72.130	-66.131	-0.780	0.00
NYCC	-37.307	-34.130	-0.150	0.00
ECOn	-185.225	-171.731	-5.520	0.00
ECOp	-183.262	-168.152	-17.000	0.00

Since the assumption is made that the UC does not have any energy of its own and the efficiency is calculated during the simulation, the efficiency calculated as round trip efficiency is shown in equation (3.22), repeated here for convenience:

$$eff_{uc} = \eta_{uc}^2 \cdot \eta_{conv}^2 \quad \textbf{(6.1)}$$

Table 6.3 shows the energies recovered into the UC on round trip efficiency. The table shows more energy being recovered and discharged by the UC module in Topology 4.

Table 6.3: Energy recovered into the UC – Top3 and Top 4 (Wh)

	Topology 3	Topology 4
NEDC	-360.02	-452.01
NYCC	-182.10	-200.00
ECOn	-690.74	-863.48
ECOp	-536.34	-656.91

In Table 6.4 the effective energy as seen by the bus is shown; i.e. the energies that have effectively left the battery and the energies that can be used, either because they have been saved in the battery or in the UC, are added. Since, these efficiencies have been established after the completion of a full drive cycle; i.e. the simulations have been successful, the only calculations involve the energy supplied by the battery and the energy returned (to battery or UC). All efficiencies reported are with the converters at 95% efficiency.

The percentages reported next to each topology are in relation to the base topology (Topology 1). The result of Topology 2 is as expected, extra energy is required to travel the same drive cycle. The result is reported to illustrate the effect of a non functioning UC module, for example, after prolonged driving at cruising conditions the UC module becomes depleted and is effectively only additional weight. Topology 3 is the most efficient only for NEDC despite higher voltage and less converter losses.

Table 6.4: Overall energy expenditure at the bus (kWh)

	Topology 1	Topology 2	%	Topology 3	%	Topology 4	%
NEDC	1.690	1.805	6.81%	1.212	-28.27%	1.215	-28.10%
NYCC	0.337	0.349	3.62%	0.111	-67.11%	0.086	-74.46%
ECOn	2.299	2.479	7.85%	1.304	-43.29%	1.244	-45.91%
ECOp	1.579	1.673	5.96%	0.831	-47.38%	0.777	-50.78%

In Topology 4 there is full control over the two converters, which means that any current supplied is fully controlled. Any discrepancies because of losses or current increases because of voltage drop are automatically corrected in the control loop, which is not possible in topology 3 since the battery current responds to a change in bus demand and the control strategy would need to compensate for the difference in voltage between the bus and the UC (power remains the same). The ripple effect in topology 3 – as reported - will affect battery life.

The higher efficiency of Topology 3 under NEDC seems to indicate that driving under highway conditions would significantly decrease the efficiency of the drive train when a converter is added as shown by Topology 2, as long as the occurrence is rare or not continuous (more city driving than highway driving) and the control strategy optimised an improved efficiency can be achieved for both Topology 3 and 4.

The biggest gain for Topology 4 is the improved control and the control over the battery current ripple which can be established by setting the inductor current ripple. The addition of a filter could solve the ripple issue for Topology 3 but introduces extra weight and losses. At the moment, the extra weight has not been taken in account; i.e. all topologies are simulated with the same amount of weight assumed for the drive train.

In Table 6.5 Topology 3 and 4 are directly compared to each other. And the efficiency difference with relation to Topology 3 is reported – positive efficiency is in favour of Topology 3.

Table 6.5: Overall energy expenditure comparison between Top3 and Top4 (kWh)

	Topology 3	Topology 4	%
NEDC	1.212	1.215	0.23%
NYCC	0.111	0.086	-22.35%
ECOn	1.304	1.244	-4.62%
ECOp	0.831	0.777	-6.45%

6.3.1. ECO negative versus ECO positive

A comparison between the ECO drivers for all four Topologies is provided in Table 6.6. A negative difference indicates improvement for ECOp driver compared to ECOn driver within the same topology. A notable observation is seen when comparing the performance of ECOp (positive) driving to ECOn driving. Whilst the ECOn driver saw an improvement of 4.62% compared to Topology 4, the ECOp driver saw 6.45% (see Table 6.5). However, when the performance of each driver is compared directly to each other a much larger increase of 36.29% for Topology 3 and 37.51% for Topology 4 can be seen.

This would imply that further improvements can be made with the combination of the three: eco driving and the optimised PEM strategy and Topology, providing weight is not increased or cost is too high.

Table 6.6: ECO driving energy expenditure at the bus (kWh)

	Topology 1	Topology 2	Topology 3	Topology 4
ECO difference	-31.32%	-32.53%	-36.29%	-37.51%

6.3.2. Weight / Volume / Cost

Battery

Table 6.7 shows details on battery density, volume and pricing. As can be seen the online details found could be classed as high power batteries, which indicates there is room for adjustments and improvements by using lower power but higher energy batteries (letting the UC support the power peaks) and as a result reduce the cost of the battery pack further. This point is argued by Miller et al. (2009a).

In the topologies simulated a battery string contained either 30 cells (Topology 1 and 3) or 25 cells (Topology 2 and 4) which would weigh 93 and 77.5 kg per string respectively.

The final calculation will include three strings in parallel to achieve a more realistic battery sized pack. The assumption is made that a 24kWh pack is approximately necessary for a vehicle of the proposed size. The paralleling of the battery packs will affect the efficiency since the current is effectively divided by three.

Table 6.7: Battery specifications

	(Lithium Batteries for Electric Vehicles, 2014)	(Tie and Tan, 2013)	(Miller et al., 2009a)		
			High Energy	High Power	
Specific Energy	93	120	200	95	Wh/kg
Specific Volume	147	220	461	199	Wh/L
Price per kWh[5]	486 (140 / cell)	208	298	595	£/kWh
Capacity	90				Ah
Cell weight	3.1				Kg

[5] Currency exchange rate $1.68 - £1 – source xe.com (last accessed 05/08/2014)

Ultra Capacitor

The UC used in this simulation are based on the Lithium-Ion capacitors from Table 2.1. To establish the necessary voltage 23 were placed in series which was 12 less (per string) if the equivalent Maxwell cell was used. The final comparison is shown in Table 6.8 which shows significant improvement despite the higher internal resistance per cell. The price for the Lithium-Ion capacitor was established through personal market research and the price range quoted was €40-€60 (£32-£48) depending on ordering quantities. In this thesis a low quantity was assumed, leaving room for improvements. The price for Maxwell ultra capacitors is stated to be between $10-20/Wh for energy or $15-30/kW based on power rating (Miller et al., 2009a).

The choice for the Li-Ion UC is based on its significant weight and volume reduction which comes at a cost in operating range. The operating range is less important since below a certain value the problems with efficiency increase as reported earlier. At high input to output voltage ratio instability also becomes an issue.

Table 6.8: Comparison UC string – 3 parallel

	Li-Ion 2200	**Maxwell 2700**			
Capacitance	286.95	231.42		F	
Ri	0.0107	0.0105		Ω	
Vmax	87.40	87.50		V	
Vmin	50.60	0		V	
Weight[6]	25.71	106.77		Kg	
Volume	22.2	88.2		L	
		energy		power	
Price[7]	€60 (£48) / cell £3 312	$2 460 (£1 429)	$4 920 (£2 929)	$1 350 (£804)	$2 700 (£1 607)

[6] Packaging factor for both weight and volume of 0.7
[7] Currency exchange rate £1 = €1.25 (last accessed 14/08/2014)

Converter

Ortuzar (2005) estimated the cost for his 45kW converter at around $1200 (approx £714). Miller (2004) reported a power density of 5kW/kg for a DC-DC converter, which is expected to rise to 14.1kW / kg in 2020 (Rosario, 2007). In terms of volume (Miller et al., 2009a) expect 25kW/L to be the current norm.

Based on this data the total mass of the module becomes: $\frac{30}{5} + 25.71 = 31.71$ kg based on the lowest converter density rating with a volume of $\frac{30}{25} + 22.2 = 23.4$ L and a cost of 714 + 3312 = £4026. The converter for the battery is rated at 80 kW (which is equivalent to the motor power of the Nissan Leaf (U.S. Department of Energy, 2012). This converter would have a mass of $\frac{80}{5} = 15$ kg and a volume of $\frac{80}{25} = 3.2$ L. As a cost indication the value of the UC converter is doubled and thus the cost for the battery converter becomes: £1428. The data calculated for the different topologies is shown in Table 6.9.

The final weight of around 300kg for the battery pack would be in line with assumptions from other research (Aguirre et al., 2012).

The value for the volume is high and the main reason for this is the off-the-shelf aspect of these batteries versus designed from the cell level up (including electronics for monitoring of SoC and temperature) as with the Nissan Leaf battery.

The calculated cost of the battery pack seems to be in the correct region for an electric vehicle battery: estimates of the Nissan Leaf battery pack vary between £12k and £15k.

Table 6.9: Topology Weight, Volume and Cost

	Topology 1	Topology 2	Topology 3	Topology 4
Battery				
Weight (kg)	93	77.50	93	77.50
Volume (L)	58.38	48.65	58.38	48.65
Price (£)/string	4 200	3 500	4 200	3 500
Price for 3 strings (£)	**12 600**	**10 500**	**12 600**	**10 500**
UC Module[89]				
Weight			31.71	31.71
Volume (L)			23.4	23.4
Price (£)			**4026**	**4026**
Converter battery				
Weight (Kg)		15		15
Volume (L)		3.2		3.2
Price (£)		**1 428**		**1 428**
Total Weight (kg)				
3 strings	279 (25.92kWh)	247.5 (21.6kWh)	310.71	279.21
Total Volume (L)				
3 strings	175.14	149.15	198.44	172.55
Total Cost (£)	**12 600**	**11 928**	**16 626**	**15 954**

6.3.3. Life span improvement

A full life cycle analysis is beyond the scope of this thesis but the life span of the battery pack is one of the most important parts of this analysis because of the cost involved. How long the battery pack will last is thus of great importance not only from a life cycle analysis but also for resale value of the vehicle.

In section 2.2.3 Life span (page 18) an average lifespan of 7 years was found. In order to achieve a ten year lifespan 43% of the battery pack would need to be replaced $\left(\frac{10\ years-3\ years}{7\ years} * 100\right)$. A virtual vehicle lifespan of ten years is chosen

[8] The module would add 202Wh extra energy when charged from the wall.
[9] This includes the converter

since it is felt that the battery development in the next ten years will be such that any replacement happening in ten years from now will provide such batteries as to be able to last for ten years or longer. It should be noted that in the author's opinion it would prove very difficult to replace only 43% of a battery pack but there are arguments that suggest this not unreasonable because of the modularity of the battery modules (Aguirre et al., 2012). In practice it is more likely that the entire pack would be replaced which makes the cost argument even more compelling. However, current convention states that only 43% will need replacing so this is the figure used.

A final simulation was run using repeated drive cycles until a final SoC of 30% was registered. In all cases Topology 2 had the shortest runtime. The comparison over the different Topologies and drive cycles was done with the runtime of Topology 2. An efficiency adjustment was made because the current as seen by the full battery pack is now calculated per string (1/3rd of the current that the whole pack sees). The battery efficiency results are shown in Table 6.10, which shows a reduction in battery efficiency compared to Table 6.1.

Table 6.10: Full battery pack efficiency, repeated drive cycles (kWh)

	Topology 1	Topology 2	%	Topology 3	%	Topology 4	%
NEDC	5.550	5.905	6.40%	5.064	-8.76%	5.332	-3.93%
NYCC	6.537	6.811	4.19%	5.332	-18.43%	5.443	-16.74%
ECOn	5.872	6.293	7.17%	4.945	-15.79%	5.345	-8.97%
ECOp	6.341	6.725	6.06%	5.153	-18.74%	5.398	-14.87%

The overall efficiency results for this simulation are shown in Table 6.11. The overall efficiencies are better compared to the single drive cycle approach (Table 6.4), which indicates that the UC module over the whole discharge cycle has a positive effect on the overall efficiency of the drive train.

Table 6.11: Full battery pack, repeated drive cycles, overall efficiency (kWh)

	Topology 1	Topology 2	%	Topology 3	%	Topology 4	%
NEDC	5.122	5.511	7.59%	3.652	-28.71%	3.520	-31.28%
NYCC	5.357	5.716	6.70%	1.519	-71.64%	1.176	-78.05%
ECOn	5.013	5.492	9.55%	2.781	-44.53%	2.666	-46.82%
ECOp	5.129	5.603	9.24%	2.640	-48.53%	2.449	-52.25%

The assumption is made that a vehicle drives on average 20 000 km per year or 60 km per discharge cycle. This would result in a distance over seven years of 140 000 km (which is around 2 333 charge / discharge cycles). Table 6.12 shows the result of the effect that the efficiency increase has on the battery energy improvement. If the assumption is made that efficiency improvement directly translates to increased km / cycle then the average increase (from a battery perspective) over the two topologies (3 & 4) is 72.62 and 66.68 km respectively on average, which in turn (based on 2 333 cycles) results in a battery improvement to 8.47 years and 7.78 years. This would be from a battery only perspective but the battery has been passing charge onto the UC module which has not been taken into account yet.

Table 6.12: Distance per cycle increase based on battery efficiency increase

	Topology 3 (%)	km / cycle	Topology 4 (%)	km / cycle
NEDC	-8.76%	65.25	-3.93%	62.36
NYCC	-18.43%	71.06	-16.74%	70.04
ECOn	-15.79%	69.47	-8.97%	65.38
ECOp	-18.74%	71.24	-14.87%	68.92
Average		69.26		66.68

If the efficiency calculation includes the whole system then the average result between topology 3 and 4 are: 89.01 and 91.26 km per charge / discharge cycle

(Table 6.13), which results in a total driveable distance after 2 333 cycles of 207 660 km and 212 909 km, which at an average of 20 000 km per year equals 10.38 and 10.65 years of use. It should be noted that Topology 3 would have generally more energy due to the larger battery pack and thus would be able to provide energy for further travel.

Table 6.13: Distance per cycle increase based on overall efficiency increase

	Topology 3 (%)	km / cycle	Topology 4 (%)	km / cycle
NEDC	-28.71%	77.22	-31.28%	78.77
NYCC	-71.64%	102.99	-78.05%	106.83
ECOn	-44.53%	86.72	-46.82%	88.09
ECOp	-48.53%	89.12	-52.25%	91.35
Average		89.01		91.26

The calculations are carried out based on the assumption that the efficiency directly improves the driving range per charge / discharge cycle and does not take in account the effects the increased aging effect as a result of cold / hot temperature changes, how often fast chargers are used and the average SoC when not in use.

From a cost perspective – see Table 6.14 -, the implications are that Topology 1 would see at least part of the battery pack replaced to reach the ten year target, which results in a higher cost for the battery pack over a 10 year cycle while Topology 3 and 4 result in a lower overall cost with Topology 4 the lowest cost over a 10 year duration.

Although Topology 3 is more efficient it also is heavier, which will reduce its efficiency. The efficiency reported here is probably on the high side since the weight was not factored into the simulation. Topology 4, although more complex

to setup and control, shows a higher km / cycle improvement than Topology 3 but at reduced weight and cost.

Table 6.14: Cost comparison based on efficiency

	Topology 1	Topology 3	Topology 4
Initial Purchase Cost	£ 12 600	£ 16 626	£ 15 954
Replaced (43%)	£ 5 418	-	-
Total Pack Cost (After 10 years)	£ 18 018	£ 16 626	£ 15 954

6.3.4. Weight adjustment

As mentioned a potential solution to the ripple effect that the battery sees in Topology 3 is the introduction of another inductor which would work together with bus capacitance as a filter to smooth the ripple. This will add weight and losses to the system reducing its efficiency. The battery operating range requires an inverter with a wide operating window which will affect inverter efficiency in contrast to the more stable bus voltage in Topology 4 where a potential saving can be made on the inverter / motor controller level by designing it with tighter tolerances, potentially reducing weight and improving efficiency and certainly as reported earlier reducing cost.

Chapter Seven

Conclusions and Future Research

7.1.Validate hypothesis

In this thesis the development of a strategy for the management and control of multiple energy sources has been presented as well as the result of this development: a novel Power and Energy Management Strategy (PEMS). This PEMS has been presented and simulated. The new strategy has proven, in simulation, to be very efficient in increasing the life span of the battery by increasing the distance driven per charge / discharge cycle. The system has proven that driveability has not been reduced and that the system will further improve efficiency when adhering to ECO driving rules. The PMS is integrated with the Operational Control which increases response times allowing for a reduced sized bus capacitor.

In Table 7.1 the developed Markov Chain EMS is compared to the energy management strategies discussed in section 2.10.3 (page 75) and compares well against the current state of the art. The effectiveness of the optimisation is given a rating on the following scale: H = High, M = Medium, L= low.

The Markov Chain Analysis allows for a low computational, practical and predictive energy management implementation and with the combination of the PMS the response rate does not have to be fast. The Markov Chain matrix provides a predictive snapshot from which the EMS control parameters can be set which allows for reduced capacity design for the UC module in combination with reduced power, resulting in a lighter system.

Different topologies have been researched and discussed:

- Topology 3 has improved efficiency compared to Topology 1 but also increased cost and weight and requires further investigation in the issues of control and adjustment to reduce the ripple effect to avoid increased heat generation in the battery.
- Topology 4 has weight and cost improvement as well as efficiency improvements over Topology 3
- Neither topology sacrifices driveability

Table 7.1: Comparison of optimisation strategies

Optimisation Strategy	Optimisation	sensitive to noise	Large data base	computationally intensive	requires baseline strategy	Fast or slow response	Self learning	Comments
Stochastic Optimal Control	H		x	x		na		offline optimisation only and both require a-priory knowledge of driving aspects
Dynamic Programming	H	x	x	x		na		
Model Predictive Control	M-H		x	x	x	slow	x	empirical tuning required
Drive Cycle Prediction	L-M	x	x	x	x			highly dependent on accuracy of the prediction
equivalent consumption minimisation strategy	M-H			x	x	fast		non predictive
rule based strategies	L					fast		limited to a selected number of variables
Neural Networks	M		x	x		slow	x	requires a lot of training data for optimal control but can be adaptive
Flexible load demand	L					fast		simple but effective
Markov Chain EMS	M		x		no[1]	slow[2]	x	

Comments:

1. A baseline strategy would not be required but would help in the initial control while the Markov Chain matrix is being populated.

2. The response of the EMS is allowed to be slow since the fast response is dealt with through the PMS.

For both topologies, the initial upfront cost is higher than the cost for Topology 1 but the operating cost over a 10 year life span from a battery perspective is less and the range per cycle has been increased which would assist in reducing range anxiety.

A Pugh analysis (Burge, 2013) was applied to the different topologies to see which one would be preferred as the best solution to replace Topology 1 (baseline), based on a limited set of criteria as discussed in this thesis. A full explanation of the individual criteria can be found in Appendix 12.

Table 7.2 shows the outcome of the analysis and shows Topology 4 as the best option. The option to design for battery ripple in Topology 4 combined with the improvement in efficiency (and range despite a reduced capacity) and the possibility for further improvement of the motor controller (in both weight (Synthesis Partners LLC, 2011) and efficiency (Estima and Marques Cardoso, 2012)) without adding weight make it the preferred topology for BEV.

Table 7.2: Pugh Analysis

	Capacity	Ripple control	weight	10 year cost	Motor controller improvement	Range	Efficiency	Rating
Topology 1	S	S	S	S	S	S	S	0
Topology 2	-1	+1	+1	-1	+1	-1	-1	-2
Topology 3	S	-1	-1	+1	S	+1	+1	+1
Topology 4	-1	+1	S	+1	+1	+1	+1	+4

It is known that choice of assessment criteria, the understanding of the criteria and the low granularity of the scoring system is a limitation to the Pugh analysis (Burge, 2013). The criteria chosen have been discussed and researched in this thesis as such the value of the outcome of the analysis is of high quality.

However, while the outcome is of significant importance to this thesis it can be considered limited to - for example – an Original Equipment Manufacturer.

The proposed PEMS has been tested and validated against real world driving cycles using different topologies and proven to be able to improve efficiency, weight, cost and life span as well as further enhance ECO driving behaviour, thus proving the hypothesis.

The PEMS is a practical design that can be implemented in a modular fashion and not affect driveability thus support the points 1 and 3 made by Crolla et al (2008). Regenerative energy recovery (point 2) while touched on in this thesis is supported in the control but as discussed will always require master control from the ABS to maintain safe braking conditions.

7.2.**Future**

The PEMS can be further improved by running the Markov chain analysis as an optimisation program while the vehicle is in use and as such further gains can be achieved this would require onboard data storage and care must be taken to keep the system practical. More research is required here. The power limit levels are currently set in a rule based function. An improvement would be to expend this through use of a fuzzy logic set. Another improvement would be to allow the Bias function to feed the rule based function or the fuzzy logic set. Thus including the Markov Chain analysis in the process.

Using a larger drive cycle set for Markov Chain analysis would allow the EMS to be further improved which could lead to a further size reduction and potentially power reduction of the UC module.

Currently all control and simulations are carried out using a current reference which from a power limiting (protection of the converter) point of view is not ideal. When the input voltage to a converter is falling any demanded power requires a rise in current as explained using the power balance equation. Suppose, the control strategy is limited at 300A for the UC, which at 80V would mean a possible 24kW of power but since the voltage will be falling - for example: after a certain amount of time the input only shows 60V then the possible power is limited to 18kW. An improved control design would be to design for a maximum power use. In that way you could design for 24kW at 60V, which would limit the current supply at 80V but allows for a more constant power delivery.

References

[1] Aguirre, K., Eisenhardt, L., Lim, C., Nelson, B., Norring, A., Slowik, P. and Tu, N. (2012) 'Lifecycle analysis comparison of a battery electric vehicle and a conventional gasoline vehicle'.

[2] Ahmadi, R., Zargarzadeh, H. and Ferdowsi, M. (2013) 'Nonlinear Power Sharing Controller for a Double-Input H-Bridge-Based Buckboost-Buckboost Converter', *Power Electronics, IEEE Transactions on,* 28(5), pp. 2402-2414.

[3] Al-Hallaj, S., Kizilel, R., Lateef, A., Sabbah, R., Farid, M. and Selman, J. 'Passive thermal management using phase change material (PCM) for EV and HEV Li-ion batteries'. *Vehicle Power and Propulsion, 2005 IEEE Conference*: IEEE, pp. 1-5.

[4] Amjadi, Z. and Williamson, S. S. (2010) 'Power-Electronics-Based Solutions for Plug-in Hybrid Electric Vehicle Energy Storage and Management Systems', *Industrial Electronics, IEEE Transactions on,* 57(2), pp. 608-616.

[5] Anderman, M. (2014) *The Tesla Battery Report* Total Battery Consulting Inc.

[6] *Average Annual Car Miles UK* (2014). Available at: http://www.car-insurance-information.org/average-annual-car-miles-uk.html (Accessed: 15 August 2014).

[7] Ayad, M.-Y., Pierfederici, S., Raël, S. and Davat, B. (2007) 'Voltage regulated hybrid DC power source using supercapacitors as energy storage device', *Energy Conversion and Management,* 48(7), pp. 2196-2202.

[8] Baglee, D., Kok, D. and Morris, A. 'Prototype Pre-Heat System for Electric Vehicles (Keynote presentation)'. *Next Generation Batteries 2014 conference* San Diego, CA, USA, April 29-30.

[9] Baisden, A. C. and Emadi, A. (2004) 'ADVISOR-based model of a battery and an ultra-capacitor energy source for hybrid electric vehicles', *Vehicular Technology, IEEE Transactions on,* 53(1), pp. 199-205.

[10] Bala, S., Tengner, T., Rosenfeld, P. and Delince, F. 'The effect of low frequency current ripple on the performance of a Lithium Iron Phosphate (LFP) battery energy storage system'. *Energy Conversion Congress and Exposition (ECCE), 2012 IEEE*, 15-20 Sept. 2012, pp. 3485-3492.

[11] Bard, A. J. and Faulkner, L. R. (2000) *Electrochemical Methods: Fundamentals and Applications.* Wiley.

[12] Barkenbus, J. N. (2010) 'Eco-driving: An overlooked climate change initiative', *Energy Policy,* 38(2), pp. 762-769.

[13] Bender, F. A., Kaszynski, M. and Sawodny, O. (2013) 'Drive Cycle Prediction and Energy Management Optimization for Hybrid Hydraulic

Vehicles', *Vehicular Technology, IEEE Transactions on,* 62(8), pp. 3581-3592.

[14] Bitsche, O. and Gutmann, G. (2004) 'Systems for hybrid cars', *Journal of Power Sources,* 127(1–2), pp. 8-15.

[15] Blanco, S. (2010) *Details on Nissan Leaf battery pack, including how recharging speed affects battery life*. Available at: http://green.autoblog.com/2010/05/27/details-on-nissan-leaf-battery-pack-including-how-recharging-sp/ (Accessed: 18 December 2012).

[16] Blanes, J. M., Gutierrez, R., Garrigos, A., Lizan, J. L. and Cuadrado, J. M. (2013) 'Electric Vehicle Battery Life Extension Using Ultracapacitors and an FPGA Controlled Interleaved Buck-Boost Converter', *Power Electronics, IEEE Transactions on,* 28(12), pp. 5940-5948.

[17] Bo, C., Yimin, G., Ehsani, M. and Miller, J. M. 'Design and control of a ultracapacitor boosted hybrid fuel cell vehicle'. *Vehicle Power and Propulsion Conference, 2009. VPPC '09. IEEE*, 7-10 Sept. 2009, pp. 696-703.

[18] Borhan, H., Vahidi, A., Phillips, A. M., Kuang, M. L., Kolmanovsky, I. V. and Di Cairano, S. (2012) 'MPC-Based Energy Management of a Power-Split Hybrid Electric Vehicle', *Control Systems Technology, IEEE Transactions on,* 20(3), pp. 593-603.

[19] Bose, B. K., Kim, M. H. and Kankam, M. D. 'Power and energy storage devices for next generation hybrid electric vehicle'. *Energy Conversion Engineering Conference, 1996. IECEC 96. Proceedings of the 31st Intersociety*, pp. 1893-1898 vol.3.

[20] Bradley, T. H. and Frank, A. A. (2009) 'Design, demonstrations and sustainability impact assessments for plug-in hybrid electric vehicles', *Renewable and Sustainable Energy Reviews,* 13(1), pp. 115-128.

[21] Burge, S. (2013) 'The systems engineering tool box', *London, UK*, pp. 1.

[22] Burke, A. F. 'Cost-effective combinations of ultracapacitors and batteries for vehicle applications'. *Second Int. Advanced Battery Conf.*, Las Vegas, Nevada.

[23] Burnett, M. B. and Borle, L. J. 'A power system combining batteries and supercapacitors in a solar/hydrogen hybrid electric vehicle'. *Vehicle Power and Propulsion, 2005 IEEE Conference*, 7-9 Sept. 2005, p. 7 pp.

[24] Byeon, G., Yoon, T., Oh, S. and Jang, G. (2013) 'Energy Management Strategy of the DC Distribution System in Buildings Using the EV Service Model', *Power Electronics, IEEE Transactions on,* 28(4), pp. 1544-1554.

[25] Camara, M. B., Gualous, H., Gustin, F. and Berthon, A. (2008) 'Design and New Control of DC/DC Converters to Share Energy Between Supercapacitors and Batteries in Hybrid Vehicles', *Vehicular Technology, IEEE Transactions on,* 57(5), pp. 2721-2735.

[26] Caponet, M. C., Profumo, F., De Doncker, R. W. and Tenconi, A. 'Low stray inductance bus bar design and construction for good EMC performance in power electronic circuits'. *Power Electronics Specialists Conference, 2000. PESC 00. 2000 IEEE 31st Annual*, pp. 916-921.

[27] Caricchi, F., Crescimbini, F., Noia, G. and Pirolo, D. 'Experimental study of a bidirectional DC-DC converter for the DC link voltage control and the regenerative braking in PM motor drives devoted to electrical vehicles'. *Applied Power Electronics Conference and Exposition, 1994. APEC '94. Conference Proceedings 1994., Ninth Annual*, pp. 381-386 vol.1.

[28] Carroll, S. (2011) *CENEX - The Smart Move Case Studies*, Leicestershire: CENEX.

[29] Carter, R., Cruden, A. and Hall, P. J. (2012) 'Optimizing for Efficiency or Battery Life in a Battery/Supercapacitor Electric Vehicle', *Vehicular Technology, IEEE Transactions on,* 61(4), pp. 1526-1533.

[30] Chan, C. C. (2007) 'The State of the Art of Electric, Hybrid, and Fuel Cell Vehicles', *Proceedings of the IEEE,* 95(4), pp. 704-718.

[31] Cho, B. H., Bae, H. S. and Lee, J. H. 'Review of current mode control schemes and introduction of a new digital current mode control method for the parallel module DC-DC converters'. *Power Electronics and Motion Control Conference, 2009. IPEMC '09. IEEE 6th International*, 17-20 May 2009, pp. 202-210.

[32] Crolla, D. A., Ren, Q., ElDemerdash, S. and Yu, F. (2008) 'Controller design for hybrid vehicles - state of the art review', *Vehicle Power and Propulsion Conference, 2008. VPPC '08. IEEE*, Harbin, China, September 3-5: IEEE, pp. 1-6.

[33] Di Napoli, A., Crescimbini, F., Rodo, S. and Solero, L. 'Multiple input DC-DC power converter for fuel-cell powered hybrid vehicles'. *Power Electronics Specialists Conference, 2002. pesc 02. 2002 IEEE 33rd Annual*, pp. 1685-1690.

[34] Di Napoli, A., Crescimbini, F., Solero, L., Caricchi, F. and Capponi, F. G. 'Multiple-input DC-DC power converter for power-flow management in hybrid vehicles'. *Industry Applications Conference, 2002. 37th IAS Annual Meeting. Conference Record of the*, pp. 1578-1585 vol.3.

[35] Di Napoli, A., Crescimbini, F., Solero, L., Pede, G., Lo Bianco, G. and Pasquali, M. 'Ultracapacitor and Battery Storage System Supporting Fuel-Cell Powered Vehicles'. *EVS 18* Berlin.

[36] Di Napoli, A., Giulii Capponi, F. and Solero, L. 'Power Converter Arrangements with Ultracapacitor Tank for Battery Load Leveling in EV Drives'. *Proceedings 8th European Conference on Power Electronics and Applications*, Lausanne, Switzerland, 7-9 September 1999: EPE.

[37] Divan, D. M. (1989) 'The resonant DC link converter-a new concept in static power conversion', *Industry Applications, IEEE Transactions on,* 25(2), pp. 317-325.

[38] Divya, K. C. and Østergaard, J. (2009) 'Battery energy storage technology for power systems—An overview', *Electric Power Systems Research,* 79(4), pp. 511-520.

[39] Dixon, J. W. and Ortuzar, M. E. (2002) 'Ultracapacitors + DC-DC converters in regenerative braking system', *Aerospace and Electronic Systems Magazine, IEEE,* 17(8), pp. 16-21.

[40] Dixon, L. 1998. Average Current Mode Control of Switching Power Supplies. *Application note.* Merrimack: Unitrode Corporation.

[41] Dobbs, B. G. and Chapman, P. L. (2003) 'A multiple-input DC-DC converter topology', *Power Electronics Letters, IEEE,* 1(1), pp. 6-9.

[42] Doerffel, D. and Sharkh, S. A. (2006) 'A critical review of using the Peukert equation for determining the remaining capacity of lead-acid and lithium-ion batteries', *Journal of Power Sources,* 155(2), pp. 395-400.

[43] Dong, T. K., Kirchev, A., Mattera, F., Kowal, J. and Bultel, Y. (2011) 'Dynamic Modeling of Li-Ion Batteries Using an Equivalent Electrical Circuit', *Journal of The Electrochemical Society,* 158(3), pp. A326-A336.

[44] Donghwa, S., Younghyun, K., Jaeam, S., Naehyuck, C., Yanzhi, W. and Pedram, M. 'Battery-supercapacitor hybrid system for high-rate pulsed load applications'. *Design, Automation & Test in Europe Conference & Exhibition (DATE), 2011*, 14-18 March 2011, pp. 1-4.

[45] Dusmez, S. and Khaligh, A. (2013) 'A Compact and Integrated Multifunctional Power Electronic Interface for Plug-in Electric Vehicles', *Power Electronics, IEEE Transactions on,* 28(12), pp. 5690-5701.

[46] Ehsani, M., Gao, Y., Gay, S. E. and Emadi, A. (2004) *Modern Electric, Hybrid Electric, and Fuel Cell Vehicles: Fundamentals, Theory, and Design.* 1 edition (20 Dec 2004) edn.: CRC Press.

[47] Eller, B., Hetet, J. F., Andre, S. and Hennequet, G. 'Electric vehicle platform for drivability analysis'. *Control and Automation (ICCA), 2010 8th IEEE International Conference on*, 9-11 June 2010, pp. 2251-2257.

[48] Erickson, R. W. and Maksimovic, D. (2001) *Fundamentals of power electronics.* 2nd ed. edn. Boston, Mass. ; [Great Britain]: Kluwer Academic Publishers.

[49] Estima, J. O. and Marques Cardoso, A. J. (2012) 'Efficiency Analysis of Drive Train Topologies Applied to Electric/Hybrid Vehicles', *Vehicular Technology, IEEE Transactions on,* 61(3), pp. 1021-1031.

[50] Etxeberria, A., Vechiu, I., Camblong, H. and Vinassa, J. M. (2012) 'Comparison of three topologies and controls of a hybrid energy storage system for microgrids', *Energy Conversion and Management,* 54(1), pp. 113-121.

[51] Ferrero, R., Marracci, M. and Tellini, B. 'Impedance spectroscopy on a single PEM fuel cell for the evaluation of current ripple effects'. *Instrumentation and Measurement Technology Conference (I2MTC), 2012 IEEE International*, 13-16 May 2012, pp. 52-56.

[52] Finch, J. W. and Giaouris, D. (2008) 'Controlled AC Electrical Drives', *Industrial Electronics, IEEE Transactions on,* 55(2), pp. 481-491.

[53] Floyd, T. L. (1997) *Principles of electric circuits.* 5th ed. edn. London: Prentice-Hall International.

[54] Froberg, A. and Nielsen, L. (2008) 'Efficient Drive Cycle Simulation', *Vehicular Technology, IEEE Transactions on,* 57(3), pp. 1442-1453.

[55] Fuyuan, Y., Languang, L., Yuping, Y. and He, Y. (2010) 'Characterization, Analysis and Modeling of an Ultracapacitor', *World Electric Vehicle Journal,* 4, pp. 358-369.

[56] Gao, Y., Chen, L. and Ehsani, M. 1999. Investigation of the Effectiveness of Regenerative Braking for EV and HEV. SAE Technical Paper 1999-01-2910.

[57] Gerard, M., Poirot-Crouvezier, J.-P., Hissel, D. and Péra, M.-C. (2010) 'Ripple Current Effects on PEMFC Aging Test by Experimental and Modeling', *Journal of Fuel Cell Science and Technology,* 8(2), pp. 021004-021004.

[58] Gerssen-Gondelach, S. J. and Faaij, A. P. C. (2012) 'Performance of batteries for electric vehicles on short and longer term', *Journal of Power Sources,* 212(0), pp. 111-129.

[59] Giaouris, D., Banerjee, S., Stergiopoulos, F., Papadopoulou, S., Voutetakis, S., Zahawi, B., Pickert, V., Abusorrah, A., Al Hindawi, M. and Al-Turki, Y. (2013) 'Foldings and grazings of tori in current controlled interleaved boost converters', *International Journal of Circuit Theory and Applications*, pp. n/a-n/a.

[60] Giaouris, D., Banerjee, S., Zahawi, B. and Pickert, V. (2008) 'Stability Analysis of the Continuous-Conduction-Mode Buck Converter Via Filippov's Method', *Circuits and Systems I: Regular Papers, IEEE Transactions on,* 55(4), pp. 1084-1096.

[61] Giaouris, D., Maity, S., Banerjee, S., Pickert, V. and Zahawi, B. (2009) 'Application of Filippov method for the analysis of subharmonic instability in dc–dc converters', *International Journal of Circuit Theory and Applications,* 37(8), pp. 899-919.

[62] Grbovic, P. J., Delarue, P., Le Moigne, P. and Bartholomeus, P. (2011) 'Modeling and Control of the Ultracapacitor-Based Regenerative Controlled Electric Drives', *Industrial Electronics, IEEE Transactions on,* 58(8), pp. 3471-3484.

[63] Gurkaynak, Y., Khaligh, A. and Emadi, A. 'State of the art power management algorithms for hybrid electric vehicles'. *Vehicle Power and Propulsion Conference, 2009. VPPC '09. IEEE*, 7-10 Sept. 2009, pp. 388-394.

[64] Hampson-Jones, H. W. 'Safe, affordable high energy batteries, powering the revolution in transportation (presentation)'. *Electric Vehicles 2012 - Accelerating adoption*, Gateshead College, Sunderland: IET.

[65] Harris, S. J., Timmons, A., Baker, D. R. and Monroe, C. (2010) 'Direct in situ measurements of Li transport in Li-ion battery negative electrodes', *Chemical Physics Letters,* 485(4–6), pp. 265-274.

[66] Hegazy, O., Van Mierlo, J. and Lataire, P. (2012) 'Analysis, Modeling, and Implementation of a Multidevice Interleaved DC/DC Converter for Fuel Cell Hybrid Electric Vehicles', *Power Electronics, IEEE Transactions on,* 27(11), pp. 4445-4458.

[67] Hofman, T., Steinbuch, M., Van Druten, R. and Serrarens, A. (2007) 'Rule-based energy management strategies for hybrid vehicles', *International Journal of Electric and Hybrid Vehicles,* 1(1), pp. 71-94.

[68] Høyer, K. G. (2008) 'The history of alternative fuels in transportation: The case of electric and hybrid cars', *Utilities Policy,* 16(2), pp. 63-71.

[69] Hredzak, B., Agelidis, V. G. and Minsoo, J. (2014) 'A Model Predictive Control System for a Hybrid Battery-Ultracapacitor Power Source', *Power Electronics, IEEE Transactions on,* 29(3), pp. 1469-1479.

[70] Husain, I. (2003) *Electric and hybrid vehicles : design fundamentals.* Boca Raton, Fla. ; London: CRC Press.

[71] Ibanez, F., Vadillo, J., Maiza, M. M.-I. and Echeverria, J. M. (2012) '30kW DC-DC Converters with Regenerative Mode for Electric Cars', *Journal of Power Electronics,* 12(2), pp. 233-241.

[72] IEEE Board of Directors 2007. Position Statement on Plug-in Electric Hybrid Vehicles. IEEE-USA.

[73] ieee.tv 2010. APEC 2010 - Exhibitor overview. ieee.tv.

[74] J.R. Miller, A. D. K. 'Electrochemical Capacitor Performance Compared with the Performance of Advanced Lithium Ion Batteries'. *Proc. 17th International Seminar on Double Layer Capacitors and Hybrid Energy Storage Devices*, Deerfield Beach, Florida, Dec. 10-12, 2007

[75] Jamshidpour, E., Nahid-Mobarakeh, B., Poure, P., Pierfederici, S. and Saadate, S. 'Distributed stabilization in DC hybrid power systems'. *Vehicle Power and Propulsion Conference (VPPC), 2011 IEEE*, 6-9 Sept. 2011, pp. 1-6.

[76] Jang, M., Ciobotaru, M. and Agelidis, V. G. (2012) 'A Single-Stage Fuel Cell Energy System Based on a Buck--Boost Inverter with a Backup Energy Storage Unit', *Power Electronics, IEEE Transactions on,* 27(6), pp. 2825-2834.

[77] Jayawickrama, Y. R. L. and Rajakaruna, S. 'Ultracapacitor based ride-through system for a DC load'. *Power System Technology, 2004. PowerCon 2004. 2004 International Conference on*, 21-24 Nov. 2004, pp. 232-237 Vol.1.

[78] Ji, B., Song, X. G., Cao, W. P. and Pickert, V. 'Active temperature control of Li-ion batteries in electric vehicles'. *Hybrid and Electric Vehicles Conference 2013 (HEVC 2013), IET*, 6-7 Nov. 2013, pp. 1-5.

[79] Jian, C. and Emadi, A. 'A new battery/ultra-capacitor hybrid energy storage system for electric, hybrid and plug-in hybrid electric vehicles'. *Vehicle Power and Propulsion Conference, 2009. VPPC '09. IEEE*, 7-10 Sept. 2009, pp. 941-946.

[80] Jian, C., Schofield, N. and Emadi, A. 'Battery balancing methods: A comprehensive review'. *Vehicle Power and Propulsion Conference, 2008. VPPC '08. IEEE*, 3-5 Sept. 2008, pp. 1-6.

[81] Jih-Sheng, L. (2009) 'Power conditioning circuit topologies', *Industrial Electronics Magazine, IEEE,* 3(2), pp. 24-34.

[82] Jin, W., Ke, Z., Chingchi, C. and Lihua, C. 'A high frequency battery model for current ripple analysis'. *Applied Power Electronics Conference and Exposition (APEC), 2010 Twenty-Fifth Annual IEEE*, 21-25 Feb. 2010, pp. 676-680.

[83] Jinrui, N., Fengchun, S. and Qinglian, R. 'A Study of Energy Management System of Electric Vehicles'. *Vehicle Power and Propulsion Conference, 2006. VPPC '06. IEEE*, pp. 1-6.

[84] Jinrui, N., Zhifu, W. and Qinglian, R. 'Simulation and Analysis of Performance of a Pure Electric Vehicle with a Super-capacitor'. *Vehicle Power and Propulsion Conference, 2006. VPPC '06. IEEE*, pp. 1-6.

[85] Jongh, P. E. d. and Notten, P. H. L. (2002) 'Effect of current pulses on lithium intercalation batteries', *Solid State Ionics,* 148, pp. 259-268.

[86] Kessels, J. T. B. A., Van den Bosch, P. P. J., Koot, M. and de Jager, B. 'Energy management for vehicle power net with flexible electric load demand'. *Control Applications, 2005. CCA 2005. Proceedings of 2005 IEEE Conference on*, 28-31 Aug. 2005, pp. 1504-1509.

[87] Khaligh, A. 'A multiple-input dc-dc positive buck-boost converter topology'. *Applied Power Electronics Conference and Exposition, 2008. APEC 2008. Twenty-Third Annual IEEE*, 24-28 Feb. 2008, pp. 1522-1526.

[88] Khaligh, A., Jian, C. and Young-Joo, L. (2009) 'A Multiple-Input DC-DC Converter Topology', *Power Electronics, IEEE Transactions on,* 24(3), pp. 862-868.

[89] Khaligh, A. and Zhihao, L. (2010) 'Battery, Ultracapacitor, Fuel Cell, and Hybrid Energy Storage Systems for Electric, Hybrid Electric, Fuel Cell, and Plug-In Hybrid Electric Vehicles: State of the Art', *Vehicular Technology, IEEE Transactions on,* 59(6), pp. 2806-2814.

[90] Knowles, M., Kok, D., Baglee, D. and Morris, A. 'Design and Development of a Electric Vehicle Drive Train Test Bed'. *Condition Monitoring and Machine Failure Prevention Technology (BINDT)*, London, UK.

[91] Knowles, M., Scott, H. and Baglee, D. (2012b) 'The effect of driving style on electric vehicle performance, economy and perception', *International Journal of Electric and Hybrid Vehicles,* 4(3), pp. 228-247.

[92] Kok, D., Knowles, M. and Morris, A. (2012) 'Building a Driving Simulator as an Electric Vehicle Hardware Development Tool', *Driving Simulation Conference 2012*, Paris, pp. 325-333.

[93] Kok, D., Morris, A. and Knowles, M. 'Novel EV drive train topology - A review of the current topologies and proposal for a model for improved drivability'. *Power Electronics and Applications (EPE), 2013 15th European Conference on*, 2-6 Sept. 2013, pp. 1-10.

[94] Kok, D., Morris, A., Knowles, M. and Baglee, D. 'Converter simulation using SimPowerSystems: a comparison of drive cycles and control strategies'. *2013 International Conference on Renewable Energy Research and Applications (ICRERA),* , 20-23 Oct. 2013, pp. 800-805.

[95] Kok, D., Morris, A., Knowles, M. and Baglee, D. (2014) 'Battery Ripple Effects in Cascaded and Parallel Connected Converters', *IET Power Electronics*

[96] Kowal, J., Gerschler, J. B., Schaper, C., Schoenen, T. and Sauer, D. U. 'Efficient battery models for the design of EV drive trains'. *Power Electronics and Motion Control Conference (EPE/PEMC), 2010 14th International*, 6-8 Sept. 2010, pp. S11-31-S11-38.

[97] Krause, P. C. and Thomas, C. H. (1965) 'Simulation of Symmetrical Induction Machinery', *Power Apparatus and Systems, IEEE Transactions on,* 84(11), pp. 1038-1053.

[98] Kroeze, R. C. and Krein, P. T. 'Electrical battery model for use in dynamic electric vehicle simulations'. *Power Electronics Specialists Conference, 2008. PESC 2008. IEEE*, pp. 1336-1342.

[99] Krutak, R., Raimund, W., Jellinek, R., Zopf-Renner, C. and Emmerling, B. (2013) *State of the Art Electric Propulsion: Vehicles and Energy Supply* Austria: Austrian Energy Agency.

[100] Ksiazek, P. F. and Ordonez, M. (2014) 'Swinging Bus Technique for Ripple Current Elimination in Fuel Cell Power Conversion', *Power Electronics, IEEE Transactions on,* 29(1), pp. 170-178.

[101] Lacey, G., Tianxiang, J., Putrus, G. and Kotter, R. 'The effect of cycling on the state of health of the electric vehicle battery'. *Power Engineering Conference (UPEC), 2013 48th International Universities'*, 2-5 Sept. 2013, pp. 1-7.

[102] Lambert, S. M., Pickert, V., Holden, J., He, X. and Li, W. 'Comparison of supercapacitor and lithium-ion capacitor technologies for power electronics applications'. *Power Electronics, Machines and Drives (PEMD 2010), 5th IET International Conference on*, 19-21 April 2010, pp. 1-5.

[103] Lane, B. and Potter, S. (2007) 'The adoption of cleaner vehicles in the UK: exploring the consumer attitude–action gap', *Journal of Cleaner Production,* 15(11–12), pp. 1085-1092.

[104] Larminie, J. and Dicks, A. (2003) *Fuel cell systems explained.* 2nd ed. edn. Chichester: Wiley.

[105] Larminie, J. and Lowry, J. (2003) *Electric Vehicle Technology Explained.* Chichester: John Wiley & Sons Ltd.

[106] Leuenberger, M. and Frischknecht, R. (2010) 'Life cycle assessment of battery electric vehicles and concept cars', *Report, ESU-Services Ltd*.

[107] Ling, Z., Chen, J., Fang, X., Zhang, Z., Xu, T., Gao, X. and Wang, S. (2014) 'Experimental and numerical investigation of the application of phase change materials in a simulative power batteries thermal management system', *Applied Energy,* 121(0), pp. 104-113.

[108] *Lithium Batteries for Electric Vehicles* (2014). Available at: http://www.everything-ev.com/index.php?main_page=index&cPath=65_128_135&zenid=esned1m9n7nh0h8nc6ms1u7723 (Accessed: 05 August 2014).

[109] Long, L. and Bauer, P. (2013) 'Practical Capacity Fading Model for Li-Ion Battery Cells in Electric Vehicles', *Power Electronics, IEEE Transactions on,* 28(12), pp. 5910-5918.

[110] Loukakou, D., Gualous, H., Yuan, C., Espanet, C. and Dubas, F. 'Sizing and experimental characterization of ultra-capacitors for small urban hybrid electric vehicle'. *Vehicle Power and Propulsion Conference (VPPC), 2010 IEEE*, 1-3 Sept. 2010, pp. 1-7.

[111] Lugert, G. and Knorr, R. G., H. (2002) '14/42 V powernet and ISG - a solution for high dynamic energy supply suitable for mass market', *INTERNATIONAL ADVANCED AUTOMOTIVE BATTERY CONFERENCE*, Las Vegas, Nevada, p. 10.

[112] Luk, P. C. K. and Rosario, L. C. 'Towards a Negotiation-Based Multi-Agent Power Management System for Electric Vehicles'. *Machine Learning and Cybernetics, 2005. Proceedings of 2005 International Conference on*, pp. 410-416.

[113] Lung-Sheng, Y. and Tsorng-Juu, L. (2012) 'Analysis and Implementation of a Novel Bidirectional DC-DC Converter', *Industrial Electronics, IEEE Transactions on,* 59(1), pp. 422-434.

[114] Lynch, B. (2003) 'Current-Mode Vs. Voltage-Mode Control in Synchronous Buck Converters'.

[115] Makansi, H. and Bergholtz, C. (2010) *Electric Vehicles and Batteries - Charging Ahead*, London: GP BullHound Ltd.

[116] Malikopoulos, A. A. (2014) 'Supervisory Power Management Control Algorithms for Hybrid Electric Vehicles: A Survey', *Intelligent Transportation Systems, IEEE Transactions on,* PP(99), pp. 1-17.

[117] Mallika, S. and Saravana Kumar, R. (2011) 'Review on Ultracapacitor-Battery Interface for Energy Management System', *International Journal of Engineering & Technology (0975-4024),* 3(1).

[118] Marchesoni, M. and Vacca, C. (2007) 'New DC-DC Converter for Energy Storage System Interfacing in Fuel Cell Hybrid Electric Vehicles', *Power Electronics, IEEE Transactions on,* 22(1), pp. 301-308.

[119] Masjosthusmann, C., Kohler, U., Decius, N. and Buker, U. 'A vehicle energy management system for a Battery Electric Vehicle'. *Vehicle Power and Propulsion Conference (VPPC), 2012 IEEE*, 9-12 Oct. 2012, pp. 339-344.

[120] Maxwell Technologies Inc. (2007) *Ultracapacitors Help P21 To Provide Fuel Cell Based Backup Power For Telecoms [case study].* p. 8.

[121] Mesbahi, T., Rizoug, N., Bartholomeus, P. and Le Moigne, P. 'A new energy management strategy of a Battery/Supercapacitor Hybrid Energy Storage System for electric vehicular applications'. *Power Electronics, Machines and Drives (PEMD 2014), 7th IET International Conference on*, 8-10 April 2014, pp. 1-7.

[122] Mestre, P. and Astier, S. 'Utilization of Ultracapacitors as a Auxiliary Power Source in Electric Vehicle'. *Proceedings of the EPE'97 Conference*, Trondheim, Norway, pp. 670-673.

[123] Miller, J. (2004) *Propulsion Systems for Hybrid Vehicles.* London: The Institution of Electrical Engineers.

[124] Miller, J., PE, Prummer, M. and Schneuwly, A. (2007) 'Power Electronic Interface For An Ultracapacitor as the Power Buffer in a Hybrid Electric Energy Storage System ', *Power Systems Design Europe*.

[125] Miller, J. M. 'Electrical and Thermal Performance of the Carbon-carbon Ultracapacitor Under Constant Power Conditions'. *Vehicle Power and*

Propulsion Conference, 2007. VPPC 2007. IEEE, 9-12 Sept. 2007, pp. 559-566.

[126] Miller, J. M. 'Energy storage technology markets and application's: Ultracapacitors in combination with Lithium-ion'. *Power Electronics, 2007. ICPE'07. 7th Internatonal Conference on*: IEEE, pp. 16-22.

[127] Miller, J. M. 'Trends in Vehicle Energy Storage Systems: Batteries and Ultracapacitors to Unite'. *Vehicle Power and Propulsion Conference, 2008. VPPC '08. IEEE*, 3-5 Sept. 2008, pp. 1-9.

[128] Miller, J. M., Bohn, T., Dougherty, T. J. and Deshpande, U. 'Why hybridization of energy storage is essential for future hybrid, plug-in and battery electric vehicles'. *Energy Conversion Congress and Exposition, 2009. ECCE 2009. IEEE*, 20-24 Sept. 2009, pp. 2614-2620.

[129] Miller, J. M., Deshpande, U., Dougherty, T. J. and Bohn, T. 'Power Electronic Enabled Active Hybrid Energy Storage System and its Economic Viability'. *Applied Power Electronics Conference and Exposition, 2009. APEC 2009. Twenty-Fourth Annual IEEE*, 15-19 Feb. 2009, pp. 190-198.

[130] Miller, J. M., Deshpande, U., Dougherty, T. J. and Bohn, T. P. (2008) 'Combination Ultracapacitor-Battery Performance Dependence on Drive Cycle Dynamics', in Marincic, N. (ed.) *The 18th International Seminar on Double Layer Capacitors and Hybrid Energy Storage Devices: December 8 - 10, 2008, Embassy Suites Deerfield Beach Resort, Deerfield Beach, Florida, USA*. United States: Redox Engineering, pp. 124-142.

[131] Miller, J. M. and Everett, M. 'Ultra-capacitor augmentation of the vehicle electrical system to reset its power budget'. *Power Electronics in Transportation, 2004*, pp. 19-26.

[132] Miller, J. M. and Sartorelli, G. 'Battery and ultracapacitor combinations - Where should the converter go?'. *Vehicle Power and Propulsion Conference (VPPC), 2010 IEEE*, 1-3 Sept. 2010, pp. 1-7.

[133] Moreno, J., Ortuzar, M. E. and Dixon, J. W. (2006) 'Energy-management system for a hybrid electric vehicle, using ultracapacitors and neural networks', *Industrial Electronics, IEEE Transactions on,* 53(2), pp. 614-623.

[134] NAIGT (2009) *An Independent Report on the Future of the Automotive Industry in the UK*, London: Department for Business, Enterprise and Regulatory Reform.

[135] Newton, D. 'Presentation on Axeon projects (Presentation)'. *Electric Vehicles 2012 - Acceleratng adoption*, Gateshead College, Sunderland, UK: IET.

[136] Niculuţă, M.-C. and Veje, C. 'Analysis of the thermal behavior of a LiFePO4 battery cell'. *Journal of Physics: Conference Series*: IOP Publishing, p. 012013.

[137] O'Loughlin, M. (2012) *Leading-edge modulation improves power-supply efficiency in PFC designs*: EETimes Design [online]. Available at: http://www.eetimes.com/design/power-management-design/4373892/Leading--edge-modulation-improves-power--supply-

efficiency-in-PFC-designsr-factor-and-supply-performance- (Accessed: 27 May 2012).

[138] Oleksowicz, S. A., Burnham, K. J., Southgate, A., McCoy, C., Waite, G., Hardwick, G., Harrington, C. and McMurran, R. (2013) 'Regenerative braking strategies, vehicle safety and stability control systems: critical use-case proposals', *Vehicle System Dynamics,* (ahead-of-print), pp. 1-16.

[139] Onar, O. and Khaligh, A. 'Dynamic modeling and control of a cascaded active battery/ultra-capacitor based vehicular power system'. *Vehicle Power and Propulsion Conference, 2008. VPPC '08. IEEE*, pp. 1-4.

[140] Ortuzar, M. E. (2005) *Design, Implementation and evaluation of auxiliary energy system for electric vehicle, based on Ultracapacitors and buck-boost converter.* Ph.D. Dissertation, Pontifificia Univeristy Catolica de Chile, Santiago de Chile.

[141] OXIS Energy (2014) email to Kok, T., 22 May.

[142] Payman, A., Pierfederici, S., Meibody-Tabar, F. and Davat, B. (2011) 'An Adapted Control Strategy to Minimize DC-Bus Capacitors of a Parallel Fuel Cell/Ultracapacitor Hybrid System', *Power Electronics, IEEE Transactions on,* 26(12), pp. 3843-3852.

[143] Pesaran, A., Vlahinos, A. and Stuart, T. 'Cooling and preheating of batteries in hybrid electric vehicles'. *6th ASME-JSME Thermal Engineering Joint Conference*.

[144] Pesaran, A. A. (2002) 'Battery thermal models for hybrid vehicle simulations', *Journal of Power Sources,* 110(2), pp. 377-382.

[145] Pickert, V., Cheng, H., Pritchard, L. and Atkinson, D. J. 'An experimental and computational study of water cooled heatsinks for HEV's'. *Power Electronics, Machines and Drives (PEMD 2010), 5th IET International Conference on*, 19-21 April 2010, pp. 1-6.

[146] Pisu, P. and Rizzoni, G. (2007) 'A Comparative Study Of Supervisory Control Strategies for Hybrid Electric Vehicles', *Control Systems Technology, IEEE Transactions on,* 15(3), pp. 506-518.

[147] Qing-Chang, Z., Wen-Long, M., Xin, C. and Krstic, M. 'Reduction of DC-bus voltage ripples and capacitors for single-phase PWM-controlled rectifiers'. *IECON 2012 - 38th Annual Conference on IEEE Industrial Electronics Society*, 25-28 Oct. 2012, pp. 708-713.

[148] Rao, Z. and Wang, S. (2011) 'A review of power battery thermal energy management', *Renewable and Sustainable Energy Reviews,* 15(9), pp. 4554-4571.

[149] Ribeiro, P. F., Johnson, B. K., Crow, M. L., Arsoy, A. and Liu, Y. (2001) 'Energy storage systems for advanced power applications', *Proceedings of the IEEE,* 89(12), pp. 1744-1756.

[150] Rosario, L. and Luk, P. C. K. 'Applying Management Methodology to Electric Vehicles with Multiple Energy Storage Systems'. *Machine Learning and Cybernetics, 2007 International Conference on*, pp. 4223-4230.

[151] Rosario, L. C. (2007) *Power and Energy Management of Multiple Energy Storage Systems in Electric Vehicles.* DOCTOR OF PHILOSOPHY in Electrical Engineering, Cranfield University, Shrivenham.

[152] Rosario, L. C. and Luk, P. C. K. 'Power and Energy Management Policy Implementation of a Dual-Energy Source Electric Vehicle'. *Power Electronics, Machines and Drives, 2006. The 3rd IET International Conference on*, pp. 464-468.

[153] Rufer, A. and Barrade, P. (2002) 'A supercapacitor-based energy-storage system for elevators with soft commutated interface', *Industry Applications, IEEE Transactions on,* 38(5), pp. 1151-1159.

[154] Rufer, A., Barrade, P., Hotellier, D. and Hauser, S. 'Sequential supply for electrical transportation vehicles: properties of the fast energy transfer between supercapacitive tanks'. *Industry Applications Conference, 2003. 38th IAS Annual Meeting. Conference Record of the*, 12-16 Oct. 2003, pp. 1530-1537 vol.3.

[155] Sadoun, R., Rizoug, N., Bartholumeus, P., Barbedette, B. and LeMoigne, P. 'Sizing of hybrid supply (battery-supercapacitor) for electric vehicle taking into account the weight of the additional Buck-Boost chopper'. *Renewable Energies and Vehicular Technology (REVET), 2012 First International Conference on*, 26-28 March 2012, pp. 8-14.

[156] Schoenung, S. (2011) 'Energy storage systems cost update', *Sandia National Laboratories, Albuquerque*.

[157] Schupbach, R. M. and Balda, J. C. '35 KW ultracapacitor unit for power management of hybrid electric vehicles: bidirectional DC-DC converter design'. *Power Electronics Specialists Conference, 2004. PESC 04. 2004 IEEE 35th Annual*, 20-25 June 2004, pp. 2157-2163 Vol.3.

[158] Scott, H., Knowles, M., Morris, A. and Kok, D. (2012) 'The Role of a Driving Simulator in Driver Training to Improve Fuel Economy', *Proceedings of Driving Simulator Conference Europe 2012*, pp. 313-325.

[159] Sharma, P. and Bhatti, T. S. (2010) 'A review on electrochemical double-layer capacitors', *Energy Conversion and Management,* 51(12), pp. 2901-2912.

[160] Shi, K. L., Chan, T. F., Wong, Y. K. and Ho, S. L. (1999) 'Modelling and Simulation of the Three-Phase Induction Motor using Simulink', *International Journal of Electrical Engineering Education,* 36(2), pp. 136-172.

[161] Siang Fui, T. and Chee Wei, T. 'A review of power and energy management strategies in electric vehicles'. *Intelligent and Advanced Systems (ICIAS), 2012 4th International Conference on*, 12-14 June 2012, pp. 412-417.

[162] Simoes, M., Blunier, B. and Miraoui, A. (2014) 'Fuzzy-Based Energy Management Control: Design of a Battery Auxiliary Power Unit for Remote Applications', *Industry Applications Magazine, IEEE,* 20(4), pp. 41-49.

[163] Sivakkumar, S. R. and Pandolfo, A. G. (2012) 'Evaluation of lithium-ion capacitors assembled with pre-lithiated graphite anode and activated carbon cathode', *Electrochimica Acta,* 65(0), pp. 280-287.

[164] Skibinski, G. L. and Divan, D. M. 'Design methodology and modeling of low inductance planar bus structures'. *Power Electronics and Applications, 1993., Fifth European Conference on*, pp. 98-105 vol.3.

[165] Smith, P. H., Tran, T. N., Jiang, T. L. and Chung, J. (2013) 'Lithium-ion capacitors: Electrochemical performance and thermal behavior', *Journal of Power Sources,* 243(0), pp. 982-992.

[166] Smith, T. A., Mars, J. P. and Turner, G. A. 'Using supercapacitors to improve battery performance'. *Power Electronics Specialists Conference, 2002. pesc 02. 2002 IEEE 33rd Annual*, 2002, pp. 124-128 vol.1.

[167] Song, Y. and Wang, B. (2013) 'Survey on Reliability of Power Electronic Systems', *Power Electronics, IEEE Transactions on,* 28(1), pp. 591-604.

[168] Souffran, G., Miegeville, L. and Guerin, P. (2012) 'Simulation of Real-World Vehicle Missions Using a Stochastic Markov Model for Optimal Powertrain Sizing', *Vehicular Technology, IEEE Transactions on,* 61(8), pp. 3454-3465.

[169] Steinmauer, G. and del Re, L. (2001) 'Optimal control of dual power sources', *Control Applications, 2001. (CCA '01). Proceedings of the 2001 IEEE International Conference on*, pp. 422-427.

[170] Stewart, S. G. S. F. C. A., Kohn, S. I. R. C. C. A., Kelty, K. R. P. A. C. A. and Straubel, J. B. M. P. C. A. (2012a) *Electric Vehicle Extended Range Hybrid Battery Pack System* Patent no. US 2012/0041624 A1. [Online]. Available at: http://www.patentlens.net/patentlens/patent/US_2012_0041624_A1/en/ (Accessed: 2013/12/08).

[171] Stewart, S. G. S. F. C. A., Kohn, S. I. R. C. C. A., Kelty, K. R. P. A. C. A. and Straubel, J. B. M. P. C. A. (2012b) *Electric Vehicle Extended Range Hybrid Battery Pack System* Patent no. US 2012/0038314 A1. [Online]. Available at: http://www.patentlens.net/patentlens/patent/US_2012_0038314_A1/en/ (Accessed: 2013/12/08).

[172] Stienecker, A. W., Stuart, T. and Ashtiani, C. 'A combined ultracapacitor-lead acid battery storage system for mild hybrid electric vehicles'. *Vehicle Power and Propulsion, 2005 IEEE Conference*, 7-9 Sept. 2005, p. 6.

[173] Synthesis Partners LLC, Energy, R.f.t.D.o. (2011) *Technology and Market Intelligence: Hybrid Vehicle Power Inverters Cost Analysis*.

[174] Taesic, K., Wei, Q. and Liyan, Q. (2012) 'Power Electronics-Enabled Self-X Multicell Batteries: A Design Toward Smart Batteries', *Power Electronics, IEEE Transactions on,* 27(11), pp. 4723-4733.

[175] Takehara, J., Miyaoka, K. and Fukuda, T. 'EV Mini-Van Featuring Series Conjunction of Ultracapacitors and Batteries for Load Leveling of its Batteries'. *Proceedings of the 14th International Electric Vehicle Symposium*, Orlando, Florida, 15-17 December: Technical Research Center, The Chugoku Electric Power Co., Inc. 3-9-1 Kagamiyama, Higashihiroshima-City, Hiroshima 739, Japan.

[176] Thounthong, P., Rael, S. and Davat, B. (2009a) 'Analysis of Supercapacitor as Second Source Based on Fuel Cell Power

Generation', *Energy Conversion, IEEE Transactions on,* 24(1), pp. 247-255.

[177] Thounthong, P., Raël, S. and Davat, B. (2006) 'Control strategy of fuel cell/supercapacitors hybrid power sources for electric vehicle', *Journal of Power Sources,* 158(1), pp. 806-814.

[178] Thounthong, P., Raël, S. and Davat, B. (2009b) 'Energy management of fuel cell/battery/supercapacitor hybrid power source for vehicle applications', *Journal of Power Sources,* 193(1), pp. 376-385.

[179] Tie, S. F. and Tan, C. W. (2013) 'A review of energy sources and energy management system in electric vehicles', *Renewable and Sustainable Energy Reviews,* 20(0), pp. 82-102.

[180] Tonicello, F. (2002) 'Peak and average current controls: Simulation techniques and comparison', *ESA SP*, pp. 99-105.

[181] Tremblay, O. (2009) 'Experimental Validation of a Battery Dynamic Model for EV Applications', *World Electric Vehicle Journal,* 3.

[182] Tremblay, O., Dessaint, L. A. and Dekkiche, A. I. 'A Generic Battery Model for the Dynamic Simulation of Hybrid Electric Vehicles'. *Vehicle Power and Propulsion Conference, 2007. VPPC 2007. IEEE*, pp. 284-289.

[183] Trovao, J. P., Pereirinha, P. G. and Jorge, H. M. 'Analysis of operation modes for a neighborhood electric vehicle with power sources hybridization'. *Vehicle Power and Propulsion Conference (VPPC), 2010 IEEE*, 1-3 Sept. 2010, pp. 1-6.

[184] Trovão, J. P., Pereirinha, P. G., Jorge, H. M. and Antunes, C. H. (2013) 'A multi-level energy management system for multi-source electric vehicles – An integrated rule-based meta-heuristic approach', *Applied Energy,* 105(0), pp. 304-318.

[185] Trzynadlowski, A. M. (2001) *Control of induction motors.* San Diego ; London: Academic Press.

[186] Tse, C. K. (2004) *Complex behavior of switching power converters.* Boca Raton: CRC Press.

[187] U.S. Department of Energy, Energy, U.S.D.o. (2012) *Advanced Vehicle Testing - Beginning-of-Test Battery Testing Results - 2011 Nissan Leaf.* online: Idaho National Laboratory.

[188] Uzunoglu, M. and Alam, M. S. (2006) 'Dynamic modeling, design, and simulation of a combined PEM fuel cell and ultracapacitor system for stand-alone residential applications', *Energy Conversion, IEEE Transactions on,* 21(3), pp. 767-775.

[189] Valentine-Urbschat, M. and Bernhart, W. (2009) 'Powertrain 2020–The future drives electric'.

[190] Van den Bossche, P., Vergels, F., Van Mierlo, J., Matheys, J. and Van Autenboer, W. (2006) 'SUBAT: An assessment of sustainable battery technology', *Journal of Power Sources,* 162(2), pp. 913-919.

[191] Wang, T., Tseng, K. J., Zhao, J. and Wei, Z. (2014) 'Thermal investigation of lithium-ion battery module with different cell arrangement

structures and forced air-cooling strategies', *Applied Energy,* 134(0), pp. 229-238.

[192] Williams, B. W. (2013) 'DC-to-DC Converters With Continuous Input and Output Power', *Power Electronics, IEEE Transactions on,* 28(5), pp. 2307-2316.

[193] Wuhua, L., Weichen, L., Yan, D. and Xiangning, H. (2010) 'Single-Stage Single-Phase High-Step-Up ZVT Boost Converter for Fuel-Cell Microgrid System', *Power Electronics, IEEE Transactions on,* 25(12), pp. 3057-3065.

[194] Xing, Y., Ma, E. W. M., Tsui, K. L. and Pecht, M. (2011) 'Battery Management Systems in Electric and Hybrid Vehicles', *Energies,* 4(11), pp. 1840-1857.

[195] Xu, N. and Riley, J. (2011) 'Nonlinear analysis of a classical system: The double-layer capacitor', *Electrochemistry Communications,* 13(10), pp. 1077-1081.

[196] Yu, H., Wang, W. and Liu, Z. (2012) 'Parameter Sizing of Hybrid Energy Storage System for Hybrid Electric Vehicle', *Advanced Materials Research,* 608-609, pp. 1643-1646.

[197] Zhang, J., Lv, C., Qiu, M., Li, Y. and Sun, D. (2013a) 'Braking energy regeneration control of a fuel cell hybrid electric bus', *Energy Conversion and Management,* 76(0), pp. 1117-1124.

[198] Zhang, X., Ruan, X., Kim, H. and Tse, C. K. (2013b) 'Adaptive Active Capacitor Converter for Improving Stability of Cascaded DC Power Supply System', *Power Electronics, IEEE Transactions on,* 28(4), pp. 1807-1816.

[199] Zhihao, L., Onar, O., Khaligh, A. and Schaltz, E. 'Design and Control of a Multiple Input DC/DC Converter for Battery/Ultra-capacitor Based Electric Vehicle Power System'. *Applied Power Electronics Conference and Exposition, 2009. APEC 2009. Twenty-Fourth Annual IEEE*, 15-19 Feb. 2009, pp. 591-596.

Appendixes

Appendixes

Appendix 1 ***Ultra Capacitor efficiency program***

```
% internal resistance
Ri = 0.0014;
% Cell open circuit voltage
Uc = 3.6;

% Power range in Watt
P = 10:10:2000;
% Current over the power range
ic = (Uc - realsqrt(Uc^2 - 4*Ri.*P))./(2*Ri);
% output voltage over the power range
Uo = Uc-Ri*ic;
% internal resistance power losses
Pri = Ri.*ic.^2;
% output power based on constant current
Pout = ic.*Uo;
% temporary holding variable
Pt = Pri./Pout;
% efficiency
eff = 1 ./ (1 + Pt);
% plot power versus efficiency
plot(P, eff)
```

Appendix 2 ***Power Converter efficiency program***

```
clear
Rds = 11e-3/3;  % 3 mosfets in parallel at 11mOhm each
RL = 6.12e-3;   % inductor esr
Vd = 1.5;       % diode voltage
Vbus = 100;     % bus voltage is constant
I = 20:20:400;  % Load demand
Vi = 50;
i = 1;

d(1,i) = 1-Vi/Vbus;         % Duty cycle

R = Vbus./I;                % load resistance
IL = Vi./((1-d(1,i))^2.*R); % inductor current

Pconv = I.*Vbus;            % power at the bus
Pdiode = IL.*Vd;            % diode power consumption
Pind = RL.*IL.^2;           % inductor power
Pswitch = Rds.*IL.^2;       % switch power
% Boost converter losses
Plosses = Pind + Pswitch.*d(1,i) + Pdiode.*(1-d(1,i));
```

```
eff(:,i) = 1 ./ (1 + Plosses ./ Pconv);

% plot
plot(Pconv./1000,eff);
legend('Vi(d) = 50(0.5)')
title('Boost Converter Efficiency plot');
xlabel('Power (kW)');
ylabel('Efficiency');
```

Appendix 3 *Karnaugh map logic*

Since there is the possibility that the reset signal is high at the beginning of the period this would mean that the set signal is ignored (the subsystem is reset and a reset RS flip flop beginning state is unknown q= 0). To avoid this a little karnaugh map was drawn and solved. Effectively there are 3 signals: 1) Set is high at the beginning of each period and always requires Q = 1; 2) Reset is high always from receiving the reset pulse Q = 0, overwrites Set; Reference is established between these values. If the value is larger than 0 than Q = 0 (reset = 1, set = 0) and when below 0 then Q remains 1 (reset 0, set = 1).

Appendix Table 3.1: Karnaugh Map

Set	reference	reset	S	R	Q
0	0	0	0	**0**	0
0	0	1	0	**1**	0
0	1	0	0	**1**	0
0	1	1	0	**1**	0
1	0	0	1	**0**	1
1	0	1	1	**x**	NA[10]
1	1	0	1	**0**	1
1	1	1	1	**x**	NA

Output result from Karnaugh mapping:

Set AND Reference OR Reset

[10] NA = Since the percentages between set and reset do not overlap these conditions do not occur

Appendix 4 ***Input current monitor***

The steady state DC equations are given by:

$$\boldsymbol{K}\frac{d\boldsymbol{x}(t)}{dt} = \boldsymbol{0} = \boldsymbol{AX} + \boldsymbol{BU}$$
$$\boldsymbol{Y} = \boldsymbol{CX} + \boldsymbol{EU} \tag{7.1}$$

The linearised model for small signal AC is given by:

$$\boldsymbol{K}\frac{d\hat{\boldsymbol{x}}(t)}{dt} = \boldsymbol{A}\hat{\boldsymbol{x}}(t) + \boldsymbol{B}\hat{\boldsymbol{u}}(t) + \{(\boldsymbol{A_1} - \boldsymbol{A_2})\boldsymbol{X} + (\boldsymbol{B_1} - \boldsymbol{B_2})\boldsymbol{U}\}\hat{\boldsymbol{d}}(t)$$
$$\hat{\boldsymbol{y}}(t) = \boldsymbol{C}\hat{\boldsymbol{x}}(t) + \boldsymbol{E}\hat{\boldsymbol{u}}(t) + \{(\boldsymbol{C_1} - \boldsymbol{C_2})\boldsymbol{X} + (\boldsymbol{E_1} - \boldsymbol{E_2})\boldsymbol{U}\}\hat{\boldsymbol{d}}(t) \tag{7.2}$$

$\boldsymbol{X}$ = state vector containing state variables under steady state conditions

$\boldsymbol{U}$ = state vector independent inputs under steady state conditions

$\boldsymbol{K}$ = matrix containing the capacitances and inductances of the system

$\boldsymbol{Y}$ = State output vector of dependent signals

$\boldsymbol{A_1}, \boldsymbol{A_2}, \boldsymbol{B_1}, \boldsymbol{B_2}, \boldsymbol{C_1}, \boldsymbol{C_2}, \boldsymbol{E_1}, \boldsymbol{E_2}$ are the respective state equations for the different operating states.

$\boldsymbol{A}, \boldsymbol{B}, \boldsymbol{C}, \boldsymbol{E}$ are the respective averaged state equations

The input impedance of the buck converter with the bus capacitance as input is derived with the state space averaging technique. The circuit is given in Appendix Figure 4.1 and the individual states are given in Appendix Figure 4.2 and 4.3.

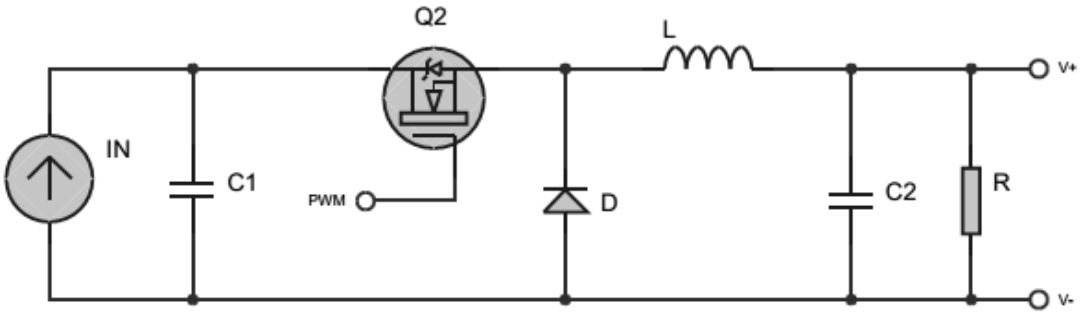

Appendix Figure 4.1: Bus Connected Buck Converter

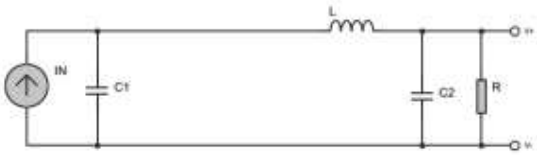

Appendix Figure 4.2: Bus Connected Buck Converter - ON

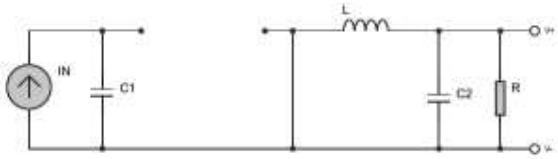

Appendix Figure 4.3: Bus Connected Buck Converter - OFF

The state variables are $x_1 = v_1(t),\ x_2 = v_2(t),\ x_3 = i(t)$. The Input variables are $u_1 = i_{in}$. The output vector is $y_1 = i_g$. Where i_g is the input current to the switch. The matrices are given by:

$$\boldsymbol{K} = \begin{bmatrix} C_1 & 0 & 0 \\ 0 & C_2 & 0 \\ 0 & 0 & L \end{bmatrix} \tag{7.3}$$

ON	OFF	
$\boldsymbol{A_1} = \begin{bmatrix} 0 & 0 & -1 \\ 0 & -1/R & 1 \\ 1 & -1 & 0 \end{bmatrix}$	$\boldsymbol{A_2} = \begin{bmatrix} 0 & 0 & 0 \\ 0 & -1/R & 1 \\ 0 & -1 & 0 \end{bmatrix}$	**(7.4)**
$\boldsymbol{B_1} = \begin{bmatrix} 1 & 0 & 0 \\ 0 & 0 & 0 \\ 0 & 0 & 0 \end{bmatrix}$	$\boldsymbol{B_2} = \begin{bmatrix} 1 & 0 & 0 \\ 0 & 0 & 0 \\ 0 & 0 & 0 \end{bmatrix}$	**(7.5)**
$\boldsymbol{C_1} = [0 \quad 0 \quad 1]$	$\boldsymbol{C_2} = [0 \quad 0 \quad 0]$	**(7.6)**

The averaged matrices are given by:

$$\boldsymbol{A} = D\boldsymbol{A_1} + D'\boldsymbol{A_2}$$
$$D' = 1 - D \tag{7.7}$$

$$\boldsymbol{A} = \begin{bmatrix} 0 & 0 & -D \\ 0 & -1/R & 1 \\ D & -1 & 0 \end{bmatrix} \tag{7.8}$$

$$\boldsymbol{B} = \begin{bmatrix} 1 & 0 & 0 \\ 0 & 0 & 0 \\ 0 & 0 & 0 \end{bmatrix} \tag{7.9}$$

$$\boldsymbol{C} = \begin{bmatrix} 0 & 0 & D \end{bmatrix} \tag{7.10}$$

The steady state equation thus becomes:

$$0 = \begin{bmatrix} 0 & 0 & -D \\ 0 & -1/R & 1 \\ D & -1 & 0 \end{bmatrix} \cdot \begin{bmatrix} V_1 \\ V_2 \\ I \end{bmatrix} + \begin{bmatrix} 1 & 0 & 0 \\ 0 & 0 & 0 \\ 0 & 0 & 0 \end{bmatrix} \cdot \begin{bmatrix} I_{in} \\ 0 \\ 0 \end{bmatrix} \tag{7.11}$$

$$\boldsymbol{I_g} = \begin{bmatrix} 0 & 0 & D \end{bmatrix} \cdot \begin{bmatrix} V_1 \\ V_2 \\ I \end{bmatrix} \tag{7.12}$$

The final small AC equation becomes:

$$\begin{bmatrix} C_1 & 0 & 0 \\ 0 & C_2 & 0 \\ 0 & 0 & L \end{bmatrix} \frac{d\hat{\boldsymbol{x}}(t)}{dt}$$
$$= \begin{bmatrix} 0 & 0 & -D \\ 0 & -1/R & 1 \\ D & -1 & 0 \end{bmatrix} \begin{bmatrix} \hat{v}_1(t) \\ \hat{v}_2(t) \\ \hat{\imath}(t) \end{bmatrix} + \begin{bmatrix} 1 & 0 & 0 \\ 0 & 0 & 0 \\ 0 & 0 & 0 \end{bmatrix} \begin{bmatrix} \hat{\imath}_{in}(t) \\ 0 \\ 0 \end{bmatrix} \tag{7.13}$$
$$+ \left\{ \begin{bmatrix} 0 & 0 & -1 \\ 0 & 0 & 0 \\ 1 & 0 & 0 \end{bmatrix} \cdot \begin{bmatrix} V_1 \\ V_2 \\ I \end{bmatrix} \right\} \hat{d}(t)$$

And

$$\hat{\boldsymbol{y}}(t) = \begin{bmatrix} 0 & 0 & D \end{bmatrix} \hat{\boldsymbol{x}}(t)$$
$$+ \{([0 \quad 0 \quad 1] - [0 \quad 0 \quad 0])\boldsymbol{X}\} \hat{d}(t) \tag{7.14}$$

The DC and AC equivalent circuit can now be drawn, see Appendix Figure 4.4.

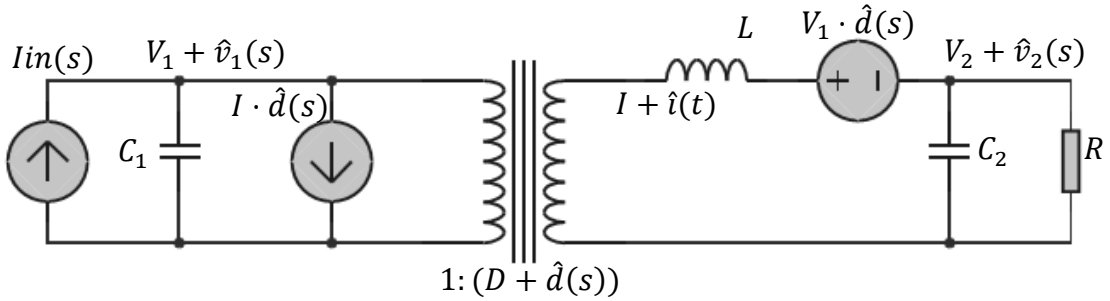

Appendix Figure 4.4: Buck Converter with Input Capacitor equivalent circuit

To find the input impedance equation the $\hat{d}(s) = 0, \hat{v}(s) = 0$ and disconnect the source. The input impedance equation then becomes:

$$Z_{in} = \frac{1}{sC_1} // \frac{1}{D^2}\ (sL + R // \frac{1}{sC_2}) \qquad \textbf{(7.15)}$$

The resulting control setup is shown in Appendix Figure 4.5.

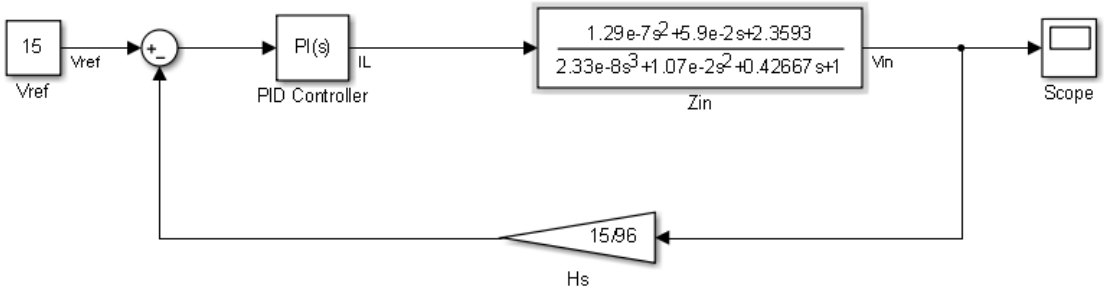

Appendix Figure 4.5: Buck converter control from Bus voltage

Appendix 5 *Battery Specifications*

Appendix Table 5.1: battery specifications

CALB SE130AHA		
Nominal Capacity	**130 Ah**	**95wh/kg**
Voltage	Nominal	3.2 V
	Cut-off charge	3.6 V
	Cut-of discharge	2.0 V
Std Discharge current	0.3 CA (39A)	
Std Charge current	< 0.3C (39A)	
int. Resistance	<0.8 ohm	
weight	4.4kg x 30	132
price	£144	excl vat
TS-LFP90AHA		
Nominal Capacity	90 Ah	93Wh/kg
Voltage	Nominal	3.2 V
	Cut-off charge	3.8 V
	Cut-off discharge	2.5 V
Std Discharge current	<45A	
Std charge current	< 45A	(<20A) suggested
weight	3.1Kg x 30	93
price	£ 140	excl vat

Appendix 6 ***Energy Management – Enabled Subsystem***

In Appendix Figure 6.1 the enabled subsystem contents is shown. The contents of the “Matlab Function is given below.

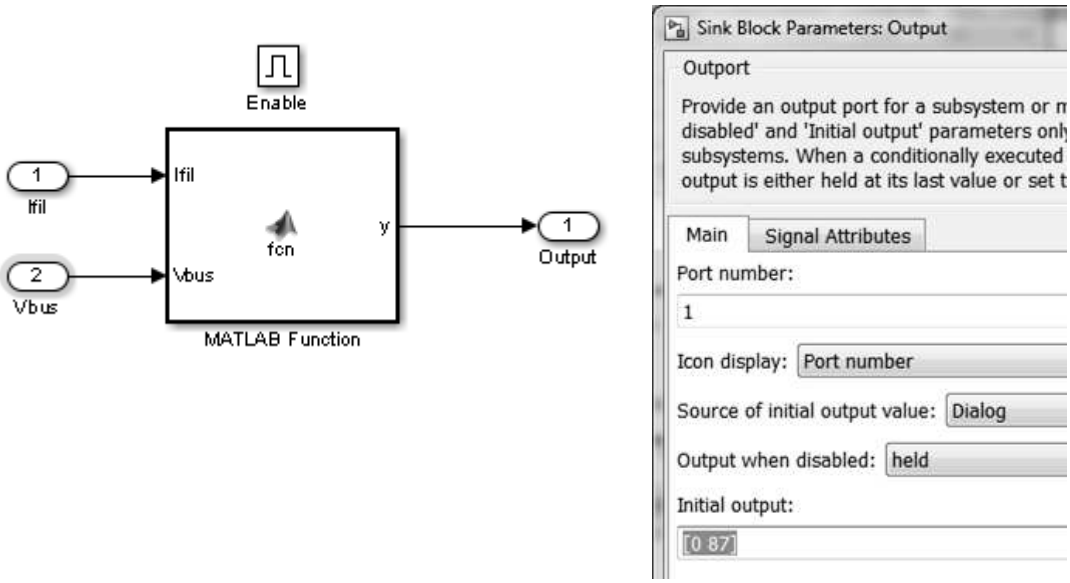

Appendix Figure 6.1: Enabled Subsystem and output port parameters

```
function y = fcn(Ifil, Vbus)
%#codegen

P = Ifil*Vbus;

if Ifil >= 0

    if P <= 1744
        Vuc_target = 87.40;
    elseif P <= 4617;
        Vuc_target = 87.03;
    elseif P <= 8108
        Vuc_target = 85.06;
    elseif P <= 13492
        Vuc_target = 79.57;
    elseif P <= 17064
        Vuc_target = 77.62;
    elseif P <= 21313
        Vuc_target = 75.41;
    else
        Vuc_target = 72.91;
    end
else
    % ensure input is not negative
    P = 0;
    Vuc_target = 87.40;
end

y = [P, Vuc_target];
```

Appendix 7 ***Ripple effects simulation setup***

In this appendix the Simulink SPS models are included for the ripple effect simulation..

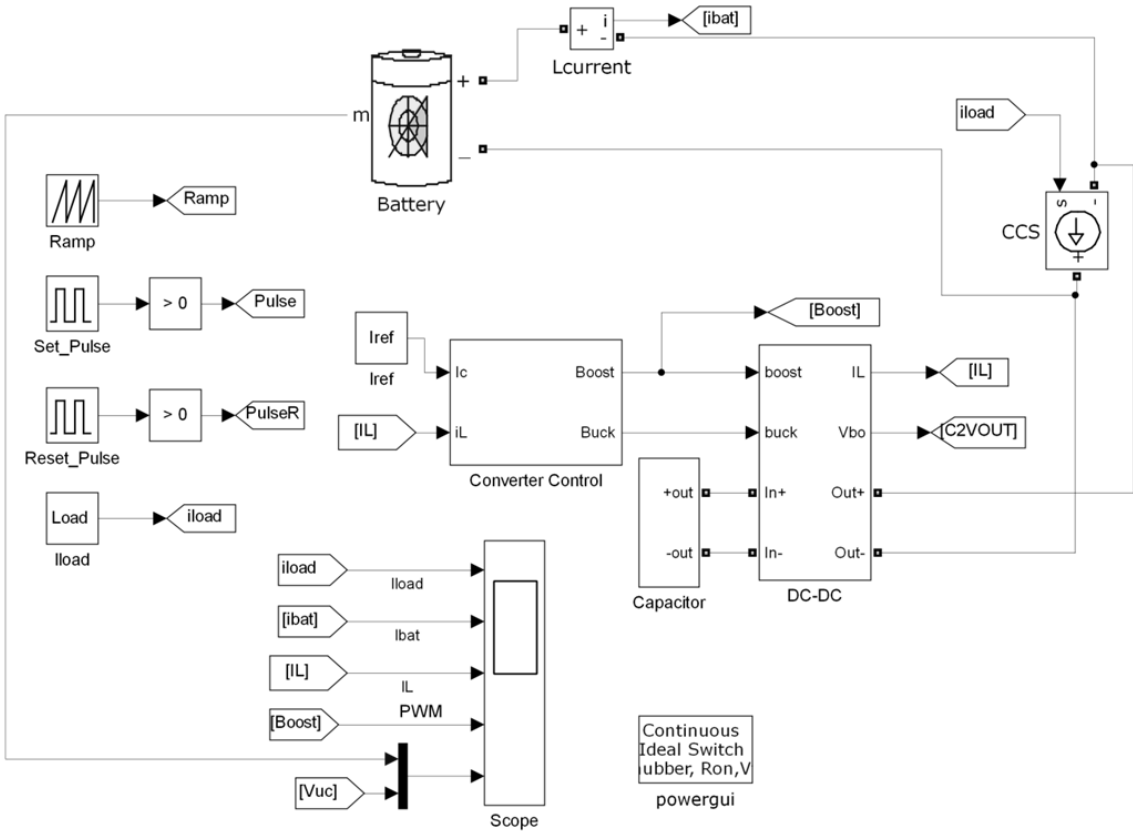

Appendix Figure 7.1: Battery + UC module ripple effect simulation

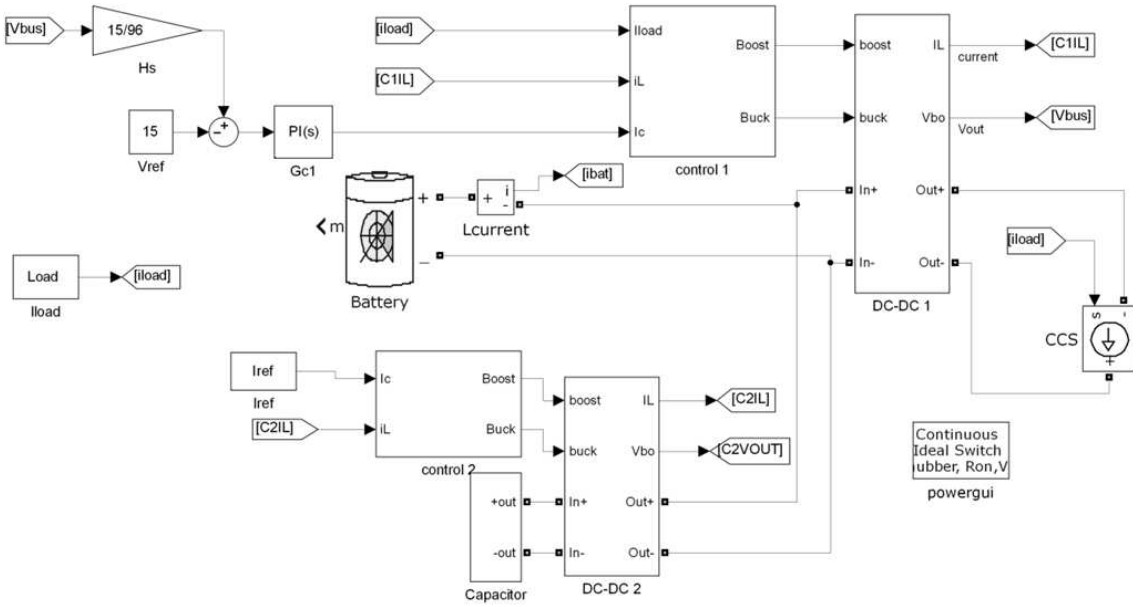

Appendix Figure 7.2: Cascaded Topology - ripple effect layout

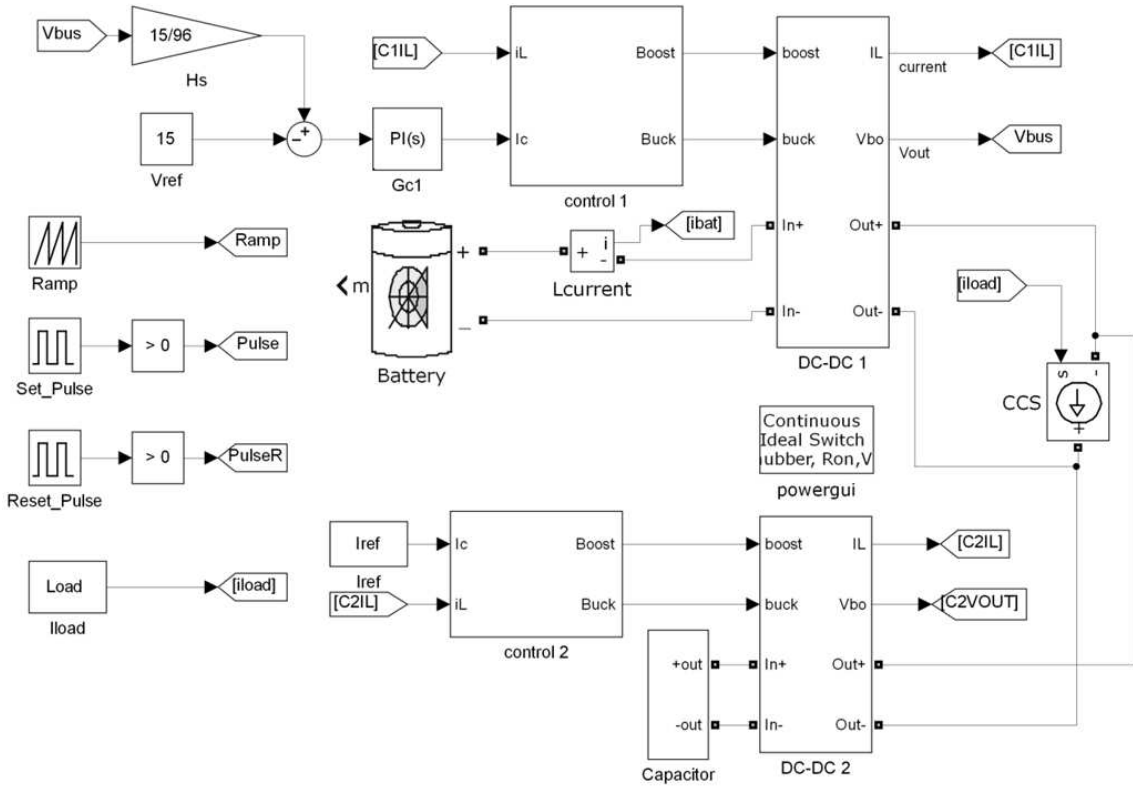

Appendix Figure 7.3: Parallel Topology - ripple effect layout

For the offset simulation the Ramp, Set_Pulse and Reset_Pulse where duplicated and offset by 50% of the timing settings (Appendix Figure 7.4). The new “Goto blocks” where updated in the “control 2” block.

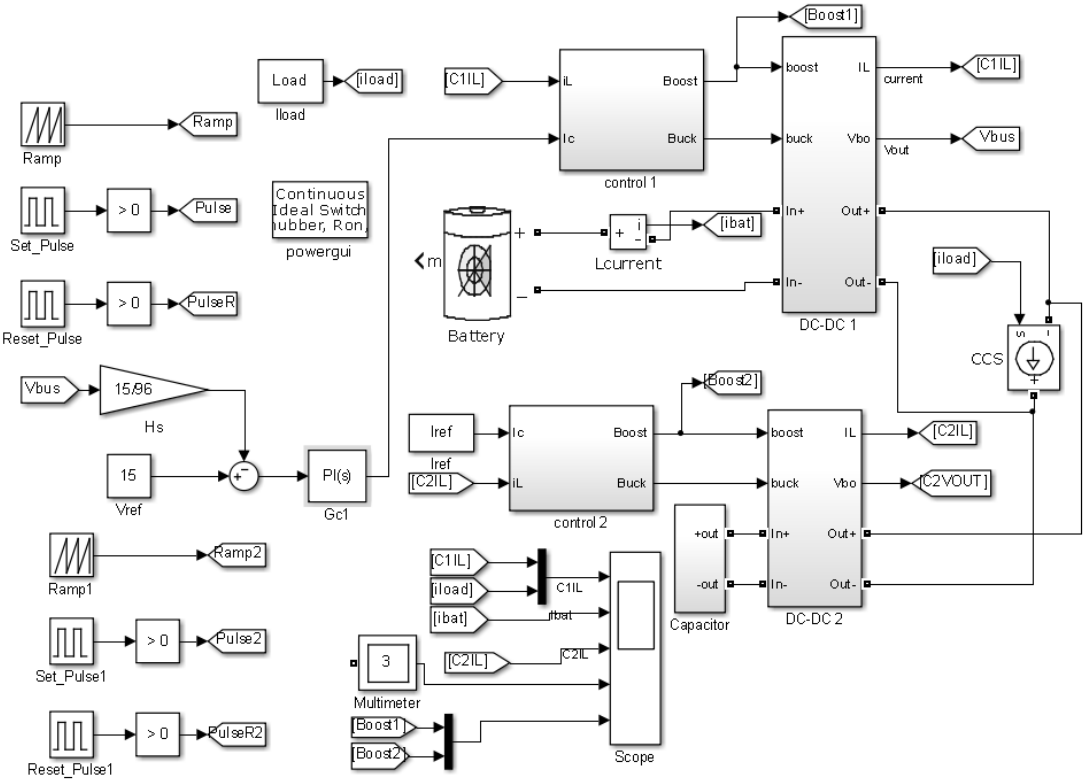

Appendix Figure 7.4: Parallel Topology - ripple effect layout with timing offset

Within this model the Scope outputs a Structure-with-Time of data to the Matlab workspace. A Matlab program then retrieves the data and outputs a graph. The Matlab code is provided below:

Retrieve data from the Simulink ScopeData

```
T = ScopeData.time;
Idem = ScopeData.signals(1).values(:,1);
Ibat = ScopeData.signals(2).values(:,1);
IL = ScopeData.signals(3).values(:,1);
PWM  = ScopeData.signals(4).values(:,1);
Vbat  = ScopeData.signals(5).values(:,1);
Vuc   = ScopeData.signals(5).values(:,2);
```

Plot single picture

```
subplot(2,1,1), plot(T,Ibat);
ylabel('Battery current (A)');

subplot(2,1,2), plot(T,IL);
ylabel('UC current (A)');
xlabel('time in seconds');
```

Zoom in at a particular area

```
xmin = 0.45;
xmax = 0.4505;
i = 0;
j = 0;
[steps, ~] = size(T);
for i = 1:steps-1
   if T(i) >= xmin
       a = i;
       break;
   end
end
for j = i:steps-1
   if T(j) >= xmax
       b = j;
       break;
   end
end
ymin = min(Ibat(a:b,1)) - 5;
ymax = max(Ibat(a:b,1)) + 5;
subplot(3,1,1), plot(T,Ibat);
axis([xmin xmax ymin ymax])
ylabel('Battery (A)');

ymin = min(IL(a:b,1)) - 5;
ymax = max(IL(a:b,1)) + 5;
subplot(3,1,2), plot(T,IL);
axis([xmin xmax ymin ymax])
ylabel('UC (A)');

ymin = -0.25;
ymax = 1.25;
subplot(3,1,3), plot(T,PWM);
axis([xmin xmax ymin ymax])
ylabel('PWM');
xlabel('time in seconds');
```

Read in Drive Cycle

```
filename = 'DC_NEDC.txt';
M =  dlmread(filename, '\t', 2, 0);
t = M(:,1);
v = M(:,2);
% speed conversion from mph to m/s if needed
if strcmp(filename,'DC_NYCC.txt')
    v = 1.609.*v ./3.6;
end
% set the duration of the drive cycle
seconds = length(t);
```

Vehicle details are based loosely on a Nissan Micra

```
m = 1200;                       % Mass in Kg including full load
g = 9.81;                       % Gravitational constant m/s^2
r = 0.266;                      % wheel radius in meters
% Frr - rolling force
% Frr = urr*m*g
urr = 0.015;                    % Rolling coefficient
Frr = urr*m*g;

% Fad = aerodynamic drag force
% Fad - drag force include 0.5
rho = 1.25;                     % air density kg/m^3
A = 2.08;                       % frontal surface m^2
Cd = 0.33;                      % drag coefficient based on frontal surface
% Fhc - hill climbing force
% Fhc = m*g*sin(alpha)
% alpha = 2.29 * pi()/ 180;     % 4% incline = 2.29 degree convert to rad
alpha = 0;
Fhc = m*g*sin(alpha);           % sine requires radians
% Fla - lateral acceleration including inertia
% Fla = m * a * I
I = 1.05;                       % intertia

% inefficiencies
Ng = 0.95;          % gear losses
kc = 0.3;           % motor losses based on 100kW induction motor
ki = 0.01;
kw = 5e-6;
C = 600;
% gear ratio of manual transmission
    % Gm = 2.861;     % 1st
    Gm = 1.562;       % 2nd
    % Gm = 1.000;     % 3rd
    % Gm = 0.697;     % 4th
Gdiff = 4.072;                   % gear ratio of diff
% final gear ratio
G = Gm * Gdiff;                  % based on AT final drive ratio

% set the ratio for regenerative braking
```

```
Regen_ratio = 0.5;
% average auxiliary power - not used
Pac = 0;

% create empty arrays
Xdd = zeros(seconds, 1);
X = zeros(seconds,1);                % Distance
Fte = zeros(seconds,1);              % Tractive effort
W = zeros(seconds,1);                % work
Pte = zeros(seconds,1);              % Power supplied by the battery
Pbat = zeros(seconds,1);
T = zeros(seconds,1);
omega = zeros(seconds,1);
```

Calculate Tractive Effort

```
for i = 1:1:seconds-1
    % Calculate Acceleration
    Xdd(i) = v(i+1)- v(i);
    % Calculate distance
    X(i+1) = v(i)*1 + X(i);
    % Calculate the lateral force
    Fla = I*m*Xdd(i);
    % calculate aero drag based on velocity
    Fad = 0.5*rho*A*Cd*v(i)^2;
    % Calculate tractive force
    Fte(i) = Frr + Fad + Fhc + Fla;
    Pte(i) = Fte(i) * v(i); %Nm/s
    omega(i) = G*v(i)/r; % omega of motor in rad/s

    if (omega(i) == 0) %stationary
        Pte(i) = 0;
        Pmot_in = 0;
        T(i) = 0;
        Nm = 0.5; % eff_mot - dummy value to make sure its not zero
    elseif (omega(i) ~= 0) % moving
        if Pte(i) < 0
            % reduce power if braking since not all will be used by motor
            Pte(i) = Regen_ratio * Pte(i);
        end
        % we now calculate the power at the motor which is different from
        % the power at the wheel because of the transmission losses
        if Pte(i) >= 0
            % motor power > shaft power
            Pmot_out = Pte(i) / Ng;
        elseif Pte(i) < 0
            % motor power diminished when if engine braking
            Pmot_out = Pte(i) * Ng;
        end

        T(i) = Pmot_out ./ omega(i); % torque equation
        % Calculate efficiency based on torque
        if T(i) > 0
            Nm = (T(i).*omega(i)) / (T(i).*omega(i) + kc.*T(i).^2 + ki.*omega(i) +
kw.*omega(i).^3 + C);
        elseif T < 0
            Nm = (-T(i).*omega(i)) / (-T(i).*omega(i) + kc.*T(i).^2 + ki.*omega(i) +
kw.*omega(i).^3 + C);
```

```
        end
        % Calculate power at the battery
        if Pmot_out >= 0
            Pmot_in = Pmot_out / Nm;
        elseif Pmot_out < 0
            Pmot_in = Pmot_out * Nm;
        end
    end
    Pbat(i) = Pmot_in + Pac;

end
mph = v*3.6/1.609;
kph = v*3.6;
```

Plot Power Profile

```
subplot(2,1,1), plot(t, kph), xlabel('time in s') ,ylabel('Velocity (kph)'), grid on
subplot(2,1,2), plot(t, Pbat), xlabel('time in seconds') ,ylabel('Power (W)'), grid on
```

Save Power Profile to File

```
saveName = regexprep(filename,'.txt', '_profile.mat');

p = zeros(2,seconds);
p(1,:) = transpose(t);
p(2,:) = transpose(Pbat);
p(3,:) = transpose(Xdd);
p(4,:) = transpose(v);
p(5,:) = transpose(X);
p(6,:) = transpose(Fte);
p(7,:) = transpose(T);
p(8,:) = transpose(omega);

S = struct('Time_S', t, 'Pbat_W', Pbat, 'Acceleration_MpS2', Xdd, 'Speed_MpS', v, ...
    'Distance_M', X, 'Fte_N', Fte, 'Torque_Nm', T, 'MotorVelo_radpS', omega.'');

save(saveName, '-struct','S', '-mat')
```

Appendix 9 ***General Simulation setup details***

Battery specifications – There are two types of battery used in these simulations. A battery for when the battery is connected directly to the bus, which requires a higher voltage and a battery connected to the bus via a converter which requires a lower voltage both battery specifications are provided in Appendix Figure 9.1 and 9.2. The battery details are based on specifications from the TS-LFP90AHA battery (see Appendix 5 - Battery Specifications).

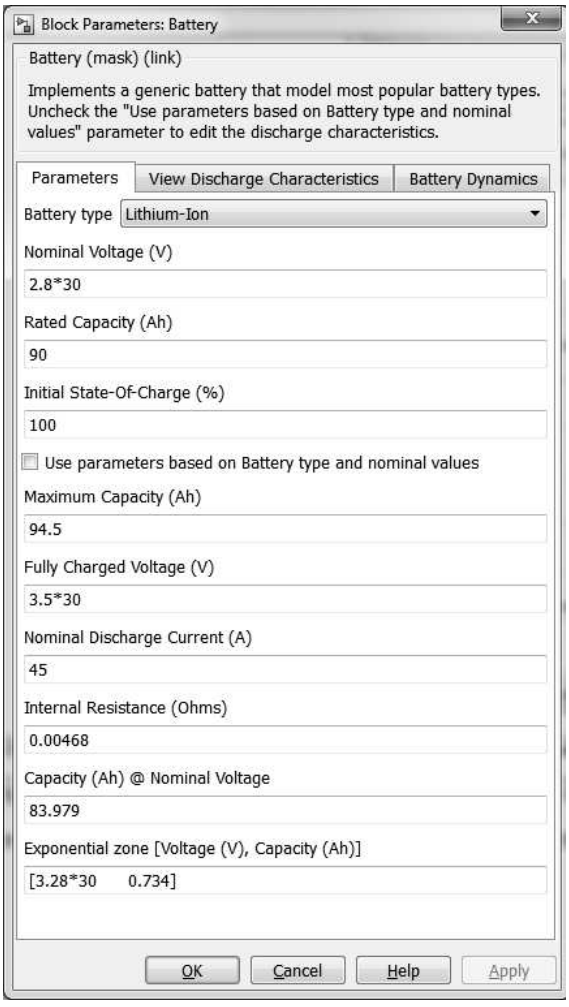

Appendix Figure 9.1: Battery specifications - bus connected

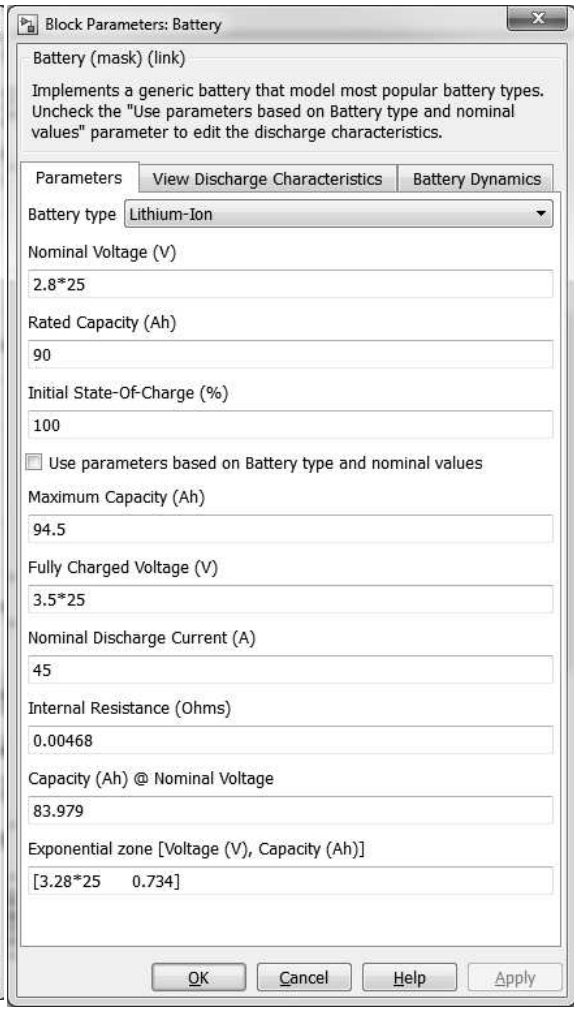

Appendix Figure 9.2: Battery specifications - Converter connected

UC Capacitor specifications – the parameters used for the UC are given in Appendix Figure 9.3.

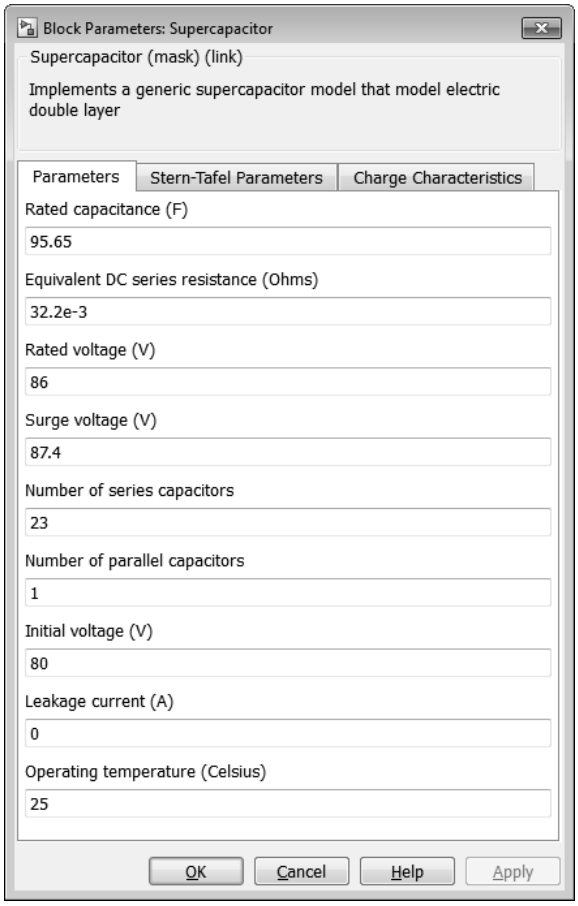

Appendix Figure 9.3: UC parameters

Timing details – within each simulation the following three blocks (Appendix Figure 9.4) provide the timing pulses for the different converters. The details for each bock are provided in Appendix Figure 9.5.

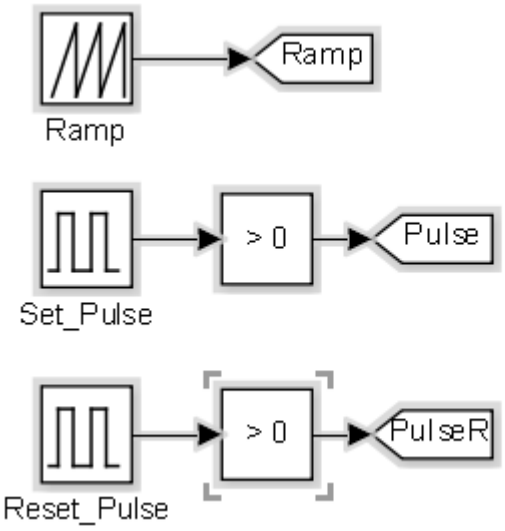

Appendix Figure 9.4: Converter Timing blocks

Ramp

Set Pulse

Reset Pulse

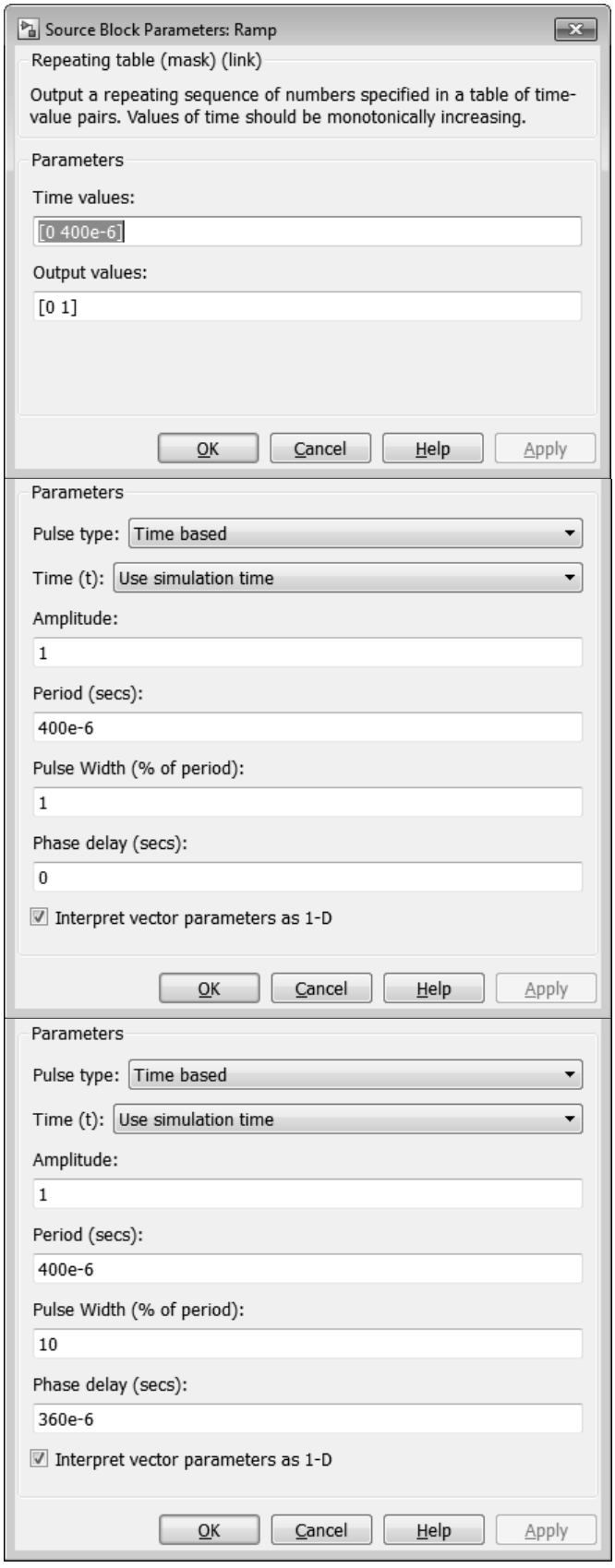

Appendix Figure 9.5: Converter Timing settings

Simulation Configuration Parameters – The Simulink Configuration Parameters are set to the following (Appendix Figure 9.6)

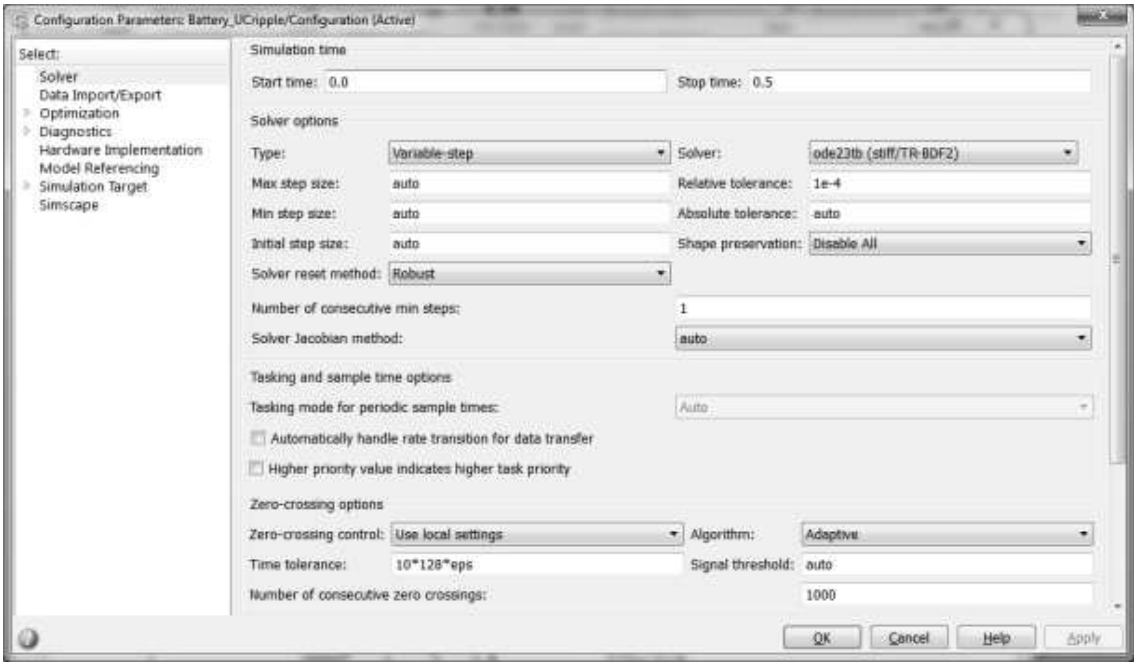

Appendix Figure 9.6: Simulation Configuration Parameters

For the Matlab graphs used in this document a program was used created by Oliver Woodford and can be found at: http://www.mathworks.co.uk/matlabcentral/fileexchange/23629-export-fig

The following figures (9.7, 9.8 and 9.9) provide the basic overview of each simulation setup in SPS. The use of the “simout” function is similar to the “To File” block except that it outputs to the Matlab workspace and is useful if interaction with a Matlab script file is necessary.

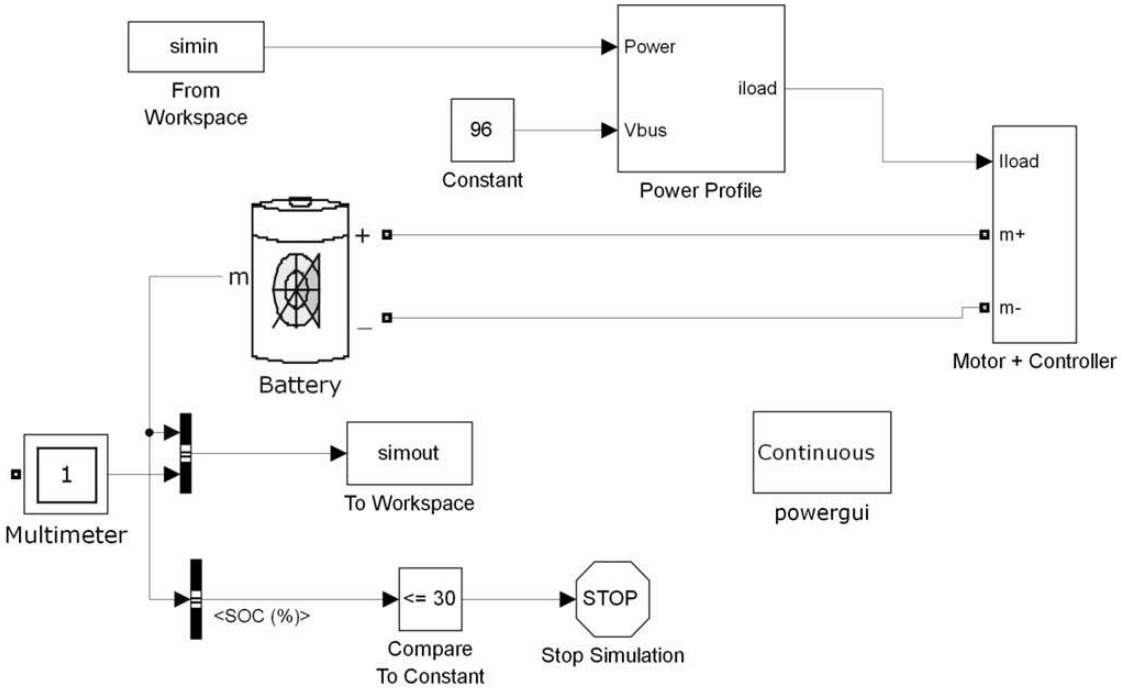

Appendix Figure 9.7: Topology 1 – Battery

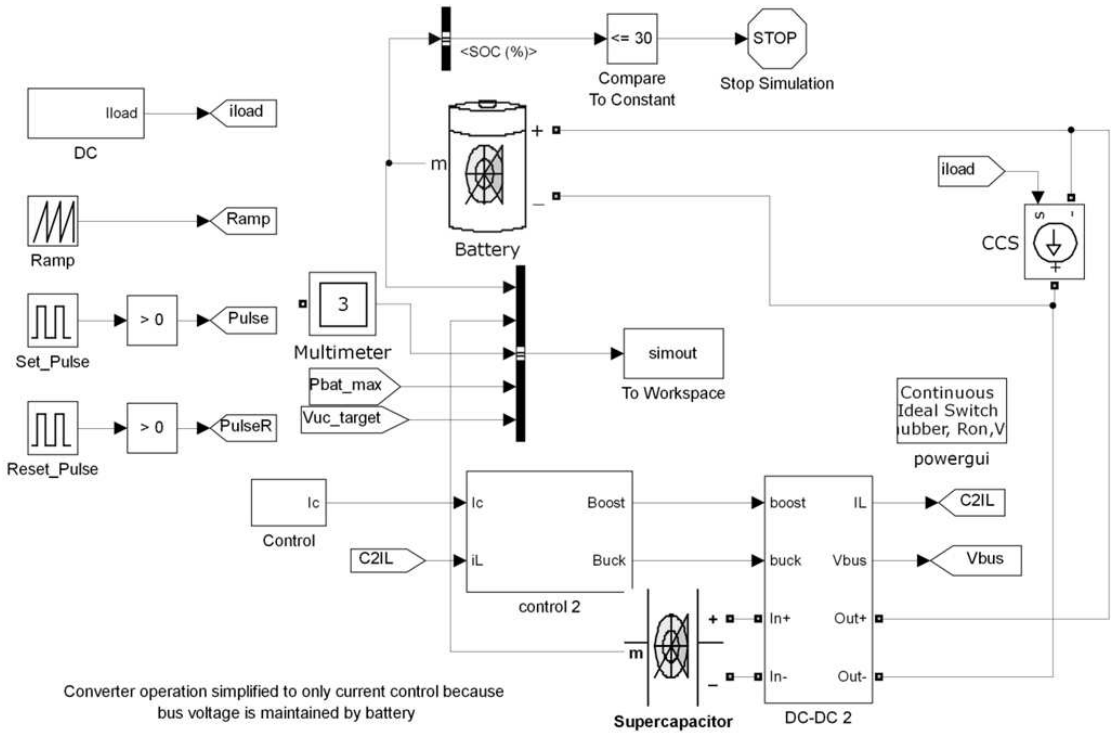

Appendix Figure 9.8: Topology 3 – Battery with UC module

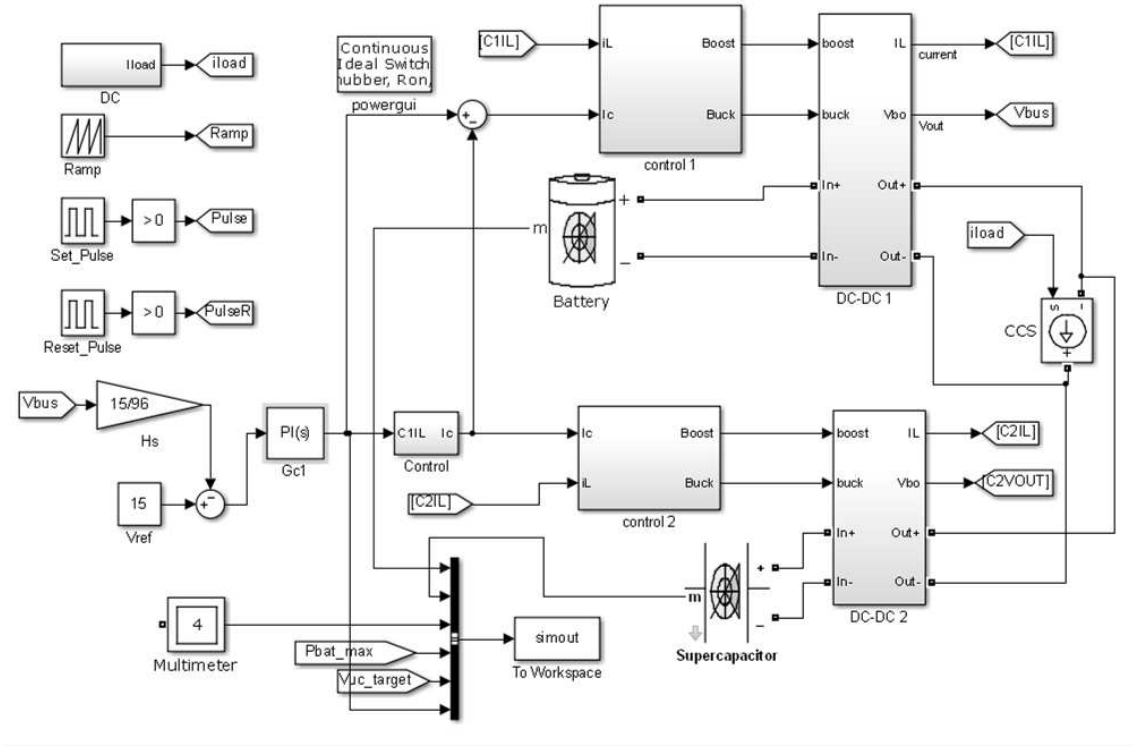

Appendix Figure 9.9: Topology 4 – Parallel

Appendix 10 ***Main Program***

Set timing

```
clear all; clc;
% output a time to command window so we know when we started
c = clock;
hrs = c(1,4);
minutes = c(1,5);
sec = c(1,6);
fprintf(1, 'Start Time = %2.0f : %2.0f : %2.0f \n', hrs, minutes, sec);
% Set mail alert specifications
setMailSpec; % Copyright (c) 2010, Benjamin Kraus
```

Load Drive Cycle Power Profile

```
DCname = 'NEDC';

% create the filenames for loading and saving
s1 = ['DC_',DCname, '_profile.mat'];
s2 = ['01_',DCname, '_Sim_Time.txt'];
% Load drive cycle
M = load(s1);

% prep data for inclusion to workspace
Time = length(M.Time_S);
simin = timeseries(M.Pbat_W,M.Time_S);
```

Run Simulink program

```
pause(1)
fprintf(1,'Start of Simulation\n' );

        % Start timer
        tic;
        % run the simulation using catch program to alert when crashed
        varargout = notifier('123adrdress@email.com', @A1_B_C_bus_run, Time);
        % sim('Battery_Converter_run.mdl',step_time);
        elapsedTime = toc;

seconds = mod(elapsedTime , 60);
minutes = fix(elapsedTime / 60);
hours = fix(minutes / 60);
minutes = mod(minutes , 60);
```

Comment file

```
fprintf(1, 'Elapsed Time = %2.0f : %2.0f : %4.3f \n', hours, minutes, seconds);
fprintf(1, 'Write time to file\n');

fid = fopen(s2, 'w');
fprintf(fid, 'drive cycle time = %5.0f \r\n',Time);
```

```
fprintf(fid, 'Elapsed Time = %2.0f : %2.0f : %4.3f \r\n', hours, minutes, seconds);
fprintf(fid, '\r\n');
fprintf(fid, '\r\n');
fprintf(fid, '\r\n');
fprintf(fid, '\r\n');
fprintf(fid, '\r\n');
fclose(fid);

fprintf(1,'End of Simulation\n' );
```

The Notifier program can be found on the Matlab File Exchange

http://www.mathworks.co.uk/matlabcentral/fileexchange/28733-notifier

The notifier function calls the following file:

```
function [result] = A1_B_C_bus_run(Time)

sim('A1_B_C_bus.slx',Time);
result = 1;
```

Appendix 11 ***Statistic report on the battery tests***

Each column represents a battery with the reported capacity with each subheading represents the used discharge current.

90Ah		**130Ah**	
22A		**22A**	
mean	89.504	**mean**	140.153
Standard Deviation	3.157	**Standard Deviation**	0.600
Confidence interval	3.920	**Confidence interval**	1.908
45A		**45A**	
mean	88.508	**mean**	140.173
Standard Deviation	3.183	**Standard Deviation**	0.685
Confidence interval	3.951	**Confidence interval**	1.090
90A		**90A**	
mean	87.852	**mean**	140.000
Standard Deviation	3.675	**Standard Deviation**	0.648
Confidence interval	4.562	**Confidence interval**	1.031
135A		**135A**	
mean	87.074	**mean**	139.915
Standard Deviation	3.794	**Standard Deviation**	0.688
Confidence interval	4.710	**Confidence interval**	1.094
180A		**180A**	
mean	86.122	**mean**	139.618
Standard Deviation	3.682	**Standard Deviation**	0.728
Confidence interval	4.571	**Confidence interval**	1.158

Confidence interval based on T distribution			
t distribution value 95%	2.776	**t distribution value 95%**	3.182
Degrees of Freedom	4	**Degrees of Freedom**	3

Appendix 12 *Pugh Analysis selection criteria discussion*

For the Pugh analysis the following assessment criteria have been defined:

- capacity – more capacity (a larger pack) is better; the limited amount of energy the UC Module could add is ignored
- ripple control – if the system requires additional ripple control this is a negative point
- weight – a higher weight than the baseline is negative
- 10 year cost – a cost improvement after 10 years is positive
- Motor controller improvement – an efficiency improvement of the energy through the motor controller is positive
- Range – an improvement in range is positive
- Efficiency – an improvement in efficiency is positive

The latter two criteria are similar but different in that an increase in capacity could give improved range but because of the increased weight also reduced efficiency, showing one of the limitations of the analysis method (the interlinking between criteria).

This page has intentionally been left blank.